OCRWM	MODEL COVER SHEET	1. QA: QA Page: 1 of 226

2. Type of Mathematical Model

☒ Process Model ☐ Abstraction Model ☐ System Model

Describe Intended Use of Model

The purpose of the site-scale saturated zone flow model is to describe the spatial distribution of groundwater as it moves from the water table below the repository, through the saturated zone, and to the point of uptake by the receptor of interest.

3. Title

Site-Scale Saturated Zone Flow Model

4. DI (Including Rev. No. and Change No., if applicable):

MDL-NBS-HS-000011 REV 01

5. Total Attachments	6. Attachment Numbers - No. of Pages in Each
1	1-X314 spk 1/27/2004

	Printed Name	Signature	Date
7. Originator	G.A. Zyvoloski	SIGNATURE ON FILE	12-17-03
8. CSO	M. Zhu	SIGNATURE ON FILE	12/17/03
9. Checker	M. Wallace	SIGNATURE ON FILE	12-17-03
10. QER	K. McFall	SIGNATURE ON FILE	12/17/03
11. Responsible Manager/Lead	S.P. Kuzio	SIGNATURE ON FILE	12/17/03
12. Responsible Manager	P.R. Dixon	SIGNATURE ON FILE	12/17/03

13. Remarks

Calculations are not attached to the document because of their extensive nature, but files reside in the Technical Data Management System.

This report addresses TERS Item TER-02-0084. Specifically, this report addresses MVSR Items O.5 in Section 7.

OFFICE OF CIVILIAN RADIOACTIVE WASTE MANAGEMENT
MODEL REVISION RECORD

2. Model Title:
Site-Scale Saturated Zone Flow Model

3. DI (including Rev. No. and Change No., if applicable):
MDL-NBS-HS-000011 REV01

4. Revision/Change No.	5. Description of Revision/Change
REV 00	Initial Issue.
REV 00, ICN 01	Change bars were used in REV 00, ICN 01, to indicated corrections to the original document.
REV 01	Change bars are not used in REV 01 because there were extensive changes to the original document.

CONTENTS

Page

1. PURPOSE 17

2. QUALITY ASSURANCE 19

3. USE OF SOFTWARE 21
   3.1 SOFTWARE TRACKED BY CONFIGURATION MANAGEMENT 21
      3.1.1 Parameter Optimization 23
      3.1.2 Flow Modeling 23
      3.1.3 Particle Tracking 23
      3.1.4 Grid Generation 23
      3.1.5 Framework Translation 23
      3.1.6 Corrections of Carbon-14 Ages in Field Data 23
   3.2 EXEMPT SOFTWARE 24

4. INPUTS 25
   4.1 DATA, PARAMETERS, AND OTHER MODEL INPUTS 25
   4.2 CRITERIA 26
   4.3 CODES AND STANDARDS 28

5. ASSUMPTIONS 29

6. MODEL DISCUSSION 31
   6.1 MODELING OBJECTIVES 31
   6.2 FEATURES, EVENTS, AND PROCESSES SUPPORTED BY THIS MODEL 31
   6.3 BASE-CASE CONCEPTUAL MODEL 35
      6.3.1 FEPs Supported by the Base-Case Model 36
      6.3.2 Components of the Base-Case Conceptual Model 39
         6.3.2.1 Groundwater Occurrence and Flow 41
         6.3.2.2 Hydrologic Features 43
         6.3.2.3 Flow Field 43
         6.3.2.4 Large, Moderate, and Small Hydraulic Gradients 46
         6.3.2.5 Vertical Gradients 47
         6.3.2.6 Lateral Boundary Conditions 49
         6.3.2.7 Recharge 49
         6.3.2.8 Discharge 50
         6.3.2.9 Heterogeneity 50
         6.3.2.10 Role of Faults 52
      6.3.3 Groundwater Flow Processes 53

CONTENTS (Continued)

Page

6.4 CONSIDERATION OF ALTERNATIVE CONCEPTUAL MODELS 57
6.4.1 Large Hydraulic Gradient 57
6.4.2 Solitario Canyon Fault 59
6.4.3 Anisotropy.....61
6.4.3.1 Vertical Anisotropy.....61
6.4.3.2 Horizontal Anisotropy 61
6.4.4 Potentiometric Surface (Horizontal Hydraulic Gradient) and Water-Level Data 62
6.4.4.1 *Water-Level Data Analysis for the Saturated Zone Site-Scale Flow and Transport Model*, REV 00 ICN 01 (Base-case model).....63
6.4.4.2 *Water-Level Data Analysis for the Saturated Zone Site-Scale Flow and Transport Model*, REV 01 (FY01 Supplemental Science and Performance Analyses) 64
6.4.4.3 *Calibration of the SZ Site-Scale Flow Model*, REV 00 ICN 01 65
6.4.4.4 UZ Model Lower Boundary for the Unsaturated Zone Flow and Transport Model.....65
6.4.5 Water-Table Rise 68
6.4.5.1 Estimating Water-Table Rise from Climate Change 68
6.4.5.2 Water-Table-Rise in the SZ Site-Scale Flow Model 72
6.4.6 Summary of the Alternative Conceptual Models.....75
6.5 MODEL FORMULATION OF BASE-CASE CONCEPTUAL MODEL.....76
6.5.1 Mathematical Description of Base-Case Conceptual Model 76
6.5.2 Computational Model 78
6.5.3 Base-Case Model Inputs 79
6.5.3.1 Hydrogeologic Framework Model Overview.....79
6.5.3.2 Grid Generation 81
6.5.3.3 Hydrogeologic Properties 86
6.5.3.4 Features.....94
6.5.3.5 Boundary Conditions 102
6.5.3.6 Recharge 102
6.5.3.7 Nodal Hydrogeologic Properties.....103
6.6 BASE-CASE MODEL RESULTS 107
6.6.1 Model Calibration 107
6.6.1.1 Calibration Criteria 107
6.6.1.2 Parameter Optimization Procedure 107
6.6.1.3 Calibration Targets.....109
6.6.1.4 Calibration Parameters.....113
6.6.2 Calibration Results.....116
6.6.2.1 Water Levels 116
6.6.2.2 Comparing Fluxes Derived from the Regional Model with Fluxes Calculated from the Calibrated Model 119
6.6.2.3 Predicted Flow Paths.....121

CONTENTS (Continued)

Page

6.6.2.4 Specific Discharge 122
6.7 EVALUATION OF ALTERNATIVE MODELS 123
6.7.1 Large Hydraulic Gradient ACM 123
6.7.1.1 Overview of Large Hydraulic Gradient ACM 123
6.7.1.2 Large Hydraulic Gradient ACM Setup 123
6.7.1.3 Large Hydraulic Gradient ACM Results 124
6.7.1.4 Assessment of the Large Hydraulic Gradient ACM 131
6.7.2 Solitario Canyon Fault ACM 132
6.7.2.1 Overview of Solitario Canyon Fault ACM 132
6.7.2.2 Solitario Canyon Fault ACM Setup 132
6.7.2.3 Solitario Canyon Fault ACM Results 133
6.7.2.4 Assessment of Solitario Canyon Fault ACM 135
6.8 UNCERTAINTY 140
6.8.1 Model Uncertainty Due to the Large Hydraulic Gradient 140
6.8.2 Model Uncertainty Due to Perched Water on Flow Paths and Specific Discharge 141
6.8.3 Model Uncertainty Due to Anisotropy 141
6.8.3.1 Vertical Anisotropy 141
6.8.3.2 Horizontal Anisotropy 142
6.8.4 Uncertainty of Representing Faults with Enhanced Permeability Grid Blocks 142
6.8.5 Quantification of Groundwater Specific Discharge Uncertainty 143
6.8.6 Discussion of the Effect of Hydrogeologic Contact Uncertainty on Specific Discharge 145
6.8.7 Uncertainty Due to Scaling Issues 146
6.8.8 Specific Discharge Uncertainty Range 146
6.8.9 Remaining Uncertainties in Specific Discharge Estimates 149
6.9 DESCRIPTION OF BARRIER CAPABILITY 149

7. VALIDATION 151
7.1 COMPARISON OF OBSERVED AND PREDICTED NYE COUNTY WATER LEVELS 153
7.2 COMPARISON OF SPECIFIC DISCHARGE BASED ON PERMEABILITY DATA AND ATC TRACER TEST RESULTS 158
7.2.1 Newer Permeability Data 159
7.2.1.1 Calico Hills 159
7.2.1.2 Alluvial Testing Complex (ATC) 160
7.2.1.3 Apache Leap 160
7.2.1.4 Ghost Dance Fault 162
7.2.1.5 Tuffaceous Formations 162
7.2.2 Implications of Permeability Data on Specific Discharge Estimates 163

CONTENTS (Continued)

Page

7.2.3 Permeability Data from the Yucca Mountain Area 164
7.2.3.1 Single-Hole Tests.....165
7.2.3.2 Cross-Hole Tests.....167
7.2.4 Permeability Data from the Nevada Test Site.....167
7.2.4.1 Lower Carbonate Aquifer (unit 4) 168
7.2.4.2 Valley-Fill Aquifer (unit 20).....169
7.2.4.3 Welded-Tuff Aquifer (unit 16) 171
7.2.4.4 Lava-Flow Aquifer (unit 17).....171
7.2.5 Inferences about Permeability from Regional Observations 173
7.2.5.1 Lower Clastic Aquitard (unit 3).....173
7.2.5.2 Upper Clastic Aquitard (unit 5) 174
7.2.5.3 Faults.....174
7.2.5.3.1 Orientation of Faults Relative to the Minimum Horizontal Stress in the Region 174
7.2.5.3.2 Amount and Type of Infilling Material in the Fault 175
7.2.5.3.3 Relative Transmissivities of Hydrogeologic Units Juxtaposed by Offset Across the Fault.....175
7.2.5.3.4 Recent Seismic History.....175
7.2.6 Comparing Permeability Data to Calibrated Permeability Values 176
7.3 COMPARISON OF HYDROCHEMICAL DATA TRENDS WITH CALCULATED PARTICLE PATHWAYS.....179
7.3.1 Hydrochemical Data Flow Path Summary 180
7.3.2 Mixing Zones.....186
7.4 THERMAL MODELING.....187
7.4.1 Conduction-Only Modeling.....187
7.4.1.1 Temperature and Thermal Properties Data 188
7.4.1.2 Thermal Conduction Model Setup.....193
7.4.1.2.1 Thermal Boundary Conditions on the Upper Boundary ..193
7.4.1.2.2 Thermal Boundary Conditions on the Lower Boundary..197
7.4.1.3 Thermal Model Calibration.....197
7.4.1.4 Sensitivity to Thermal Conductivity in the Alluvium.....201
7.4.1.5 Results and Discussion of Conduction-Only Thermal Modeling 202
7.4.2 Coupled Thermal Modeling.....202
7.4.2.1 SZ Site-Scale Coupled Thermal Model Setup 203
7.4.2.2 Results and Discussion of Coupled Thermal Modeling.....205
7.5 VALIDATION SUMMARY 207

8. CONCLUSIONS.....208
8.1 SUMMARY OF MODELING ACTIVITIES 209
8.1.1 Saturated-Zone Flow Characterization 209
8.1.2 Conceptual Model of Site-Scale Flow 210
8.1.3 Mathematical Model and Numerical Approach.....211
8.1.4 Model Validation and Confidence Building.....211

CONTENTS (Continued)

Page

8.2 OUTPUTS....211
8.3 OUTPUT UNCERTAINTY....212
8.3.1 Specific Discharge Uncertainty Range....212
8.3.2 Flow Paths Uncertainty....213

9. INPUTS AND REFERENCES....214
9.1 DOCUMENTS CITED....214
9.2 CODES, STANDARDS, REGULATIONS, AND PROCEDURES....223
9.3 SOFTWARE....224
9.4 SOURCE DATA, LISTED BY DATA TRACKING NUMBER....225
9.5 OUTPUT DATA, LISTED BY DATA TRACKING NUMBER....226

ATTACHMENT I: DUNE WASH AND GHOST DANCE FAULT TRACES

INTENTIONALLY LEFT BLANK

FIGURES

Page

1. Important Physiographic Features Near Yucca Mountain Including Boundaries of the Site-Scale Saturated-Zone Flow Model 40
2. Site-Scale Potentiometric Map and Structural Features 44
3. Potentiometric Surface Map and Gradient Areas Developed Using Water-Level Data from 1993 45
4. Features of the Base-Case Saturated-Zone Model with East-West Barrier Included 58
5. Features of the LHG-ACM Saturated-Zone Model without the East-West Barrier 59
6. Location of Faults in the Yucca Mountain Region 60
7. Horizontal Anisotropy is Applied to the Blue Cross-Hatched Area 62
8. Contour Plot of Water-Level Data for the *Saturated Zone Flow and Transport Model*, REV 01 66
9. Simulated Water-Level Data with Residual Heads in *Calibration of the SZ Site-Scale Flow Model*, REV 00 ICN 01 66
10. Overview of Contour Lines Representing Qualified (solid lines, blue points and labels) and Unqualified (dashed lines, black points and labels) Data Sets for the UZ Lower Model Boundary 67
11. Estimated Water-Table Elevations for Future Glacial Climatic Conditions 71
12. Estimated Depth to the Water Table for Future Glacial Climatic Conditions 72
13. Hydrogeologic Framework Model Units at the Water Table for Present Conditions 73
14. Hydrogeologic Framework Model Units at the Water Table for Estimated Future Glacial Climatic Conditions 74
15. 500-meter Computational Grid 82
16. View of 500-m Computational Grid (3x Elevation) Showing Node Points Colored by Hydrogeologic Unit Values from the HFM 84
17. Close-up View of Computational Grid (3x Elevation) Showing Cut Away at X = 549000 and Y = 4078000 through the Yucca Mountain Repository 85
18. Comparison of HFM Layer Thicknesses (Vertical) and Grid Nodes by Hydrogeologic Unit

18a. Units 2, 3, 4 87
18b. Units 5, 6, 7 88
18c. Units 8, 9, 10 89
18d. Units 11, 12, 13 90
18e. Units 14, 15, 16 91
18f. Units 17, 18, 19 92
18g. Unit 20 93

19. Geologic Features in the Area of the Site-Scale Flow Model 101
20. Comparison of Recharge Data (left panel) with FEHM Input Data (right panel) 104
21. Map of Modeled Temperature at the Water Table for the Saturated-Zone Site-Scale Flow Model Domain 106
22. Location of Observation Wells 114

FIGURES (Continued)

Page

23. Contour Plot of Water-Level Data (left panel) and Simulated Water-Level Data with Residual Heads (right panel) 118
24. Flux Zones Used for Comparing Regional and Site-Scale Fluxes 121
25. Flow Paths from the Repository with Simulated Hydraulic Head Contours 122
26. Predicted Flow Paths from the Water Table Beneath the Repository for the ANF Model 127
27. Predicted Flow Paths from the Water Table Beneath the Repository for the AWF Model 128
28. Predicted Flow Paths from the Water Table Beneath the Repository for the AWF/GDF Model 129
29. Groundwater Flow Paths in SZ Interpreted From Groundwater Chemistry and Isotope Compositions (enlarged from Figure 39a) 130
30. Simulated Groundwater Flow Paths from Beneath the Repository (Blue Lines) for the Base-Case (Deep Solitario Canyon Fault) SZ Site-Scale Flow Model 136
31. Simulated Groundwater Flow Paths from the West Side of Solitario Canyon Fault (Blue Lines) for the Base-Case (Deep Solitario Canyon Fault) SZ Site-Scale Flow Model 137
32. Simulated Groundwater Flow Paths from Beneath the Repository (Blue Lines) for the Alternative Case (Shallow Solitario Canyon Fault) SZ Site-Scale Flow Model ... 138
33. Simulated Groundwater Flow Paths from the West Side of Solitario Canyon Fault (Blue Lines) for the Alternative Case (Shallow Solitario Canyon Fault) SZ Site-Scale Flow Model 139
34. Locations of Nye County EWDP Wells 154
35. Measured and Simulated Head Along Flow Path 157
36. Comparison of Unsaturated-Zone and Saturated-Zone Permeabilities 164
37. Logarithms of Permeabilities Estimated during Model Calibration Compared to Mean Logarithms of Permeability Determined from Pump-Test Data from Yucca Mountain 176
38. Logarithms of Permeabilities Estimated during Model Calibration Compared to Mean Logarithms of Permeability Determined from Pump-Test Data from the Nevada Test Site 177
39a. Groundwater Flow Paths and Mixing Zones Interpreted From Groundwater Chemistry and Isotope Compositions 181
39b. Transport Pathways Deduced from Hydrochemistry Data (in red, enlarged from Figure 39a) Overlaying Flow Paths Calculated from the SZ Transport Model (in black) for Tracer Particles Starting at the Repository Footprint 182
40. Computed Average Annual Surface Temperature for the SZ Site-Scale Thermal Model Area 195
41. Depth to the Water Table in the SZ Site-Scale Model Area 196
42. Simulated Temperatures at the Water Table for the Thermal Conduction Model 198

FIGURES (Continued)

Page

43. Simulated Temperatures Versus Observed Temperatures for the Thermal Conduction Model 199
44. Histogram of Residuals in Simulated Temperature for the Thermal Conduction Model 200
45. Residuals in Simulated Temperature at the Water Table for the Thermal Conduction Model 201
46. Simulated Temperatures at the Water Table for the Coupled Thermal Model 204
47. Simulated Temperatures Versus Observed Temperatures for the Coupled Thermal Model 205
48. Residuals in Simulated Temperature at the Water Table for the Coupled Thermal Model 206

INTENTIONALLY LEFT BLANK

TABLES

Page

1. Computer Codes Used in the Site-Scale Saturated-Zone Flow Model.....21
2. Input Data Sources.....25
3. Project Requirements and YMRP Acceptance Criteria Applicable to This Model Report 26
4. Assumptions 29
5. Included FEPs for the Saturated Zone TSPA-LA.....32
6. Saturated-Zone Included FEPs for Which This Model Report Provides the Technical Basis.....33
7. Saturated-Zone Included FEPs Supported by the Results in This Model Report.....35
8. Alternative Conceptual Models Considered.....75
9. Bounding Box.....81
10. Vertical Grid Spacing Used in the Site-Scale SZ Flow Model 83
11. Hydrogeologic Units.....94
12. Hydrological Features in the Saturated-Zone Flow Model 96
13. Observation Wells with Computed Head Data..... 110
14. Calibration Parameters Used in the Saturated-Zone Site-Scale Model 116
15. Comparison of Regional and Site-Scale Fluxes 120
16. Selected Residuals from Models 125
17. Comparison of Selected Parameter Values for Different Conceptual Models..... 126
18. Observation Wells with Computed Head Data Compared to Shallow Fault ACM 133
19. Statistical Summary of Permeabilities Calculated from Single-Hole and Cross-Hole Tests at Yucca Mountain 148
20. Nye County EWDP Wells Used as Calibration Targets in the Base-Case Model Calibration with Observed and Predicted Water Levels..... 153
21. Comparison of Water Levels Observed and Predicted at Nye County EWDP Wells..... 155
22. Predicted and Observed Hydraulic Gradient for Identified Wells..... 158
23. Transmissivities, Hydraulic Conductivities, and Permeabilities Determined in the Single-Well Hydraulic Tests Conducted in the Alluvium in NC-EWDP-19D1 between July and November 2000..... 166
24. Permeabilities Calculated for the Lower Carbonate Aquifer 168
25. Permeability Estimates for the Valley-Fill Aquifer..... 170
26. Permeability Estimates for the Welded-Tuff Aquifer..... 171
27. Permeabilities of the Lava-Flow Aquifer 172
28. Temperature Data from Boreholes 188
29. Thermal Conductivity of SZ Hydrogeologic Units 191

INTENTIONALLY LEFT BLANK

ACRONYMS AND ABBREVIATIONS

3-D	three-dimensional
ACM	alternative conceptual model
ANF	altered, no fault
AP	administrative procedure
ATC	Alluvial Testing Complex
AVS	Advanced Visualization System
AWF	altered, with fault
AWF/GDF	altered, with fault/Ghost Dance Fault
BSC	Bechtel/SAIC Company
CRWMS M&O	Civilian Radioactive Waste Management System Management and Operating Contractor
CVFE	control-volume finite element
DIRS	Document Input Reference System
DOE	U.S. Department of Energy
DTN	data tracking number
FEHM	finite-element heat and mass transfer numerical analysis computer code
GDF	Ghost Dance Fault
GFM	Geologic Framework Model
GMRES	generalized minimum residual method
HFM	Hydrogeologic Framework Model
INEEL	Idaho National Engineering and Environmental Laboratory
LaGriT	Los Alamos grid generation software package
LANL	Los Alamos National Laboratory
LHG	large hydraulic gradient
LM	Levenberg-Marquardt, the name of the optimization algorithm for PEST
MVA	middle volcanic aquifer
NRC	U.S. Nuclear Regulatory Commission
NTS	Nevada Test Site
NC-EWDP	Nye County Early Warning Drilling Program
OCRWM	Office of Civilian Radioactive Waste Management

ACRONYMS AND ABBREVIATIONS (Continued)

PA	Performance Assessment
PEST	parameter estimation code
QA	quality assurance
REV	revision
SCM	Software Configuration Management
SR	Site Recommendation
SSD	sum-of-squares difference
STN	software tracking number
SZ	saturated zone
Tac	Calico Hills formation
TBD	to be determined
TBV	to be verified
Tcb	Bullfrog Tuff of the Crater Flat Group
Tcp	Prow Pass Tuff of the Crater Flat Group
Tct	Tram Tuff of the Crater Flat Group
Tlr	Lithic Ridge Tuffs
TSPA	Total Systems Performance Assessment
TSPA-LA	Total Systems Performance Assessment for the License Application
TSPA-SR	Total Systems Performance Assessment for the Site Recommendation
USGS	U.S. Geological Survey
UTM	Universal Transverse Mercator
UZ	unsaturated zone
V	version
YMP	Yucca Mountain Project

1. PURPOSE

The purpose of this model report is to document the components of the site-scale saturated-zone flow model at Yucca Mountain, Nevada, in accordance with administrative procedure (AP)-SIII.10Q, *Models*. This report provides validation and confidence in the flow model that was developed for site recommendation (SR) and will be used to provide flow fields in support of the Total Systems Performance Assessment (TSPA) for the License Application. The output from this report provides the flow model used in the *Site-Scale Saturated Zone Transport*, MDL-NBS-HS-000010 Rev 01 (BSC 2003 [162419]). The Site-Scale Saturated Zone Transport model then provides output to the SZ Transport Abstraction Model (BSC 2003 [164870]). In particular, the output from the SZ site-scale flow model is used to simulate the groundwater flow pathways and radionuclide transport to the accessible environment for use in the TSPA calculations.

Since the development and calibration of the saturated-zone flow model, more data have been gathered for use in model validation and confidence building, including new water-level data from Nye County wells, single- and multiple-well hydraulic testing data, and new hydrochemistry data. In addition, a new hydrogeologic framework model (HFM), which incorporates Nye County wells lithology, also provides geologic data for corroboration and confidence in the flow model.

The intended use of this work is to provide a flow model that generates flow fields to simulate radionuclide transport in saturated porous rock and alluvium under natural or forced gradient flow conditions. The flow model simulations are completed using the three-dimensional (3-D), finite-element, flow, heat, and transport computer code, FEHM Version (V) 2.20 (software tracking number (STN): 10086-2.20-00; LANL 2003 [161725]). Concurrently, process-level transport model and methodology for calculating radionuclide transport in the saturated zone at Yucca Mountain using FEHM V 2.20 are being carried out in the model report, *Site-Scale Saturated Zone Transport*, MDL-NBS-HS-000010 Rev 01 (BSC 2003 [162419]). The velocity fields are calculated by the flow model, described herein, independent of the transport processes, and are then used as inputs to the transport model. Justification for this abstraction is presented in the model report, *Saturated Zone Flow and Transport Model Abstraction*, MDL-NBS-HS-000021 (BSC 2003 [164870]).

This model report is governed by the Office of Civilian Radioactive Waste Management (OCRWM) *Technical Work Plan For: Saturated Zone Flow and Transport Modeling and Testing*, TWP-NBS-MD-000002 Rev 01 (BSC 2003 [163965], Section 2.2), Work Package ASZM04. All activities listed in the TWP that are appropriate to the flow model are documented in this report.

This report supercedes previous reports of the MDL-NBS-HS-000011 series (i.e., BSC 2001 [155974] controlled version, CRWMS M&O 2000 [139582] historical version) in that there is a more extensive validation section, a presentation of alternate conceptual models (ACMs), and a more rigorous treatment of all assumptions.

Model-validation activities presented in this report lead to increased confidence that the model is a reasonable representation of groundwater flow likely to occur at Yucca Mountain in the vicinity of the repository site. Comparisons are presented between:

- Predicted and observed heads.
- Hydraulic properties obtained from model calibrations and those obtained from hydraulic field and laboratory testing.
- Groundwater temperature data predicted by the model to those measured in wells.
- Fluid path lines obtained from the model with those inferred from analysis of field hydrochemistry and isotopic data.

Alternate conceptual models and the implications of these models for flow field, flow paths, and transport times predictions are evaluated relative to the base-case model. A number of relevant features, events, and processes (FEPs) are included in this report (Section 6.2). The rationale for their inclusion and their dispositions are described as well. The excluded FEPs are discussed in an upcoming revision to the report, *Features, Events, and Processes in SZ Flow and Transport*, ANL-NBS-MD-000002 (BSC 2003 [163128]).

Uncertainty inherent in the input parameters is discussed in Section 4, and, as appropriate, propagated in Section 8. Uncertainty inherent to conceptualization and modeling is discussed in Section 6 and propagated, if necessary, in Section 8.

When using the SZ site-scale flow model for TSPA calculations, there are limitations that must be noted in regard to the following: changes to input parameter values, useable path-line distances, and overall model recharge fluxes. These are discussed more fully in Section 8.

(Note: In this report, the six-digit numerical identifier in brackets next to each reference callout is the Yucca Mountain Project's (YMP) Document Input Reference System [DIRS] number, the purpose of which is to assist the reader in locating a specific reference in the DIRS database).

Important technical issues addressed by this model report, and the sections in which they are discussed, include

- Horizontal and vertical anisotropy, reasonable range for uncertainty (Sections 6.4.3 and 8.3.2)
- Updated potentiometric data (Section 6.4.4)
- Alternative conceptual flow model for Solitario Canyon fault (Section 6.7.2)
- Validation for SZ site-scale model (Section 7)
- Comparison of fluxes with those of the Death Valley Regional Flow Model (Section 6.6.2.2)
- Modeling objectives: (1) reflect the current understanding of the SZ flow, (2) enhance model validation and uncertainty analyses, and (3) incorporate new data collected since the TSPA-SR (Section 6.1)

2. QUALITY ASSURANCE

Development of this model report and the supporting modeling activities have been determined to be subject to the OCRWM quality assurance (QA) program (BSC 2003 [163965], Section 8, Work Package ASZM03). Approved QA procedures identified in the technical work plan (BSC 2003 [163965], Section 4) have been used to conduct and document the activities described in this model report. The technical work plan also identifies the methods used to control the electronic management of data (BSC 2003 [163965], Section 8).

This model report provides calibrated values for hydrologic properties of the saturated zone natural barrier, which is important to the demonstration of compliance with the post-closure performance objectives prescribed in 10 CFR 63.113. Therefore, the saturated zone is classified as "Quality Level – 1" with regard to importance to waste isolation, as defined in AP-2.22Q, *Classification Analyses and Maintenance of the Q-List*. This report contributes to the analysis and modeling data used to support performance assessment; the conclusions do not directly impact engineered features important to safety, as defined in AP-2.22Q.

No variation from the TWP (BSC 2003 [163965]) was required to complete this work.

INTENTIONALLY LEFT BLANK

3. USE OF SOFTWARE

3.1 SOFTWARE TRACKED BY CONFIGURATION MANAGEMENT

The computer codes used directly in the SZ flow model are summarized in Table 1. The qualification status of the software is indicated in the Software Configuration Management (SCM) database. All software was obtained from SCM and is appropriate for the application. Qualified codes were used only within the range of validation as required by AP-SI.1Q, *Software Management.*

Table 1. Computer Codes Used in the Site-Scale Saturated-Zone Flow Model

Software Name and Version (V)	Software Tracking Number (STN)	Description	Computer Type, Platform, and Location	Date Baselined
FEHM V 2.20 LANL (2003 [161725])	10086-2.20-00	Flow modeling / flow and transport modeling (particle tracking)	Sun Ultra Sparc with Sun Solaris 5.7 or 5.8 operating system at the Los Alamos National Laboratory (LANL)	1/28/03
LaGriT V 1.0 LANL (2001 [149148])	10212-1.0-00	Software package for grid generation, analysis, and visualization.	Sun Ultra Sparc with Sun Solaris 5.7 or 5.8 operating system at LANL	8/8/01
NETPATH V 2.13 LANL (2001 [149910])	10303-2.13-00	Groundwater age correction for figures in document	PC with Windows DOS operating system at LANL	8/8/01
PEST V 5.5 Watermark Computing (2002 [161564])	10289-5.5-00	Pre-conditioning and parameter optimization for FEHM (LANL 2003 [161725]) runs	Sun Ultra Sparc with Sun Solaris 5.7 or 5.8 operating system at LANL	12/3/02
* prepare_ features_for_ surfer V 1.0	11091-1.0-00	Post-processor to write visualization for Surfer	Sun Ultra Sparc with Sun Solaris 5.7 or 5.8 operating system at LANL	1/23/03
STRAT2AVS V 1.0 LANL (2003 [163069])	11028-1.0-00	Pre-processor used to extract hydrogeologic surface data from the USGS Hydrogeologic Framework Model.	SGI with Irix64 operating system at LANL	3/3/03
*READPATHS _3D V 1.0 LANL (2000 [150459])	11089-1.0-00	Post-processor for FEHM (LANL 2003 [161725]) to view flow lines	Sun Ultra Sparc with Sun Solaris 5.7 or 5.8 operating system at LANL	6/23/03
* write_temps V 1.0	11090-1.0-00	Pre-processor for FEHM (LANL 2003 [161725]) to adjust viscosity values	Sun Ultra Sparc with Sun Solaris 5.7 or 5.8 operating system at LANL	6/27/03

Table 1. Computer Codes Used in the Site-Scale Saturated-Zone Flow Model (Continued)

Software Name and Version (V)	Software Tracking Number (STN)	Description	Computer Type, Platform, and Location	Date Baselined
Extract V 1.0 SNL (2002 [163070])	10955-1.0-00	Pre/post-processor used to extract lateral flow data from the USGS 1999 regional flow model	Sun UltraSPARC - SunOS 5.7 operating system at the Sandia National Laboratories (SNL)	12/11/02
Extract V 1.1 SNL (2002 163071])	10955-1.1-00	Pre/post-processor used to extract lateral flow data from the USGS 2001 regional flow model	Sun UltraSPARC - SunOS 5.7 operating system at SNL	12/11/02
Ext_Rech V 1.0 SNL (2002 [163072])	10958-1.0-00	Pre/post-processor used to extract recharge data from the USGS 2001 regional flow model	Sun UltraSPARC - SunOS 5.7 operating system at SNL	12/11/02
Mult_Rech V 1.0 SNL (2002 [163073])	10959-1.0-00	Pre/post-processor that scales recharge data from the USGS 2001 regional flow model and maps the data to a new grid	Sun UltraSPARC - SunOS 5.7, Solaris 2.7 operating system at SNL	12/18/02
WTCONVYD V 1.00 SNL (2002 [163835])	10815-1.00-00	Used to calculate the estimated elevation of the water table for wetter climatic conditions	Sun, PC with Windows 98 at SNL	7/15/02
Xread_Distr_Rech V 1.0 SNL (2002 [163074])	10960-1.0-00	Pre/post-processor used to extract recharge data from the USGS 1999 regional flow model	Sun UltraSPARC - SunOS 5.7 operating system at SNL	12/11/02
Xread_Distr_Rech_-UZ V 1.0 SNL (2002 [163075])	10961-1.0-00	Pre/post-processor that maps recharge data onto a new grid excluding the unsaturated zone (UZ) flow model region	Sun UltraSPARC - SunOS 5.7 operating system at SNL	12/11/02
Xread_ Reaches V 1.0 SNL (2002 [163076])	10962-1.0-00	Pre/post-processor that maps local recharge from four stream channels onto a new grid	Sun UltraSPARC - SunOS 5.7 operating system at SNL	12/11/02
Xwrite_Flow_ New V 1.0-125 SNL (2002 [163077])	10963-1.0-125-00	Used both to map the combined UZ and SZ site-scale fluxes onto a 125-m grid and to create a flux file that is compatible with FEHM LANL 2003 [161725]) flow macros	Sun UltraSPARC - SunOS 5.7 operating system at SNL	12/11/02
Zones V 1.0 SNL (2002 [163078])	10957-1.0-00	Used to extract zonal designation data from the USGS 2001 regional flow model.	Sun UltraSPARC - SunOS 5.7 operating system at SNL	12/11/02

NOTE: * These routines are not used outside of this report.

3.1.1 Parameter Optimization

In this report, the parameter estimation (PEST) code V 5.5, (STN: 10289-5.5-00; Watermark Computing 2002 [161564]) is used to perform the parameter optimization for the hydrogeologic and feature permeabilities. The PEST code is based on the Levenberg-Marquardt (LM) algorithm.

3.1.2 Flow Modeling

The FEHM V 2.20 code (STN: 10086-2.20-00; LANL 2003 [161725]) is used to solve for a steady-state flow solution.

3.1.3 Particle Tracking

FEHM V 2.20 (STN: 10086-2.20-00; LANL 2003 [161725]) is used to determine the streamlines (particle tracks) with the steady-state flow solution (see Section 3.1.2). FEHM has two different particle-tracking routines. This study uses the *sptr* macro for particle tracking. The particle-tracking portion of FEHM has been verified in a related report (*Site-Scale Saturated Zone Transport*, MDL-NBS-HS-000010 (BSC 2003, Section 6.5.2 [162419])).

3.1.4 Grid Generation

The Los Alamos Grid Generation software package (LaGriT), V 1.0 (STN: 10212-1.0-00; LANL 2001 [149148]) is used for creation, analysis, and visualization of grids. LaGriT is a set of software macros that uses the Hydrogeologic Framework Model (HFM) data to create computational grids. The software macros translate the coordinate and attribute information into a form that is valid for finite-element heat and mass compilations (FEHM V 2.20, STN: 10086-2.20-00; LANL 2003 [161725]).

3.1.5 Framework Translation

The software STRAT2AVS V1.0 (STN: 11028-1.0-00; LANL 2003 [163069]) is used to read Stratamodel Geocellular Modeling (SGM) files representing a three-dimensional (3-D) Hydrogeologic Framework and then write ASCII surface files with *x,y,z* coordinate locations and quadrilateral element connectivity. These binary SGM files are both written and read by Stratamodel V 4.0 or above and represent the hydrogeologic framework for a model (HFM). This HFM provides the geologically defined internal geometry for flow and transport process models and can be converted into a mesh for use in groundwater flow and transport modeling codes.

3.1.6 Corrections of Carbon-14 Ages in Field Data

NETPATH V 2.13 (STN: 10303-2.13-00; LANL 2001 [149910]) is a public-domain geochemical software, which was used in this report to correct carbon-14 ages for the effects of chemical reactions. The results of all calculations using NETPATH were checked with order-of-magnitude estimations.

3.2 EXEMPT SOFTWARE

The following commercially available, exempt software was used in the preparation of this report.

- EXCEL 98-SR-1 was used to pre-process data from the U.S. Geological Survey (USGS) traces for FEHM V 2.20 (STN: 10086-2.20-00; LANL 2003 [161725]) zone definitions. The calculation of basic statistics was used with standard functions only (see Attachment I for input, output, and formula used).

- SURFER for Windows, V6.03 was used for plotting and visualization of analysis results in figures shown in this report. The results were visually checked for correctness.

- TECPLOT, V7.5 was used for plotting and visualization of analysis results in figures shown in this report. The results were visually checked for correctness.

- FORTNER PLOT SUN Workstations V 1.3 was used in the visualization of this analysis and the documentation for plotting graphs.

- GMV and Adobe Illustrator V 10 were used to visualize and illustrate the computational mesh and related data.

4. INPUTS

4.1 DATA, PARAMETERS, AND OTHER MODEL INPUTS

Input information used in this model report comes from several sources, which, along with their data tracking numbers (DTNs), are summarized in Table 2. The data referenced in Table 2 contain information necessary to construct the numerical model, set boundary conditions, calibrate the model, and check the calibration. The data are fully appropriate for the site-scale saturated zone flow model. The qualification status of the input sources is provided in the TDMS and listed in the DIRS database.

Table 2. Input Data Sources

Data Set	Data Description	Data Tracking Number	Source
Water level and heads	Water level and head distributions	GS000508312332.001 [149947]	USGS (2001 [154625])
Stratamodel Framework files	Hydrogeologic Framework Model (HFM) for SZ site-scale flow and transport model, containing unit surfaces	GS030208312332.001 [163087]	USGS 2001 [158608]
Recharge map and lateral fluxes	Distribution of recharge flux and lateral fluxes	SN9908T0581999.001 [132867]	CRWMS M&O (1999, [130979], Section 4)
Geologic features	Feature and fault distributions	GS010908314221.001 [162874] TBV #5396	Potter et al. 2001 [159398]
Temperature profiles in wells	Plots of temperature profiles in wells	MO0102DQRBTEMP.001 [154733]	Sass et al. (1988 [100644], Figures 4 to 8, Figure 10)

The data listed in Table 2 are direct model inputs, after appropriate manipulation by the software listed in Table 1, with the exception of the lateral fluxes, which are described below. The water-level data in Table 2 have been updated with the addition of new wells in DTN: GS010908312332.002 [163555] and do not affect model input or results. Wherever possible, the most recent DTN is used for tables referencing data (see Section 6.6.2.1 for further discussion on water levels). This document may be affected by technical product input information that requires confirmation. Any changes to the document that may occur as a result of completing the confirmation activities will be reflected in subsequent revisions. The status of the input information may be confirmed by review of the TDMS.

<u>Boundary Fluxes</u>

The SZ site-scale flow model uses the same recharge as the 1997 Death Valley Regional Flow System (DVRFS) model (D'Agnese et al. 1997 [100131]) in the area represented by the site scale model. These recharge data are included in the DTN SN9908T0581999.001 [132867]. The lateral boundary fluxes from the DVRFS were used in the calibration of the saturated zone (SZ) site-scale flow model. Lateral boundary fluxes play an important role in the SZ site-scale flow model. These fluxes provide the communication with the DVRFS model, which is based on a regional mass balance and calibrated to spring flow data. There are differences between the

SZ site-scale flow model and the regional model largely due to the HFMs used for the two models. These differences are exacerbated because the two models also used different grid resolutions and methods to simulate hydrogeology. These facts made it necessary to average the fluxes over many grid blocks on each side of the model. The link between the two models is through the calibration code PEST V 5.5 (STN: 10289-5.5-00; Watermark Computing 2002 [161564]). (Watermark Computing is not a direct input but is cited here as the reference to the PEST code). Averaged fluxes derived from the DVRFS model are used for calibration targets in the SZ site-scale flow model calibration process in much the same way water levels are used for targets. (The DVRFS is not a direct input but is cited as the reference for the DTN for recharge and lateral fluxes in Table 2). These targets are weighted differently based on the importance of a given average flux to the SZ site-scale flow model. Because of the differences in the two models, only general agreement regarding fluxes is expected, and obtained, between the two models.

The bottom boundary condition of the SZ site-scale flow model is "no-flow." This is consistent with the DVRFS model. The top boundary condition is the specified flux recharge map described in Section 6.3.2.7.

4.2 CRITERIA

The general requirements to be satisfied by the TSPA are stated in 10 CFR 63.114 [156605]. Technical requirements to be satisfied by the TSPA are identified in the *Project Requirements Document* (Canori and Leitner 2003 [161770]). The acceptance criteria that will be used by the Nuclear Regulatory Commission (NRC) to determine whether the technical requirements have been met are identified in the *Yucca Mountain Review Plan* (YMRP; NRC 2003 [163274]). The pertinent requirements and criteria for this report are summarized in Table 3.

Table 3. Project Requirements and YMRP Acceptance Criteria Applicable to This Model Report

Requirement Number[a]	Requirement Title[a]	10 CFR 63 Link	YMRP Acceptance Criteria[b]
PRD-002/T-014	Performance Objectives for the Geologic Repository After Permanent Closure	10 CFR 63.113	2.2.1.1.3, criteria 1 to 2
PRD-002/T-015	Requirements for Performance Assessment	10 CFR 63.114	2.2.1.3.8.3, criteria 1 to 3
PRD-002/T-016	Requirements for Multiple Barriers	10 CFR 63.115	2.2.1.1.3, criteria 1 to 2

NOTE: [a] from Canori and Leitner (2003 [161770]).
[b] from NRC (2003 [163274]).

The acceptance criteria identified in Sections 2.2.1.1.3 and 2.2.1.3.8.3 of the YMRP (NRC 2003 [163274] are given below, followed by a short description of their applicability to this model report.

Section 2.2.1.1.3 *Acceptance Criteria* [for 2.2.1.1 *System Description and Demonstration of Multiple Barriers*], which are based on meeting the requirements of 10 CFR 63.113 [156605] (a) and 63.115(a)–(c):

- Acceptance Criterion 1, Identification of Barriers is Adequate:

  Barriers relied on to achieve compliance with 10 CFR 63.113 [156605] (b), as demonstrated in the total system performance assessment, are adequately identified, and are clearly linked to their capability. The barriers identified include at least one from the natural system. This model report describes the saturated-zone flow system part of the natural system.

- Acceptance Criterion 2, Description of Barrier Capability to Isolate Waste is Acceptable:

  The capability of the identified barriers to prevent or substantially delay the movement of water or radioactive materials is adequately identified and described:

  1. The information on the time period over which each barrier performs its intended function, including any changes during the compliance period, is provided. This model report uses water-level data for the development of the model. Other data, including water-level data and hydrochemical data, are used for validation and confidence building. Hydrochemical data integrate the behavior of the system over a long period of time and provide indication of how the system will behave during the compliance period.
  2. The uncertainty associated with barrier capabilities is adequately described in Sections 6.8 and 6.9 of this report.

Section 2.2.1.3.8.3 *Acceptance Criteria* [for 2.2.1.3.8 *Flow Paths in the Saturated Zone*], which are based on meeting the requirements of 10 CFR 63.114 [156605] (a)–(c) and (e)–(g), relating to flow paths in the saturated zone model abstraction:

- Acceptance Criterion 1, System Description and Model Integration are Adequate:

  1. The description of the aspects of hydrology, geology, geochemistry, design features, physical phenomena, and couplings, that may affect flow paths in the saturated zone, is adequate. In particular, the hydrology and geology are described in Section 6 of this report. The geochemistry is summarized in Section 7 and described in detail in the scientific analysis report, *Geochemical and Isotopic Constraints on Groundwater Flow Directions and Magnitudes, Mixing, and Recharge at Yucca Mountain* (BSC 2003 [162657]). Conditions and assumptions in the abstraction of flow paths in the saturated zone are readily identified in Sections 5, 6, 7, and 8, and are consistent with the body of data presented in the description.
  2. The abstraction of flow paths in the saturated zone uses assumptions, technical bases, data, and models that are appropriate and consistent with other related DOE abstractions. The descriptions and technical bases listed in Sections 6, 7, and 8 provide transparent and traceable support for the abstraction of flow paths in the saturated zone.
  3. Flow paths in the saturated zone are adequately delineated, considering natural site conditions. This delineation is documented in Section 7.
  4. Potential geothermal and seismic effects on the ambient saturated zone flow system

are adequately described and accounted for. Geothermal effects as they affect viscosity and hydraulic conductivity are described in Section 6.

- Acceptance Criterion 2, Data are Sufficient for Model Justification:

  1. Geological, hydrological, and geochemical values used in the safety case to evaluate flow paths in the saturated zone are adequately justified and documented in Sections 6, 7, and 8. Adequate descriptions of how the data were used, interpreted, and appropriately synthesized into the parameters are provided in Sections 4, 6, 7, and 8.
  2. Sufficient data have been collected on the natural system to establish initial and boundary conditions for the abstraction of flow paths in the saturated zone. Data are described in Sections 4 and 6.
  3. Data on the geology, hydrology, and geochemistry of the saturated zone used in the total system performance assessment abstraction are based on appropriate techniques and described in this model report and in other saturated-zone reports: *Saturated Zone In-Situ Testing*, (BSC 2003 [162415]), *Geochemical and Isotopic Constraints on Groundwater Flow Directions and Magnitudes, Mixing, and Recharge at Yucca Mountain* (BSC 2003 [162657]), *Hydrogeologic Framework Model for the Saturated Zone* (USGS 2001 [158608], Section 4), *Site-Scale Flow and Transport Model* (BSC 2003, Section 6.3 [162419]), and *Water-Level Data Analysis for the Saturated Zone Site-Scale Flow and Transport Model* (USGS 2001 [157611]).
  4. Sufficient information is provided to substantiate that the proposed mathematical groundwater modeling approach and proposed model(s) are calibrated and applicable to site conditions as described in Sections 6 and 7.

- Acceptance Criterion 3, Data Uncertainty is Characterized and Propagated Through the Model Abstraction:

  1. Models use parameter values, assumed ranges, and/or bounding assumptions that are technically defensible and reasonably account for uncertainties and variabilities (see Sections 5 and 6.4.5).
  2. Where sufficient data do not exist, the definition of parameter values and conceptual models is based on appropriate use of expert elicitation, conducted in accordance with NUREG-1563 (Kotra et al. 1996 [100909]) (see Sections 5, 8.3.1, and 8.3.2).
  3. Uncertainty is adequately represented in parameter development for conceptual models, process-level models, and alternative conceptual models considered in developing the abstraction of flow paths in the saturated zone as described in Sections 6 and 7 of this report.

4.3 CODES AND STANDARDS

No industrial or technical codes or standards other than those discussed in Section 4.2 apply directly to the modeling activity described in this report.

5. ASSUMPTIONS

A list of the assumptions used in this model report is provided in Table 4. Subsections where assumptions are used are identified in the table. The rationale and confirmation status for each status is also provided. The upstream assumptions associated with the rational below do not impact the results of the model.

Table 4. Assumptions

Number	Assumption	Rationale	Confirmation Status	Location in this Report
1	It is assumed that a steady-state model is sufficient for calibration purposes and the intended uses of the SZ flow model. There are two potential causes of transient flow that are relevant to this assumption: (1) changes in climate over the past 15 thousand years, and (2) pumping from wells south of the model domain during approximately the last 40 years. Use of the steady-state assumption requires that the modern-day flow system has had sufficient time to completely equilibrate to both of these perturbations to the natural system. It is noted that transient tests (C-wells and ATC) were performed and that derived permeability values from those tests were considered in the validation of the numerical model. It is not expected that the model can reproduce the transient tests, largely due to the 500-m grid blocks. Because transient pumping is not used in any Yucca Mountain radionuclide migration simulations and steady state gradients are modeled accurately with the model, this does not invalidate the steady-state assumption.	The conceptual model of the long-term groundwater flow in this region holds that recharge rates and, consequently, the elevation of the water table and groundwater flow rates were larger during the last glacial pluvial period. The time required for the flow system to equilibrate to a more arid climate depends mainly on the hydraulic conductivity of the rocks and the amount of water that must be drained from storage in order to lower the water table. It is likely that equilibration to the dryer climate has occurred given (1) the long time (thousands of years) since the climate change was completed, (2) the relatively small amount of water stored (small specific yield) in fractured volcanic rocks that make up much of the model domain near the water table, and (3) the relatively large hydraulic conductivity of the fractured volcanic rocks. The time required for the flow field to arrive at steady state with respect to pumping from wells is much shorter than the time required for equilibration to climate change. It depends mainly on the time required for changes in water level to be transmitted through the saturated zone. Fast transmittal is expected in fractured volcanic rocks because of their relatively large hydraulic conductivity and small specific storage. That the modern-day flow system has, in fact, equilibrated to pumping is supported by the lack of consistent, large-magnitude variations in water levels observed in wells near Yucca Mountain (Luckey et al. 1996, pp. 29 to 32 [100465]). A transient response to pumping would be expected, instead, to result in a continued decrease in water levels.	This assumption does not require confirmation for LA submittal.	Used through-out this report.

Table 4. Assumptions (Continued)

Number	Assumption	Rationale	Confirmation Status	Location in this Report
2	Particle tracking is a numerical technique that is acceptable for simulating the transport of fluid particles in the saturated zone at Yucca Mountain.	Particle-tracking techniques have a long history of use in such applications (e.g., Pollock 1988 [101466]; Tompson and Gelhar 1990 [101490]; Wen and Gomez-Hernandez 1996 [130510]), thereby justifying this assumption.	This assumption does not require confirmation for LA submittal.	Used through-out this report.
3	A horizontal to vertical anisotropy ratio of 10:1 is appropriate for most of the hydrogeologic units in the SZ flow model.	This assumption is justified by common usage and by the Yucca Mountain Expert Elicitation Panel (CRWMS M&O 1998 [100353], Table 3-2). The 10:1 ratio is the geometric mean of the 1:1 TO 100:1 range given by the experts	This assumption does not require confirmation for LA submittal.	Used through-out this report.
4	Anisotropy in the horizontal permeability field (north-south and east-west components) is sufficient to represent fracture sets at the sub-grid scale.	The use of just the principal values of permeability without cross terms is justified because this form of anisotropy is to represent the predominately north-south trending faults east of Yucca Mountain and west of Fortymile Wash (see Figure 4 in previous version of this model report for the location) (BSC 2001 [155974[). Because of the fault direction, they only enhance the N-S flow in that region.	This assumption does not require confirmation for LA submittal.	Used through-out this report.
5	The hydrogeologic properties for all units in the SZ flow model may be represented as homogeneous values.	The calibration process provides “best fit” parameters for the SZ model. Where appropriate, additional zones or parameters are supplied to represent spatial differences in hydrogeology. These zones are justified in the sections they are used. See , for example, Sections 6.5.3.1 and 6.5.3.4	This assumption can be confirmed against stochastic data when available.	Used through-out this report.

6. MODEL DISCUSSION

6.1 MODELING OBJECTIVES

The purpose of the site-scale SZ flow model is to describe the steady-state flow of groundwater as it moves from the water table below the repository, through the SZ, and to the accessible environment. The SZ advective processes that control the movement of groundwater and the movement of dissolved radionuclides and colloidal particles that might be present are described.

The current site-scale SZ flow model was developed in support of the upcoming TSPA-LA. The current model was built upon the model used for the TSPA-SR (CRWMS M&O 2000 [153246]) but includes a number of modifications to (1) reflect the current understanding of the SZ flow, (2) enhance model validation and uncertainty analyses, and (3) incorporate new data collected since the TSPA-SR. Changes introduced since the TSPA-SR iteration include the following.

- Use of field and laboratory tests (hydraulic and tracer data collected since TSPA-SR) to establish and confirm the conceptual model for flow, constrain model parameter calibration, and provide data for model validation.
- Use of thermal data for model validation.
- For validation purposes, use of recently collected hydraulic and geologic data that were obtained from the Nye County Early Warning Drilling Program (NC-EWDP).

This modeling analysis is a direct feed to the *Site-Scale Saturated Zone Transport*, MDL-NBS-HS-000010 Rev 01 (BSC 2003 [162419]) as it provides the saturated zone flow fields and specific discharge in transport calculations.

6.2 FEATURES, EVENTS, AND PROCESSES SUPPORTED BY THIS MODEL

The development of a comprehensive list of features, events, and processes (FEPs) potentially relevant to post-closure performance of the Yucca Mountain repository is an ongoing, iterative process based on site-specific information, design, and regulations. The approach for developing an initial list of FEPs in support of the TSPA-SR (CRWMS M&O 2000 [153246]) was documented in Freeze et al. (2001 [154365]). The initial FEPs list contained 328 FEPs, of which 176 were included in TSPA-SR models (CRWMS M&O 2000 [153246], Tables B-9 through B-17). To support the TSPA-LA, the FEPs list was re-evaluated in accordance with the Enhanced FEP Plan (BSC 2002 [158966], Section 3.2). The assignments of included FEPs to SZ reports for documentation are found in the *Technical Work Plan For: Saturated Zone Flow and Transport Modeling and Testing*, TWP-NBS-MD-000002 (BSC 2003 [163965]).

The included FEPs abstractions incorporated in the TSPA-LA model, which is implemented through specific process models or input parameters, are presented as TSPA-LA dispositions and are specifically addressed in saturated zone model reports (Table 5). The rationale for excluding a FEP from the TSPA-LA model will be given in the upcoming revision (REV 02) of *Features, Events, and Processes in SZ Flow and Transport* (BSC 2003 [163128]).

Table 5. Included FEPs for the Saturated Zone TSPA-LA

FEP Number	FEP Name	Responsible SZ Report
1.2.02.01.0A	Fractures	*SZ Flow and Transport Model Abstraction*, MDL-NBS-HS-000021 (BSC 2003 [164870])
1.2.02.02.0A	Faults	*SZ Flow and Transport Model Abstraction*, MDL-NBS-HS-000021 (BSC 2003 [164870])
1.4.07.02.0A	Wells	*SZ Flow and Transport Model Abstraction*, MDL-NBS-HS-000021 (BSC 2003 [164870])
2.2.03.01.0A	Stratigraphy	This report
2.2.03.02.0A	Rock Properties of Host Rock and Other Units	*SZ Flow and Transport Model Abstraction*, MDL-NBS-HS-000021 (BSC 2003 [164870])
2.2.07.12.0A	Saturated Groundwater Flow in the Geosphere	This report
2.2.07.13.0A	Water-Conducting Features in the SZ	*SZ Flow and Transport Model Abstraction*, MDL-NBS-HS-000021 (BSC 2003 [164870])
2.2.07.15.0A	Advection and Dispersion in the SZ	*Site-Scale Saturated Zone Transport*, (BSC 2003 [162419])
2.2.07.16.0A	Dilution of Radionuclides in Groundwater	*SZ Flow and Transport Model Abstraction*, MDL-NBS-HS-000021 (BSC 2003 [164870])
2.2.07.17.0A	Diffusion in the SZ	*Site-Scale Saturated Zone Transport*, (BSC 2003 [162419])
2.2.08.01.0A	Chemical Characteristics of Groundwater in the SZ	*Site-Scale Saturated Zone Transport*, (BSC 2003 [162419])
2.2.08.06.0A	Complexation in the SZ	*Site-Scale Saturated Zone Transport*, (BSC 2003 [162419])
2.2.08.08.0A	Matrix Diffusion in the SZ	*Site-Scale Saturated Zone Transport*, (BSC 2003 [162419])
2.2.08.09.0A	Sorption in the SZ	*Site-Scale Saturated Zone Transport*, (BSC 2003 [162419])
2.2.08.10.0A	Colloid Transport in the SZ	*SZ Flow and Transport Model Abstraction*, MDL-NBS-HS-000021 (BSC 2003 [164870])
2.2.08.11.0A	Groundwater Discharge to Surface Within the Reference Biosphere	*SZ Flow and Transport Model Abstraction*, MDL-NBS-HS-000021 (BSC 2003 [164870])
2.2.10.03.0A	Natural Geothermal Effects on Flow in the SZ	This report
2.2.12.00.0B	Undetected Features in the SZ	*SZ Flow and Transport Model Abstraction*, MDL-NBS-HS-000021 (BSC 2003 [164870])
3.1.01.01.0A	Radioactive Decay and Ingrowth	*SZ Flow and Transport Model Abstraction*, MDL-NBS-HS-000021 (BSC 2003 [164870])

Table 6 both lists the FEPs included in the TSPA-LA for which this model report provides the technical basis and provides a summary of their disposition in TSPA-LA. Table 7 lists the FEPs that are partially addressed by the results of this model report. These results are used elsewhere (as shown in Table 5) to determine the include/exclude status of the FEP and/or its implementation in the TSPA-LA.

Table 6. Saturated-Zone Included FEPs for Which This Model Report Provides the Technical Basis

FEP Number	FEP Name	Section Where Disposition is Described
2.2.03.01.0A	Stratigraphy	Sections 6.3, 6.5
TSPA-LA Disposition The stratigraphic (i.e., hydrogeologic) nature of the host rock as it affects flow and transport is incorporated into the TSPA-LA site scale flow and transport models (*Site-Scale Saturated Zone Flow Model* (BSC 2003 [162649]), *SZ Flow and Transport Model Abstractions* (BSC 2003 [164870]), and *Site-Scale Saturated Zone Transport* (BSC 2003 [162419]). The primary hydrogeologic subdivisions are based on and coincide with, 1) common permeability and porosity characteristics (on a regional scale) of the host rock, and 2) whether the host rock's primary mode of origin is volcanic, clastic, sedimentary (carbonates), or alluvial in nature (BSC 2003 [162649] Section 6.3.2, *Site-Scale Saturated Zone Flow Model*). The hydrogeologic subdivisions employed for the TSPA-LA are a synthesis of hydrogeologic framework model (HFM - USGS 2001 [158608]) and the calibrated *Site-Scale Saturated Zone Flow Model* (BSC 2003 [162649]). In all, there are 19 hydrogeologic units employed in the formulation of the base case SZ flow model (BSC 2003 [162649] Section 6.5.3.1, *Site-Scale Saturated Zone Flow Model*), *Site-Scale Saturated Zone Transport* (BSC 2003 [162419]), and SZ flow and transport abstraction (Section 6.3, *SZ Flow and Transport Model Abstraction*, BSC 2003 [164870]). These are listed below:The 19 hydrogeologic units can be grouped into five basic SZ hydrogeologic subdivisions, these are; the upper volcanic aquifer, upper volcanic confining unit, lower volcanic aquifer, lower volcanic confining unit, and lower carbonate aquifer (BSC 2003 [162649] Section 6.3.2, *Site-Scale Saturated Zone Flow Model*). In SZ base case flow model (BSC 2003 [162649] Sections 6.3.2 and 6.5.3.4, *Site-Scale Saturated Zone Flow Model*) major discontinuities between the 19 hydrostratigraphic units are implemented by including 17 discrete features. These features reflect degree of fracturing, faulting, fault orientation, and mineralogical alteration of glassy materials to zeolites and clay minerals. In the hydrogeologic units where flow and transport is expected to take place (Units 15 through Units 11 (BSC 2003 [162649] Section 6.6.2.2), variability in transport properties between the major hydrogeologic units is implemented using a range of sampled parameters assigned to each unit for a particular realization (Section 6.5.2, *SZ Flow and Transport Model Abstractions,* BSC 2003 [164870]). How the physical properties of stratigraphic units are modeled is discussed in the FEP, Rock Properties of Host Rock and Other Units (2.2.03.02.0A)		
2.2.07.12.0A	**Saturated Groundwater Flow in the Geosphere**	**Sections 6.3, 6.5**
TSPA-LA Disposition Steady-state, saturated, 3-D groundwater flow within the Yucca Mountain vicinity is modeled through the *Site Scale Saturated Zone Flow Model* (BSC 2003 [162649]) using the numerical code FEHM V 2.20 (LANL 2003 [161725], STN: 10086-2.20-00). The model domain is a 50-km^2 region within the confines of the Death Valley groundwater basin (BSC 2003 [162649] Section 6.3.2, *Site Scale Saturated Zone Flow Model*). Inputs include faults and fault zones (BSC 2003 [162649] Section 6.3.2.10, *Site Scale Saturated Zone Flow Model*) and variable permeabilities associated with the 19 hydrostratigraphic units (FEP 2.2.03.01.0A) identified through hydrogeologic framework model (HFM - USGS 2001 [158608]). The most significant flow units are the volcanic Crater Flat Tuff hydrogeologic units and the shallow alluvial aquifer of Fortymile Wash. Flow through fractures is modeled through an effective continuum flow model (BSC 2003 [162649] Section 6.3.3, *Site Scale Saturated Zone Flow Model*). Recharge is modeled through underflow, surface flow infiltration, and UZ infiltration components (BSC 2003 [162649] Section 6.3.2.7, *Site Scale Saturated Zone Flow Model*). The impact of future climate conditions on flow are modeled in the *SZ Flow and Transport Model Abstractions* (BSC 2003 [164870]) using a convolution integral method (SZ_Convolute V 2.2 software code (STN: 10207-2.2-00, SNL 2003 [163344]), and Section 6.5 *SZ Flow and Transport Model Abstractions* (BSC 2003 [164870]) which scales radionuclide breakthrough curve simulations representing current climate conditions using representative scaling factors (Section 6.5.1, *SZ Flow and Transport Model Abstractions,* BSC 2003 [164870]).		

Table 6. Saturated-Zone Included FEPs for Which This Model Report Provides the Technical Basis (Continued)

2.2.10.03.0A	Natural Geothermal Effects on Flow in the SZ	Section 7.3
TSPA-LA Disposition		
Natural geothermal effects, as it influences fluid properties, are implicitly included in the SZ site scale flow model. Groundwater flow is simulated in the *Site-Scale Saturated Zone Flow Model* (BSC 2003 [162649]) using a conservation of fluid-rock energy equation in the numerical code FEHM V 2.20 (STN: 10086-2.20-00, LANL 2003 [161725]). The fluid-rock energy equation is, in part, a function of permeability, density, viscosity, and temperature (Section 6.5.3, *Site-Scale Saturated Zone Flow Model* (BSC 2003 [162649]). For temperatures that range between 20° C to 100° C the density of water changes by only a few percent. The variation in water viscosity changes by a factor of 3.3 over the temperature range. Consequently, natural geothermal effects on groundwater flow are more effectively captured by spatially varying viscosity rather than density. The *Site-Scale Saturated Zone Flow Model* (BSC 2003 [162649]) assigns a specified temperature to each node, which varies with depth and is based on variable temperature measurements reported in Sass et al. (1988) [100644]. Permeability and viscosity are also assigned to each node. Temperatures are used to calculate nodal viscosities. Using the spatially varying viscosity, a fluid property, allows the calibration of intrinsic permeability, a lumped rock property parameter. Estimated intrinsic permeability at each node is calibrated to hydraulic head measurements, while nodal viscosities and temperatures remain fixed (Section 6.5.3.7, *Site-Scale Saturated Zone Flow Model,* (BSC 2003 [162649]). Hydraulic heads are, in part, manifestations of multiple processes within the system, including geothermal effects. By calibrating intrinsic permeability to hydraulic heads and keeping spatially varying temperature and viscosity fixed, geothermal effects on flow are implicitly captured. Additionally, the *Site-Scale Saturated Zone Flow Model* (BSC 2003 {162649]) performed a set of heat transport and flow simulations using measured temperature values in the SZ (Section 7.4, BSC 2003 [162649]). The results of the coupled thermal modeling provide a general independent validation of the SZ site-scale flow model, and validate the implicit modeling of geothermal effects in SZ flow.		

Table 7 lists the FEPs that are supported by the results of this model report. Table 7 also lists the reports in which the TSPA dispositions are located.

Table 7. Saturated-Zone Included FEPs Supported by the Results in This Model Report

FEP Number and Name	FEP Description	Report in Which TSPA Disposition is Located
1.2.02.01.0A Fractures	Groundwater flow in the Yucca Mountain region and transport of any released radionuclides may take place along fractures. The rate of flow and the extent of transport in fractures are influenced by characteristics such as orientation, aperture, asperity, fracture length, connectivity, and the nature of any linings or infills.	*SZ Flow and Transport Model Abstraction*, MDL-NBS-HS-000021 (BSC 2003, [164870])
1.2.02.02.0A Faults	Numerous faults of various sizes have been noted in the Yucca Mountain Region and in the repository area in specific. Faults may represent an alteration of the rock permeability and continuity of the rock mass, alteration or short-circuiting of the flow paths and flow distributions close to the repository, and represent unexpected pathways through the repository.	*SZ Flow and Transport Model Abstraction*, MDL-NBS-HS-000021 (BSC 2003, [164870])
1.4.07.02.0A Wells	One or more wells drilled for human use (e.g., drinking water, bathing) or agricultural use (e.g., irrigation, animal watering) may intersect the contaminant plume.	*SZ Flow and Transport Model Abstraction*, MDL-NBS-HS-000021 (BSC 2003, [164870]).
2.2.03.02.0A Rock Properties of Host Rock and Other Units	Physical properties such as porosity and permeability of the relevant rock units, soils, and alluvium are necessary for the performance assessment. Possible heterogeneities in these properties should be considered. Questions concerning events and processes that may cause these physical properties to change over time are considered in other FEPs	*SZ Flow and Transport Model Abstraction*, MDL-NBS-HS-000021 (BSC 2003, [164870]).
2.2.07.13.0A Water-Conducting Features in the SZ	Geologic features in the saturated zone may affect groundwater flow by providing preferred pathways for flow.	*SZ Flow and Transport Model Abstraction*, MDL-NBS-HS-000021 (BSC 2003, [164870]).
2.2.07.15.0A Advection and Dispersion in the SZ	Advection and dispersion processes affect contaminant transport in the SZ.	*Site-Scale Saturated Zone Transport*, MDL-NBS-HS-000010 (BSC 2003 [162419]).
2.2.08.01.0A Chemical Characteristics of Groundwater in the SZ	Chemistry and other characteristics of groundwater in the saturated zone may affect groundwater flow and radionuclide transport of dissolved and colloidal species. Groundwater chemistry and other characteristics, including temperature, pH, Eh, ionic strength, and major ionic concentrations, may vary spatially throughout the system as a result of different rock mineralogy.	*Site-Scale Saturated Zone Transport*, MDL-NBS-HS-000010 (BSC 2003 [162419]).

6.3 BASE-CASE CONCEPTUAL MODEL

The base-case model presented in this section describes our current state of knowledge of the saturated flow system. The general conceptual model of SZ flow in the site-scale SZ flow model area is that groundwater flows southerly from recharge areas of higher precipitation at higher elevations north of Yucca Mountain, through the Fortymile Wash and toward the Amargosa Desert. Within the site-scale model area, recharge occurs from infiltration of both precipitation and flood-flows from Fortymile Wash and its tributaries. In the southeastern part of the model area (within the Ash Meadows groundwater basin), considerable flows enter and exit the area in the lower Carbonate Aquifer system (CRWMS M&O 1999, Section 6.2 [130979]). This aquifer

system is believed to underlie much of the Alkali Flat-Furnace Creek groundwater basin based on inferences from Death Valley regional groundwater flow data as explained below. However, the flow patterns of groundwater in this area and their relationship to flow in the Ash Meadows flow system are poorly understood. Outflow from the SZ site-scale flow model area mostly occurs across the southern boundary of the model. The boundary conditions on the southern boundary include discharge by irrigation wells in the Amargosa Farms area.

Within the boundaries of the site-scale flow model area, there are several components that strongly affect the local flow system and potential radionuclide transport.

- The Solitario Canyon Fault
- Recharge on Yucca Mountain
- The Crater Flat Tuff hydrogeologic units
- The shallow alluvial aquifer of Fortymile Wash
- The regional Carbonate Aquifer.

The Solitario Canyon Fault is important because it provides a fast vertical flow path from the surface to the saturated zone. It also can provide a barrier for water flowing laterally under Yucca Mountain that originated in Crater Flat. Recharge to the saturated zone is important because the travel time of potential radionuclides is directly dependent on it. The Crater Flat Tuffs, particularly the Bullfrog unit, are likely to be the most permeable hydrogeologic units near the repository and, thus, are most-likely paths for potential radionuclide transport. The shallow alluvial aquifer in Fortymile Wash is important because it both contains the likely flow paths for fluid leaving the repository area and has desirable retardation characteristics for many radionuclides. The regional Carbonate Aquifer underlies the likely flow area for fluid leaving the repository area. This aquifer also provides an upward gradient that keeps the flow lines shallow and, effectively, isolates the local Yucca Mountain system from the regional aquifer.

6.3.1 FEPs Supported by the Base-Case Model

This model report provides the technical basis for three FEPs (Table 6). Following is a listing of these FEPs, their descriptions, and discussion regarding their dispositions in the TSPA-LA.

- 2.2.03.01.0A (Stratigraphy)

FEP Description:

Stratigraphic information is necessary for the performance assessment. This information should include identification of the relevant rock units, soils and alluvium, their thicknesses, lateral extents, and relationships to each other. Major discontinuities should be identified.

FEP Disposition in the TSPA:

The stratigraphic (i.e., hydrostratigraphic) nature of the host rock as it affects flow and transport is incorporated into the TSPA-LA site-scale flow and transport models, which are presented in this model report and in two other model reports in preparation: *Site-Scale Saturated Zone Transport*, MDL-NBS-HS-00010 (BSC 2003, Sections 6.3 and 6.4 [162419]), and *SZ Flow and Transport Model Abstractions*, MDL-NBS-HS-000021 (BSC 2003 [164870]). The primary hydrostratigraphic subdivisions are based on and coincide with: (1) common permeability and porosity characteristics (on a regional scale) of the host rock, and (2) the host rock's primary mode of origin (i.e., volcanic, clastic, sedimentary (carbonates), or alluvial in nature (Section 6.3.2).

The hydrostratigraphic subdivisions employed for the TSPA-LA are a synthesis of the hydrogeologic framework model (HFM) (USGS 2001 [158608]) and the calibrated SZ flow model described in the previous version of this report (BSC 2001 [155974]). There are 19 hydrostratigraphic units employed in the formulation of the base-case SZ flow model (Section 6.5.3.1), the site-scale SZ transport model, and the SZ flow and transport abstraction (Section 6.3). These units are listed below and described in detail in Section 6.5.3.

> *Unit 20* - Alluvium, *Unit 19* - Valley-Fill Confining Unit, *Unit 18* - Limestones, *Unit 17* - Lava Flows, *Unit 16* - Upper Volcanic Aquifer, *Unit 15* - Upper Volcanic Confining Unit, *Unit 14* - Crater Flat-Prow Pass, *Unit 13* – Crater Flat-Bullfrog, *Unit 12* – Crater Flat-Tram, *Unit 11* - Lower Volcanic Confining Unit, *Unit 10* - Older Volcanic Aquifer, *Unit 9* - Undifferentiated Valley Fill, *Unit 8* – Upper Carbonate Aquifer, *Unit 7* – Lower Carbonate Aquifer, *Unit 6* - Lower Carbonate Aquifer Thrust, *Unit 5* – Upper Clastic Confining Unit, *Unit 4* – Lower Carbonate Aquifer, *Unit 3* – Lower Clastic Confining Unit, *Unit 2* – Granites.

The 19 hydrogeologic units can be grouped into five basic SZ hydrostratigraphic subdivisions: the upper volcanic aquifer, upper volcanic confining unit, lower volcanic aquifer, lower volcanic confining unit, and lower Carbonate Aquifer (Section 6.3.2). Major discontinuities between the 19 hydrostratigraphic units are implemented by including 17 discrete features. These features reflect degree of fracturing, faulting, fault orientation, and mineralogical alteration of glassy materials to zeolites and clay minerals. In the hydrostratigraphic units where transport is expected to take place (Units 11 through Units 15), variability in transport properties between the major hydrostratigraphic units is implemented using a range of sampled parameters assigned to each unit for a particular realization (Section 6.5.2, *SZ Flow and Transport Model Abstractions*, MDL-NBS-HS-000021 (BSC 2003, [164870]).

The stratigraphic model, also known as the HFM (USGS 2001 [158608]), is used as a basis for building the numerical SZ flow model. The stratigraphic model must be represented accurately in the numerical model. Tests conducted to determine an adequate resolution (Bower et al. 2000 [149161]) have shown that the resolution used in the base-case model is sufficient to represent the stratigraphy accurately.

Uncertainty with respect to contact points for individual hydrostratigraphic units is discussed in Section 6.8.

- 2.2.07.12.0A (Saturated Groundwater Flow in the Geosphere)

FEP Description:

Groundwater flow in the saturated zone below the water table may affect long-term performance of the repository. The location, magnitude, and direction of flow under present and future conditions and the hydraulic properties of the rock are all relevant.

FEP Disposition in the TSPA:

Steady-state, saturated, 3-D groundwater flow within the Yucca Mountain vicinity is modeled as the main thrust of this report using the numerical code FEHM V 2.20 (STN: 10086-2.20-00; LANL 2003 [161725]). The model domain is a 1350-km^2 region within the confines of the Death Valley groundwater basin (Section 6.3.2). Inputs include faults and fault zones (Section 6.3.2.10) and variable permeabilities associated with the 19 hydrostratigraphic units (FEP 2.2.03.01.0A) identified through the HFM (USGS 2001 [158608]). The most significant flow units are the volcanic Crater Flat Tuff hydrogeologic units and the shallow alluvial aquifer of Fortymile Wash. Flow through fractures is modeled through an effective continuum flow model.

Recharge is modeled through underflow, surface flow infiltration, and UZ infiltration components (Section 6.3.2.7). Future climate simulation is discussed in 6.4.5 of this report. The impact of future climate conditions on flow and transport are modeled in the report *SZ Flow and Transport Model Abstractions*, MDL-NBS-HS-000021 (BSC 2003 [164870]), using a convolution integral method (SZ_Convolute V 2.2 software code (STN: 10207-2.2-00) Section 6.5), which scales radionuclide-breakthrough-curve simulations representing current climate conditions using representative scaling factors (Section 6.5.1 of BSC 2003 [164870]).

- 2.2.10.03.0A (Natural Geothermal Effects on Flow in the SZ).

FEP Description:

The existing geothermal gradient, and spatial or temporal variability in that gradient, may affect groundwater flow in the SZ.

FEP Disposition in the TSPA:

Natural geothermal effects, as they influence fluid properties, are included implicitly in the SZ site scale flow model. Groundwater flow is simulated in the flow model using a conservation of fluid-rock energy equation in the numerical code FEHM V 2.20 (STN: 10086-2.20-00; LANL 2003 [161725]). This equation is, in part, a function of permeability, density, viscosity, and temperature (Section 6.5.3). For temperatures that range between 20^oC to 100^oC, the density of water changes by only a few percent. The variation in water viscosity changes by a factor of 3.55 over the temperature range. Consequently, natural geothermal effects on groundwater flow are more effectively captured by spatially varying viscosity rather than by density. In this report, a specified temperature is assigned to each node, which varies with depth and is based on variable temperature measurements reported in Sass et al. (1988 [100644], Figures 4 to 8, 10). Permeability and viscosity are also assigned to each node. Temperatures are used to calculate nodal viscosities. Using the spatially varying viscosity, a fluid property, allows the calibration of

intrinsic permeability, a lumped rock property parameter. Estimated intrinsic permeability at each node is calibrated to hydraulic head measurements, while nodal viscosities and temperatures remain fixed (Section 6.5.3.7). Because hydraulic heads are, in part, manifestations of geothermal effects, calibrating intrinsic permeability to hydraulic heads, and keeping spatially varying temperature and viscosity fixed, geothermal effects on flow are implicitly captured.

6.3.2 Components of the Base-Case Conceptual Model

Yucca Mountain is located in the Great Basin about 150 km northwest of Las Vegas, Nevada. The mountain consists of a series of fault-bounded blocks of ash-flow and ash-fall tuffs and a smaller volume of lava deposited between 14 and 11 Ma (million years before present) from a series of calderas located a few to several tens of kilometers (km) to the north (Sawyer et al. 1994 [100075]). Yucca Mountain itself extends southward from the Pinnacles Ridge toward the Amargosa Desert, where the tuffs thin and pinch out beneath the alluvium (Figure 1). The tuffs dip 5 to 10 degrees to the east over most of Yucca Mountain. Crater Flat is west of Yucca Mountain and separated from it by Solitario Canyon, which is the surface expression of the Solitario Canyon Fault—a steeply dipping scissors fault with down-to-the-west displacement of as much as 500 meters (m) in southern Yucca Mountain (Day et al. 1998 [100027], pp. 6 to 7). Underlying Crater Flat is a thick sequence of alluvium, lavas, and tuffs that has been locally cut by faults and volcanic dikes. East of Yucca Mountain, and separated from it by Fortymile Wash, is Jackass Flats, which is underlain by a thick sequence of alluvium and volcanic rocks. Timber Mountain, approximately 25 km to the north of the repository area, is a resurgent dome within the larger caldera complex that erupted the tuffs at Yucca Mountain.

The central block of Yucca Mountain, into which waste would be emplaced if the site were licensed, is bounded by Drill Hole Wash on the north, the Solitario Canyon Fault on the west, the Bow Ridge fault on the east, and is dissected by the Ghost Dance and Dune Wash faults. Topography is highly variable and, north of the central block, is controlled by long, northwest-trending, fault-controlled washes. Within and south of the central block, washes are shorter and trend eastward. Topography in the southern part of Yucca Mountain is controlled by south-trending faults.

The boundaries of the numerical model for SZ flow and transport are shown in Figure 1. The hydrogeologic setting of the SZ flow system in the vicinity of Yucca Mountain was summarized by Luckey et al. (1996 [100465], p. 13). Yucca Mountain is part of the Alkali Flat-Furnace Creek sub-basin of the Death Valley groundwater basin, as described by Waddell (1982 101062], pp. 15 to 16). Discharge within the sub-basin occurs at Alkali Flat (Franklin Lake Playa) and, possibly, Furnace Creek in Death Valley (Figure 1). Water inputs to the sub-basin include groundwater inflow along the northern boundary of the sub-basin, recharge from precipitation in high-elevation areas of the sub-basin, and recharge from surface runoff in Fortymile Canyon and Fortymile Wash. North and northeast of Yucca Mountain, recharge from precipitation also probably occurs at Timber Mountain, Pahute Mesa, Rainier Mesa, and Shoshone Mountain (Luckey et al. 1996 [100465], p. 13).

.

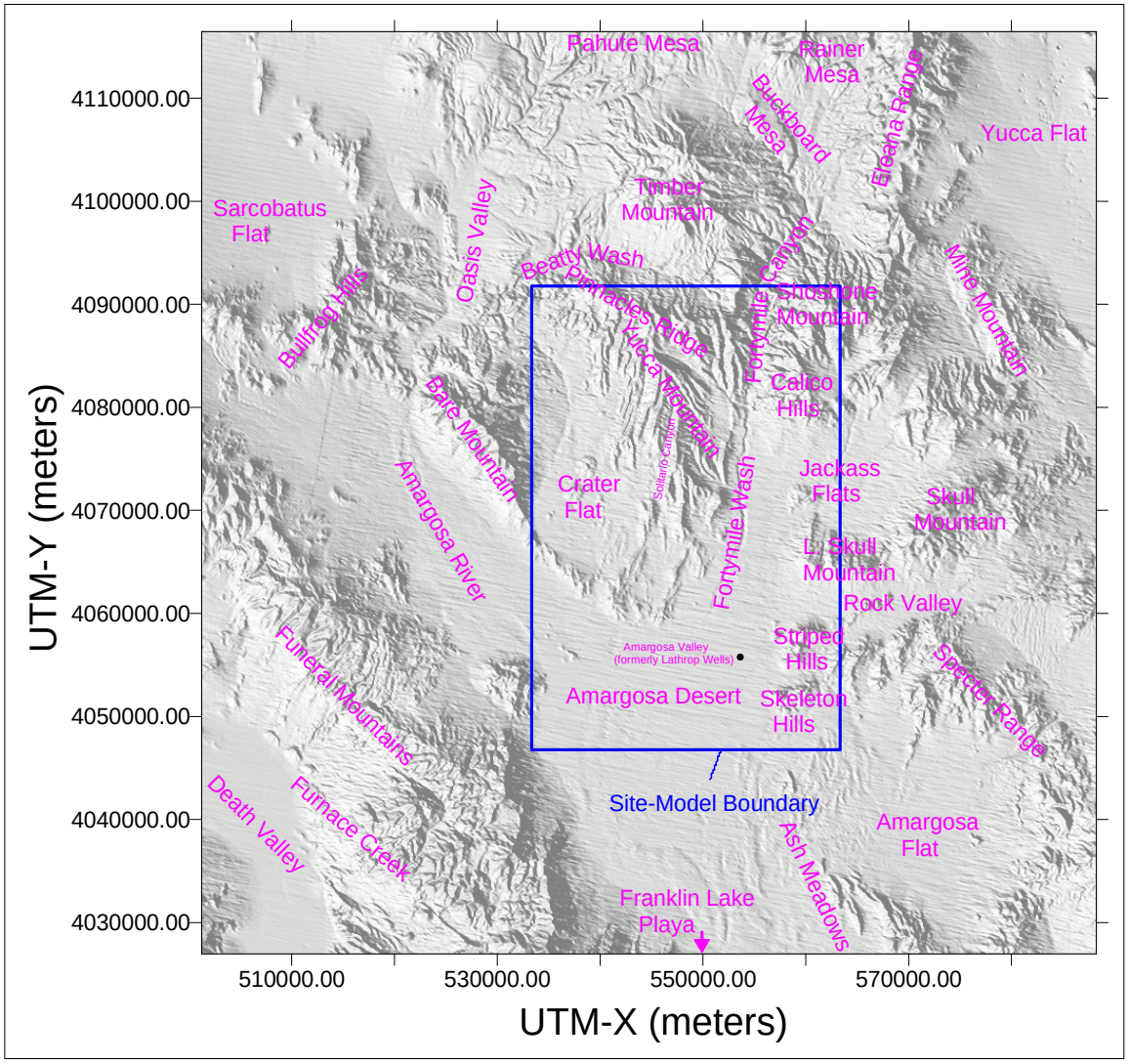

For illustration purposes only.

NOTE: The blue rectangle is the boundary of the numerical model for SZ flow and transport.

Figure 1. Important Physiographic Features Near Yucca Mountain Including Boundaries of the Site-Scale Saturated Zone Flow Model

6.3.2.1 Groundwater Occurrence and Flow

As described by Luckey et al. (1996 [100465], p. 17), the Tertiary volcanic section at Yucca Mountain consists of a series of ash-flow and bedded ash-fall tuffs that contain minor amounts of lava and flow breccia. Individual ash-flow tuffs may be several hundred meters thick, whereas bedded tuffs generally are less than a few tens of meters thick. Ash-flow tuffs range from nonwelded to densely welded, and the degree of welding varies both horizontally and vertically in a single flow unit. Nonwelded ash-flow tuffs, when unaltered, have moderate to low matrix permeability but high porosity. Permeability is decreased by secondary alteration, and fractures are infrequent and often closed in the low-strength nonwelded tuffs. Consequently, these rocks generally constitute laterally extensive SZ confining units in the Yucca Mountain area. The properties of partly welded tuffs vary between those of fractured, welded tuffs and those of altered, nonwelded tuffs. The densely welded tuffs generally have minimal primary porosity and water-storage capacity, but they can be highly fractured. Where interconnected, fractures can easily transmit water, and highly fractured units function as aquifers. In general, the bedded tuffs have high primary porosity and can store large amounts of water. Their matrix permeability is moderate to low, depending on the degree of alteration. The bedded tuffs generally function as confining units, at least when compared to less porous but densely fractured ash-flow tuffs. Lavas, flow breccias, and other minor rock types are neither thick nor widely distributed in the Yucca Mountain area. Their hydraulic properties probably are as variable as the properties of the ash-flow tuffs, but the relatively limited spatial distribution of these minor rock types makes them generally unimportant to the hydrology of Yucca Mountain.

As described by Luckey et al. (1996 [100465], p. 17), even fractured tuffs and lavas may not easily transmit water because lithostatic loading keeps the fractures closed. In addition, where volcanic glass has been partly replaced by zeolites and clays, particularly in the originally glassy nonwelded tuffs, these secondary minerals substantially decrease permeability and slow groundwater flow through the rock. The degree of alteration can affect the water-transmitting characteristics of the volcanic sequence. Alteration, particularly in the Calico Hills Formation, increases toward the north of Yucca Mountain and probably accounts for the apparent decrease in hydraulic conductivity to the north. Alteration also tends to increase with depth and is pervasive below the Calico Hills Formation.

Fractures vary in length, orientation, connectivity, aperture width, and amounts and types of coatings, all of which may affect the flow of water. The physical parameters of fractures are characterized by outcrop mapping, borehole logging, and mapping in the Exploratory Studies Facility; however, seeps of water have not been observed in outcrop mapping or in mapping in the Exploratory Studies Facility.

Fractures at Yucca Mountain originated as a result of initial cooling of the volcanic deposits and as a result of tectonic activity. For example, in the Tiva Canyon welded hydrologic unit, two sets of vertically orientated cooling fractures were observed dipping nearly vertically and striking towards the northwest and northeast. A third set of tectonic joints commonly abut the cooling joints, and these three sets of joints form an orthogonal, 3-D network. An extensive discussion of fractures in the Yucca Mountain area is presented in CRWMS M&O (1998 [100126], Section 3.6.3).

Fracture aperture characteristics are poorly known from direct observation, and for modeling, reliance is placed on indirect effects such as changes in air and water permeability. In general, the stress due to overburden loading across high-angle fractures will be less than across low-angle fractures, resulting in higher vertical than horizontal permeability. Stratification effects will also be present in many units. This will tend to have the opposite effect; that is, the horizontal permeability will be larger than the vertical permeability.

The volcanic rocks consist of alternating layers of welded and nonwelded ash-flow and ash-fall (bedded) tuff deposits. Each of the ash-flow units is underlain by an associated bedded-tuff layer. The ash-flow units vary in degree of welding (or recrystallization) with the maximum welding generally found near the center of the flow, where heat was retained the longest, and the degree of welding decreasing upward and downward toward the flow boundaries.

The welded units typically have low matrix porosities and high fracture densities, whereas the nonwelded and bedded tuffs have relatively higher matrix porosities and lower fracture densities. The fracture density is correlated with the degree of welding of the volcanic rocks.

Where glassy tuff has been saturated for long time periods (e.g., beneath the water table), the original glassy material generally has been altered to zeolite or clay minerals. Such alteration does not affect porosity greatly because it does not fill the pore spaces, but the permeability of the rocks is greatly reduced by alteration of the connections between the pore spaces. Alteration of silica to zeolites or clay minerals is not an important factor in densely welded zones because cooling fractures dominate permeability.

The saturated zone flow system to the south of Yucca Mountain transitions from a fractured tuff aquifer to a valley-fill (alluvium) aquifer before reaching the ~18-km performance compliance boundary at the southern boundary of the Nevada Test Site. Underlying Crater Flat is a thick sequence of alluvium, lavas, and tuffs that has been locally cut by faults and volcanic dikes. East of Yucca Mountain, and separated from it by Fortymile Wash, is Jackass Flats, which is underlain by a thick sequence of alluvium and volcanic rocks. Characterization of the valley-fill system was conducted just outside the southwest corner of NTS at the Alluvial Testing Complex (ATC), which is the site of the Nye County Early Warning Drilling Program (NC-EWDP) well 19D/D1. Single-well hydraulic and tracer tests were conducted in NC-EWDP-19D/D1 in FY 2001. These tests indicated producing zones with permeabilities consistent with other alluvial systems ($1\text{-}10 \cdot 10^{-12}$ m^2) interbedded with lower permeability (10^{-15} m^2) clay-rich zones. These Nye County well locations are shown in Figure 34.

In addition to flow within the volcanic rocks and alluvial material, groundwater also flows in the carbonate rocks of the lower Carbonate Aquifer. In general, it is believed that the matrix porosity of the ancient marine limestones and dolomites of the lower Carbonate Aquifer is negligible (Winograd and Thordarson 1975 [101167], p. C14), and that the large discharge from that aquifer system at Ash Meadows is due to flow through solution-enlarged fractures and along faults (Dudley and Larson 1976 [103415], pp. 5 and 9). One borehole, UE-25 p#1 in Figure 3, penetrates the lower Carbonate Aquifer near Yucca Mountain. The ongoing Nye County Early Warning Drilling Program has completed a deep well, NC-EWDP2-DB, in the Carbonate Aquifer. These deep wells, plus additional planned deep wells, will improve understanding of hydrologic conditions in the aquifers, including the deep Carbonate Aquifer, and will help to

confirm the direction and magnitude of groundwater flow in that aquifer at Yucca Mountain. However, large groundwater flows have been modeled in the Carbonate Aquifer by D'Agnese et al. (1997 [100131], Figures 46 to 47, p. 90) in the Death Valley Regional Groundwater Flow Model within the southern part of the site-scale flow model. These results are discussed in Section 6.3.2.4.

More data are available on the transmissive properties (transmissivity and hydraulic conductivity) of the rocks of the SZ, chiefly from aquifer tests in boreholes. However, a wide margin of uncertainty exists about the quantitative validity and extrapolation of such data far from the test sites (Luckey et al. 1996 [100465], pp. 53 to 54). Groundwater flow models have been used to estimate transmissivity over large areas, but these have a large uncertainty associated with them (Luckey et al. 1996 [100465], p. 54).

6.3.2.2 Hydrologic Features

The hydrogeologic framework model (HFM) for the base-case model (USGS 2001 [158608], Section 6.3.3) represents faults and other hydrogeologic features, such as zones of hydrothermal alteration, that affect SZ flow. Information on faults includes fault trace maps, which show both faults on cross sections and locations where faults intersect the land surface. Faults in the model area can dip at almost any angle, but most are high-angle faults. Faults deemed important to flow near Yucca Mountain are modeled explicitly in the numerical SZ flow model. Given software constraints and the numerical flow model resolution, faulting in the area is simplified in the numerical model, and the faults are treated as vertical features. Section 6.5.3.1 discusses how these features were constructed in the HFM.

6.3.2.3 Flow Field

Using the potentiometric surface map (Figure 2) and the supposition that hydraulic conductivity is isotropic, the general direction of groundwater flow within the site-scale SZ flow and transport model area can be deduced as being from north to south. Under this assumption, the direction of flow is perpendicular to the water-level contours. Under the USGS (2001 [158608], Section 6.3.6) interpretation of the water-level data, the water table exhibits a steep gradient throughout the northern part of the model area (north of the repository) and the contours curve southward to the west of Crater Flat.

Several faults are interpreted as barriers to groundwater flow, as indicated by offsets of contours where they cross faults (Figure 2). This interpretation is supported only by field data at the Solitario Canyon Fault, west of the repository, which is interpreted as causing a differential of about 45 m (148 ft) in the potentiometric surface. In Crater Flat and on the southern part of Yucca Mountain, the flow direction is nearly easterly toward Fortymile Wash. A more detailed water-level map of the immediate vicinity of Yucca Mountain (Figure 3) indicates that flows from the west and east converge at Fortymile Wash and turn southward toward the Amargosa Desert. The cause of the easterly gradient in Crater Flat and southern Yucca Mountain is not evident, but it suggests that a groundwater barrier exists near the northern margin of the Amargosa Desert. In any event, the potentiometric surface upgradient of the 725-m (2,379 ft) contour and the Highway 95 fault appears to have little north-south flow over an area of about

259 km^2 (100 mi^2). It is noted here that Figure 3 is a water-level map using 1993 data. Newer data do not contradict any of the discussion of this paragraph.

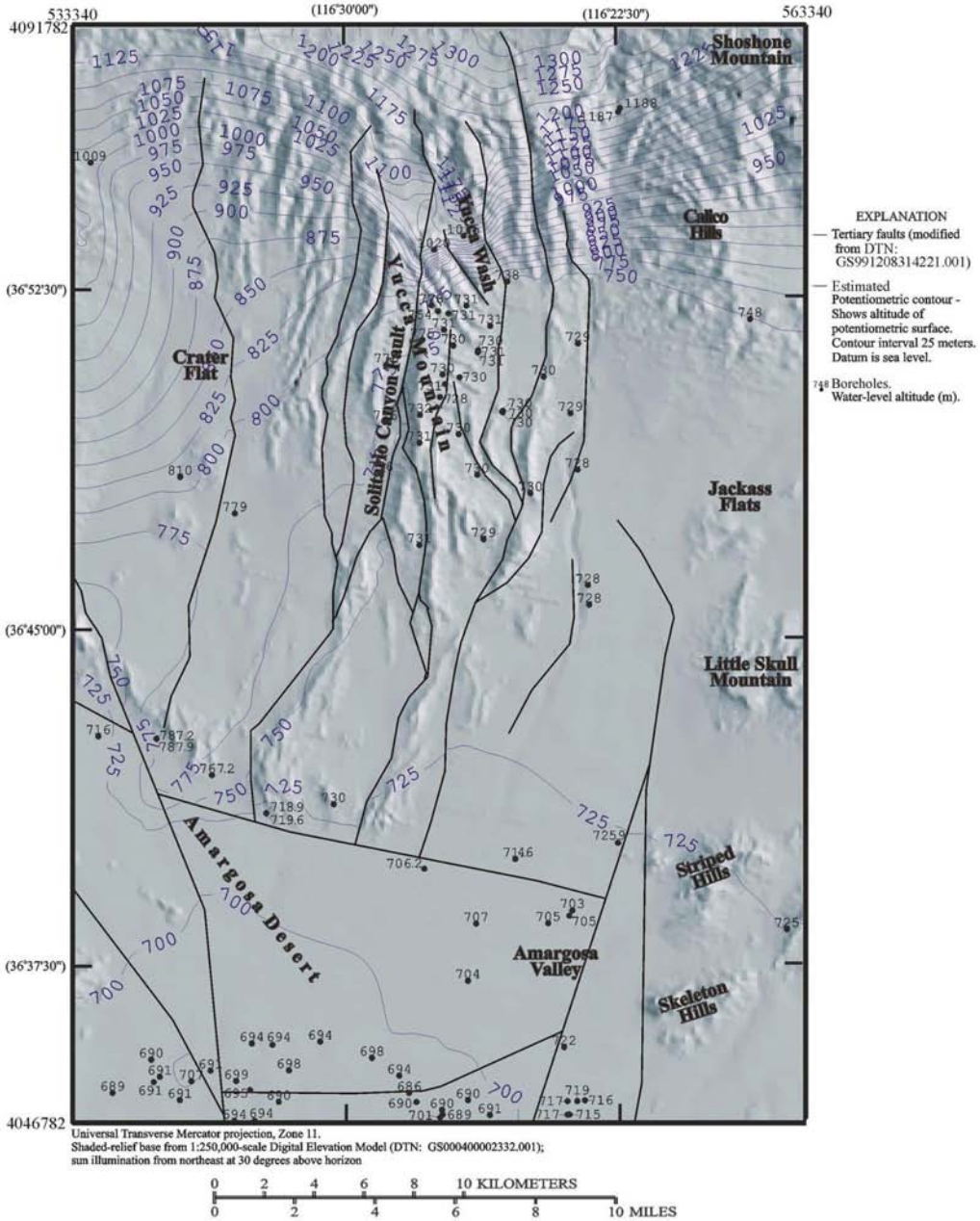

Source: USGS (2001 [154625], Figure 1-2).

NOTE: Potentiometric contours show elevation of the potentiometric surface. Datum is sea level.

Figure 2. Site-Scale Potentiometric Map and Structural Features

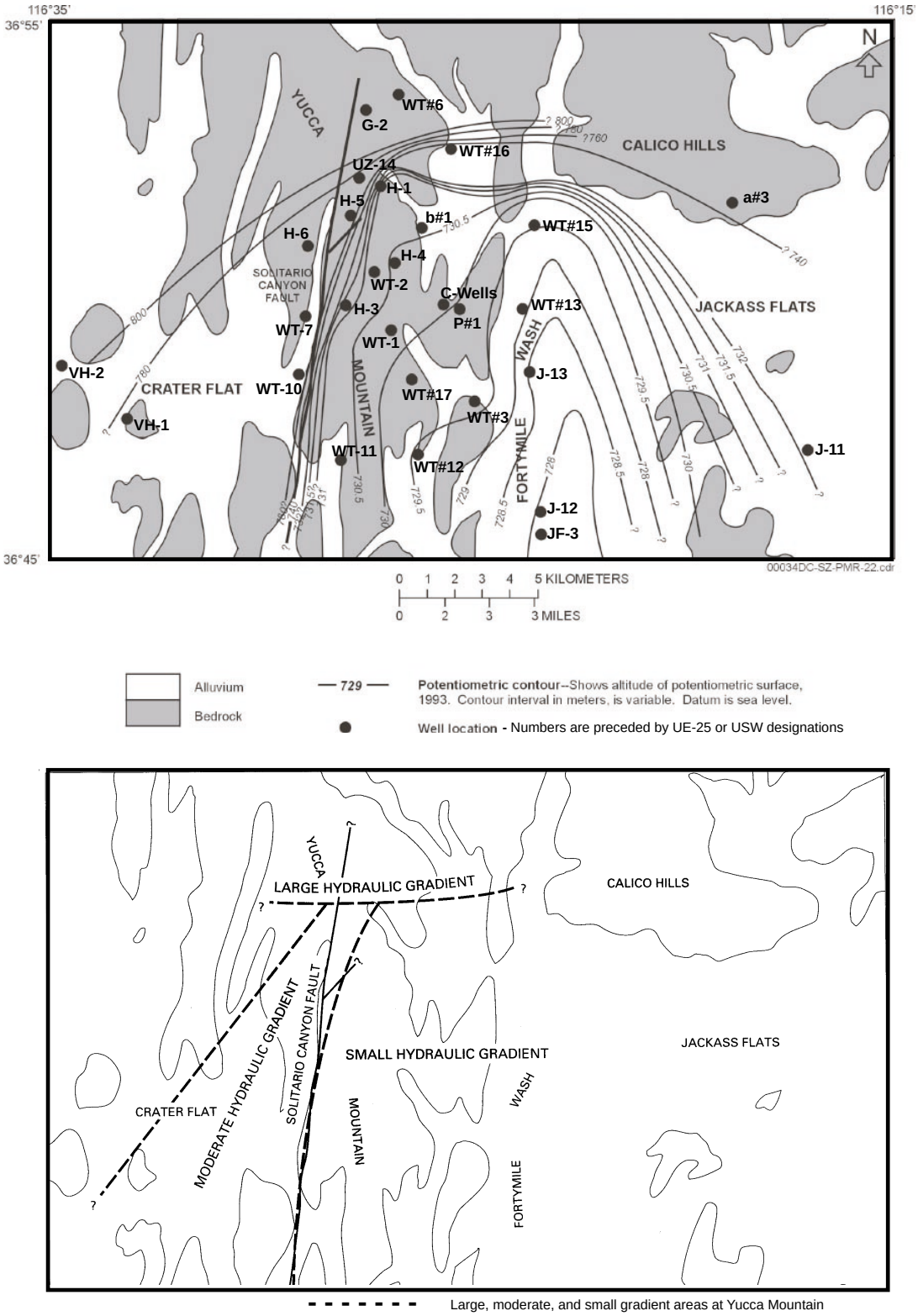

Source: Tucci and Burkhardt (1995 [101060], Figures 2, 4, and 5).

Figure 3. Potentiometric Surface Map and Gradient Areas Developed Using Water-Level Data from 1993

As discussed in Section 6.3.2.5, the potentiometric level in well UE-25 p#1, which penetrates the lower Carbonate Aquifer, is about 752 m (2,467 ft), 21 m (69 ft) higher than in nearby wells tapping the lower volcanic aquifer. This result indicates a potential for upward flow from the lower Carbonate Aquifer; however, other lines of evidence suggest that such flow is small. The direction of flow and hydraulic gradient cannot be determined from a single well; however, regional relationships suggest that the general direction of flow in the lower Carbonate Aquifer should be southerly to southeasterly in the site-scale SZ flow model domain (NRC 1998 [107770], p. 109). We do note, however, that south of the site-scale model domain, there is geochemical evidence for a westward component of flow in the Carbonate Aquifer. See BSC (2003 [162657]) for details.

Most monitoring wells in the Yucca Mountain area show little variation in water level over time (Luckey et al. 1996 [100465], p. 29). In contrast, water levels in the heavily pumped Amargosa Farms area have declined substantially since intensive irrigation development began in the 1950s. Kilroy (1991 [103010], p. 18) reported a water-level decline of as much as 9 m (30 ft) by 1987, and La Camera and Locke (1997 [103011], Figure 4) show an additional decline of about 3.4 m (11 ft) through 1996 at well AD-5, about 14 km (8.7 mi) southwest of the Amargosa Valley.

6.3.2.4 Large, Moderate, and Small Hydraulic Gradients

Three distinctive hydraulic gradients of the potentiometric surface at Yucca Mountain are recognized: (1) a large hydraulic gradient of 0.13 between water-level altitudes of 1,030 m (3,380 ft) and 750 m (2,460 ft) at the northern end of Yucca Mountain, (2) a moderate hydraulic gradient of 0.05 west of the crest of Yucca Mountain, and (3) a small hydraulic gradient of 0.0001 to 0.0003 extending from Solitario Canyon to Fortymile Wash. These gradients have been portrayed on detailed potentiometric surface maps presented by Ervin et al. (1994 [100633]), and Tucci and Burkhardt (1995 [101060]), as well as on the maps with large contour intervals compiled by D'Agnese et al. (1997 [100131]) and by the USGS (USGS 2001 [157611], Section 7.2). The large contour-interval maps do not portray the small or moderate gradients well because of limitations imposed by contour intervals; however, the large gradient is recognizable on all of these maps.

Luckey et al. (1996 [100465]) present detailed descriptions of these gradient features and discuss interpretations of their causes. The large hydraulic gradient has been the subject of numerous theories. The large gradient is summarized by Luckey et al. (1996 [100465], pp. 21 to 25):

- The gradient is simply the result of flow through the upper volcanic confining unit, which is nearly 300-m (984-ft) thick near the large gradient.
- The gradient represents a semi-perched system in which flow in the upper and lower aquifers is predominantly horizontal, whereas flow in the upper confining unit would be predominantly vertical.
- The gradient represents a drain down a buried fault from the volcanic aquifers to the lower Carbonate Aquifer.

- The gradient represents a spillway in which a fault marks the effective northern limit of the lower volcanic aquifer.

- The large gradient results from the presence at depth of the Eleana Formation, a part of the Paleozoic upper confining unit, which overlies the lower Carbonate Aquifer in much of the Death Valley region. The Eleana Formation is absent at borehole UE-25 p#1 at Yucca Mountain, which penetrated the lower Carbonate Aquifer directly beneath the lower volcanic confining unit.

The cause of the moderate hydraulic gradient is less controversial than that of the large gradient, and Luckey et al. (1996 [100465], p. 25) suggest that the Solitario Canyon Fault and its splays function as a barrier to flow from west to east due to the presence of low-permeability fault gouge or to the juxtaposition of more permeable units against less permeable units.

The small hydraulic gradient occupies most of the repository area and the downgradient area eastward to Fortymile Wash. Over a distance of 6 km (3.7 mi), the hydraulic gradient declines only about 2.5 m (8.2 ft) between the crest of Yucca Mountain and Fortymile Wash. The small gradient could indicate highly transmissive rocks, little groundwater flow in this area, or a combination of both causes (Luckey et al. 1996 [100465], p. 27).

The potentiometric map (USGS 2000 [157611]), which includes head data from the recently drilled NC-EWDP boreholes, indicates that the small hydraulic gradient extends southward to an east-west fault approximately along Highway U.S. 95.

6.3.2.5 Vertical Gradients

Information on vertical hydraulic gradients in the SZ is concentrated near Yucca Mountain, although Kilroy (1991 [103010]) presents some information indicating the existence of vertical gradients in the Amargosa Desert. The following discussion of vertical gradients primarily is extracted from Luckey et al. (1996 [100465], pp. 27–29).

Luckey et al. (1996 [100465], pp. 27–29) report on potentiometric level measurements in multiple depth intervals in 10 boreholes at Yucca Mountain. Differences in potentiometric levels at different depth intervals in the same borehole ranged from as little as 0.15 m (0.5 ft) in borehole USW H-4 to as much as 54.83 m (180 ft) in USW H-1 (Luckey et al. 1996 [100465], Table 3). The largest differences were between the lower Carbonate Aquifer or the adjoining lowermost lower volcanic confining unit and the overlying lower volcanic aquifer. Within the upper part of the lower volcanic confining unit and the lower volcanic aquifer, the differences in potentiometric levels generally were 1 m (3.3 ft) or less.

Potentiometric levels generally were higher in the lower intervals of the volcanic rocks than in the upper intervals, indicating a potential for upward groundwater movement. However, at four boreholes (USW G-4, USW H-1, USW H-6, and UE-25 b#1), potentiometric levels in the volcanic rocks were slightly higher in the uppermost intervals than in the next lower intervals. Overall, it appears that an upward gradient between the lower and upper volcanic aquifer is maintained at these locations.

Potentiometric levels in the Paleozoic Carbonate Aquifer in borehole UE-25 p#1 are about 752 m (2,467 ft), or about 21 m (69 ft) higher than levels in the lower volcanic aquifer. A potential for upward groundwater movement from the Paleozoic rocks to the volcanic rocks was, therefore, indicated. Because of the large difference in potentiometric levels in these two aquifers, they seem to be hydraulically separate (Luckey et al. 1996 [100465], p. 28). Testing at the C-wells complex in 1984 suggested a hydraulic connection between the lower volcanic aquifer and the Carbonate Aquifer; however, testing in 1995 and 1996, using more reliable water-level measurement equipment, did not confirm the hydraulic connection (Luckey et al. 1996 [100465], p. 28).

In borehole UE-25 p#1, the lowermost 70 m (230 ft) of the older tuffs (lower volcanic confining unit) had potentiometric levels similar to those in the Carbonate Aquifer, indicating an hydraulic connection between the lowermost part of the lower volcanic confining unit and the Carbonate Aquifer. Such a connection could be expected in the hanging-wall rocks adjacent to a fault; and, this type of connection is supported by calcification of the basal tuffs in the borehole. The remaining 237 m (778 ft) of the lower volcanic confining unit had a potentiometric level similar to that of the lower volcanic aquifer (Luckey et al. 1996 [100465], p. 28).

No obvious spatial patterns in the distribution of vertical hydraulic gradients around Yucca Mountain are apparent; however, some generalizations can be made as to the distribution of potentiometric levels in the lower sections of the volcanic rocks. Potentiometric levels in the lower volcanic confining unit are relatively high (altitude greater than 750 m [2,460 ft]) in the western and northern parts of Yucca Mountain and are relatively low (altitude about 730 m [2,395 ft]) in the eastern part of Yucca Mountain. Based on potentiometric levels that were measured in borehole UE-25 p#1, the potentiometric levels in the lower volcanic confining unit in boreholes USW H-1, USW H-3, USW H-5 and USW H-6 may reflect the potentiometric level in the Carbonate Aquifer. Boreholes UE-25 b#1 and USW H-4 do not seem to fit the pattern established by the other boreholes. These two boreholes penetrated only 31 m (102 ft) and 64 m (210 ft), respectively, into the lower volcanic confining unit and had potentiometric levels (about 730 m [2,395 ft]) that were similar to potentiometric levels in the lower volcanic aquifer. Penetration of the other four boreholes into the lower volcanic confining unit ranged from 123 m (403 ft) in borehole USW H-3 to 726 m (2,382 ft) in borehole USW H-1. Only in boreholes USW H-1, USW H-3, USW H-5, and USW H-6 are the potentiometric levels in the lower volcanic confining unit influenced by the potentiometric level in the Carbonate Aquifer (Luckey et al. 1996 [100465], p. 29).

Vertical hydraulic gradients could have an important impact on the analysis of the effectiveness of the SZ as a barrier to radionuclide transport in that they keep the flow path for the potential repository in the shallow groundwater. Based on available data, a spatially extensive upward gradient can be inferred between the Carbonate Aquifer and the volcanic aquifers, which indicates that, at least for the immediate Yucca Mountain area, radionuclide transport would be restricted to the volcanic system (Luckey et al. 1996 [100465], p. 29).

Kilroy (1991 [103010], pp. 11–16, Table 3) presents vertical gradient data for 21 nested piezometers, 1 well cluster, and 1 river and well pair in the Amargosa Desert area. However, none of these locations are within the area of the site-scale SZ model, so the results are not discussed in detail here. Upward gradients generally were associated with freshwater limestones,

carbonate rock outcrops, and structural features (Kilroy 1991 [103010], p. 16). The association with carbonate rocks is attributed to an hydraulic connection with the Carbonate Aquifer regional flow system and, especially, to the Spotted Range-Mine Mountain fault zone, which is a conduit for flow from the Carbonate Aquifer to the basin fill.

6.3.2.6 Lateral Boundary Conditions

The boundary conditions are derived from regional water-level and head data (DTN: GS000508312332.001 [149947]). The data are used to form fixed-head boundary conditions on the lateral sides of the model. By fixed heads, it is meant that the heads may vary in space along the boundary but not in the vertical direction or in time. Because of constant vertical head, this condition produces no vertical flow. This model contrasts with a known upward gradient in the area near well UE-25 p#1. Nevertheless, some upward gradient can be obtained away from the boundaries with the present boundary conditions. This is because permeability differences between the hydrogeologic units propagate the head changes for the higher permeability carbonate rocks slower than the lower permeability volcanic confining unit overlaying the carbonate rocks. This upward gradient, though smaller in magnitude than that measured in well UE-25 p#1, is sufficient to keep the modeled transport path lines leaving the repository from reaching the deep Carbonate Aquifer. This situation will be discussed further in Section 6.7. Of special note is the southern boundary of the model, which coincides with a large number of wells in the Amargosa Valley. Here there are a variety of measurements over the time of usage. Some of the earlier measurements represent pre-development states, and the later measurements generally represent water levels with pumping. The boundary conditions represent water levels with pumping and are described in USGS (2001 [158608], Section 6.3.6). (See Section 6.4.4 for a discussion of the water level used in this report and the other analyses that are available.) Most of the inflows to, and outflow from, the site-scale SZ flow model occurs as groundwater flows across the lateral boundaries. The best estimates of flow rates are the cell-by-cell fluxes calculated by the regional-scale model. These fluxes are compiled in four tables (CRWMS M&O 1999 [130979], Tables 7.2-1, 7.2-2, 7.2-3, and 7.2-4) corresponding to the rectangular boundaries of the site-scale flow model. The flows are compiled by the three depth layers (0 to 500 m [0 to 1,640 ft], 500 to 1,250 m [1,640 to 4,100 ft], and 1,250 to 2,750 m [4,100 to 9,020 ft] below the water table) of the regional-scale flow model (D'Agnese et al. 1997 [100131], p. 75). These lateral fluxes constitute calibration targets for the SZ flow model and are discussed in that context in Section 6.6.1.3.

6.3.2.7 Recharge

The three recharge components (site-scale UZ model, regional-scale SZ model, and Fortymile Wash) take different forms and must be combined into a single result. Recharge from the site-scale UZ model (percolation flux) is taken as the flow through the base of that model, the domain of which includes approximately 50 km^2 (19.3 mi^2). The UZ flow model uses dual permeability; accordingly, the output includes fluxes for fracture and matrix flow. These data are combined into a total volumetric flow rate and an average percolation flux (CRWMS M&O 1999 [130979], Figure 6.1.3-2).

Estimates of recharge from the infiltration of surface flows in Fortymile Wash are given by linear reaches along the wash. Recharge estimates were interpolated to a 500-m (1,640-ft) wide

recharge zone for most of the wash and a broader area of distributary channels in the Amargosa Desert (CRWMS M&O 1999 [130979], Table 6.1.3-1, Figure 6.1.3-2).

The distributed vertical recharge, limited to the northern-most portion of the site-scale model area, was extracted from the regional-scale SZ flow model (D'Agnese et al. 1997 [100131]). No recharge within the UZ model area was included from the regional scale SZ flow model as this was included separately (see above). A plot of distributed recharge is provided by CRWMS M&O (1999 [130979], Figure 6.1.1-1).

Estimated recharge from all three sources is displayed by CRWMS M&O (1999 [130979], Figure 6.1.3-2). Total recharge was about 1,550,000 m^3/yr (1,256 acre-ft/yr). Of this total, about 212,000 m^3/yr (172 acre-ft/yr) was attributed to flux from the UZ model area and about 95,000 m^3/yr (77 acre-ft/yr) was attributed to infiltration along Fortymile Wash, leaving a remainder of about 1,240,000 m^3/yr (1,007 acre-ft/yr) from distributed recharge.

Groundwater inflows along the eastern, northern, and western boundaries of the site-scale SZ flow model total 17.8 x 10^6 m^3/yr (14,430 acre-ft/yr), 6.21 x 10^6 m^3/yr (5,034 acre-ft/yr), and 3.74 m^3/yr (3,032 acre-ft/yr), respectively (CRWMS M&O 1999 [130979]). These inflows, totaling 27.75 x 10^6 m^3/yr (22,500 acre-ft/yr), represent nearly 18 times the estimated recharge from the surface in the model area. Of the total inflow for the eastern boundary, 17.6 x 10^6 m^3/yr (14,273 acre-ft/yr), or 99 percent, occurs in the Amargosa Desert sector (CRWMS M&O 1999 [130979]), and nearly all of that occurs in layers 2 and 3 of the regional-scale flow model (CRWMS M&O 1999 [130979], Table 7.2-2) and represents flows in the lower Carbonate Aquifer (D'Agnese et al. 1997 [100131], p. 90, Figures 46-47).

6.3.2.8 Discharge

There is no measurable present day natural discharge (i.e., springs or evapotranspiration within the site-scale model domain; therefore, natural discharge to the surface is not represented in the simulations.

6.3.2.9 Heterogeneity

Physical and chemical heterogeneity of the rocks and water in the SZ can affect groundwater flow and the transport of contaminants in the SZ. The principal forms of heterogeneity in the site-scale SZ model area are physical and may be primary (i.e., related to the formation of the rocks) or secondary (i.e., related to events subsequent to their formation).

The most obvious form of primary heterogeneity is the mode of origin (i.e., volcanic rocks, clastic rocks, carbonate rocks, and alluvial deposits), which is the primary basis for subdividing the rocks into hydrogeologic units. Within each major category, further subdivisions are possible. Probably the major form of primary heterogeneity affecting groundwater flow in the site-scale SZ model area results from the origin of the volcanic rocks (i.e., ash-flow or air-fall pyroclastic deposits, lava flows, and volcanic breccias). The pyroclastic rocks (termed tuffs) primarily are nonwelded to densely welded, vitric to devitrified ash-flow deposits separated by nonwelded vitric air-fall deposits. Thus, the primary heterogeneity in physical character relates to whether the deposits resulted from massive eruptions of hot volcanic ash from volcanic

centers that moved downslope as flows of fragmental material or whether they resulted from explosive eruptions that injected volcanic fragments into the air to fall out as bedded tuffs.

The thicker flow deposits, up to several hundred meters thick, were very hot, resulting in welding of the fragments into a dense mass. Thinner flows retained heat less effectively, resulting in partly welded to nonwelded ash-flow tuffs. Ash-fall tuffs, generally less than tens of meters thick, cooled in the atmosphere and characteristically are glassy (vitric) (Luckey et al. 1996 [100465], p. 17).

The mode of origin controls the porosity and permeability of the volcanic rocks. The densely welded tuffs generally have minimal primary porosity and water-storage capacity but commonly are highly fractured and function as aquifers (Luckey et al. 1996 [100465], p. 17). Nonwelded ash-flow tuffs, when unaltered, have moderate to low matrix permeability but high porosity, and commonly constitute confining units. Bedded tuffs have high primary porosity and moderate to low permeability, and they generally function as confining units.

As the tuff deposits cooled, they were subjected to secondary processes, including formation of cooling fractures, recrystallization or devitrification, and alteration of the initial glassy fragments to zeolite minerals and clay minerals, all of which affect the hydrologic properties of the rocks. Beginning with deposition and throughout their subsequent history, the rocks have been subjected to tectonic forces resulting in further fracturing and faulting. They also have been subject to changes in the position of the water table, which greatly affects the degree of alteration of the initially glassy deposits.

The forms of secondary heterogeneity most affecting the SZ are fracturing, faulting, and alteration of glassy materials to zeolites and clay minerals. Fractures, where interconnected, transmit water readily, which accounts for the permeable character of the welded tuffs. Cooling fractures, which are pervasive in welded tuffs, tend to be strata-bound, that is, confined to the welded portions of flows, whereas tectonic fractures tend to cut through stratigraphic units, as do faults.

Nonwelded deposits are less subject to fracturing and more subject to alteration of the initial glassy deposits to zeolites and clay minerals, both of which reduce permeability. The presence of perched-water bodies in the UZ is attributed to the ubiquitous presence of a smectite-zeolite interval at the base of the Topopah Spring Tuff, which, in the absence of through-going fractures, essentially stops the vertical movement of water (Luckey et al. 1996 [100465], p. 46).

The heterogeneity in permeability of different types of deposits led to the subdivision of the Yucca Mountain geologic section into five basic SZ hydrologic units: upper volcanic aquifer, upper volcanic confining unit, lower volcanic aquifer, lower volcanic confining unit, and lower Carbonate Aquifer. To accommodate the more extensive area of the site-scale flow model, the HFM (USGS 2001 [158608], Section 6.3.4) includes several additional units above and below these basic five units.

In the vicinity of Yucca Mountain, volcanic deposits generally form laterally-extensive stratigraphic units; however, due to physical heterogeneity, porosity and permeability are highly variable both laterally and vertically. As noted previously, the properties of each hydrogeologic

unit is taken as uniform with the value being established during the calibration process. The model is still complex because of the lateral distribution of the hydrogeologic units. It should be noted here that the heterogeneity of the rocks at scales less than the grid-block size (500 m in the lateral directions) will be smoothed by the average permeability applied to that block. The heterogeneity is accounted for in the TSPA calculations through dual-porosity calculations and effective porosity.

Within the site-scale model area, little specific information is available on the lower Carbonate Aquifer. However, information from nearby areas (D'Agnese et al. 1997 [100131], p. 90, Figures 46 and 47) suggests that the lower Carbonate Aquifer is highly and uniformly permeable, and that the high permeability is attributed to pervasive solution-enlarged fractures.

In the southern part of the site-scale SZ flow model domain, the volcanic deposits thin and interfinger with valley-fill deposits. The latter are heterogeneous (sand and gravel) because of their mode of deposition (Walker and Eakin 1963 [103022], p. 14), but are not subject to the fracturing, faulting, and alteration types of heterogeneity that affect the volcanic rocks.

6.3.2.10 Role of Faults

Faults, fault zones, and zones of chemical alteration are hydrogeologic features that require special treatment in the site-scale SZ flow and transport model. Faulting and fracturing are pervasive at Yucca Mountain, and they greatly affect groundwater flow patterns because they may act as preferred conduits or barriers to groundwater flow. The role that faults play in facilitating or inhibiting groundwater flow depends on the nature of the fault (i.e., whether the faults are in tension, compression, or shear) and other factors such as the juxtaposition of varying geologic units along the fault plane, the rock types involved, fault zone materials, and depth below land surface.

Faunt (1997 [100146]) investigated the effect of faulting on groundwater movement in the Death Valley region and developed a map of fault traces (Faunt 1997, [100146] Figure 10) and rose diagrams (Faunt 1997 [100146], Figure 11) showing the orientation of faults within the principal structural provinces of region. Faunt (1997 [100146], p. 38) grouped the faults into three categories depending on their orientations relative to the present-day stress field (i.e., those in relative tension, compression, or shear).

Faults in relative tension are more likely to be preferential conduits for groundwater, and faults in shear or compression are more likely to deflect or block groundwater movements. Within the site-scale model area, faults assumed to have the most evident effects on groundwater movement, such as effects on potentiometric contours (Figure 1), include the Solitario Canyon, Stagecoach Road, Highway 95, Crater Flat, and Bare Mountain faults, all of which appear to act as barriers to groundwater flow. Faults within the site-scale model area of hydrologic importance include the Spotted Range-Mine Mountain shear zone, which Faunt (1997 [100146], p. 34) describes as a major high-permeability zone in the lower Carbonate Aquifer, and the following features to which special treatment is accorded in the site-scale SZ flow model: Crater Flat Fault, Solitario Canyon Fault, Highway 95 Fault, Bare Mountain Fault, Imbricate Fault zone (between the Ghost Dance and Paintbrush Canyon Faults at Yucca Mountain), Fortymile Wash zone (which may not be a fault), and the east-west barrier (which appears to cause the large

hydraulic gradient north of Yucca Mountain). These features fall into three categories depending on their hydrologic impacts: (1) zones of permeability enhancement parallel to faults and zones of permeability reduction perpendicular to faults (Crater Flat and Solitario Canyon faults), (2) zones of permeability enhancement (Bare Mountain Fault, Imbricate Fault zone, Fortymile Wash zones, and Spotted Range-Mine Mountain zone), and (3) zones of unknown behavior (Highway 95 fault).

6.3.3 Groundwater Flow Processes

Assumptions used in modeling the groundwater flow process include those of the regional-scale models and the site-scale SZ flow model, and those made in estimating parameters that are used as input to these models. For the following reasons, the effective continuum representation of fracture permeability is used.

- On the scale represented by the site-scale SZ flow model, the site is well represented by a continuum flow model. Pumping tests show evidence of fracture flow near Yucca Mountain (Geldon et al. 1997 [100397]). Numerical modeling of fracture properties is done in one of two ways: discrete fracture models, effective continuum models, or dual-continuum models. Dual-continuum models are not needed because transient simulations are not performed. For steady-state flow calculations, dual-continuum formulations are equivalent to single-continuum formulations. Discrete fracture models represent each fracture as a distinct object within the modeling domain. Although a discrete fracture model might reproduce the flow system more accurately, flow modeling is adequately conducted using a continuum model for the following reasons:
    - At Yucca Mountain, studies of the density and spacing of flowing intervals generally indicate that flow occurs through fracture zones (BSC 2001 [156965], Figure 15). The fractures or fracture zones are located in various geological units, and in most cases, no single zone dominates the flow through a well. Geochemical studies (BSC 2001 [158606], Section 6) independently confirm a south-southeasterly trace of the particle flow path. For the limited set of wells (Luckey et al. 1996 [100465], Figure 11), flow appears to be carried through fracture zones separated by a few tens of meters rather than by a few individual fractures.
    - Part of the flow system is an alluvium unit for which flow and transport is appropriately modeled using a continuum model.
    - The drawdown response to pumping at wells surrounding the C-wells complex in multi-well pump tests indicates a well-connected fracture network in the Miocene tuffaceous rocks in this area (Geldon et al. 1998 [129721], p. 31).

The following assumptions also apply to both the TSPA-SR continuum modeling approach (BSC 2001 [157132]) and to the TSPA-LA.

- Estimates of discharge from the volcanic aquifer, elicited from the SZ expert elicitation panel, are applicable to the entire flow path from the repository to the accessible environment. The estimates of specific discharge from the SZ expert elicitation primarily

were based on data from hydraulic testing in wells in volcanic units and the hydraulic gradient inferred from water level measurements (CRWMS M&O 1998 [100353], p. 3-8). The relative values of groundwater flux in the volcanic aquifer and along the flow path farther to the south are constrained by the calibration of the site-scale SZ model; that is, the limits of permeability values of important hydrological units that allow reasonable calibration are used to set limits on specific discharge. It is reasonable to extrapolate the degree of uncertainty in the absolute value of groundwater flux from the volcanic aquifer to the flow path farther to the south.

- Horizontal anisotropy in permeability is adequately represented by a permeability tensor that is oriented in the north-south and east-west directions. In support of the TSPA-LA, horizontal isotropy and anisotropy are considered for radionuclide transport (BSC 2003 [162415]). The numerical grid of the site-scale SZ flow model is aligned north-south and east-west, and values of permeability may be specified only in directions parallel to the grid. Analysis of the probable direction of horizontal anisotropy shows that the direction of maximum transmissivity is N 33° E (Winterle and La Femina 1999 [129796], p. iii), indicating that the anisotropy applied on the site-scale SZ model grid is within approximately 30° of the inferred anisotropy. Horizontal isotropy was assumed in the calibrated flow model. Inclusion of a 5:1 (north-south to east-west) horizontal anisotropy in the calibrated flow model resulted in head residuals that were less than the calibrated isotropic model along the transport path (BSC 2001 [157132], Figures 7 and 8).

- Horizontal anisotropy in permeability applies to the fractured and faulted volcanic units of the SZ system along the groundwater flow paths that run from the repository to points south and east of Yucca Mountain. The inferred flow path from beneath the repository extends to the south and east. This is the area in which potential anisotropy could have an important impact on radionuclide transport in the SZ. Given the conceptual basis for the anisotropy model, it is appropriate to apply anisotropy only to those hydrogeologic units that are dominated by groundwater flow in fractures.

- Anisotropy in permeability represents an alternative conceptual model of groundwater flow at the Yucca Mountain site. Sufficient uncertainty in the analysis of horizontal anisotropy exists to warrant consideration of two possible conceptual models: one with anisotropy and one without anisotropy (i.e., isotropic permeability).

- Changes in the water-table elevation (due to future climate changes) will have negligible effect on the direction of the groundwater flow near Yucca Mountain although the magnitude of the groundwater flux will change. This assumption has been studied in regional-scale (D'Agnese et al. 1999 [120425]) and subregional-scale (Czarnecki 1984 [101043]) flow models. These studies found that the flow direction did not change significantly under increased recharge scenarios. The studies were based on 2-D confined aquifer models that did not take into account the free surface boundary at the water table or the saturation of geological units that currently are in the UZ overlying the present-day SZ. These UZ tuffs generally have a lower permeability than those in the SZ, and as such, UZ units are not likely to introduce faster flow paths.

- Future water supply wells that might be drilled near Yucca Mountain (including outside the regulatory boundary) will have a negligible effect on the hydraulic gradient. Water levels at the southern boundary of the site-scale SZ flow and transport model (in the Amargosa Valley) currently reflect the effect of well pumpage (Luckey et al. 1996 [100465], p. 41).

- In the analysis presented in this report, it is assumed that temperature is approximately proportional to the depth below the ground surface. This assumption of a uniform temperature gradient with depth is equivalent to assuming uniform geothermal heat flux through a medium of homogeneous thermal conductivity. In addition, the temperature at the ground surface is assumed to be equal to a uniform value. The data on temperature in boreholes presented in Sass et al. (1988 [100644], Figures 4 to 8, Figure 10) indicate that there is significant variability in the temperature gradient at different locations and within individual wells, presumably due to advective redistribution of heat from infiltration and vertical groundwater flow. However, these data also indicate that the temperature gradients generally become more linear with increasing depth below the water table. It is important to note that the goal of assigning temperature variations with depth in the SZ site-scale flow model is to account for resulting variations in fluid viscosity at different depths in the SZ. The viscosity of water changes by a factor of only about 3.3 over the temperature range of 20°C to 100°C (Streeter and Wylie 1979 [145287], p. 536) that is expected within the range of depths in the SZ site-scale model domain. Thus, the linear approximation of the temperature gradient is adequate to capture the general effects of variations in groundwater viscosity with depth in the SZ site-scale flow model. The density also varies with temperature, but the effect is much smaller than viscosity. Over the temperature range of 20°C to 100°C, water density varies only a few percent. Using a variable viscosity allows the calibration of intrinsic permeability to be made instead of hydraulic conductivity. The former is a rock property, whereas the latter is a rock and fluid property. This approach, in turn, allows for more accurate flux calculations on the boundaries of the model.

- The confined-aquifer solution approach is used in the SZ flow model. The approach assumes no UZ and, therefore, solves a simplified and computationally more efficient numerical model. In the numerical model, the top surface has boundary conditions of applied recharge flux. The confined aquifer solution was enforced in the FEHM V 2.20 (STN: 10086-2.20-00; LANL 2003 [161725]) code by adding a large artificial head to the numerical solution. This artificial head was later subtracted after the computer run to recover the true solution. Because none of the fluid or rock properties depend on head, no changes to the true solution occur other than forcing the bookkeeping coding in FEHM to assume fully saturated conditions. If this procedure was not adopted, small variations in head around the water-level value would result in FEHM testing for an air phase, thus decreasing the efficiency. The negative side of this approach is that the top surface of the numerical model corresponds to the measured water-table surface and may be inconsistent with the model-derived water-table surface. This discrepancy affects the flux through the model. The error is generally small because the flowing area is proportional to the thickness of the model in the North-South direction, and the average error between the calibrated and field data is 16 m, compared to a model thickness of approximately 3000 m. Furthermore, the discrepancy can be checked after the model is

run. The numerical model averaged about 16-m discrepancy for the more than 100 head observations. Assuming that the water-table solution is in error by this amount, error for the "flow area" for the horizontal head gradient is small. Care was taken in the calibration process to model the low head gradient area to the south and east of Yucca Mountain accurately. Specified head boundary conditions on the lateral boundaries were set with no vertical gradient. It should be noted that the model allows for vertical flows that arise from recharge and heterogeneity. The numerical approach used is similar to the classical Dupuit-Forcheimer method.

6.4 CONSIDERATION OF ALTERNATIVE CONCEPTUAL MODELS

The site-scale saturated zone flow model is used in the Performance Assessment (PA) calculations to evaluate the potential risks to groundwater users downgradient from the repository area. The results of these PA calculations depend strongly on the specific discharge of groundwater leaving the repository area, as well as on the flow paths and the distribution of flow among the various hydrostratigraphic units that carry, deflect, or otherwise affect the flow. The alternative conceptual models (ACMs) presented here were investigated because they represented a well-publicized hydrologic concern (Large Hydraulic Gradient) or were related to a model feature (anisotropy or fault), or conceptualization (potentiometric surface), that had a possibility of strongly affecting the specific discharge calculations. Thus, it is important to understand how ACMs and their representations may affect the specific discharge and flow paths. This section presents analyses of the ACMs, their representation in the numerical model, and a discussion about possible impacts on the model outputs (specific discharge and flow paths). ACMs affecting model outputs are discussed in Section 6.7, and their associated uncertainty is propagated to the stochastic generation of radionuclide breakthrough curves in the TSPA calculations.

The base-case site-scale model described in detail in Section 6.5 also provides the basis for the alternate conceptual models discussed here. That is, the same numerical grid and HFM are used throughout. Various parameterization schemes are used to define the ACMs. For example, the Large Hydraulic Gradient HFM uses a different feature set (without the east-west barrier) than the base-case model. Otherwise the models are the same.

6.4.1 Large Hydraulic Gradient

It is important to understand how the presence or absence of the large hydraulic gradient (LHG) and its representation in the numerical model affect estimates of groundwater specific discharge and flow paths. By absence of the LHG we mean that the high heads/high gradients are an artifact of interpreting water levels as the regional water table when they are representing a perched water body. In the alternate conceptual models of the LHG that follow, the absence of the LHG is implicitly accounted for by assigning a low weight (relative to other observations) in the numerical calibrations to those wells that are suspected as perched.

The LHG north of Yucca Mountain is a feature of the flow system near Yucca Mountain that has been the subject of interest over the years (see Figures 2 and 3). Compared to the very gentle gradient from the repository to points south, the gradient north of the site is much larger. The cause of this gradient is unknown. To model the LHG, a low-permeability east-west feature has been incorporated into the base-case conceptual model north of Yucca Mountain. Because there is little field evidence for the presence of this feature, alternate conceptualizations are plausible. The Claim Canyon Caldera, north of Yucca Mountain, is an area of extensive hydrothermal alteration, which may result in a generalized reduction in permeability in the hydrogeologic units in this area. Permeability changes in similar environments have been studied by economic geologists (Norton and Knapp 1977 [147379]).

The fact that the LHG is north of Yucca Mountain means that if the downstream gradients of Yucca Mountain are modeled accurately, the change in the model's potentiometric surface due to

LHG conceptualizations are minimal. The different model-generated potentiometric surfaces, though similiar, lead to considerable differences in flow paths for fluid particles leaving the repository as well as large differences in flow directions for fluid entering the repository area. These are important points in the overall understanding of the flow system, and, thus, a detailed evaluation of the ACMs are warranted. Fortunately, after a small change in the parameterization, the flow paths generated with the LHG ACM was consistent with the base case model.

The site-scale saturated zone flow model has been used to evaluate three different conceptual models of the LHG. In addition to the original conceptualization described above, a second conceptual model was evaluated that assumes the apparent LHG to be a result of low-permeability hydrothermally altered rock north of Yucca Mountain. A third conceptual model of the LHG was evaluated that takes into account not only the area of hydrothermally altered rock north of Yucca Mountain but also the observed faults in the northwest-southeast trending washes in northern Yucca Mountain. The feature sets for the alternate conceptual models of the LHG are shown in Figures 4 and 5 (see a more detailed discussion of these feature sets in Section 6.5.3). Regardless of their conductivity, these faults tend to divert water along their strike and have the potential for segregating flow regimes near Yucca Mountain.

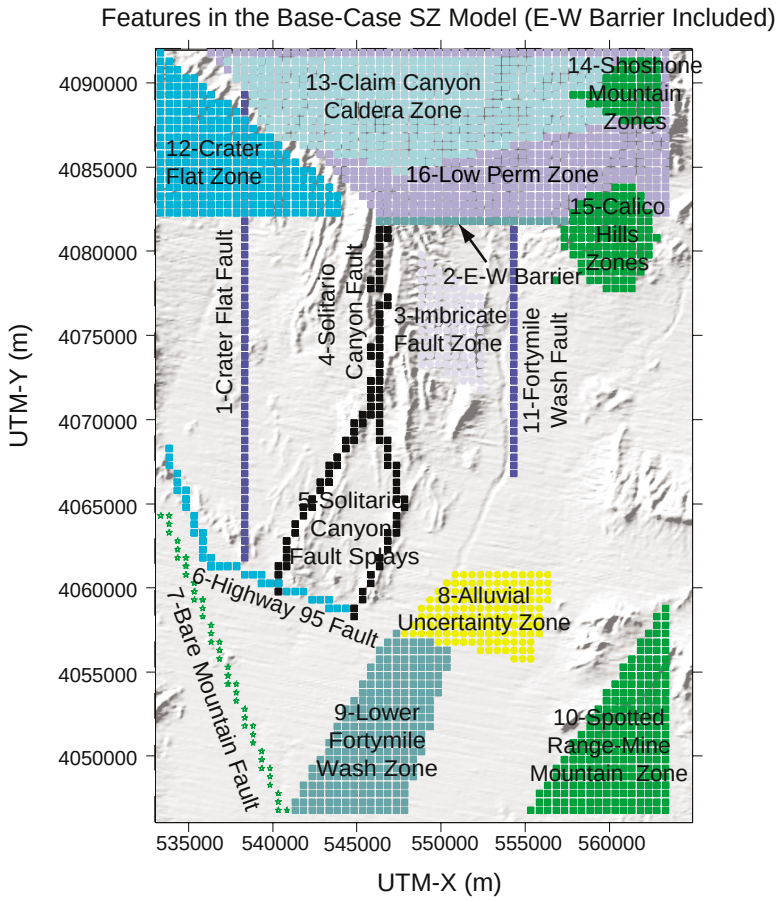

Source: Zyvoloski et al. (2003 [163341], Figure 2b).

Figure 4. Features of the Base-Case Saturated-Zone Model with East-West Barrier Included

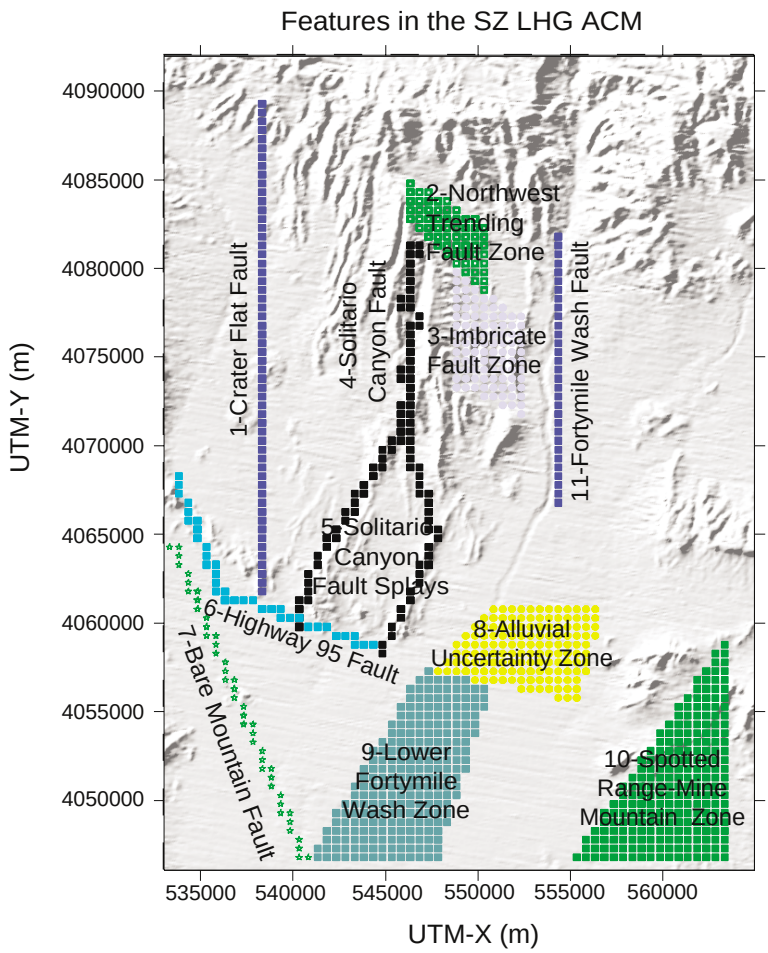

Source: Zyvoloski et al. (2003 [163341], Figure 2c).

Figure 5. Features of the LHG-ACM Saturated-Zone Model without the East-West Barrier

6.4.2 Solitario Canyon Fault

The Solitario Canyon Fault separates Crater Flat from Yucca Mountain and is shown in Figure 6. The representation of the Solitario Canyon Fault is an important part of the SZ site-scale flow model because it can potentially control flow from Crater Flat to Fortymile Wash in the area of the repository. The impact on the model of these features is to generate a higher head gradient to the west of Yucca Mountain and to impede flow from Crater Flat to Yucca Mountain. This in turn affects the eastern extent of travel of fluid leaving the repository area. Thus, the conceptual model of the Solitario Canyon Fault influences the path length in the alluvial material of fluid that originated from beneath the repository region.

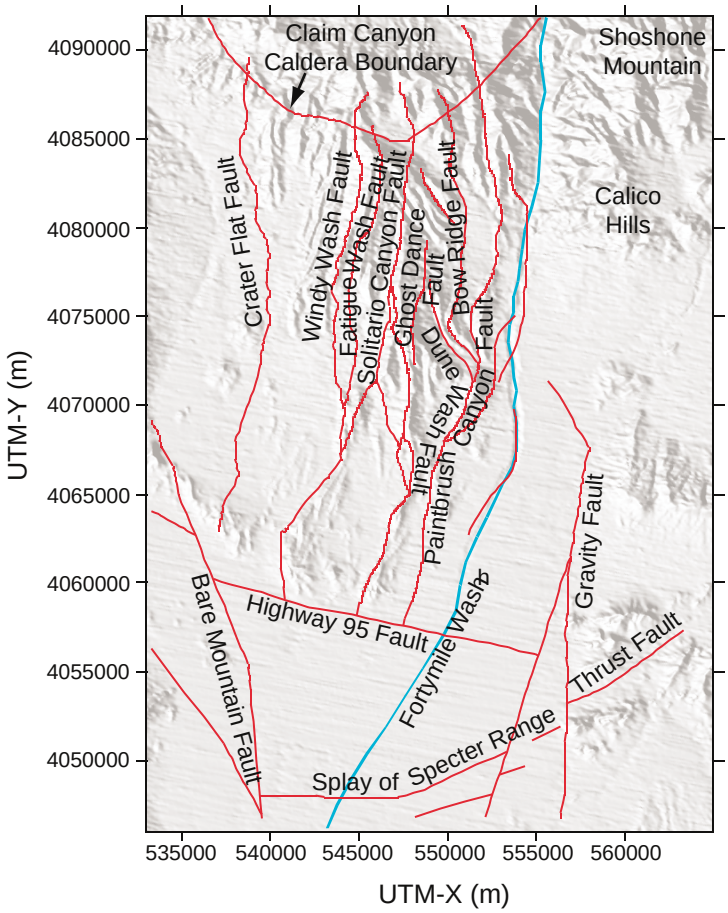

Source: DTN: GS010908314221.001 [162874]

Figure 6. Location of Faults in the Yucca Mountain Region

While the Solitario Canyon Fault has been identified as a major fault in the site-scale model region, conceptual uncertainty remains in the HFM as to the depth of this fault (USGS 2001 [158608], Section 6.3.3). This uncertainty translates into uncertainty regarding the likely hydraulic behavior of this feature at depth. The SZ site-scale flow model includes the Solitario Canyon Fault as a discrete feature that extends from the bottom of the model to the top of the water table. The fault is modeled as an anisotropic feature with larger permeability along the plane of the fault than across it. It is possible that this treatment of the anisotropy is inappropriate where it cuts the Carbonate Aquifer deep in the model domain. To investigate the importance of the Solitario Canyon Fault depth, an alternative conceptualization has been simulated in which the fault extends from the water table only to the top of the Carbonate Aquifer.

6.4.3 Anisotropy

Anisotropy occurs when hydraulic properties have different values in the three different directions: vertical, horizontal along the direction of maximum permeability, and horizontal along the direction of minimum permeability.

6.4.3.1 Vertical Anisotropy

A fractured or porous media exhibits anisotropy when hydraulic properties are not uniform in all directions. For Yucca Mountain, anisotropic permeability potentially affects the specific discharge, the flowpaths, and the flowpath lengths in the volcanic tuffs and alluvium. The base-case flow model includes a horizontal to vertical anisotropy ratio of 10:1, a typical value, in many of the units (see Section 6.1.6 of the previous version of this model report, BSC 2001 [155974]). For the base-case flow model, anisotropy ratios were generally kept constant during the analysis of the groundwater flow regime. Conceptual models both with and without vertical anisotropy are considered.

6.4.3.2 Horizontal Anisotropy

The faults in the SZ site-scale flow model include both vertically and horizontally anisotropic features that have high conductivity in the strike and vertical directions and low conductivity in the direction across the fault (Table 12). In general the x direction permeability of major faults were calibration parameters. However, the anisotropy ratios were kept constant during the calibration process. Also, the predominant north-south trending faults in the vicinity of Yucca Mountain were investigated using an alternate conceptual model (ACM) with variable horizontal anisotropy ratios (north-south to east-west permeabilities).

As described in the previous version of this model report, *Calibration of the Site-Scale Saturated Zone Flow Model*, MDL-NBS-HS-000011 REV 00 ICN 01 (BSC 2001, Section 6.1.6 [155974]), the predominately north-south trending faults in the vicinity of Yucca Mountain were also investigated using an alternative conceptual model with variable horizontal anisotropy ratios (north-south to east-west permeabilities). The area to which the anisotropy ratio was applied is bounded by a quadrilateral shown in Figure 7. This effect was investigated by re-running the SZ calibrated model with a 5:1 permeability ratio and checking the sensitivity of the calibration. A detailed description of the development of the horizontal anisotropy distribution used in this model is found in BSC (2003 [162415], Section 6.2.6). The TSPA calculations generated flow fields with the distribution described in BSC (2003 [162415], Figure 6.2-44). Incorporating the 5:1 permeability anisotropy in the area of the north-south trending faults at Yucca Mountain into the calibrated model resulted in predicted hydraulic heads that were slightly closer to the observed heads than for the model calibration without anisotropy. The differences in predicted heads and their impacts on the specific discharge, the flow-path direction, and flow-path lengths in volcanic tuffs and alluvium were within the uncertainty ranges used in the TSPA-SR (CRWMS M&O 2000 [153246]. Because horizontal anisotropy impacts model results, this parameter has been included in the TSPA analysis and, thus, is fully accounted for in terms of effect on repository performance.

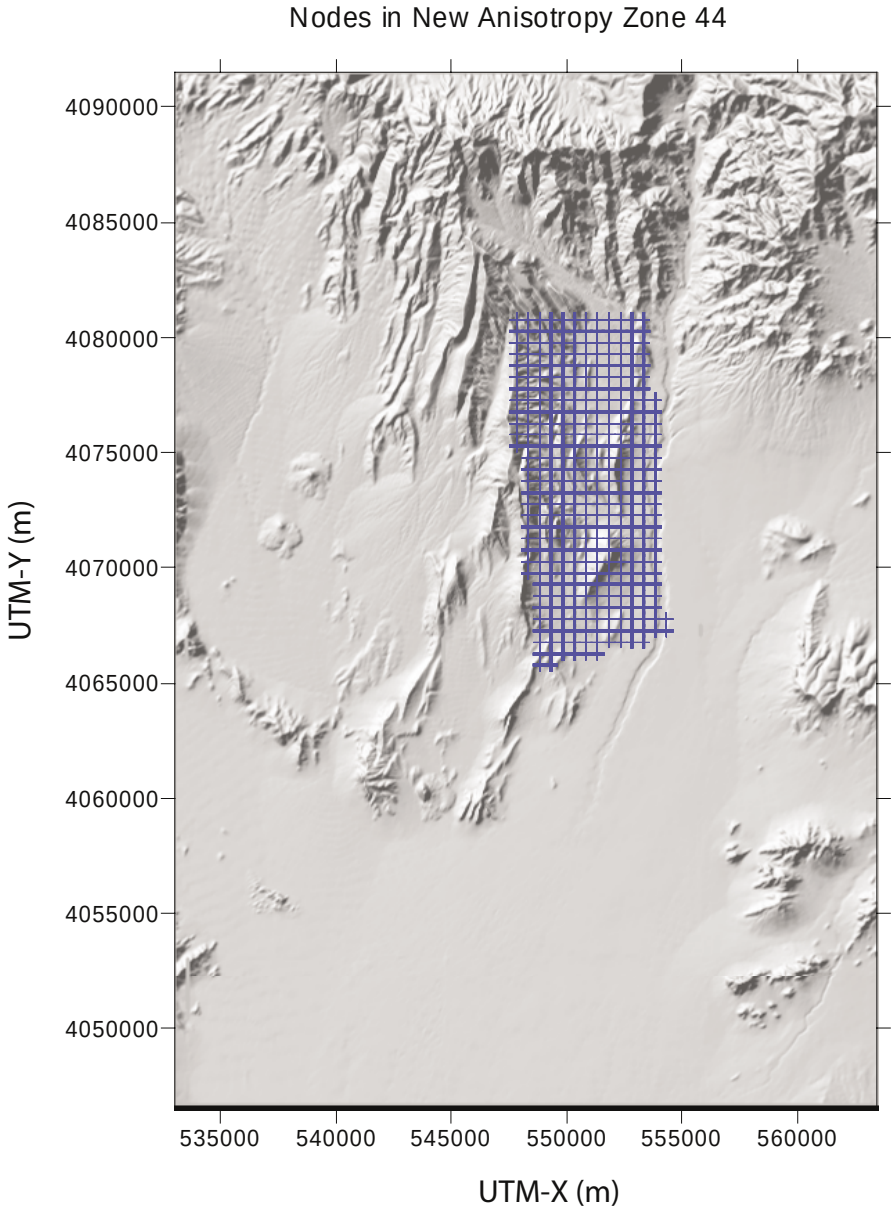

Output DTN: LA0304TM831231.002

Figure 7. Horizontal Anisotropy Is Applied to the Blue Cross-Hatched Area

6.4.4 Potentiometric Surface (Horizontal Hydraulic Gradient) and Water-Level Data

Water-level data (heads) are important parameters for model development. Water levels are used directly as calibration targets and to construct potentiometric surfaces used to derive horizontal and vertical hydraulic gradients. Additionally, water-level responses to pumping are used to estimate a distribution of horizontal anisotropies for certain model zones.

The purpose of this section is to compare four versions of the potentiometric surface of the uppermost part of the saturated zone for the SZ site-scale flow and transport model domain. There are differences in the potentiometric surface represented in each of these versions due to differences in purpose, assumptions, conceptual models, and methods by which the surfaces were constructed. The four versions considered here are derived from the following:

1) *Water-Level Data Analysis for the Saturated Zone Site-Scale Flow and Transport Model* REV 00 ICN 01 (USGS 2001 [154625], Section 6.2)

2) *Water-Level Data Analysis for the Saturated Zone Site-Scale Flow and Transport Model* REV 01 (USGS 2001 [157611])

3) *Calibration of the SZ Site-Scale Flow Model* REV 00 ICN 01 (the previous version of this model report, BSC 2001 [155974]).

4) The lower boundary for the *Unsaturated Zone Flow and Transport Model* (UZ model) REV 00 ICN 01 (BSC 2001 [159356]).

These are not the only versions of the potentiometric surface produced for this area; however, model comparisons will be limited to these four, all of which have been developed since the year 2000.

It is noted here that the base-case model calibration described in this report used a relatively low weighting for observations in the high-head, high-gradient area because of the uncertainty associated with those observations. Some of these uncertainties are due to the data in wells G-2 and WT-24.

6.4.4.1 *Water-Level Data Analysis for the Saturated Zone Site-Scale Flow and Transport Model,* REV 00 ICN 01 (Base-case model)

A potentiometric surface map (see Figure 2) was presented in ANL-NBS-HS-000034 REV 00 ICN 01, *Water-Level Data Analysis for the Saturated Zone Site-Scale Flow and Transport Model* (USGS 2001 [154625], Figures 1-1 and 1-2). The purpose of the analysis documented in this USGS report was to provide the SZ site-scale flow model with the configuration of the potentiometric surface and target water-level data for model calibration. This analysis was used to support the Site Recommendation. The source data consisted of water-level data from boreholes within and from one borehole (UE-25 J-11) adjacent to the SZ site-scale model domain. The SZ site-scale model domain coordinates range from Universal Transverse Mercator (UTM) Easting of 533,340 meters to 563,340 meters and from UTM Northing of 4,046,782 meters to 4,091,782 meters (Zone 11, North American Datum 1927) (USGS 2001 [154625], Figure 1-2).

Water levels were used from a number of wells in the northern part of the domain that defined a region of the LHG. An important assumption for this analysis was that while the wells defining the LHG were suspected to represent perched water (USW G-2, UE-25 WT #24), it was decided that there was insufficient data to exclude these water levels from the analysis. The output of this analysis (DTN: GS000508312332.001 [149947]) was used to construct the potentiometric surface using gridding software.

6.4.4.2 *Water-Level Data Analysis for the Saturated Zone Site-Scale Flow and Transport Model,* REV 01 (FY01 Supplemental Science and Performance Analyses)

A potentiometric surface map was presented in ANL-NBS-HS-000034 REV 01, *Water-Level Data Analysis for the Saturated Zone Site-Scale Flow and Transport Model* (USGS 2001 [157611], p. 6). The purpose of the analysis documented in the revision to this USGS report discussed in Section 6.4.4.1 was to provide the SZ site-scale flow model with an updated configuration of the potentiometric surface. The updated water-level data (for Site Recommendation) included water levels obtained from the Nye County Early Warning Drilling Program (EWDP) and data from borehole USW WT-24. This analysis was used in BSC 2001 [154657], *FY01 Supplemental Science and Performance Analyses, Volume 1: Scientific Bases and Analyses*. Source data included data used for the USGS water-level data analysis (USGS 2001 [154625], Sections 6.2 and 7.2), and the potentiometric surface was constructed for the same domain. An alternative conceptual model was considered in this revision by incorporating the following two assumptions**:**

- Water levels in boreholes USW G-2 and UE-25 WT#6 in the northern part of Yucca Mountain and in borehole NC-EWDP-7S in southern Crater Flat represent perched conditions.

- Water levels in USW WT-24, at approximately 840 meters above sea level, represent the regional potentiometric level.

The output of this analysis was a potentiometric surface map assuming perched conditions north of Yucca Mountain (DTN: GS010908312332.002 [163555]). The method used to construct this potentiometric surface differed from that used for the map discussed in the preceding section (USGS 2001 [154625]). Automatic gridding software was used for one USGS water-level data analysis (USGS 2001 [154625]), while contours for the other USGS water-level data analysis (USGS 2001 [157611], Sections 6.1 and 7.2) were hand drawn.

The potentiometric surface maps developed in the USGS water-level data analyses (USGS 2001 [154625]; USGS 2001 [157611], Figure 1-1) are compared in USGS 2001 [157611]). Because the two maps were based on similar data, the general characteristics of the surfaces were similar. The most significant difference noted is the representation of the LHG area north of Yucca Mountain. Exclusion of water-level data from boreholes USW G-2 and UE-25 WT #6 considered to represent perched conditions reduced the LHG significantly. Another difference noted is that potentiometric contours in USGS 2001 [157611] are no longer offset where they cross faults. Offsets in the USGS (USGS 2001 [154625]) map were noted in the USGS water-level data analysis (USGS 2001 [157611]) and were described as unexpected where contours are perpendicular or nearly perpendicular to faults. The contour interval for this map (Figure 8) is variable with an interval of 50 meters for contours greater than 800 meters and 25 meters for contours less than 800 meters. Two additional contours, 730 meters and 720 meters, are also included to improve visualization of the effect of the fault along Highway 95 south of Yucca Mountain on the groundwater flow system.

6.4.4.3 *Calibration of the SZ Site-Scale Flow Model,* REV 00 ICN 01

Calibration of the SZ site-scale flow model is described in the previous version of this model report, MDL-NBS-HS-000011, *Calibration of the Site-Scale Saturated Zone Flow Model* (BSC 2001 [155974]). The purpose of the flow-model calibration was to adjust model parameters until the simulated water levels best matched target water levels. Target water levels for the SZ site-scale flow model calibration were those developed by the USGS (USGS 2001 [154625]) water-level data analysis. Once the flow model was calibrated, simulated water levels were contoured to produce a potentiometric surface (Figure 9), and measured and simulated water-level surfaces were compared. Given that the intent of the calibration was to match the simulated water levels with the measured water levels, it is not surprising that the simulated potentiometric surface is qualitatively similar to the surface in the report USGS 2001 ([154625]). The calibrated model qualitatively reproduced important features of the potentiometric surface, such as the low-gradient region in the Fortymile Wash area, the LHG in the area north of Yucca Mountain, and the flow disruption caused by the Solitario Canyon Fault. Differences between the USGS 2001 ([154625], Figure 1-2) potentiometric surface and the simulated surface were the greatest in the LHG area north of Yucca Mountain where differences in water levels were on the order of 100 m. Differences on the order of 50 m were noted in the area of the east-west barrier and the Solitario Canyon Fault.

6.4.4.4 UZ Model Lower Boundary for the Unsaturated Zone Flow and Transport Model

The development of numerical grids of the unsaturated hydrogeologic system beneath Yucca Mountain is described in ANL-NBS-HS-000015, *Development of Numerical Grids for UZ Flow and Transport Modeling* (BSC 2003 [160109]). A representation of the potentiometric surface was an output of this analysis report because this surface defined the lower UZ model boundary (see Figure 10). The domain for this interpretation of the potentiometric surface is smaller than the SZ site-scale model domain encompassing approximately 40 km^2 (BSC 2001 [159356], Sections 5 and 6.2) as compared to the approximately 1,350 km^2 of the SZ site-scale model domain (USGS 2001 [154625], Figures 1-1 and 1-2).

The lower boundary for the UZ model was established using water levels consistent with the perched water interpretation of the USGS water-level data analysis (USGS 2001 [157611]). Two gridding steps were used to create a reference horizon file representing the lower boundary. This gridding process was noted in BSC (2001 [159356]) as producing small deviations in the resulting potentiometric surface with respect to the original surface. These deviations were considered to be relatively minor (i.e., less than 5 m in the vicinity of the repository footprint). Larger differences of up to 60 m between the output potentiometric surface and the USGS (2001 [157611]) surface were attributed to errors associated with contour digitization prior to generation of the potentiometric surface (BSC 2001 [159356], Sections 5 and 6.2) and Attachment IV.

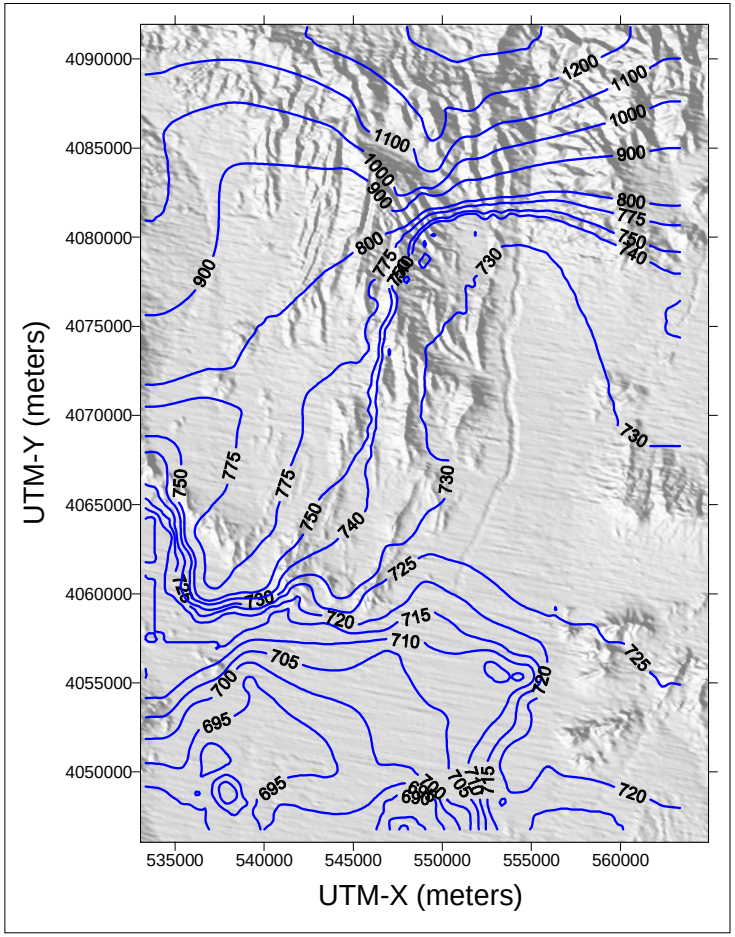

DTN: GS000508312332.001 [149947].

Figure 8. Contour Plot of Water-Level Data for the *Saturated Zone Flow and Transport Model*, REV 01

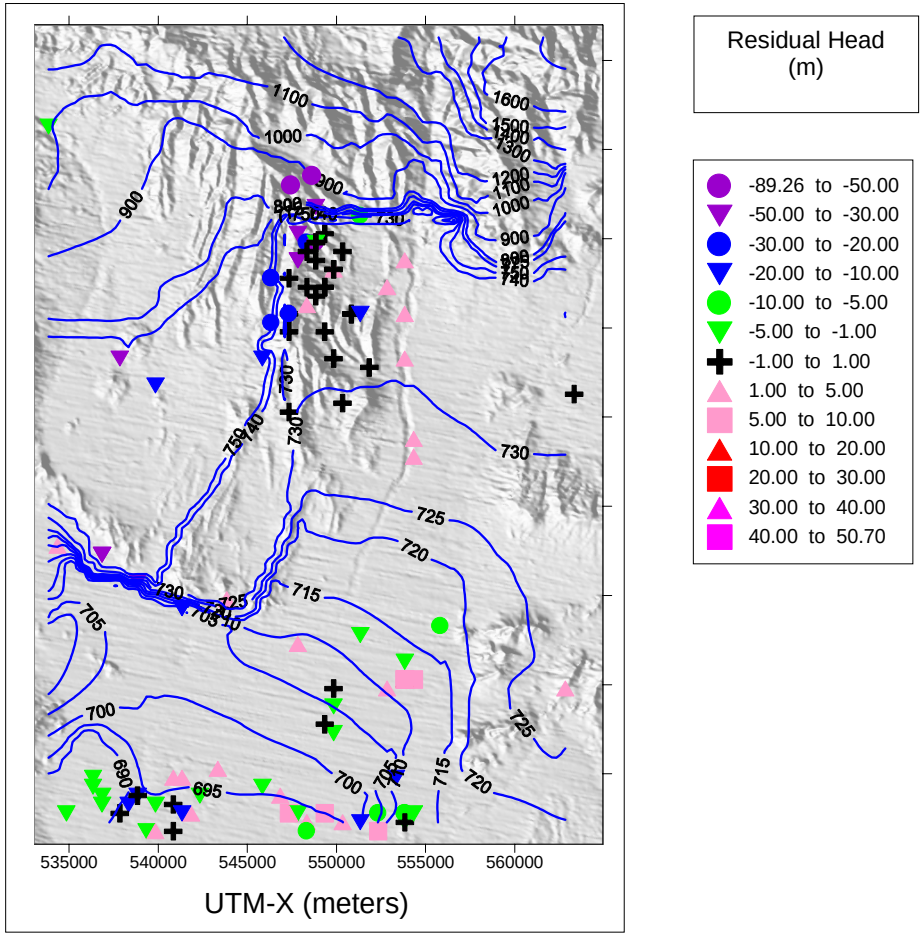

Source : BSC (2001 [155974], Figure 7).

NOTE: Symbols indicate well locations.

Figure 9. Simulated Water-Level Data with Residual Heads in *Calibration of the SZ Site-Scale Flow Model,* REV 00 ICN 01

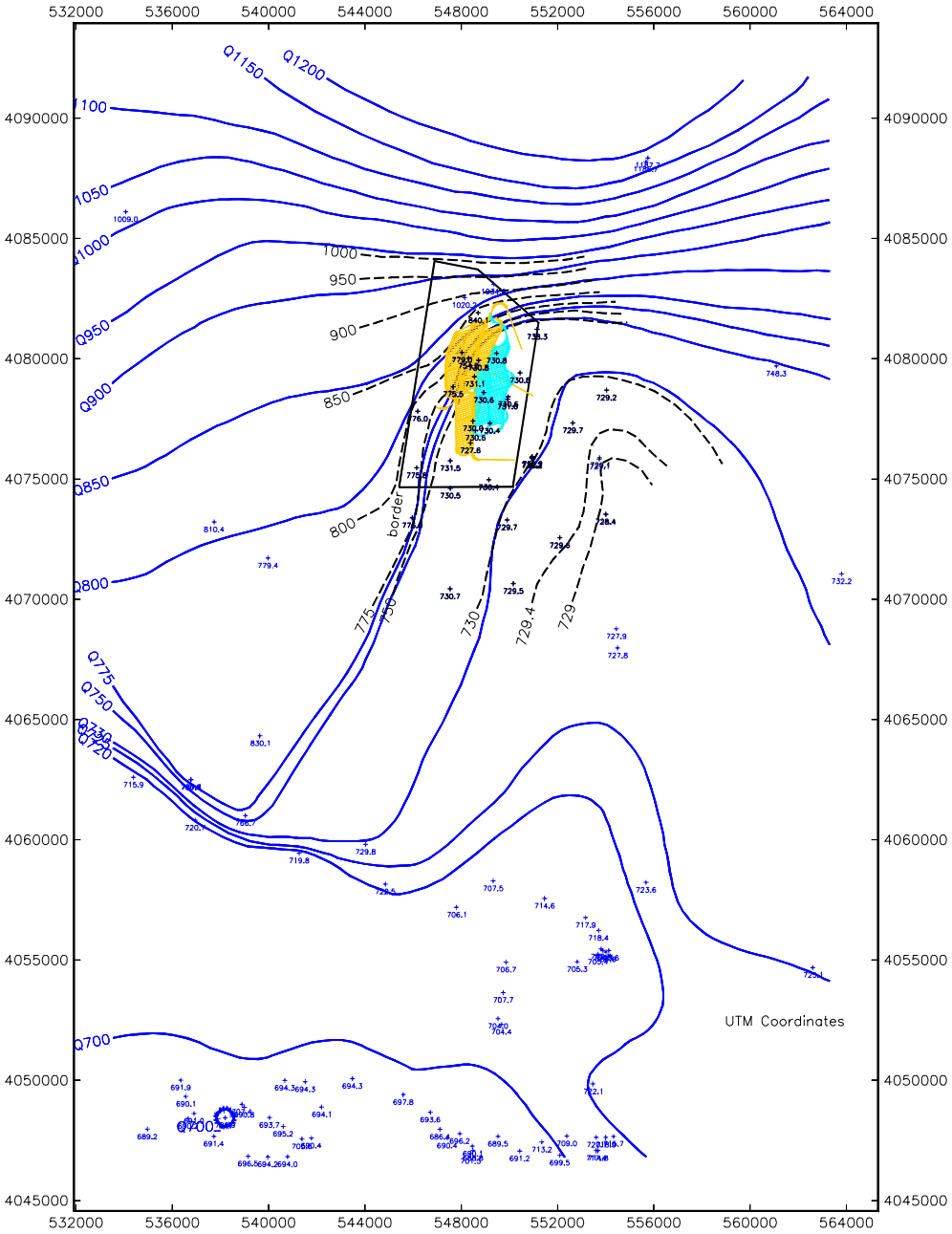

Source: BSC (2003 [160109], Attachment IV-11, Figure IV.2-1).

NOTE: 2002 Repository Lower Block (shown in turquoise) will not be used in any LA calculations.

Figure 10. Overview of Contour Lines Representing Qualified (solid lines, blue points and labels) and Unqualified (dashed lines, black points and labels) Data Sets for the UZ Lower Model Boundary

In summary, the potentiometric surface derived from the base-case flow model calibration in the previous version of this model report (BSC 2001 [155974], Section 6.4.2) qualitatively reproduces important features of the potentiometric surfaces presented in the reports: USGS (2001 [154625]), USGS (2001 [157611], Section 6-2), and BSC (2001 [159356]), such as the low-gradient region in the Fortymile Wash area, the LHG in the area north of Yucca Mountain, and the flow disruption caused by the Solitario Canyon Fault. Due to its smaller domain, comparison of the surface derived from the base-case flow model calibration to BSC (2001 [159356]) is limited. Differences in potentiometric surfaces can be attributed to differences in purpose, assumptions, conceptual models, and methods by which the surfaces were constructed.

6.4.5 Water-Table Rise

Wetter, glacial climatic conditions are expected to occur in the future at the Yucca Mountain site within the 10,000 year period of regulatory concern (CRWMS M&O 2000, Section 2 [143665]). These changes in the climate relative to present conditions would affect groundwater flow in the SZ by significantly increasing the amount of recharge to the regional groundwater flow system. These regional and local increases in recharge will tend to increase the groundwater flux through the SZ system and lead to a rise in the water table beneath Yucca Mountain.

The effects of climate change on radionuclide transport simulations in the SZ are incorporated into the TSPA analyses by scaling the simulated SZ breakthrough curves by a factor representative of the alternative climate state (BSC 2001, Section 6.2.5 [157132]). The scaling factor used in this approach is the ratio of average SZ groundwater flux under the future climatic conditions to the flux under present conditions. This approach approximates the impacts of future, wetter climatic conditions in which the SZ groundwater flux will be greater. However, this approach implicitly assumes the same flow path for radionuclide transport through the SZ under wetter climatic conditions of the future. In reality, significant rise in the water table due to climatic changes would result in different flow paths through the SZ system, including the potential for encountering different hydrogeologic units by radionuclides during transport.

The objective of this modeling task is to adapt the SZ site-scale flow model to include the effects of estimated water-table rise and to compare the results of particle-tracking simulations using this adapted model to the simple flux scaling approach used in TSPA analyses. It has been assumed, based on qualitative arguments, that the flux scaling approach to simulation of climate change is conservative with regard to radionuclide transport in the SZ, relative to the more realistic situation in which water-table rise is included in the modeling. The purpose of this section is to both verify that assumption and provide an upper bound on the future climate fluxes.

6.4.5.1 Estimating Water-Table Rise from Climate Change

Rise in the water table during wetter climatic conditions at Yucca Mountain is a complex function of greater recharge to the SZ and changes to the amount and spatial distribution of discharge from the regional SZ system. Simulations of groundwater flow under wetter, glacial climatic conditions with the SZ regional-scale flow model (D'Agnese et al. 1999 [120425]) indicate that groundwater flow paths from beneath Yucca Mountain do not change much under glacial climatic conditions. These simulations also show that groundwater discharge from the SZ

for the wetter glacial climate would not occur along the flow path from Yucca Mountain at any location closer than the regulatory limit of about 18 km south of the repository.

The estimated elevation of the water table under wetter, glacial climatic conditions within the domain of the SZ site-scale flow model is calculated using the software code WTCONVYD V.1.00 (STN: 10815-1.00-00; Sandia National Laboratories 2002 [163835]). This software code uses an algorithm that incorporates qualitative information on the paleo-flow system, an estimate of increased -groundwater flux under glacial conditions, and physical limits to the position of the water table. The software code calculates the estimated rise in the water table using this algorithm, along with data on the present water-table surface and the elevations of the topographic surface.

Estimates of the elevation of the water table under Yucca Mountain for wetter, glacial-transition climatic conditions indicate that the water table could have been on the order of 100 m higher under these conditions. The water table is calculated by the WTCONVYD V.1.00 (STN: 10815-1.00-00; Sandia National Laboratories 2002 [163835]) software code as 100 m higher than present conditions in the area beneath Yucca Mountain. In those areas of the model domain where the present water table has an elevation of greater than 730 m (the approximate water level observed beneath Yucca Mountain), the elevation of the water table under glacial conditions is also calculated to be 100 m higher than present conditions by the software code, except where the topographic surface is less than 100 m above the present water table. This exception occurs in the canyon of Fortymile Wash in the northern part of the model domain where the water table under glacial conditions is calculated by the software code to occur within 1 m of the topographic surface. There is little information upon which to base estimates of the water table configuration under glacial-transition climatic conditions in the area to the north of Yucca Mountain in the SZ site-scale flow model domain. However, the approach used in the WTCONVYD V.1.00 (STN: 10815-1.00-00; Sandia National Laboratories 2002 [163835]) software code is reasonable and has little impact on the flow system down gradient of Yucca Mountain in the SZ site-scale flow model.

Simulations of groundwater flow under wetter glacial climatic conditions with the SZ regional-scale flow model (D'Agnese et al. 1999 [120425]) indicate that the groundwater flux in the area of Yucca Mountain would be about four times greater than at present (BSC 2001, Section 6.2.5 [157132]). The software code WTCONVYD V.1.00 (STN: 10815-1.00-00; Sandia National Laboratories 2002 [163835]) calculates the higher water-table elevations for glacial conditions such that the approximate hydraulic gradient would be greater by a factor of four for locations in the model domain where the present water table is between 700-m and 730-m elevation. This range of water-table elevations covers that portion of the SZ flow system along the flow path from beneath the repository to the regulatory limit of about 18 km south of the repository. The approximation used by the software code in this approach assumes that the average permeability along the flow path would not differ significantly between present conditions and the glacial climatic conditions and that a four-fold increase in the gradient would result in an approximately four-fold increase in the groundwater flux. Finally, the software code increases the elevation of the water table by a uniform value of 10 m for locations within the model domain where the present water table is less than 700 m elevation. This condition occurs only in the southern part of the SZ site-scale flow model domain where the water table is located in the valley-fill alluvium unit and the hydraulic gradient is relatively low. The elevation of the water table under

glacial climatic conditions is relatively unimportant with regard to the hydrogeologic unit configuration because of the thick alluvium in this area of the model domain.

The software code WTCONVYD V.1.00 (STN: 10815-1.00-00; Sandia National Laboratories 2002 [163835]) also limits the estimated rise in the water table under glacial climatic conditions to within one meter of the topographic surface, which constitutes a physical limit to the rise in the water table within the domain of the SZ site-scale flow model. Rise of the water table to within one meter of the surface would induce significant groundwater discharge by evapotranspiration and the formation of local springs.

The estimated elevations of the water table under wetter, glacial climatic conditions, as calculated by the WTCONVYD V.1.00 software code (STN: 10815-1.00-00; Sandia National Laboratories 2002 [163835]), are shown in Figure 11. Note that the pattern of the contours for the water table surface is generally similar to the present water table, with the exception of the area in Fortymile Canyon in the northern part of the model domain and in some areas in the south-central and southwestern parts of the model domain. These areas, in which the contours of the estimated higher water table are more irregular, are areas of shallow groundwater under glacial climatic conditions.

Figure 12 shows the estimated depth to the water table under wetter, glacial climatic conditions, as calculated by the WTCONVYD V.1.00 software code (STN: 10815-1.00-00; Sandia National Laboratories 2002 [163835]). The areas in which the estimated water table is within 5 m of the topographic surface are shown with the light blue shading. The larger light-blue area of shallow estimated groundwater in the southwestern part of the domain contains the three areas of paleo-spring deposits located along Highway 95 and at the southern end of Crater Flat. This shows a certain degree of consistency between the estimated higher water table and the geologic features associated with Pleistocene spring discharge. The specific paleo-spring locations are probably controlled by structural features that are below the resolution of the analysis of the estimated water-table elevation under glacial climatic conditions. The other site of shallow estimated groundwater shown in Figure 12 is Fortymile Canyon. Although paleo-spring deposits are not observed in Fortymile Canyon, it is not unreasonable to postulate that such deposits would not be preserved in such an active geomorphic location as the bottom of this canyon. In any event, the large block sizes of the numerical model would average out heterogeneities of this scale.

In summary, a reasonable estimate of the water table elevation under wetter, glacial climatic conditions is developed for the SZ site-scale flow model domain. The estimated rise in the water table is consistent with the estimated increase in groundwater flux along the inferred flow path from beneath the repository. In addition, the pattern of the estimated rise in the water table is generally consistent with the locations of paleo-spring deposits within the domain.

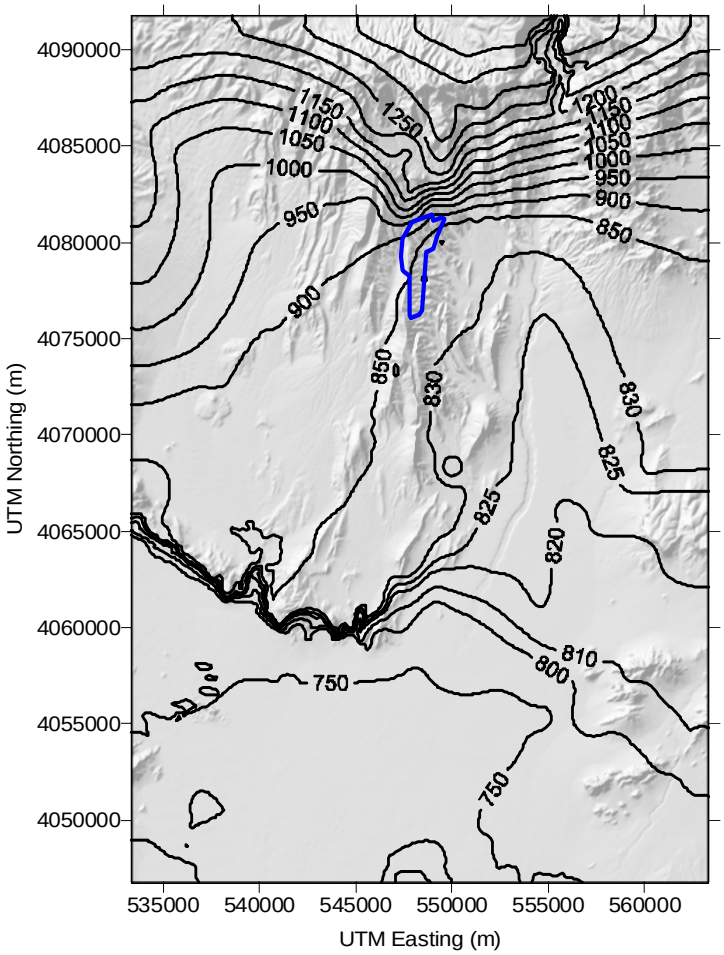

Source for repository outline (BSC 2003 [162289]). For illustration purposes only.

NOTE: Repository outline shown with bold blue line.

Figure 11. Estimated Water-Table Elevations for Future Glacial Climatic Conditions

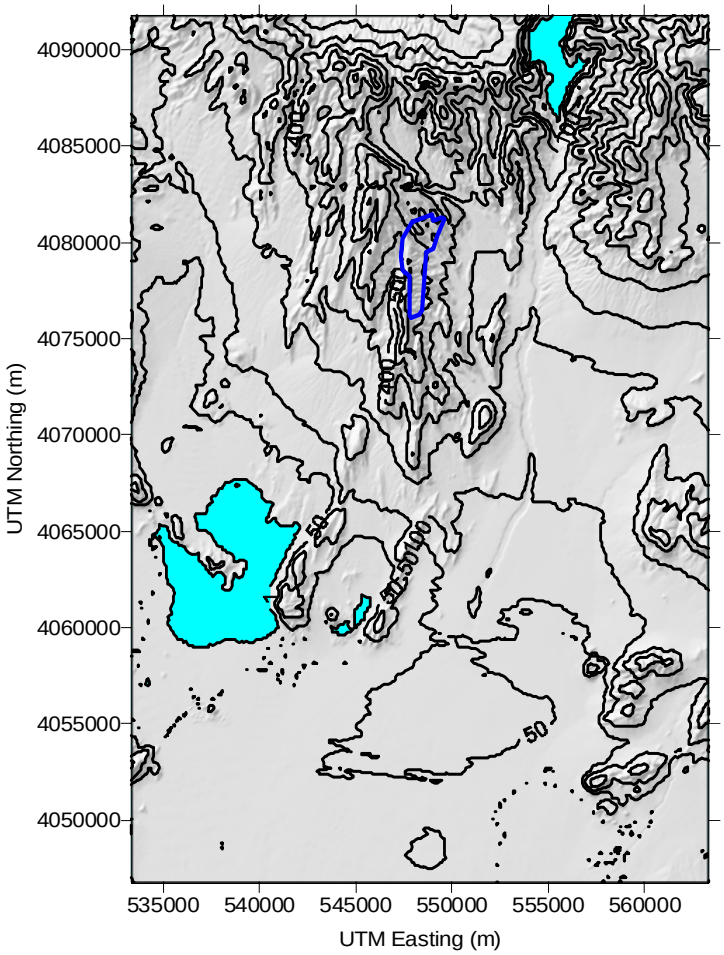

Source for repository outline (BSC 2003 [162289]). For illustration purposes only.

NOTE: Repository outline shown with bold blue line. Areas with estimated depth to the water table of less than 5 m are shown with light blue shading.

Figure 12. Estimated Depth to the Water Table for Future Glacial Climatic Conditions

6.4.5.2 Water-Table Rise in the SZ Site-Scale Flow Model

The SZ site-scale flow model is adapted to the higher estimated water table for glacial climatic conditions by creating a new grid with an upper surface corresponding to the higher water table. The lateral and bottom boundary locations remain the same in this adaptation of the model. The spatial distributions of hydrogeologic units at the water table in the flow model under present conditions and in the adapted model with the higher estimated water table are shown in Figures 13 and 14, respectively.

Comparison of Figures 13 and 14 indicates potentially significant differences in the hydrogeologic units present in the shallow SZ beneath the repository and along the inferred flow path to the south and east of the repository at depths corresponding to the position of the water

table at the different climatic conditions. The upper volcanic confining unit is much more widely distributed at the water table beneath the repository under estimated future glacial climatic conditions than it is under present conditions, particularly under the northern and eastern parts of the repository. To the south and east of the repository, the alluvium unit is present at the water table over a broad area under estimated future conditions, where this unit is absent under the present conditions.

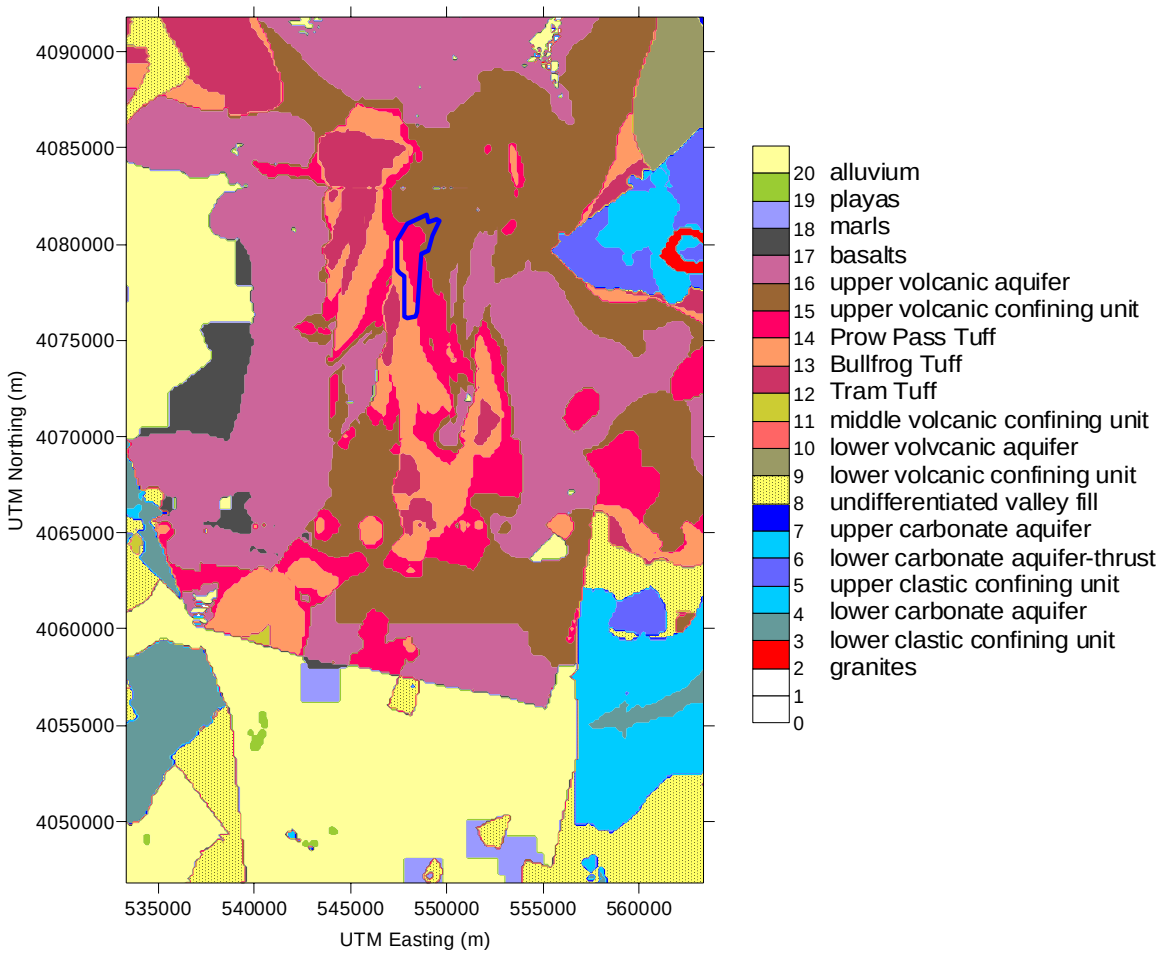

Source for repository outline (BSC 2003 [162289]). For illustration purposes only.

NOTE: Repository outline shown with bold blue line.

Figure 13. Hydrogeologic Framework Model Units at the Water Table for Present Conditions

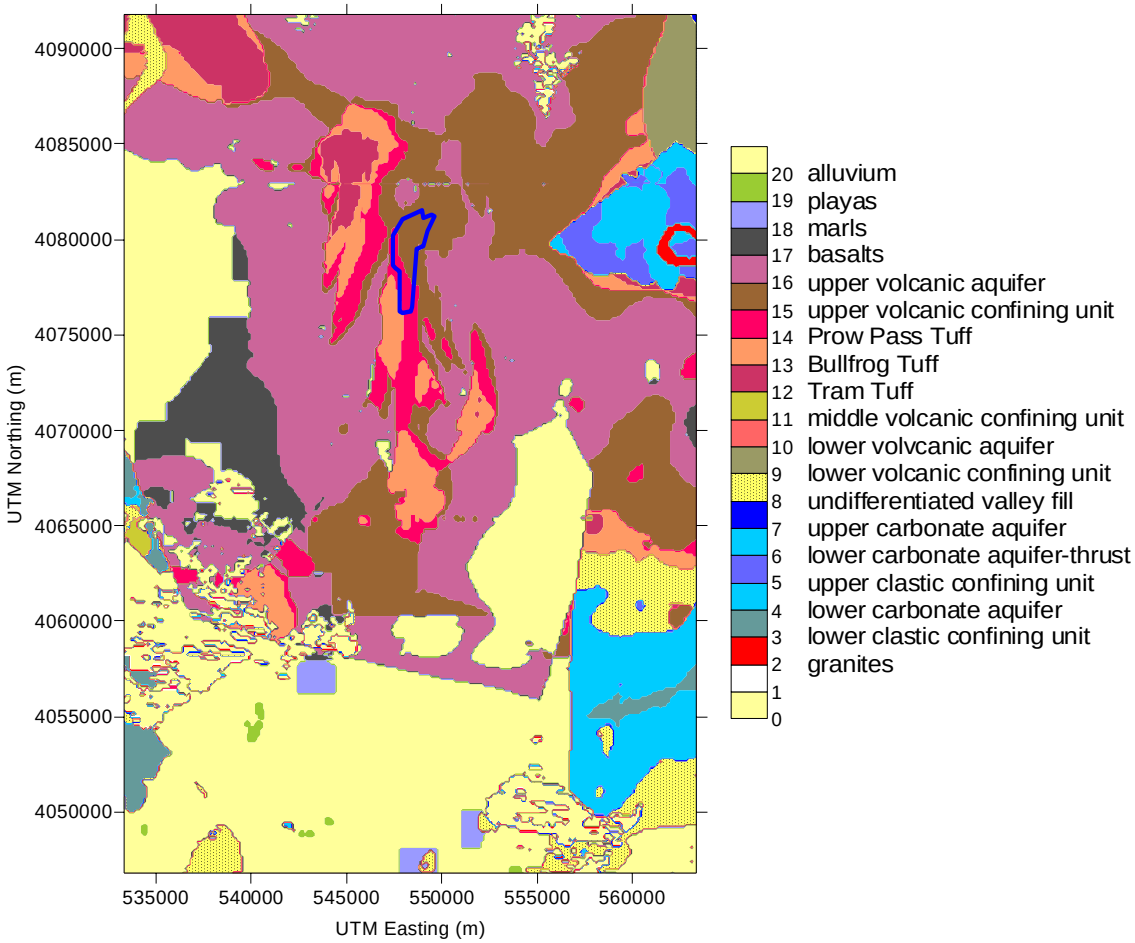

Source for repository outline (BSC 2003 [162289]). For illustration purposes only.

NOTE: Repository outline shown with bold blue line.

Figure 14. Hydrogeologic Framework Model Units at the Water Table for Estimated Future Glacial Climatic Conditions

6.4.6 Summary of the Alternative Conceptual Models

Table 8 summarizes the ACMs considered and their screening status. Based on the screening out of the ACMs considered, the SZ site-scale flow model discussed in this model report was determined to be the most appropriate model for use in TSPA-LA calculations.

Table 8. Alternative Conceptual Models Considered

Alternative Conceptual Model	Key Assumptions	Screening Assessment and Basis	Uncertainty Propagation Forward
Large Hydraulic Gradient	The large hydraulic gradient (LHG) is a result of perched water or a result of flow permeability or large head.	Different conceptualizations of a LHG do not result in different flow field or specific discharge results. This is based on analysis of the various conceptualizations of the LHG.	This is not necessary to propagate forward.
Solitario Canyon	Solitario Canyon goes deep into the Carbonate Aquifer or it only goes to the top of the Carbonate Aquifer.	Different conceptualizations of the role of Solitario Canyon do not result in different flow field or specific discharge results. This is based on computer analysis and simulation of the representation of Solitario Canyon. See Section 6.7.2.1.	This is not necessary to propagate forward.
Vertical anisotropy	Vary the range of the vertical to horizontal permeability.	The range of vertical to horizontal permeability affects the flow field and the specific discharge.	This is not necessary to propagate forward.
Horizontal anisotropy	Vary the range of the horizontal maximum to horizontal minimum permeability.	The range of horizontal maximum to horizontal minimum permeability affects the flow field and the specific discharge.	This uncertainty needs to be propagated in the generation of breakthrough curves.
Potentiometric surface	Different potentiometric interpretations of water-level data.	Compare model predictions of potentiometric surface to the different interpretations. The different interpretations do not affect the flow field or specific discharge results.	This is not necessary to propagate forward.
Water table rise due to future climates	Future climates can change water table levels.	Compare model predictions of using different water table levels. The different interpretations do not affect the flow-field spatial distribution (only the magnitude).	This is not necessary to propagate forward. Specific discharge calculations involve only the scaling of base-case results.

6.5 MODEL FORMULATION OF BASE-CASE CONCEPTUAL MODEL

6.5.1 Mathematical Description of Base-Case Conceptual Model

An effective continuum approach is adopted for simulating groundwater flow through the fractured rock and alluvial materials within the domain of the site-scale SZ flow model. Based on this conceptualization, the equations governing groundwater flow can be derived by combining the equations describing the conservation of fluid mass and Darcy's Law (Freeze and Cherry 1979, Section 2.11 [101173]). The equations presented below are for an isotropic, isothermal medium. The conservation of fluid mass is

$$\frac{\partial A_{mass}}{\partial t} + \overline{\nabla} \cdot \overline{f}_{mass} + q_{mass} = 0 \qquad \text{(Eq. 1)}$$

where

A_{mass} is the fluid mass per unit volume given by

$$A_{mass} = \phi \rho_l \qquad \text{(Eq. 2)}$$

$\overline{f}_{mass}$ is the fluid mass flux given by

$$\overline{f}_{mass} = \rho_l \overline{v} \qquad \text{(Eq. 3)}$$

ϕ is the porosity in the system (dimensionless)
ρ_l is the fluid density (kg/m^3)
$\overline{v}$ is the fluid velocity (m/s)
q_{mass} is the fluid mass source (kg/s).

The velocity of the fluid can be expressed by Darcy's Law:

$$\overline{v} = -\frac{k}{\mu}(\overline{\nabla} P - \rho_l g) \qquad \text{(Eq. 4)}$$

where

μ is the dynamic viscosity of the fluid (kg/m/s)
P is the fluid pressure (pa)
k is the permeability (m^2)
g is the acceleration resulting from gravity(m^2/s)

Equations 1 and 4 can be combined to yield:

$$-\overline{\nabla} \cdot D_{mass} \overline{\nabla} P + q_m + \frac{\partial}{\partial z} g D_{mass} \rho_l + \frac{\partial A_{mass}}{\partial t} = 0 \qquad \text{(Eq. 5)}$$

which is the fundamental equation describing groundwater flow. Here z is oriented in the direction of gravity and the transmissibility is given by

$$D_{mass} = \frac{k\rho_l}{\mu}.$$

Groundwater flow is simulated in the site-scale SZ flow model by obtaining a numerical solution to this equation. Solution of this equation requires the specification of the pressure at the boundaries of the solution domain. For steady-state calculations, solution of this equation does not require specification of initial conditions (initial pressure distribution throughout the solution domain), because Equation 5 (at very large times) represents steady-state flow, which is independent of initial conditions.

Conservation of fluid-rock energy is expressed by the equation

$$\frac{\partial A_e}{\partial t} + \overline{\nabla} \cdot \overline{f_e} + q_e = 0, \qquad \text{(Eq. 6)}$$

where the energy per unit volume, A_e, is given by

$$A_e = (1-\phi)\rho_r u_r + \phi \rho_l u_l, \qquad \text{(Eq. 7)}$$

with $u_r = c_{pr} T$, and the energy flux, $\overline{f_e}$, is given by

$$\overline{f_e} = \rho_l h_l \overline{v} + K \overline{\nabla} T. \qquad \text{(Eq. 8)}$$

Here,

the subscript r refers to the rock matrix
the subscript l refers to the liquid
u_r and u_l are specific internal energies
c_{pr} is the specific heat
h_l is specific enthalpy
K is an effective thermal conductivity
T is the temperature and
q_e is the energy contribution from sources and sinks.

Equations (6) and (4) can be combined to yield:

$$-\overline{\nabla} \cdot (D_e \overline{\nabla} P) - \overline{\nabla} \cdot (K \overline{\nabla} T) + q_e + \frac{\partial}{\partial z} g D_e \rho_l + \frac{\partial A_e}{\partial t} = 0, \qquad \text{(Eq. 9)}$$

where the transmissibility term is given by

$$D_e = h_l D_{mass} \qquad \text{(Eq. 10)}$$

Here, the subscript *e* refers to energy.

6.5.2 Computational Model

The FEHM software code V 2.20 (STN: 10086-2.20-00; LANL 2003 [161725]) is used in site-scale SZ modeling to obtain a numerical solution to the mathematical equation describing groundwater flow (Equation 5). FEHM is a nonisothermal, multiphase flow and transport code that simulates the flow of water and air, and the transport of heat and solutes, in 2-D and 3-D saturated or partially saturated heterogeneous porous media. The code includes comprehensive reactive geochemistry and transport modules and a particle-tracking capability. Fractured media can be simulated using an equivalent continuum, discrete fracture, dual porosity, or dual permeability approach. A subset of the FEHM code capabilities is used in the SZ site-scale flow model. Single-phase, isothermal flow is simulated in the SZ site-scale flow model.

The control-volume finite element (CVFE) method is used in FEHM to obtain a numerical solution to the groundwater flow equation over the model domain. Finite-element methods are based on the assumption that a continuum may be modeled as a series of discrete elements. For each element, equations based on a discretized form of the groundwater flow equation are written that describe the interaction of that element with its neighbors. These equations describe the hydrologic behavior of the elements. This discretization leads to a set of equations that must be solved numerically to obtain the values of groundwater pressure at each node throughout the model domain.

The CVFE method has been used extensively in petroleum reservoir engineering (Forsyth 1989 [144110]). The CVFE method treats the potentials in a finite-element approach while the control-volume aspect allows local mass conservation and upstream weighting (Verma and Aziz 1997 [143606]). Quadrilaterals and triangles in two dimensions and hexahedra and tetrahedra in three dimensions are divided into volumes associated with gridblocks and areas associated with interblock distances. The gridblock volumes are the Voronoi volumes (Forsyth 1989 [144110]) associated with each gridblock. Voronoi volumes are also called perpendicular bisector volumes. The Voronoi volume is formed by boundaries that are orthogonal to the lines joining adjacent gridblocks and that intersect the midpoints of the lines (Verma and Aziz 1997 [143606]). Any point within a Voronoi volume is closer to its associated gridblock than to any other node in the grid. The CVFE method can be shown on simple elements with constant properties to be equivalent to traditional finite-element methods.

The stiffness coefficients (e.g., elements of the stiffness matrix) of the traditional finite-element method can be interpreted as a linear function of the area through which the fluid passes traveling from one node to its neighbor. A stiffness coefficient uses the area of the boundary of the Voronoi volume that intersects the line joining adjacent nodes. LaGriT V1.0 (STN: 10212-1.0-00; LANL 2001 [149148]) is designed to produce CVFE grids.

These terms are used to form control-volume difference equations for the conservation equations. This method is not traditional because equation parameters are defined by node, not

element, but the method leads to an intuitive understanding of the numerical method.

In FEHM, the nodal definition of equation parameters leads naturally to a separation of the nonlinear and purely geometric parts. This separation is explained in detail in Zyvoloski (1983 [101171]) and is valid over lower-order elements. The nonlinear part uses average inverse kinematic viscosity,

$$D = \frac{\rho}{\mu} \qquad \text{(Eq. 11)}$$

between two nodes, which is usually taken to be the upstream nodal value. The result is a much more stable code for solving nonlinear problems while still retaining much of the geometric flexibility of finite elements. This method has been used in FEHM since 1983 (Zyvoloski 1983 [101171]) and has been extensively verified (*Validation Test Report (VTR) for FEHM V 2.20*, SDN: 10086-VTR-2.20-00, LANL 2003 [161725]). An harmonic weighting of the intrinsic permeability is used. It is noted that even though the SZ flow model is linear, the fact that it uses spatially varying viscosity terms (due to spatially varying temperatures), upwinding the viscosity terms is the standard way of modeling the interblock fluid fluxes. The Newton-Raphson iteration is applied to the system of equations, which is solved with a multi-degree of freedom and preconditioned, conjugate gradient methods using Generalized Minimum Residual (GMRES) or biconjugate gradient-squared acceleration techniques.

6.5.3 Base-Case Model Inputs

The development of the base-case site-scale SZ flow model involves the input of data from a number of sources, including water level and head distributions, definition of the hydrogeologic units, distribution of recharge flux and lateral fluxes into the model domain, feature and fault distribution, temperature profiles in wells, and boundary conditions. The data sources for these inputs are identified in Table 2.

Incorporation of these inputs into the site-scale SZ flow model first requires the generation of a hydrogeologic framework and a computational grid. The hydrogeologic framework model (HFM) and known features of the site are used to design a grid for flow modeling. Once a computational grid is formulated, these data inputs are used to assign the hydrogeologic units and features, recharge fluxes, hydrogeologic properties, and boundary conditions at node points throughout the computation grid. Each of these elements of model development is discussed below.

6.5.3.1 Hydrogeologic Framework Model Overview

The geometry of geologic units is defined in Stratamodel Framework files (DTN: GS030208312332.001 [163087]), which characterize a three-dimensional (3-D) Geocellular model of the site base-case HFM for the SZ (output from USGS 2001 [158608]). In depth, the HFM domain extends from the interpreted potentiometric surface (DTN: GS000508312332.001 [149947]) to the base of the regional groundwater flow model. The data in the Stratamodel Framework files conform to the Geologic Framework Model (GFM) (USGS 2001 [158608], Section 6.3.2) in areas where the GFM is valid and comprises additional information for the

other areas of the SZ model. The HFM is constructed by combining a set of structured contour maps representing the tops of hydrogeologic units using the Stratamodel software product (Landmark Graphics 1998 [153238]). The construction of the HFM includes data from geologic maps and sections, borehole data, geophysical data, and existing geologic models. This representation enables the computational grid to be populated with an initial set of hydrologic properties for the calibration of the flow model. The HFM and its development are documented in the model report USGS 2001 [158608]. It is noted that the base-case HFM also includes, as its top surface, the base-case water-table definition.

The HFM grid consists of a rectangular array of nodes with a spacing of 125 meters. This selection simplifies the available data near the repository and extrapolates from very widely spaced data in other areas of the model domain. The 3-D HFM was constructed by stacking the set of structure contour maps using "geologic rules" of the Stratamodel software (Landmark Graphics 1998 [153238]). The software allows for the specification of sedimentary depositional units, as well as truncation and faulting. Stratigraphic intrusions are included by arranging the order of the stacking sequence. This ordering begins at a depth that is the same as the base of the HFM regional flow model (DTN: GS960808312144.003 [105121]) and the granitic intrusions as the first geologic unit. The lower clastic confining unit was input and truncated where the granitic intrusions were above this grid. The remaining units were entered in order onto the lower clastic confining unit and intrusions, and a special surface was placed within the sequence to represent the thrust-faulted geometries. The valley-fill aquifer and confining units were then emplaced in the valleys.

The HFM was constructed to represent faults and other hydrogeologic features (such as zones of hydrothermal alteration) that affect SZ flow. Information on faults included fault trace maps, which show faults on cross sections and the locations where faults intersect the land surface. Faults in the model area can dip at almost any angle, but most are high-angle faults. Given software constraints and the numerical flow model resolution, faulting in the area was simplified, and the faults were treated as vertical features. Faults deemed important to flow near Yucca Mountain were modeled explicitly in the numerical SZ flow model. The hydrogeologic features that influence the flow field are identified separately (Potter et al. 2001 [159398]) and discussed in Section 6.5.3.3. These features are included in the SZ numerical model by permeability zones in FEHM V 2.20 (STN: 10086-2.20-00; LANL 2003 [161725]).

Important thrust faults were represented by repeating hydrogeologic units in the HFM. When geologic structural or stratigraphic surfaces are stored as arrays, they cannot have multiple *z*-values at one location. This limitation means that thrust faults and mushroom-shaped intrusions cannot be represented by an array. To deal with these problems, simplifying techniques were used. Where units were repeated by thrust faults, two different grids were created for the same hydrogeologic unit. A unit boundary map was then added to define an outline for the perimeter of the thrust sheet. Within this boundary, hydrogeologic structural altitude values were treated as defining unique additional hydrogeologic unit(s). Where units were continuous across this boundary, altitudes of surfaces are the same on each side of the boundary, making the boundary "invisible." Because of the large number of faults in the SZ site-scale model area and limitations in modeling technology, only those faults and other features of hydrologic importance were constructed in the HFM (USGS 2001 [158608], Figure 6-2).

Most of the special features are defined as extending from the top of the carbonate aquifer to the top of the model (water table). Exceptions to this generalization are the Spotted Range-Mine Mountain zone, which extends from the top of the model to the bottom; the Alluvial uncertainty zone, which extends from the top of the model down through the undifferentiated valley fill; and the Imbricate fault zone, which extends from the top of the model to the top of the undifferentiated valley fill (Table 12).

The top of the HFM is truncated by an interpreted water-table surface as described in USGS (2001 [154625], Section 6.2). A surface contour map was constructed using potentiometric data from various borehole locations (USGS 2001 [158608], Figure 6-2, p. 27). Data from the uppermost completed borehole intervals were used. Borehole data for this HFM were estimated from the digital elevation model (DEM) for data model consistency. The elevations were derived from USGS 3-arc-second 1-by1 degree DEM files. The water table forms the upper surface of the HFM with grid values sampled from the potentiometric map to 125-m spacing coincident to the HFM. These water-level data have been updated in USGS (2001 [157611]). Additional borehole data and a potentiometric-surface map represent an alternate conceptual model from that presented in USGS 2001 [154625] of water levels north of Yucca Mountain. These can be found on p. 25 of USGS 2001 [157611].

6.5.3.2 Grid Generation

The computational grid for the site-scale SZ flow model is developed using LaGriT V 1.0 (STN: 10212-1.0-00, LANL 2001 [149148]) grid-generation software. The computational grid is designed so that the horizontal grid is coincident with the grid cells in the regional-scale SZ flow model. The extent of the computational grid is shown in Figure 15 and Table 9. The depth of the computational grid is approximately the same as depth of the regional-scale SZ flow model. The top of the computational grid begins at the water table surface and extends to a depth of 2,750 m (9,020 ft) below sea level.

Table 9. Bounding Box

Box Direction	UTM coordinates (m)
west to east	533,340 to 563,340
south to north	4,046,780 to 4,091,780
bottom to water table	–2,200 to 1,200

Source: USGS (2001 [158608]).

A structured grid using orthogonal hexahedral elements is chosen for the site-scale SZ flow model. Previous models (Czarnecki et al. 1997 [100377]) of Yucca Mountain SZ flow and transport have used both unstructured (finite element) meshes and structured orthogonal grids. However, the principal reason structured grids are used for this work is to allow for the use of the streamline particle-tracking transport capability of FEHM V 2.20 (STN: 10086-2.20-00; LANL 2003 [161725]). Although the structured meshes are not as flexible as unstructured meshes in fitting complex geometry, tests have shown that they provide accurate solutions as long as there is adequate resolution to represent the geometry of the different materials in each hydrogeologic layer. Moreover, there must be enough resolution to account for any large gradients present in

the flow or transport model. The adequacy of grid resolution is investigated by running a flow model using various grids of differing resolutions. If little difference is found among model results using grids of increasing resolution, those resolutions at which the model differences become minimal can be used to identify suitable grid resolutions. An exhaustive study (Bower et al. 2000 [149161]) of the accuracy of both the flow and transport solution was performed on 10 grids with horizontal resolutions ranging from 500 m to 10,000 m to determine the appropriate horizontal grid resolution for the flow model. Although the study was based on an earlier GFM, the results show that the 500-m grid is entirely adequate to meet the objectives of the site-scale SZ flow model. Consequently, a horizontal grid spacing of 500 m is used in this model.

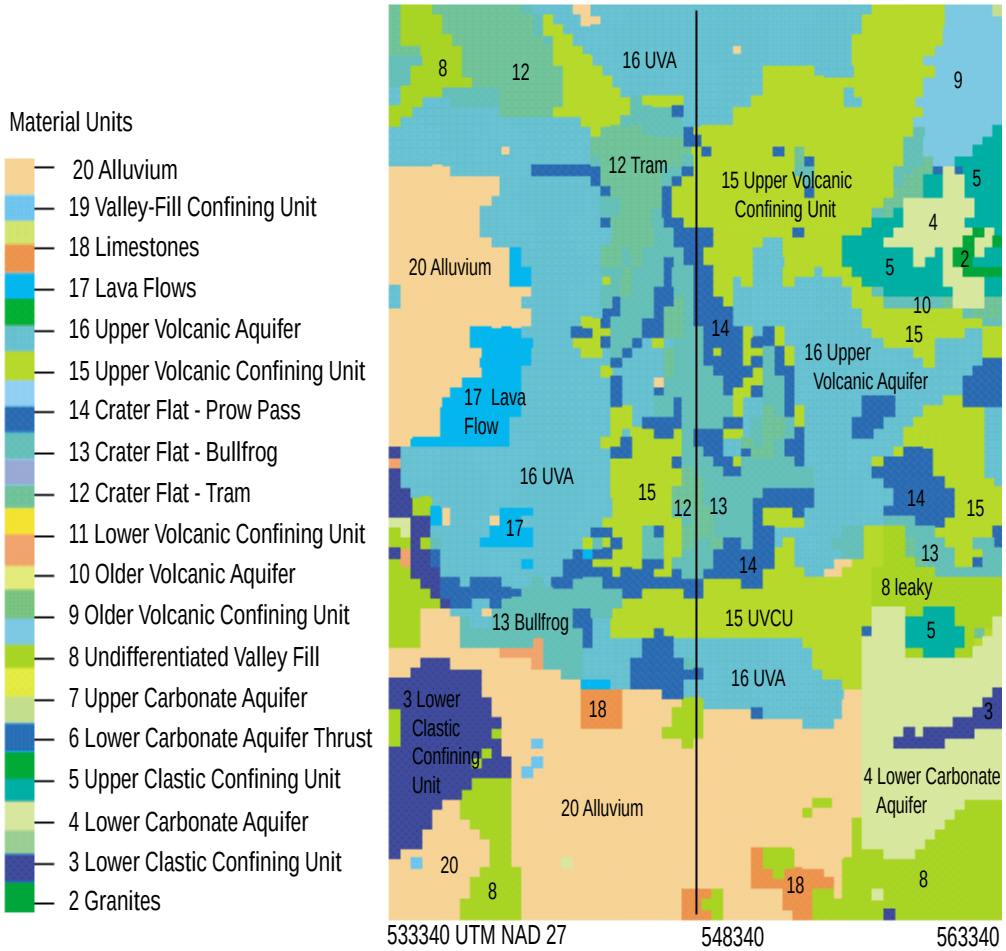

For illustration purposes only.

NOTE: This view is showing the top of the 500-meter computational grid. The different colors in the figure show the material units as defined by hydrogeologic surfaces. The black vertical line is half way between the east and west boundaries and is for reference only. The grid top is the water-table surface.

Figure 15. 500-meter Computational Grid

The grid resolution in the vertical dimension is important for adequately representing groundwater flow and transport in the SZ. Each layer in the structured grid is horizontal, but the layers of the physical hydrogeologic units are gently sloping with approximately 7 percent dip to the east. Therefore, a finer and non-uniform grid resolution is used in the vertical dimension, and this is sufficient to capture the geometry of the hydrogeologic units. The vertical grid spacing is selected to provide the resolution for accurately representing flow and transport along critical flow and transport path ways in the SZ. A finer resolution is used at shallower portions of the model, and a progressively coarser resolution is used for deeper portions of the aquifer. The vertical grid spacing ranges from 10 m (33 ft) near the water table to 550 m (1,805 ft) at the bottom of the model domain. The vertical dimension of the model domain is divided into 11 zones, and constant vertical grid spacing is adopted in each of these zones. The structure of the vertical layering used in the site-scale SZ flow and transport model grid is summarized in Table 10 and shown in the full 3-D Figure 16. In total, 38 layers are included in the vertical dimension that extends from +1,200 m (4,100 ft) to -2,750 m (-9,020 ft) elevation. Figure 17 shows a close up view of the horizontal and vertical resolution in the grid.

Table 10. Vertical Grid Spacing Used in the Site-Scale SZ Flow Model

Gridblock Elevation Zone Boundaries (m)		Grid Spacing (m)	Zone Width (m)	Grid Lines per Zone
Upper	Lower			
1200	1000	50	200	4
1000	840	40	160	4
840	760	20	80	4
760	700	10	60	6
700	640	20	60	3
640	600	40	40	1
600	300	50	300	6
300	0	100	300	3
0	–600	200	600	3
–600	–2200	400	1600	4
–2200	–2750	550	550	1
				Total: 39

Output DTN: LA0304TM831231.002.

NOTE: Of the 39 grid lines, one defined the lower boundary of the model and, thus, was not considered in the model. Therefore, there were only 38 grid lines in the model.

A 3-D representation of the computational grid is provided in Figure 16. Not all unit layers extend throughout the entire horizontal extent of the model domain. Because the model domain is both truncated at the water table and the water table exhibits some variation in altitude over the model domain (700 to 1200 meters), those layers in the higher water table areas (i.e., to the north of the model domain) are truncated as the water table decreases in altitude toward the south.

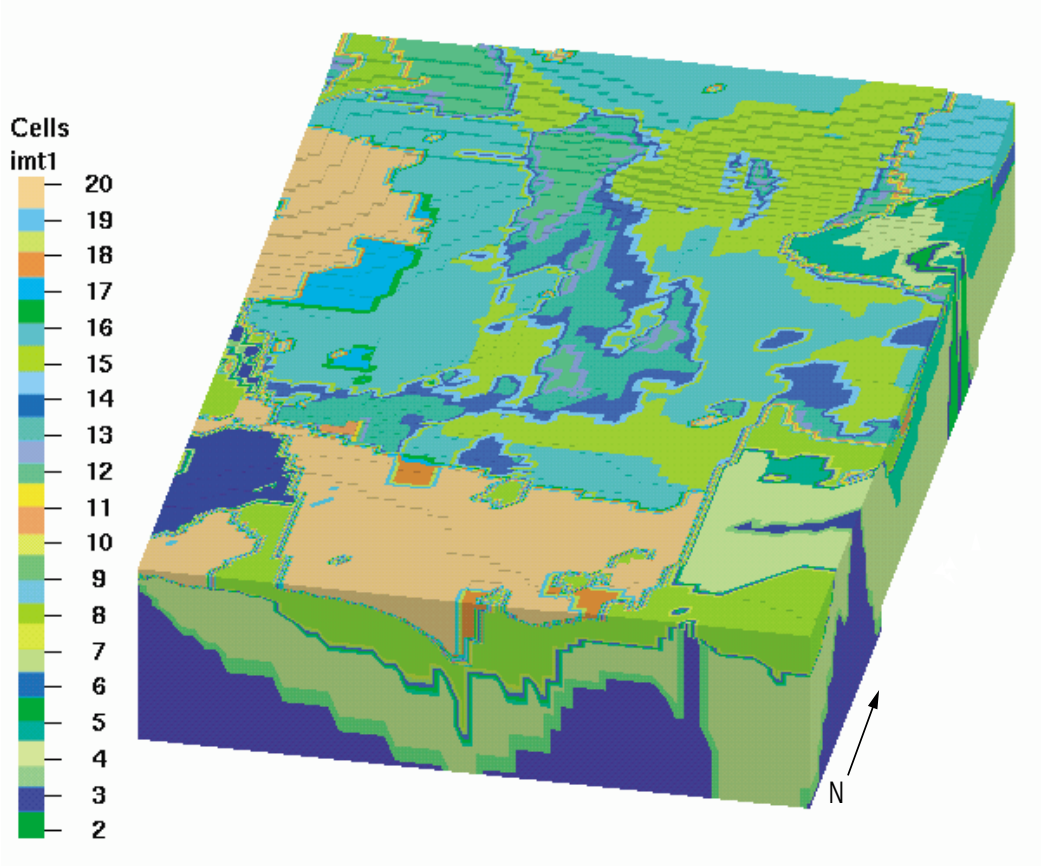

For illustration purposes only.

NOTE: The grid is truncated at the water table surface, which is at 1200 meters in the north and 700 meters in the south. The grid extends 533,340 to 563,340 m in the east and west, and 4,046,780 to 4,091,780 m north and south (Coordinates UTM NAD 27).

Figure 16. View of 500-m Computational Grid (3x Elevation) Showing Node Points Colored by Hydrogeologic Unit Values from the HFM

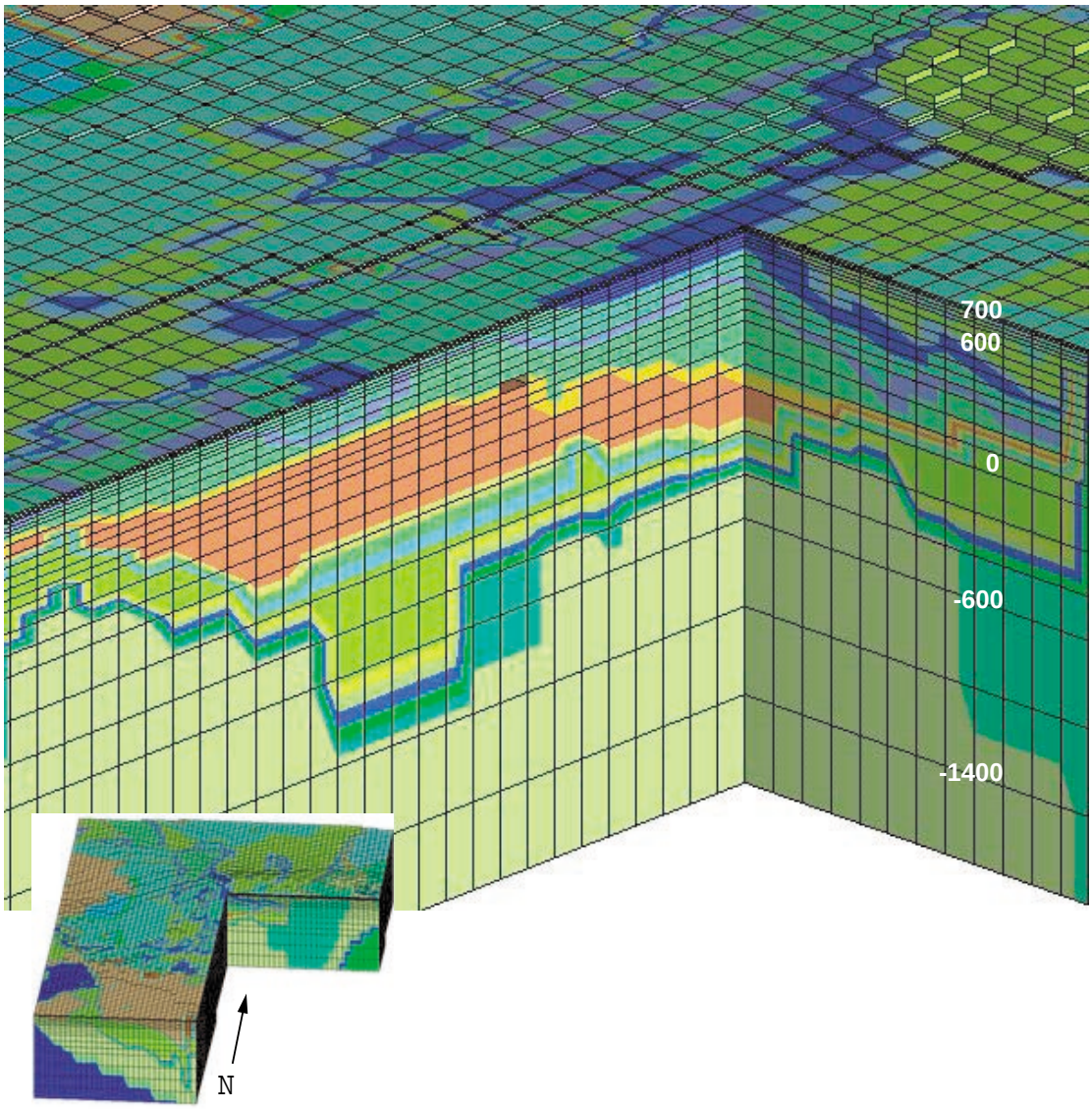

For illustration purposes only.

NOTE: Grid spacing at the bottom of the grid is at 400 meters, then 200, 100, 50, 40, 20, with 10 meters near an elevation of 700 meters. Spacing then increases with elevation from 10 meters to 20, 40, with 50-meter spacing near the higher elevations in the north. The inset at the bottom of the image shows the location of the cut out in relation to the full grid. The grid points are colored with the values of the Hydrogeologic Units 2 through 20.

Figure 17. Close-up View of Computational Grid (3x Elevation) Showing Cut Away at *X* = 549000 and *Y* = 4078000 through the Yucca Mountain Repository

6.5.3.3 Hydrogeologic Properties

After establishing the grid, the physical hydrogeologic unit present at each node in the computational grid is established. The HFM Stratamodel files are converted to Advanced Visualization System (AVS) quadrilateral surfaces (Output DTN: LA0304TM831231.001) using STRAT2AVS V1.0 (STN: 11028-1.0-00, LANL 2003 [163069]). These surface files represent the top surface of each hydrogeologic layer in the Stratamodel framework. The structured grid and the AVS surfaces that define the hydrogeologic layers are imported into LaGriT (STN: 10212-1.0-00; LANL 2001 [149148]) and are used to identify the hydrogeologic layer designation for each node and cell of the computational grid. Cells above the water table and below the bottom unit are removed from the grid. Once the grid geometry conforms to the HFM, FEHM V 2.20 (STN: 10086-2.20-00; LANL 2003 [161725]) input files are output. These files include the mesh geometry, lists of nodes on external boundaries, and node lists sorted by material property.

Quality checks are performed to ensure that the final grid is correct. These include histograms of element volume and element aspect ratio. All nodes are automatically and visually checked to ensure that they are assigned the correct material identification corresponding to the input HFM. Lists of the number of nodes associated with each material are compared to the volume of each material in the Stratamodel framework to confirm that the hydrogeologic units are identified correctly.

The grid units are checked and compared visually to HFM units. Figure 15 shows the top of the grid with the nodes colored by each of the 19 hydrogeologic units. This image compares favorably with the same view of the HFM in the USGS (2001 [158608], p. 57) model report. Further comparisons can be made with each individual unit by comparing HFM layer thickness (isopach) to the shape of the grid nodes for each hydrogeologic unit (Figures 18, a-g). Both sets of images are views looking straight down at the top, with south towards the page bottom. The HFM isopach images are formed using LaGriT (STN: 10212-1.0-00; LANL 2001 [149148]) to read each of two surfaces defining the top and bottom of a unit. LaGriT then calculates the thickness at each *x*,*y* point. The images show the HFM unit thickness with zero thickness removed. Images for the computational grid show all points within each selected unit, colored by the node elevation. A comparison of each unit shows that the grid units correspond adequately with the HFM unit images. Note that each unit distribution is also shown in the model report (USGS 2001 [158608] pp. 35 to 51) but before being clipped by the water-table surface. The images (in Figures 18, a-g) still compare favorably with USGS images, with some differences in the upper units as they approach the top surface and are clipped by the water table.

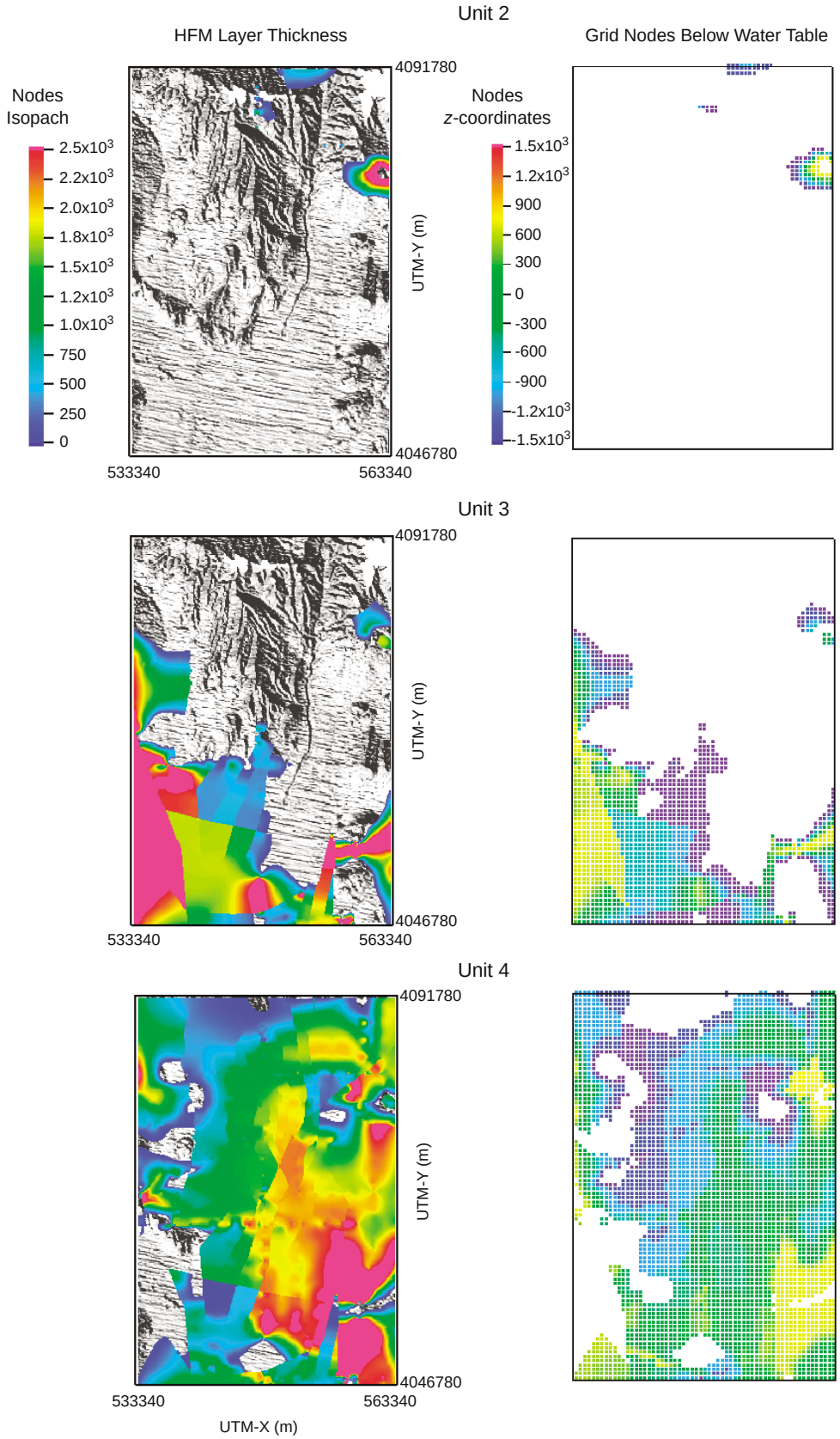

Figure 18a. Units 2, 3, 4 (see notes following Figure 18g)

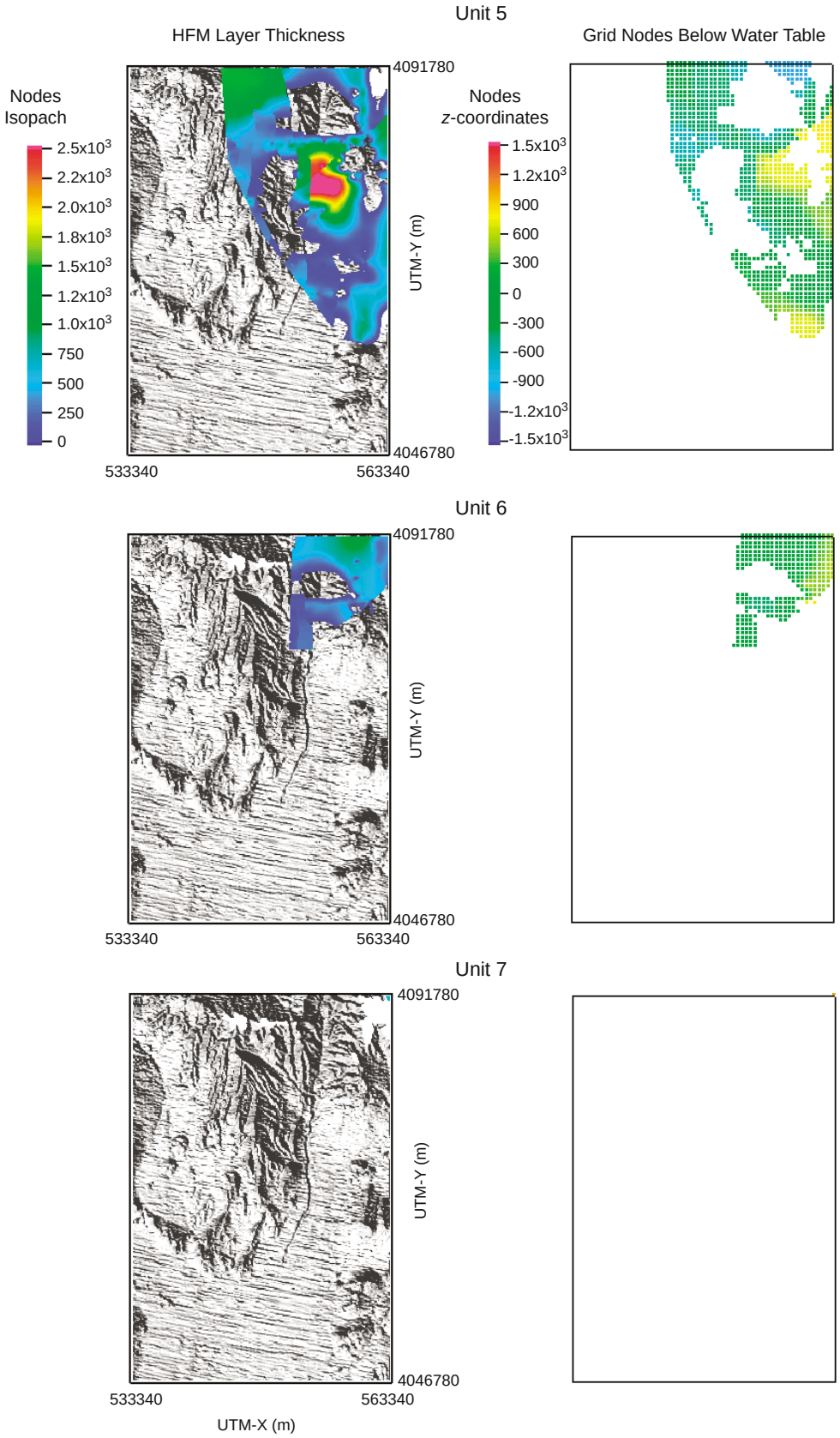

Figure 18b. Units 5, 6, 7 (see notes following Figure 18g)

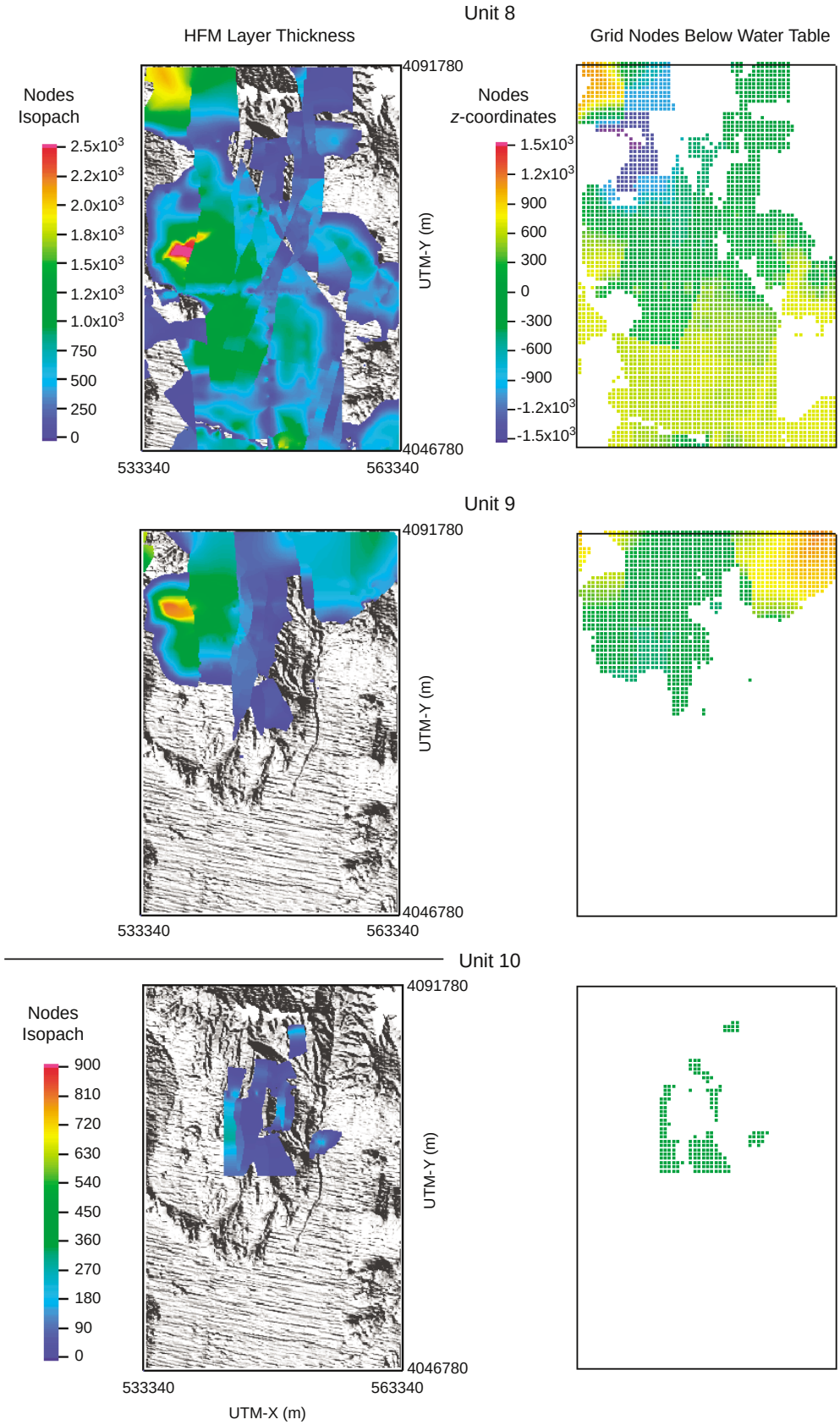

Figure 18c. Units 8. 9, 10 (see notes following Figure 18g)

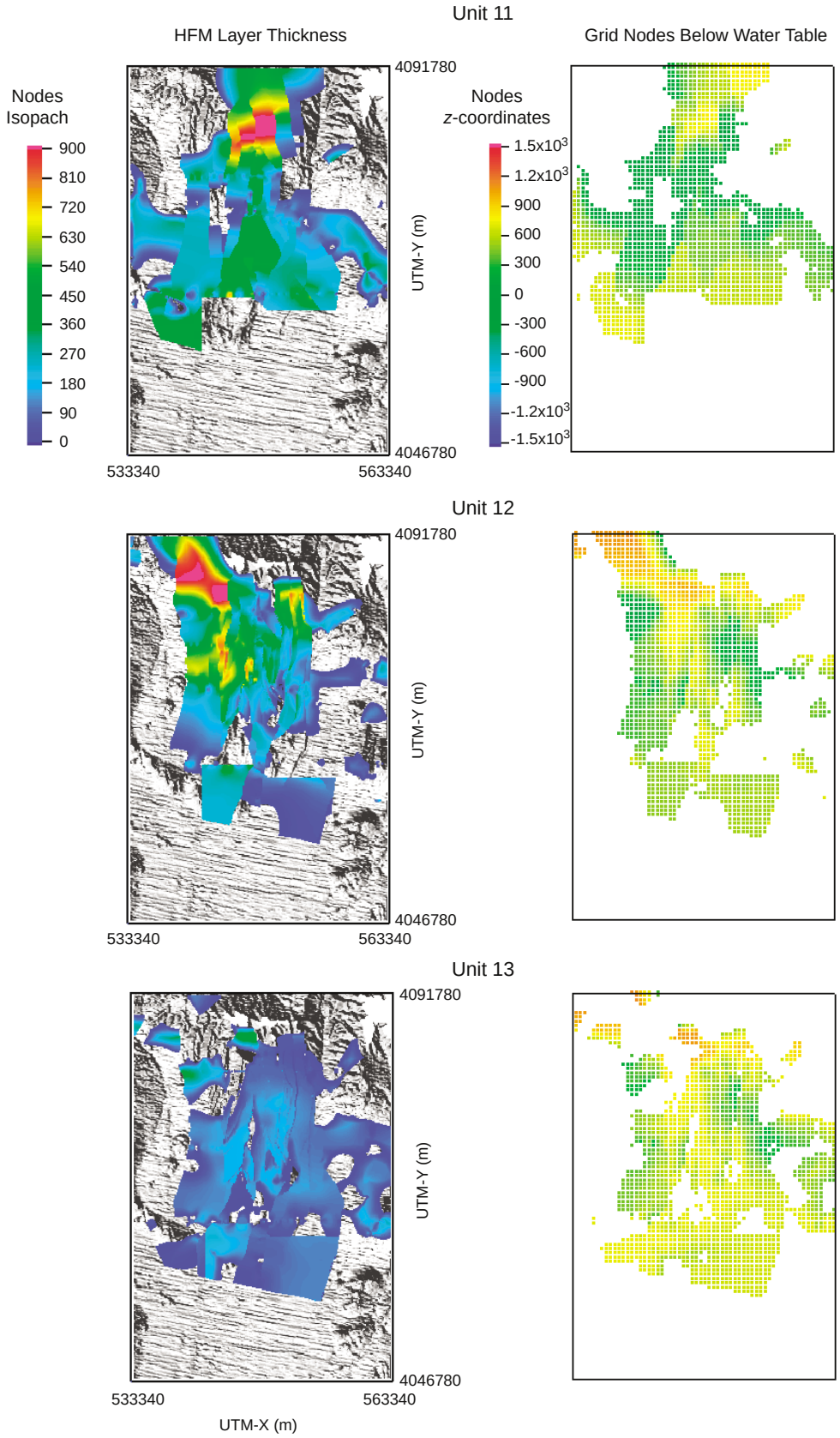

Figure 18d. Units 11, 12, 13 (see notes following Figure 18g)

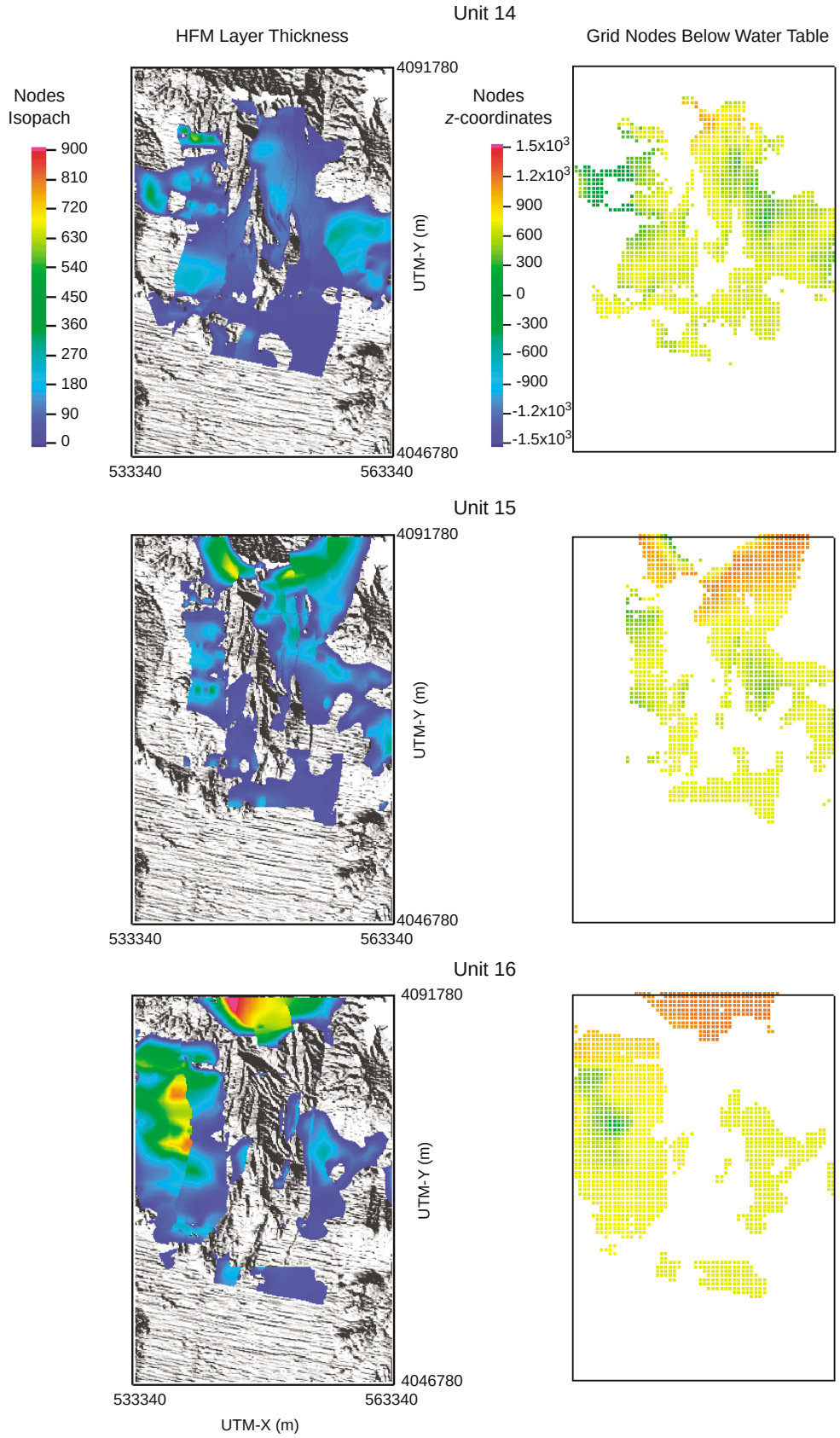

Figure 18e. Units 14, 15, 16 (see notes following Figure 18g)

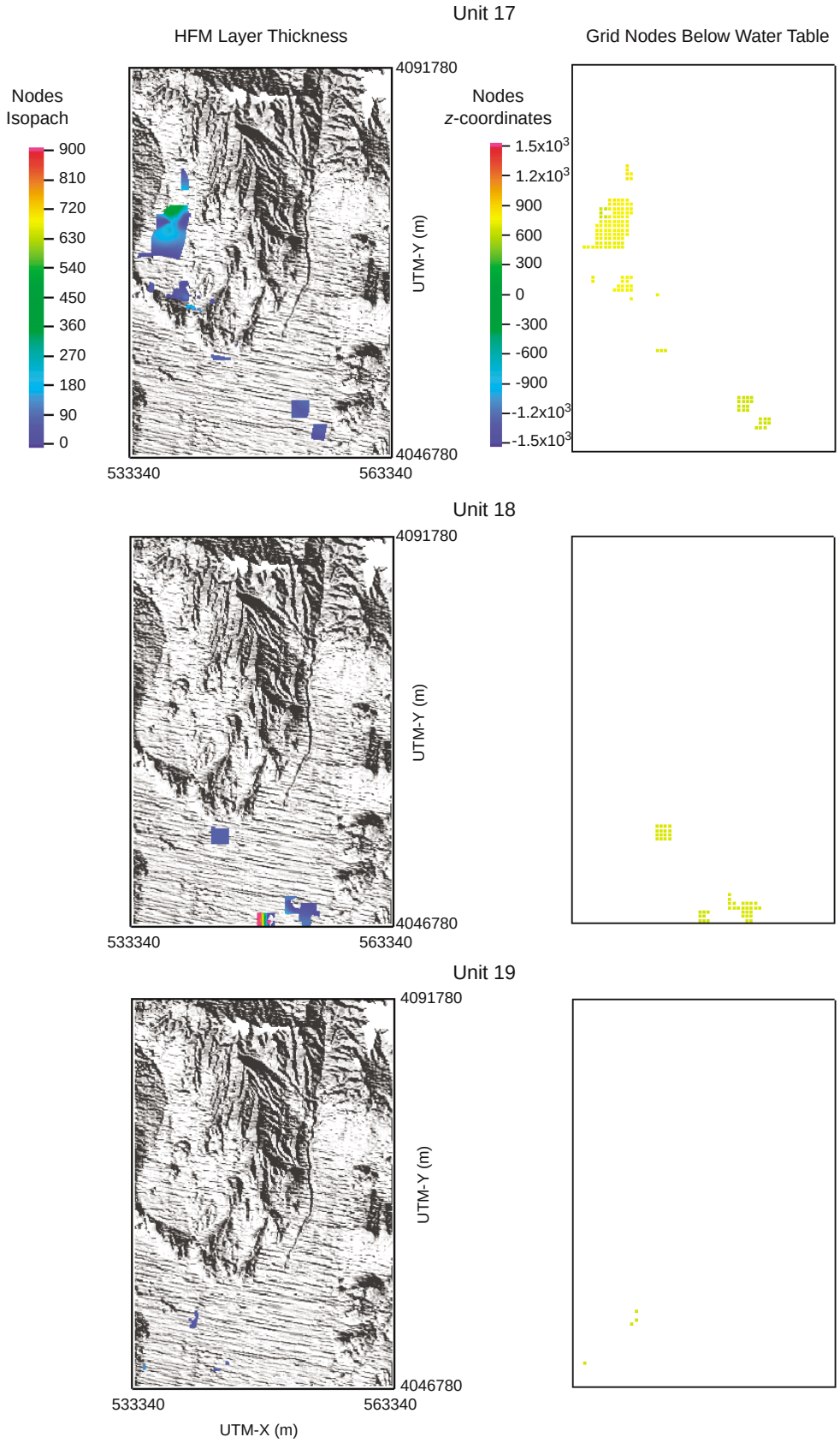

Figure 18f. Units 17, 18, 19 (see notes following Figure 18g)

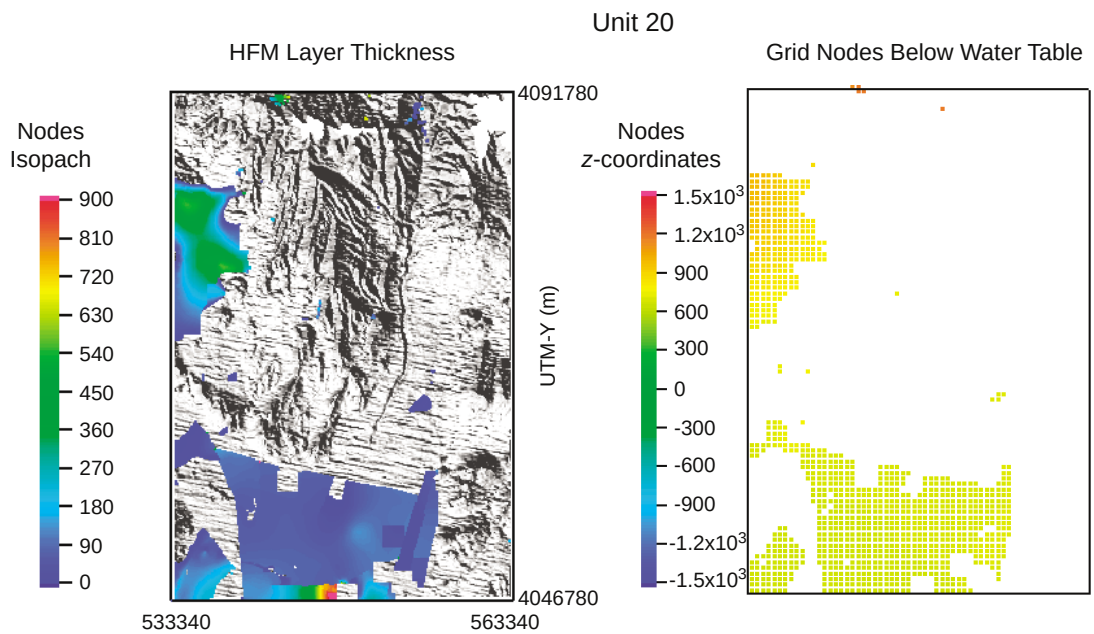

Figure 18g. Unit 20

All parts of Figure 18 are for illustration purposes only.

NOTE: Left panels of HFM Layer Thicknesses:
Color in the grid indicates vertical thickness between each of two unit surfaces. Each image is a view looking down at the input HFM and is formed by the surfaces extracted from the HFM. The bottom surface of each hydrogeologic unit is subtracted from the top surface resulting in the unit thickness at each point. Points of zero thickness have been removed, and the points are shown in relation to the topographic surface. These points are at a resolution of 125, the same as the HFM (USGS 2001, Section 6.1 [158608]).

Right panels of Grid Nodes by Hydrogeologic Unit:
Color in the grid indicates elevation at the top of the unit. Each image is a view looking down at the 500-m computational grid. Images are formed by selecting node points for each of the unit numbers 2 through 20. There are no points where the units are truncated.

Figure 18. Comparison of HFM Layer Thicknesses (Vertical) and Grid Nodes by Hydrogeologic Unit

The LaGriT V1.0 (STN: 10212-1.0-00; LANL 2001 [149148]) code writes FEHM V 2.20 (STN: 10086-2.20-00; LANL 2003 [161725]) input files; these files include the mesh geometry, lists of nodes on external boundaries, and node lists sorted by hydrogeologic unit. The number of nodes assigned to each hydrogeologic unit is presented in Table 11.

Table 11. Hydrogeologic Units

Surface Number	Hydrogeologic Units	Number of Gridblocks 500 m
20	Alluvium (Valley-Fill Aquifer)	6,188
19	Valley-Fill Confining Unit	13
18	Limestones	227
17	Lava Flows	891
16	Upper Volcanic Aquifer	13,831
15	Upper Volcanic Confining Unit	7,845
14	Crater Flat - Prow Pass	5,666
13	Crater Flat – Bullfrog	6,472
12	Crater Flat – Tram	11,676
11	Lower Volcanic Confining Unit	9,142
10	Older Volcanic Aquifer	210
9	Older Volcanic Confining Unit	11,012
8	Undifferentiated Valley Fill	21,578
7	Upper Carbonate Aquifer	23
6	Lower Carbonate Aquifer Thrust	1,192
5	Upper Clastic Confining Unit	5,923
4	Lower Carbonate Aquifer	27,097
3	Lower Clastic Confining Unit	13,259
2	Granites	608
1	Base	0
	Total Number of Gridblocks	142,853

Output DTN: LA0304TM831231.002.

6.5.3.4 Features

To represent discrete features and regions having distinct hydrological properties within the model domain, a set of 17 hydrogeologic features complementary to the HFM were identified and incorporated into the flow model. The hydrogeologic features included in the flow model primarily represent faults, fault zones, and areas of mineralogical alteration. The features described here are essentially vertical: some being linear in the horizontal extent, and some being

of areal extent. These features are distinct from the subhorizontal geological formations, which form zones with distinct geometry and material properties and are described in Section 6.5.3.2. Each of the features described in this report includes multiple geologic formations and represents zones of altered permeability within the individual formations: enhanced permeability, reduced permeability, or anisotropic permeability. Each feature has a significant impact on the flow model. The geometric definition, description, nature of permeability alteration, and impact on the model for each of these features are described in Table 12. In the table, the numbers in the parentheses refer to zone numbers in the input file for FEHM V 2.20 (STN: 10086-2.20-00; LANL 2003 [161725]). The features are shown in Figure 19, which is based on the Yucca Mountain area geologic map (DTN: GS010908314221.001 [162874]) and shows feature representation in the SZ flow model. Also shown in the figure are the zone numbers used in the input files for FEHM. The permeability values associated with the features described in Table 12 are presented and discussed in Section 6.6.1.4. Because of their importance to PA, two proposed zones in the alluvium deserve special consideration. These zones are (1) the alluvial uncertainty zone and (2) the lower Fortymile Wash zone. The alluvial uncertainty zone was added to incorporate the new geology obtained with the recently drilled 2-D and Washburn wells (DTN: MO9909NYEEWDP0.000 [119613]). This data source is not direct input to the base-case model. It is cited only to support the assertion that the base-case HFM does not accurately represent the volcanic alluvium contact in the vicinity of the above-mentioned wells. The location of this zone is given in Table 12. The drilling records of these wells show that alluvium extends further north and east than the geologic model (created without benefit of the two wells) indicates. Because of the importance to PA, the alluvial zone was added to the model. The lower Fortymile Wash zone was added because of the distinct character of the Fortymile Wash in the southern part of the model. Field observations indicate possible channelization with attendant textural contrasts with surrounding alluvial material (Oatfield and Czarnecki 1989 [149438]).

The Claim Canyon, Calico Hills, Shoshone Mountain fault zones (known collectively as the Northern Low Perm zone), and the East-West barrier deserve additional comment because they form the Large Hydraulic Gradient zone (Luckey et al. 1996 [100465]) north of Yucca Mountain. The East-West barrier was required to have a low permeability (10^{-18} m^2) during the calibration in order to separate the high heads in the north from the lower heads in the vicinity of Yucca Mountain. This feature has no other geologic significance. Though there are several theories proposed to explain the large hydraulic gradient, the expert elicitation panel (CRWMS M&O 1998 [100353], pp. 3-5 to 3-6) favored the idea of semi-perched water in that area. If several of the wells were semi-perched to the north of Yucca Mountain, then the hydraulic head gradient in the saturated zone would be smaller. This would likely result in different calibrated values for the Northern Low Perm zone and the East-West barrier than that obtained with the present model

Table 12. Hydrological Features in the Saturated-Zone Flow Model

Feature Name and Description	Geometric Definition (UTM)	Hydrogeological Characteristics	Impact on Model
1. Northern Zone (entire Claim Canyon, Calico Hills, and Shoshone Mt.; #81) This zone is wedge-shaped, spanning almost the entire northern boundary (except the western corner of the northern boundary) and approximately the upper fourth of the eastern boundary. Vertically, it extends from the top to the bottom of the model, and its areal extent is shown by the four points.	*x* = 546436, *y* = 4.08211E+006, *x* = 563657, *y* = 4.08211E+006, *x* = 563549, *y* = 4.09208E+006, *x* = 535832, *y* = 4.09202E+006, and *z* = top to bottom of model	It represents the general region of lowered permeability caused by hydrothermal alteration associated with the Claims Canyon Caldera`.	Impact of the model on this zone is mainly to control the flow of water into the model from the north boundary.
2. Northern Crater Flat Zone (#82) This wedge-shaped zone is at the northern third of the western boundary of the model. Vertically, it extends from the top to the bottom of the model, and its areal extent is shown by the four points.	*x* = 533077, *y* = 4.07458E+006, *x* = 544206, *y* = 4.07453E+006, *x* = 544103, *y* = 4.08349E+006, *x* = 532974, *y* = 4.09223E+006, and *z* = top to bottom of model	It is a permeability reduction zone, representing a hydrothermally altered area associated with the Claims Canyon Caldera.	Impact of the model on this zone is to control influx from the northwest corner of the model.
3. Fortymile Wash Zones (#57 and #58) These two north-south linear features are located approximately halfway between Yucca Mountain and the eastern model boundary. Vertically, it extends from the top to the bottom of the model, and its areal extent is shown by the four points.	*x* = 554330, *y* = 4066770, *x* = 554350, *y* = 4066770, *x* = 554350, *y* = 4081790, *x* = 554330, *y* = 4081790, and *z* = top to bottom of model	It is an enhanced permeability zone representing the faulted area associated with the wash.	Impact on the model is to channel the flow of the east-central portion of the model in the Jackass Flat area in a southern direction, lower the hydraulic gradient in the area, and act as a regional drain.
4. Spotted Range-Mine Mountain Zone (#59) This triangular feature is in the southeast corner of the model. Vertically, it extends from top of the model down to the bottom. Its areal extent is shown by the four points.	*x* = 555000, *y* = 4046770, *x* = 563350, *y* = 4046770, *x* = 563350, *y* = 4059000, *x* = 563310, *y* = 4059000, and *z* = top to bottom of model	It is a zone of enhanced permeability associated with the Spotted Range Thrust Region	Impact on the model is to control the water flow into the model from the southern end of the east boundary and water flow out of the model of the eastern end of the southern boundary.

Table 12. Hydrological Features in the Saturated-Zone Flow Model (Continued)

Feature Name and Description	Geometric Definition	Hydrogeological Characteristics	Impact on Model
5. Claim Canyon Caldera (east and west, #61 and #62) These zones span much of the northern boundary of the model, extending south as triangular shapes and terminating north of the Yucca Wash. Vertically, it extends from the top to the bottom of the model, and its areal extent is shown by the eight points. This zone is part of the Northern Low Perm zone used in calibration.	*x* = 536800, *y* = 4091760, *x* = 540000, *y* = 4086700, *x* = 547600, *y* = 4084700, *x* = 547600, *y* = 4091760; and *x* = 547677, *y* = 4091760, *x* = 547631, *y* = 4084710, *x* = 560000, *y* = 4087660, *x* = 560000, *y* = 4091760, and *z* = top to bottom of model	These are zones of reduced permeability due to the hydrothermal alteration associated with the caldera; but the permeability reduction is somewhat less than the rest of the Northern zone, probably due to faulting associated with the vertical movement due to caldera collapse and the greater thickness of welded zones within the caldera.	Impact on the model is mainly to control the water flow into the model from the northern boundary.
6. Shoshone Mt. Zone (north and south, #63 and #64) These two zones are in the northeastern corner of the model. They extend from the top of the carbonate aquifer up to the top of the model. Vertically, it extends from the top to the bottom of the model, and its areal extent is shown by the eight points. This zone is part of the Northern Low Perm zone used in calibration.	*x* = 560634, *y* = 4.09153E+006, *x* = 559362, *y* = 4.08957E+006, *x* = 563090, *y* = 4.08962E+006, *x* = 563044, *y* = 4.09148E+006; and *x* = 557045, *y* = 4.08962E+006, *x* = 560953, *y* = 4.08748E+006, *x* = 563137, *y* = 4.08775E+006, *x* = 563090, *y* = 4.08962E+006, and *z* = top to bottom of model	These are zones of permeability reduction due to hydrothermal alteration associated with the Claim Canyon Caldera.	Impact on the model is mainly to control the water flow into the model from the northern portion of the eastern boundary.
7. Calico Hills Zone (north and south #65 and #66) These two zones are near the eastern end of the model, south of the Shoshone Mountain Zones, at approximately the same northing as the Yucca Wash. Vertically, it extends from the top to the bottom of the model, and its areal extent is shown by the eight points. This zone is part of the Northern Low Perm zone used in calibration.	*x* = 556864, *y* = 4.08102E+006, *x* = 562957, *y* = 4.08102E+006, *x* = 561499, *y* = 4.08407E+006, *x* = 558589, *y* = 4.08343E+006; and *x* = 556818, *y* = 4.08102E+006, *x* = 558821, *y* = 4.07807E+006, *x* = 561273, *y* = 4.07716E+006, *x* = 563142, *y* = 4.08098E+006, and *z* = top to bottom of model	These are zones of permeability reduction due to hydrothermal alteration associated with the Calico Hills	Impact on the model is mainly to control the water flow into the model from the northern portion of the eastern boundary.

Table 12. Hydrological Features in the Saturated-Zone Flow Model (Continued)

Feature Name and Description	Geometric Definition	Hydrogeological Characteristics	Impact on Model
8. Crater Flat Fault (north-1, north-2, south-3, and south-4, #69, #70, #71, and #72) This is a linear feature running north-south in the western half of the model, starting to the south of the Claims Canyon and terminating near Highway 195, almost halfway between the western boundary and the Solitario Canyon. Vertically, it extends from the top to the bottom of the model, and its areal extent is shown by the sixteen points.	*x* = 538330, *y* = 4.08380E+006, *x* = 538350, *y* = 4.08380E+006, *x* = 538350, *y* = 4.08943E+006, *x* = 538330, *y* = 4.08943E+006; and *x* = 538330, *y* = 4.07475E+006, *x* = 538350, *y* = 4.07475E+006, *x* = 538350, *y* = 4.08380E+006, *x* = 538330, *y* = 4.08380E+006; and *x* = 538330, *y* = 4.06650E+006, *x* = 538350, *y* = 4.06650E+006, *x* = 538350, *y* = 4.07475E+006, *x* = 538330, *y* = 4.07475E+006; and *x* = 538330, *y* = 4.06140E+006, *x* = 538350, *y* = 4.06140E+006, *x* = 538350, *y* = 4.06650E+006, *x* = 538330, *y* = 4.06650E+006; and *z* = top to bottom of model	These are zones of permeability reduction normal to the fault orientation and permeability enhancement parallel to the fault orientation.	Impact on the model of these zones is to generate a somewhat high head gradient in the western half of the model and control the influx coming from the western boundary, and to restrict the flow towards the eastern half of the model.
9. Solitario Canyon Fault (#74, # 83 and #84) These are generally north-south trending linear features just to the west of Yucca Mountain. Vertically, it extends from the bottom of the model to the top of the model. Its areal extent is shown by the twelve points.	*x* = 546451, *y* = 4.07754E+006, *x* = 545632, *y* = 4.07355E+006, *x* = 546384, *y* = 4.07355E+006, *x* = 547018, *y* = 4.07754E+006; and *x* = 546451, *y* = 4.07754E+006, *x* = 545632, *y* = 4.07752E+006, *x* = 546384, *y* = 4.08158E+006, *x* = 547018, *y* = 4.08158E+006; and *x* = 545638, *y* = 4.07111E+006, *x* = 546379, *y* = 4.07108E+006, *x* = 546647, *y* = 4.07355E+006, *x* = 546008, *y* = 4.07352E+006; and *z* = top to bottom of model	These are zones of permeability enhancement in the vertical and fault-parallel direction and permeability reduction normal to the fault.	Impact on the model of these features is to generate a higher head gradient to the west of Yucca Mt. and to impede flow from Crater Flat to Yucca Mountain.

Table 12. Hydrological Features in the Saturated-Zone Flow Model (Continued)

Feature Name and Description	Geometric Definition	Hydrogeological Characteristics	Impact on Model
10. Solitario Canyon Fault, East Branch (#75, #76) These are generally north-northeast trending linear features just to the west of Yucca Mountain. Vertically, it extends from the bottom of the model to the top of the model. Its areal extent is given by the eight points.	*x* = 545632, *y* = 4.07111E+006, *x* = 547450, *y* = 4.06468E+006, *x* = 547996, *y* = 4.06468E+006, *x* = 546384, *y* = 4.07109E+006; and *x* = 547450, *y* = 4.06468E+006, *x* = 544520, *y* = 4.05833E+006, *x* = 545040, *y* = 4.05815E+006, *x* = 548022, *y* = 4.06468E+006; and *z* = top to bottom of model	These are zones of permeability enhancement in the vertical and fault-parallel direction and permeability reduction normal to the fault.	Impact on the model of these features is to generate a higher head gradient to the west of Yucca Mt. and to impede flow from Crater Flat to Yucca Mountain.
11. Solitario Canyon Fault, West Branch (#77, #78) These are generally north-northeast trending linear features just to the west of Yucca Mountain. Vertically, it extends from the bottom of the model to the top of the model. Its areal extent is given by the eight points.	*x* = 545632, *y* = 4.06109E+006, *x* = 540452, *y* = 4.06259E+006, *x* = 541018, *y* = 4.06261E+006, *x* = 546384, *y* = 4.07106E+006; and *x* = 540426, *y* = 4.06259E+006, *x* = 540132, *y* = 4.05972E+006, *x* = 540699, *y* = 4.05947E+006, *x* = 541018, *y* = 4.06259E+006; and *z* = top to bottom of model	These are zones of permeability enhancement in the vertical and fault-parallel direction and permeability reduction normal to the fault.	Impact on the model of these features is to generate a higher head gradient to the west of Yucca Mt. and to impede flow from Crater Flat to Yucca Mountain.
12. Highway 95 Fault (West, #79) This is a linear feature in the lower half of the western portion of the model. It is east-southeast trending. Vertically, it extends from the bottom of the model to the top of the model. Its areal extent is given by the four points.	*x* = 536625, *y* = 4.06124E+006, *x* = 544355, *y* = 4.05838E+006, *x* = 544716, *y* = 4.05833E+006, *x* = 536486, *y* = 4.06184E+006, and *z* = top to bottom of model	This is a zone of permeability enhancement in the vertical and fault-parallel direction and permeability reduction normal to the fault.	Impact on this model is to restrict flow in the north-south direction and support high head gradients in that portion of the model.
13. Bare Mountain Fault (#80 and #90) This is a northwest- to southeast-trending linear feature in the southwestern corner of the model. Vertically, it extends from the bottom of the model to the top of the model. Its areal extent is given by the eight points.	*x* = 533628, *y* = 4.06757E+006, *x* = 536126, *y* = 4.06102E+006, *x* = 536672, *y* = 4.06125E+006, *x* = 533628, *y* = 4.06898E+006, and *x* = 540330, *y* = 4.04678E+006, *x* = 540850, *y* = 4.04678E+006, *x* = 533850, *y* = 4.06429E+006, *x* = 533330, *y* = 4.06429E+006; and *z* = top to bottom of model	This is a zone of permeability enhancement representing the Bare Mountain fault.	Impact on the model is to drain the flow from Crater Flat to the Amargosa Desert.

Table 12. Hydrological Features in the Saturated-Zone Flow Model (Continued)

Feature Name and Description	Geometric Definition	Hydrogeological Characteristics	Impact on Model
14. Alluvial Uncertainty Zone (expected case, #88) This is a roughly rectangular region to the south of Yucca Mountain in the southern half of the model. Vertically, it extends from the top of the model down through the undifferentiated units. Its areal extent is given by the four points.	x = 547622, y = 4.05731E+006, x = 555503, y = 4.05542E+006, x = 556740, y = 4.06206E+006, x = 550691, y = 4.06206E+006, and z = top of model to +400	This zone represents uncertainty in the border between the alluvium and tuff.	Although it does not strongly influence the flow model, it is expected to be important to PA calculations due to its effect on solute transport.
15. Imbricate Fault Zone (#91) This is a highly faulted area bounded in the west by the Ghost Dance fault, south by the Dune Wash, east by the Paintbrush Canyon fault, and to the north by the Drillhole Wash. Vertically, it extends from the top of the model down through the middle volcanics to the top of the undifferentiated units. Its areal extent is given by the four points.	x = 548830, y = 4073270, x = 552350, y = 4071770, x = 552350, y = 4077290, x = 548830, y = 4079790, and z = top of model to +400	This is a region of permeability enhancement.	It allows the model to represent higher permeabilities due to faulting while retaining regional scale permeability values of the middle volcanic layers in the expected range.
16. East-West Barrier (#56) This linear feature runs east-west just to the north of Yucca Mountain, starting at the western edge of Yucca Mt. and extending eastwards but short of the Calico Hills. Vertically, it extends from the bottom of the model to the top of the model. Its areal extent is given by the four points.	x = 546000, y = 4081440, x = 559000, y = 4081440, x = 559000, y = 4082000, x = 546000, y = 4082000, and z = top to bottom of model	This is a zone of permeability reduction.	The impact of this barrier on the model is mainly to create the steep hydraulic gradient to the north of Yucca Mountain between the wells G2, WT6 to the north and the wells WT18, H1 to the south.
17. Lower Fortymile Wash Zone (#45) This quadrilateral feature (plan view) encompasses the Lower Fortymile Wash part of the model . The depth of the zone includes the alluvium unit to the top of the model. Its areal extent is given by the four points.	x = 546965, y = 4057460, x = 550691, y = 4056450, x = 547893, y = 4046760, x = 540833, y = 4046760, z = 400m to top	This is a zone of permeability enhancement.	The impact on the model of this barrier is mainly to create the low hydraulic gradient observed in the Fortymile wash area where it intersects the Southern Boundary.

Source: GS010908314221.001 [162874]. Output DTN: LA0304TM831231.002.

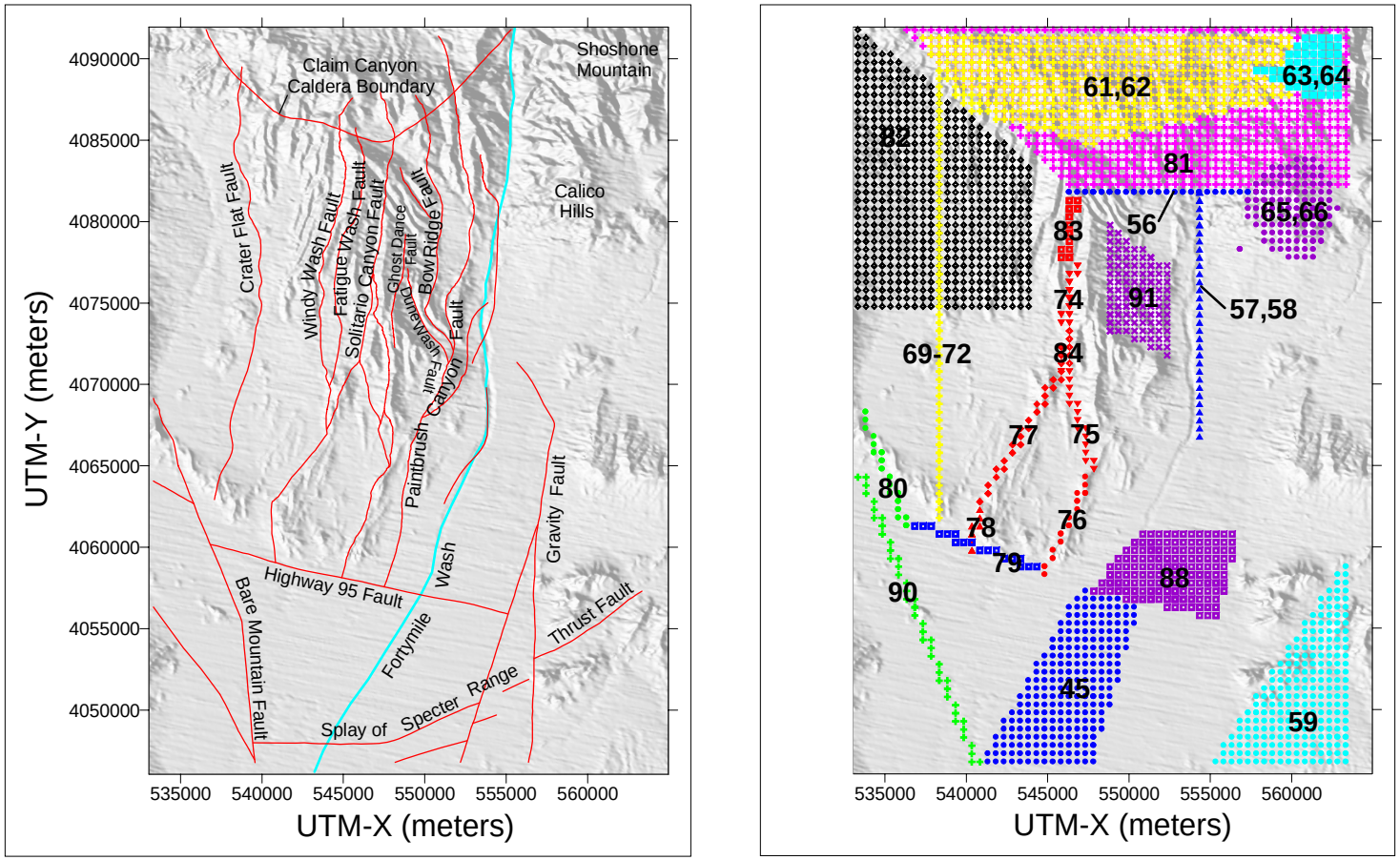

DTN: GS010908314221.001 (left panel) Output DTN: LA0304TM831231.002 (right panel).

NOTE: Field data are on the left panel, and the SZ model representation is on the right panel. Numbers designate the following regions: 45 - Lower FortyMile Wash Zone; 56 - East-West Barrier Zone; 57 and 58 - Fortymile Wash Zones; 59 - Spotted Range-Mine Mountain Zone; 61 and 62 - Claim Canyon Caldera Zones; 63 and 64 - Shoshone Mountain Zones; 65 and 66 - Calico Hills Zones; 69, 70, 71, and 72 - Crater Flat Fault Zones; 74, 83, and 84 - Solitario Canyon Fault Zones; 75 and 76 - Solitario Canyon Fault Zones (East Branch); 77 and 78 - Solitario Canyon Fault Zones (West Branch); 79 - Highway 95 Fault Zone; 80 and 90 - Bare Mountain Fault Zones; 81 - Northern Zone; 82 - Northern Crater Flat Zone; 88 - Alluvial Uncertainty Zone (expected case); 91 - Imbricate Fault Zone.

Figure 19. Geologic Features in the Area of the Site-Scale Flow Model

6.5.3.5 Boundary Conditions

The lateral boundary conditions are described in Section 6.3.2.6. It should be noted that historically, groundwater has been extracted from wells in the Amargosa Valley south of the site-scale model domain. Drawdown from the wells is represented in the potentiometric surface map that was used to establish southern boundary head conditions. Consequently, the effect of pumping on flow within the model domain is accounted for by the head values specified along the southern boundary. A small amount of pumping also has occurred from the southern portion of the site-scale model. This pumping was included in the regional-scale model, but not the site-scale model. Ignoring this pumping is assumed to have very little effect on the calculated flow paths and flow times to compliance boundaries.

6.5.3.6 Recharge

Recharge is applied to the top surface of the computational grid as a flux boundary condition. The recharge map in CRWMS M&O (1999, Section 6.1 [130979]) is mapped (with changes to be described later) to the top surface of the numerical grid described in this report. An important characteristic of the recharge data is that they were developed with the assumption that they are applied at the land's surface. It is really net infiltration. The exception is the recharge in the area of the UZ model, where the actual output of the UZ model is used. Thus, except for the area beneath the UZ model, redistribution of infiltration in the UZ is likely to produce recharge at the water table that is different than that described in CRWMS M&O (1999 [130979]). Because most of the recharge occurs at higher elevations in rocks that are less permeable than in other regions, there are nodes at the top of the model (i.e., at the water table surface) where the permeability is too small to accept the recharge developed for the land surface at that location. This has necessitated the increase in the permeability of the top layer in the SZ model in some areas. This change allows the flow to redistribute locally and avoid artificially high heads. This method conserved recharge mass flux and was deemed better than any procedure that modified the spatial distribution of the recharge. Sensitivity to this procedure on calibration and flow direction is small because this procedure is applied to the low perm rocks that exist to the North of Yucca Mountain. The effect on the flow field to the south and east of Yucca Mountain, provided the heads and gradients are well matched, is therefore minimal.

To assign recharge values to the top surface of the computational grid, an infiltration map (DTN: SN9908T0581999.001 [132867]) is interpolated onto the computational mesh to provide the top surface flux boundary condition. The interpolation procedure is designed to ensure that the local small-scale features of the infiltration map are represented in the boundary conditions and that the total flux is preserved. This procedure is accomplished by first providing the infiltration map (DTN: SN9908T0581999.001 [132867]) as an ASCII file with two coordinates, x and y, for each data point, the area associated with that point, and the flux (mm/yr) for each point. The computational mesh has a regular point distribution with points spaced at 500-m horizontal intervals. However, the mesh numbering was irregular. A geometric sorting program is used to identify each point in the infiltration data with the corresponding gridblock in the computational mesh. This step is equivalent to determining the grid block number for the 500-m mesh and determining to which node each point of the infiltration map belongs. Figure 20 shows a comparison of the data in the above-mentioned DTN and that recharge used in the FEHM V 2.20

(STN: 10086-2.20-00; LANL 2003 [161725]) input files for the SZ flow model. They are identical, thus proving the mapping used preserves the recharge distribution.

6.5.3.7 Nodal Hydrogeologic Properties

Hydrogeologic properties must be specified for each node in the computational grid. Using the hydrogeologic unit sets created in the grid-building process, flow parameters such as permeability, viscosity, and porosity are assigned to each node.

The parameter values for viscosity depend on the temperature at each node, and a uniform temperature gradient is assumed. This assumption of a uniform temperature gradient with depth is equivalent to assuming uniform geothermal heat flux through a medium of homogeneous thermal conductivity. In addition, the temperature at the ground surface is assumed to be equal to a uniform value. The data on temperature in boreholes presented in Sass et al. (1988 [100644], p. 2) indicate that there is significant variability in the temperature gradient at different locations and within individual wells, presumably due to advective redistribution of heat from infiltration and vertical groundwater flow. However, these data also indicate that the temperature gradients generally become more linear with increasing depth below the water table. It is important to note that the goal of assigning temperature variations with depth in the SZ site-scale flow model is to account for resulting variations in fluid viscosity at different depths in the SZ. The viscosity of water changes by a factor of only about 3.3 over the temperature range of 20°C to 100°C (Streeter and Wylie 1979, [145287], p. 536) that is expected within the range of depths in the SZ site-scale model domain. Thus, the linear approximation of the temperature gradient is adequate to capture the general effects of variations in groundwater viscosity with depth in the SZ site-scale flow model. The density also varies with temperature, but the effect is much smaller than viscosity.

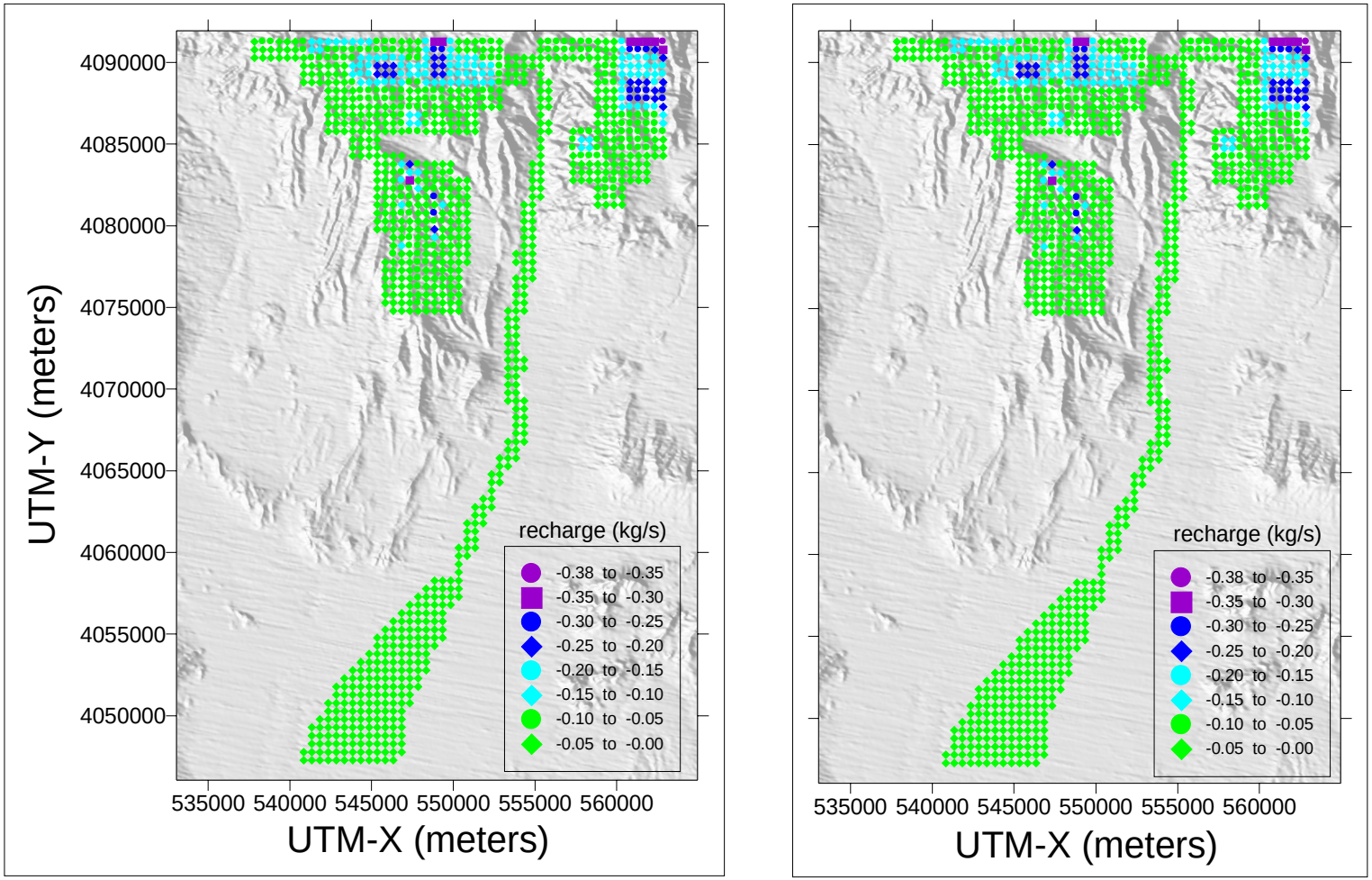

DTN: SN9908T0581999.001 [132867] (left panel); Output DTN: LA0304TM831231.002 (right panel).

Figure 20. Comparison of Recharge Data (left panel) with FEHM Input Data (right panel)

Over the temperature range of 20°C to 100°C, water density varies only a few percent, and, thus, density was treated as a constant. Using a variable viscosity allows the calibration of intrinsic permeability to be made instead of hydraulic conductivity. The former is a rock property, whereas the latter is both a rock and fluid property. This approach, in turn, allows for more accurate flux calculations on the boundaries of the model.

The approach taken to the incorporation of groundwater temperature in the SZ site-scale model is to evaluate the average temperature gradient using temperature measurements in boreholes and to use that temperature gradient to specify temperature at grid nodes in the SZ site-scale flow model. As implemented in the SZ site-scale flow model, temperatures remain fixed at the specified value, and the heat-transport equations are not solved in the simulation. Thus, the specified values of temperatures are used to calculate the local groundwater viscosity, but temperature variations do not result in any variable-density flow processes as the density in all calculations was treated as a constant.

Temperature profiles in a number of wells near Yucca Mountain are presented in Sass et al. (1988 [100644]). The data in Sass et al. (DTN: MO0102DQRBTEMP.001 [154733], Figures 4, 5, 6, 7, 8, and 10) were used to estimate an approximate average temperature gradient and representative surface temperature for the site. As noted by Sass et al. (1988 [100644], p. 2), there is considerable variability (about 15°C/km to nearly 60°C/km) in the temperature gradients among the wells. However, the approximately average value of the temperature gradient in the wells is 25°C/km, and the average surface temperature is about 19°C. By using these values for the average temperature gradient and surface temperature, along with the water table and topographic surface evaluations, the estimated temperature at the water table is calculated as shown in Figure 21. The lower temperatures in the figure correspond to areas of relatively small unsaturated thickness, and the higher temperatures correspond to a thick unsaturated zone.

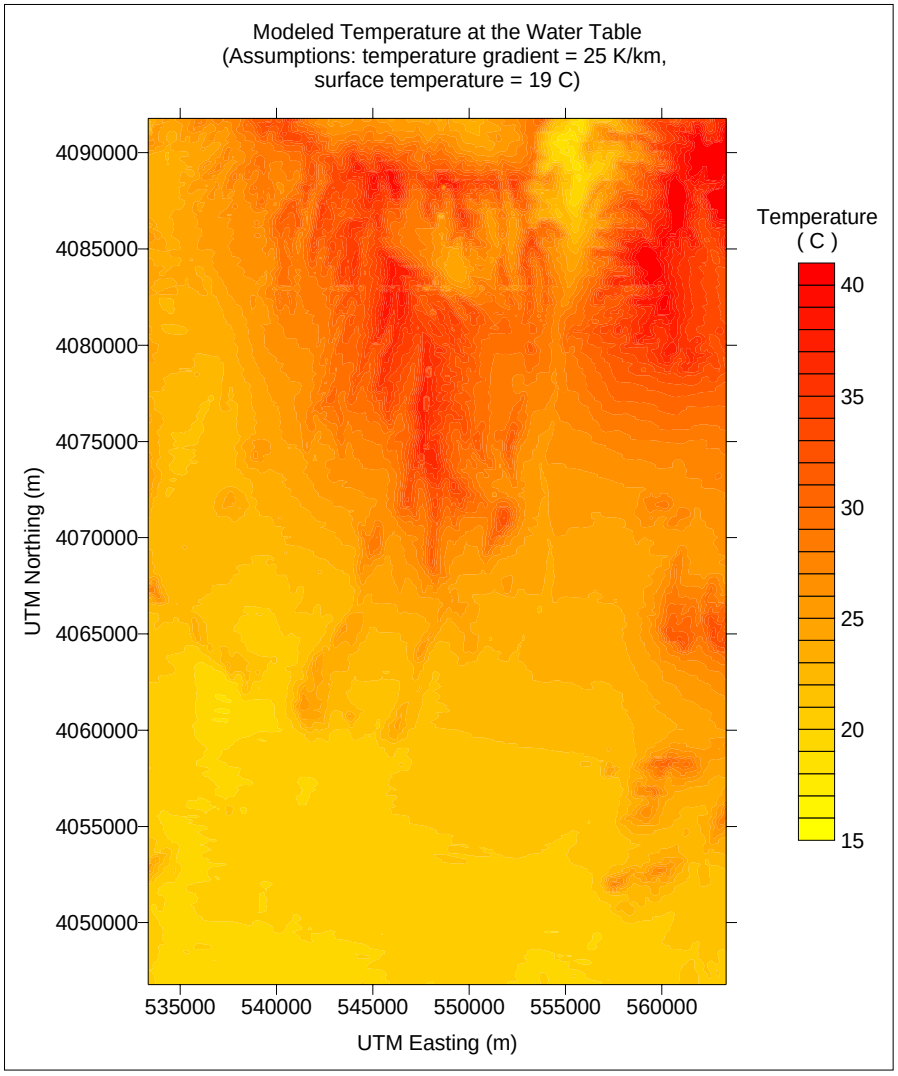

DTN: MO0102DQRBTEMP.001 [154733].

Figure 21. Map of Modeled Temperature at the Water Table for the Saturated-Zone Site-Scale Flow Model Domain

6.6 BASE-CASE MODEL RESULTS

6.6.1 Model Calibration

Calibration is the process by which values of important model parameters are estimated and optimized to produce the best fit between the model output and the observed data. Calibration generally is accomplished by adjusting model input parameters (e.g., permeability) to minimize the difference between observed and simulated conditions (in this case, comparing predicted and observed head values and lateral boundary fluxes). Model calibration may be performed through manual methods or through automated optimization procedures. Automated optimization procedures generally employ a carefully prescribed mathematical process that selects the optimal set of parameters based on minimizing an objective function describing the difference between observed and simulated conditions. These procedures generally provide the most structured and thorough means of calibrating a model, and, frequently, they provide useful additional information regarding model sensitivity to parameters and other useful statistical measures. Consequently, an automated optimization procedure is used to calibrate the site-scale SZ flow model. However, manual adjustments to the calibration also are performed to ensure an accurate representation of fluxes in the low head gradient portion of Fortymile Wash in the numerical model.

Discussed below are the criteria used to guide calibration, optimization procedures used during calibration, those model outputs for which the difference between predicted and observed values were minimized (calibration targets) during calibration, and those parameters that were optimized during calibration.

6.6.1.1 Calibration Criteria

Proper calibration of the site-scale SZ flow model requires consideration of the full range of available data, which include field data for water levels and hydraulic heads, permeability data from field and laboratory tests, locations of known faults and other geologic data, and hydrochemical data. Opinions expressed during the expert elicitation process (CRWMS M&O 1998 [100353]) also must be considered. The goal during development of site-scale SZ flow model was to deliver to PA a model that is realistic where data exist and is conservative where data are lacking.

6.6.1.2 Parameter Optimization Procedure

Calibration of the site scale SZ flow model was accomplished with the PEST-FEHM computer code, which is a combination of FEHM V 2.20 (STN: 10086-2.20-00, LANL 2003 [161725]; Zyvoloski et al. 1997 [100615]) and a commercial parameter estimation code named PEST V 5.5 (STN: 10289-5.5-00; Watermark Computing 2002 [161564]). PEST is a Levenberg-Marquardt (LM)-based optimization algorithm. The LM package is a well-established algorithm (Press et al. 1992 [103316], pp. 678 to 683), very robust, and widely applicable. It will search for the minima of a multidimensional function. In this case, the “function” is the sum-of-squares difference (SSD) between a set of observations (the heads in the 100+ wells in the Yucca Mountain region plus side-boundary fluxes from the regional flow model) and the solution to the partial differential equation that describes SZ flow at Yucca Mountain. PEST computes the

derivatives of the SSD function with respect to the various parameters. As discussed below in Section 6.6.1.3, those parameters optimized during calibration are the intrinsic permeability of each of the various hydrogeologic units and the permeability multipliers for some of the hydrogeologic features established in the model. An initial estimate or guess for each unknown parameter is specified at the beginning of the fitting process.

- FEHM computes the resulting heads for the initial estimate of parameters.
- The results are returned to the PEST code.
- Through a series of FEHM simulations with perturbations in the parameters, the LM package (PEST) computes the derivative of the SSD function with respect to each of the parameters.
- The LM package (PEST) then determines the amount to change each parameter's current value to improve the fit to the data. It does this through a mathematical process that combines gradient information and second derivative (approximated) information.

This process is repeated until the fit to data is within a prescribed tolerance or until no further improvement is possible. This coupling between PEST V 5.5 (STN: 10289-5.5-00; Watermark Computing 2002 [161564]) and FEHM V 2.20 (STN: 10086-2.20-00; LANL 2003 [161725]) allows any variable in FEHM to be considered as a fitting parameter, if desired, whether it be a flow-related or a transport-related parameter. PEST will find local minima of the target function. To enable the PEST-FEHM code to search for the global minimum, a procedure is attached to the code that carries out a simulated annealing process, which allows the PEST-FEHM code to move from one local minimum to another, better local minimum. This process is repeated until no further improvement occurs. The simulated annealing process (Press et al. 1992 [103316], pp. 436 to 448) is simple in principle. The approach is to reject an improved solution occasionally, move to a new location in parameter space, and continue the search. Theory indicates that this will eventually find the global or a near-global minimum. In the Yucca Mountain case, the procedure involves resetting the value of the LM step-size parameter after each local minimum is found.

In addition to the PEST V 5.5 (STN: 10289-5.5-00; Watermark Computing 2002 [161564]) optimization described above, several manual adjustments were made to the model. These were made to improve the model in ways that were not possible during the PEST run. The most important of these adjustments was to ensure that the specific discharge near Yucca Mountain was realistic with respect to the estimates given by the SZ expert elicitation panel (CRWMS M&O 1998 [100353]). Because the specific discharge was calculated with the particle-tracking feature of FEHM V 2.20 (STN: 10086-2.20-00; LANL 2003 [161725]) after the flow calculations were performed, this adjustment could not easily be incorporated in the PEST optimization. The specific discharge was adjusted by changing the permeability of the Bullfrog unit. Because of the large permeability of that unit, the specific discharge could be manipulated by changing the unit's permeability without adversely affecting the heads in the low-gradient area near Yucca Mountain. Adjustments were also made to the permeability in the lower Fortymile Wash area so water levels in the 2-D and Washburn wells in lower Fortymile wash would be more consistent with those in the upper Fortymile Wash area, thus preserving the

observed head gradient. The well locations will be discussed in Section 6.6.1.3. Adjustments to the permeability of the alluvial uncertainty zone and the permeability of the valley-fill aquifer were also made to better match eastern boundary fluxes of the regional model.

It is important to note that while the SZ model was calibrated with the application of the PEST code, the final product (a suite of FEHM files) does not include any PEST files. Thus, the SZ flow model may be used for PA or other purposes without the inclusion of the PEST executable code or related files.

6.6.1.3 Calibration Targets

The site-scale SZ flow model was calibrated to achieve a minimal difference between observed water levels and predicted water levels as well as between fluxes along specific boundary segments predicted by the regional model and the site-scale SZ model. For calibration targets, 115 water-level and head measurements were used. This was the complete set of wells available at the time of calibration. The measurements (DTN: GS00058312332.001 [149947]) represent water levels and deeper head measurements. The deeper measurements represent average values over "open" or "packed-off" intervals, and the coordinates of the observation represent mid-points of the interval. The calibration targets also represent steady-state values. Where pumping is taking place, as in the Amargosa Valley, current water levels are used. When comparing simulated water levels to target water levels, the model represents water levels at the target locations by assigning the target head value to the nearest grid block that is in the same hydrostratigraphic unit as the measurement.

During the calibration process, emphasis is given to minimizing the difference between observed and simulated water levels for selected calibration targets (i.e., at selected target locations) based on probable fluid pathways. This is accomplished by multiplying the squared differences at that location by a weighting factor. A weighting factor of 1.0 (i.e., no particular importance) normally is applied to calibration targets. However, a preferential weighting factor (20) is applied to approximately 30 calibration targets in the low-gradient region to the south and east of Yucca Mountain. These calibration targets are given high weighting because they are in the likely pathway of fluid leaving the repository site and because small changes in head in this area could produce a large effect on the flow direction. Calibration targets north of Yucca Mountain are given a low weighting (0.05; i.e., little importance). The five wells in this category are given low weights primarily because of the possibility of perching and the attendant uncertainty in water-level measurements in this region. For the base-case model, the moderate gradient wells or those wells that provide a transition between the high and low gradients proved to be relatively unimportant. The East-West barrier incorporated in the base-case model to establish the LHG was that primary reason for this. Other ACMs of the LHG without the East-West barrier were more sensitive to the moderate gradient wells and additional parameters were required for these models. The one head measurement in the Carbonate Aquifer is given a preferential weighting factor (20) because of the importance of this calibration target for reproducing an upward gradient in the calibrated model. The inclusion of an upward gradient within the calibrated site-scale SZ flow model is considered to be important for generating a realistic model because an upward gradient tends to force flow along shallower path lines as indicated by geochemical data. A complete listing of all target water-level values, target locations, and the weighting applied to each target is provided in Table 13.

Table 13. Observation Wells with Computed Head Data

Site Name	Fig. 22	*x* (UTM) (m)	*y* (UTM) (m)	*z* (elevation) (m)	Head Data* (m)	Model Data (m)	Model Data New Recharge Map (m)	Weight
UE-29 a #2	1	555753	4088351	990.8	1187.7	1165.96	1165.94	0.05
GEXA Well 4	2	534069	4086110	859.2	1009.0	1017.9	1017.89	0.05
UE-25 WT#6	3	549352	4083103	983.2	1034.6	945.34	945.26	0.05
USW G-2	4	548143	4082542	371.5	1020.2	933.87	933.79	0.05
UE-25 WT #16	5	551146	4081234	714.1	738.3	734.51	734.49	1
USW UZ-14	6	548032	4080260	793.4	779.0	734.89	734.86	1
UE-25 WT #18	7	549468	4080238	722.1	730.8	734.67	734.63	20
USW G-1	8	548306	4080016	125.7	754.2	735	734.98	1
UE-25 a #3	9	561084	4079697	681.4	748.3	798.99	798.99	1
UE-25 WT #4	10	550439	4079412	709	730.8	734.46	734.43	20
UE-25 WT #15	11	554034	4078694	698.7	729.2	733.87	733.85	20
USW G-4	12	548933	4078602	542.2	730.6	734.5	734.48	20
UE-25 a #1	13	549925	4078330	584	731.0	734.36	734.33	1
UE-25 WT #14	14	552630	4077330	703.6	729.7	733.79	733.77	20
USW WT-2	15	548595	4077028	702	730.6	734.18	734.16	20
UE-25 c #1	16	550955	4075933	473.2	730.2	733.92	733.89	20
UE-25 c #3	17	550930	4075902	474.3	730.2	733.92	733.89	20
UE-25 c #2	18	550955	4075871	553.2	730.2	733.9	733.88	20
UE-25 WT #13	19	553730	4075827	703.8	729.1	733.35	733.33	20
USW WT-7	20	546151	4075474	740.9	775.8	768.09	768.34	1
USW WT-1	21	549152	4074967	708.4	730.4	733.86	733.83	20
USW G-3	22	547543	4074619	318.1	730.5	734.96	734.94	20
UE-25 J-13	23	554017	4073517	354.8	728.4	732.74	732.73	20
USW WT-10	24	545964	4073378	734.2	776.0	781.48	781.41	1
UE-25 WT #17	25	549905	4073307	705.4	729.7	733.58	733.56	20
USW VH-2	26	537738	4073214	282.8	810.4	794.35	794.3	1
UE-25 WT #3	27	552090	4072550	705.8	729.6	733.08	733.06	20
USW VH-1	28	539976	4071714	490.5	779.4	783.68	783.62	1
UE-25 WT #12	29	550168	4070659	702.6	729.5	732.92	732.9	20
USW WT-11	30	547542	4070428	691.9	730.7	733.71	733.69	20
UE-25 J-12	31	554444	4068774	659.6	727.9	731.44	731.43	20
UE-25 JF #3	32	554498	4067974	662.7	727.8	731.15	731.14	20
Cind-R-Lite Well	33	544027	4059809	710.2	729.8	737.49	737.48	20
Ben Bossingham	34	553704	4056228	697.4	718.4	715.41	715.41	1
Fred Cobb	35	553808	4055459	675.6	702.8	713.61	713.61	1
Bob Whellock	36	553883	4055398	682	704.1	713.61	713.61	1
Louise Pereidra	37	554131	4055399	698	705.6	714.16	714.16	1
Joe Richards	38	554008	4055337	679.3	701.6	713.61	713.61	1
NDOT Well	39	553685	4055242	682.1	705.4	713.61	713.61	1
James H. Shaw	40	549863	4054911	664.3	706.7	707.46	707.46	1
Airport Well	41	552818	4054929	636.5	705.3	711.65	711.65	1
TW-5	42	562604	4054686	688.7	725.1	726.67	726.67	1

Table 13 (Continued). Observation Wells with Computed Head Data

Site Name	Fig. 22	*x* (UTM) (m)	*y* (UTM) (m)	*z* (elevation) (m)	Head Data* (m)	Model Data (m)	Model Data New Recharge Map (m)	Weight
Richard Washburn	43	549746	4053647	669.9	707.7	706	705.99	1
Richard Washburn	44	549679	4052322	675.3	704.4	703.92	703.91	1
Nye County Develop. Co.	45	543481	4050069	638.6	694.3	696.65	696.66	1
Fred Wooldridge	46	536350	4050006	673.8	691.9	688.06	688.1	1
Fred J. Keefe	47	540673	4049994	676.7	694.3	696.14	696.16	1
Leslie Nickels	48	541518	4049937	654.7	694.3	696.35	696.38	1
L. Mason	49	553471	4049848	699.2	722.1	711.75	711.78	1
Unknown	50	545596	4049403	667.6	697.8	695.99	695.99	1
Davidson Well	51	536552	4049329	672	690.1	688.07	688.11	1
Eugene J. Mankinen	52	538889	4049000	678.6	707.4	691.83	691.85	1
Donald O. Heath	53	542194	4048892	651.6	694.1	694.5	694.5	1
Elvis Kelley	54	536903	4048621	685.1	691.0	688.16	688.19	1
Manuel Rodela	55	546718	4048669	686.7	693.6	695.3	695.29	1
Charles C. DeFir Jr.	56	538196	4048442	685.7	706.9	691.1	691.12	1
William R. Monroe	57	540035	4048450	669.5	693.7	694.8	694.82	1
DeFir Well	58	536655	4048405	671.1	690.2	688.21	688.24	1
Edwin H. Mankinen	59	540608	4048083	662.8	695.2	694.4	694.41	1
Bill Strickland	60	534967	4047966	677	689.2	687.22	687.23	1
M. Meese	61	547120	4047963	664.6	686.4	693.47	693.46	1
Theo E. Selbach	62	547941	4047782	673.3	696.2	693.99	694	1
C.L. Caldwell	63	537727	4047670	654.5	691.4	690.7	690.72	1
Leonard Siegel	64	552390	4047685	667.2	709.0	703.7	703.75	1
James K. Pierce	65	541778	4047596	664	690.4	693.41	693.42	1
James K. Pierce	66	541381	4047563	677.1	705.6	693.64	693.65	1
Cooks West Well	67	553609	4047631	690.2	720.1	712.24	712.33	1
Cooks East Well	68	554006	4047633	693.4	718.9	712.24	712.33	1
Nye County Land Co.	69	548466	4047261	715.4	690.1	693.28	693.27	1
Amargosa Town Complex	70	548492	4047077	668.3	688.8	693.28	693.27	1
Nye County Develop. Co.	71	550431	4047057	615.4	691.2	694.89	694.72	1
Lewis C. Cook	72	553612	4047076	702.5	717.4	714.02	714.13	1
Lewis C. Cook	73	553687	4047077	688.7	714.8	714.02	714.13	1
Amargosa Valley Water	74	548393	4046953	673.9	701.3	691.81	691.81	1

Table 13 (Continued). Observation Wells with Computed Head Data

Site Name	Fig. 22	*x* (UTM) (m)	*y* (UTM) (m)	*z* (elevation) (m)	Head Data* (m)	Model Data (m)	Model Data New Recharge Map (m)	Weight
Earl N. Selbach	75	539147	4046844	672.1	696.5	694.05	694.05	1
Lewis N. Dansby	76	539968	4046817	664.7	694.2	695.22	695.22	1
Edwin H. Mankinen	77	540788	4046821	686.2	694.0	693.64	693.64	1
Willard Johns	78	552097	4046882	678.9	699.5	708.82	708.82	1
USW WT-24	79	548697	4081909	734.8	840.1	830.76	830.72	1
USW H-1 tube 1	79	548727	4079926	–495.5	785.5	741.96	741.94	1
USW H-1 tube 2	80	548727	4079926	193	736.0	734.68	734.65	1
USW H-1 tube 3	81	548727	4079926	562.5	730.6	734.63	734.6	20
USW H-1 tube 4	82	548727	4079926	680.5	730.8	734.65	734.62	20
USW H-5 upper	83	547668	4078841	704.2	775.5	734.65	734.62	1
USW H-5 lower	84	547668	4078841	446.4	775.6	734.66	734.63	1
UE-25 b #1 lower	85	549949	4078423	–8.8	729.7	735.53	735.51	20
UE-25 b #1 upper	86	549949	4078423	366.2	730.6	734.34	734.32	20
USW H-6 upper	87	546188	4077816	662.9	776.0	764.08	763.61	1
USW H-6 lower	88	546188	4077816	315.8	775.9	763.93	763.76	1
USW H-4 upper	89	549188	4077309	395.5	730.4	734.25	734.23	20
USW H-4 lower	90	549188	4077309	45	730.5	735.1	735.08	20
USW H-3 upper	91	547562	4075759	576.9	731.5	734.48	734.44	20
USW H-3 lower	92	547562	4075759	343.2	755.9	734.51	734.48	1
UE-25 p #1 (Lwr Intrvl)	93	551501	4075659	–410.3	752.4	739.69	739.67	1
USW SD-7	95	548384	4076499	637.7	727.6	734.13	734.1	20
USW SD-9	96	548550	4079256	678.3	731.1	734.64	734.61	20
USW SD-12	97	548492	4077415	696.7	730.0	734.31	734.28	20
NC-EWDP-1DX, shallow	99	536768	4062502	413.5	786.8	763.9	764.01	1
NC-EWDP-1S probe 1	100	536771	4062498	747.8	787.1	773.29	773.26	1
NC-EWDP-2D	101	547744	4057164	507.2	706.1	709.26	709.26	1
NC-EWDP-3D	102	541273	4059444	376.7	718.3	703.88	704.07	1
NC-EWDP-3S probe 2	103	541269	4059445	719.1	719.8	702.54	702.75	1
NC-EWDP-5SB	104	555676	4058229	603.9	723.6	717.98	717.97	1

Table 13 (Continued). Observation Wells with Computed Head Data

Site Name	Fig. 22	*x* (UTM) (m)	*y* (UTM) (m)	*z* (elevation) (m)	Head Data* (m)	Model Data (m)	Model Data New Recharge Map (m)	Weight
NC-EWDP-9SX probe 2	105	539039	4061004	721.2	767.3	732.49	732.69	1
NC-Washburn-1X	106	551465	4057563	668.8	714.6	714.55	714.55	1
UE-25 J-11	107	563799	4071058	687.2	732.2	731.57	731.57	20
BGMW-11	108	534386	4062600	673.4	715.9	724.56	724.91	1
Richard Washburn	109	549529	4052567	739.9	704.0	704.05	704.04	1
L. Cook	110	551348	4047432	704.1	713.2	699.01	698.95	1
Unknown	111	549532	4047668	691.8	689.5	695.05	694.89	1
Amargosa Water	112	547420	4047594	714.3	690.4	693.47	693.46	1
Lewis C. Cook	113	554329	4047666	735.5	715.7	713.71	713.75	1
Unknown	114	538989	4048877	710.1	690.8	691.83	691.85	1
USW UZ-N91	115	555680	4088196	1180.6	1186.7	1165.78	1165.76	0.05

Source: DTN: GS010908312332.002 [163555]; Output DTN: LA0304TM831231.002.

* Head Data is the mean water-level altitude (m).

NOTE: The “Fig. 22” label in the second column of the table refers to the numbers given in Figure 22 below.

In addition to water levels, fluxes around certain boundary segments were used as calibration targets. Fluxes from all of the boundary segments on the eastern and northern boundaries of the site-scale SZ flow model domain were used as calibration targets during parameter optimization. Fluxes from the five western boundary segments were not used during parameter optimization. Preliminary calibration runs indicated that it was difficult to match the fluxes along these segments predicted by the site-scale model with those predicted by the regional-scale model. This difficulty largely was a result of the different HFMs used in the site-scale and regional-scale models. The goal of ensuring that the total flux through the site-scale model domain is close to that predicted by the regional-scale model was achieved by not forcing a close match along those boundary segments for which the rock types (because of differences in the grid resolution and the HFMs) were different in the two models. Thus, a weighting scheme was used with the target fluxes. Zero weight was applied to the Western boundary segments and weights between one and two were used for the Eastern and Northern segments.

6.6.1.4 Calibration Parameters

Permeability is optimized during calibration of the site-scale SZ flow model. The model formulation and the FEHM V 2.20 (STN: 10086-2.20-00; LANL 2003 [161725]) code allow for the specification of a permeability value at each node. However, there is not sufficient water-level and permeability data to warrant identifying a specific value of permeability for each individual node during calibration. Consequently, sets of nodes are grouped into specific permeability zones based on similar permeability characteristics. A single permeability value is assigned to each zone. These zonal values of permeability serve as the parameters that are optimized during model calibration. Permeability zones are created for hydrogeologic units identified in the HFM and for specific hydrogeologic features. With the exception of the basal

unit that serves as a lower boundary for the model, a permeability zone is established for each hydrogeologic unit. All of the nodes within a specific hydrogeologic unit are assigned to that permeability zone unless they are included in one of the permeability zones established for specific hydrogeologic features. It should be noted that the zone sizes are fixed, largely based on the hydrogeologic framework model provided by the USGS. Some on the uncertainty associated with geologic contacts is discussed in Section 6.8.6.

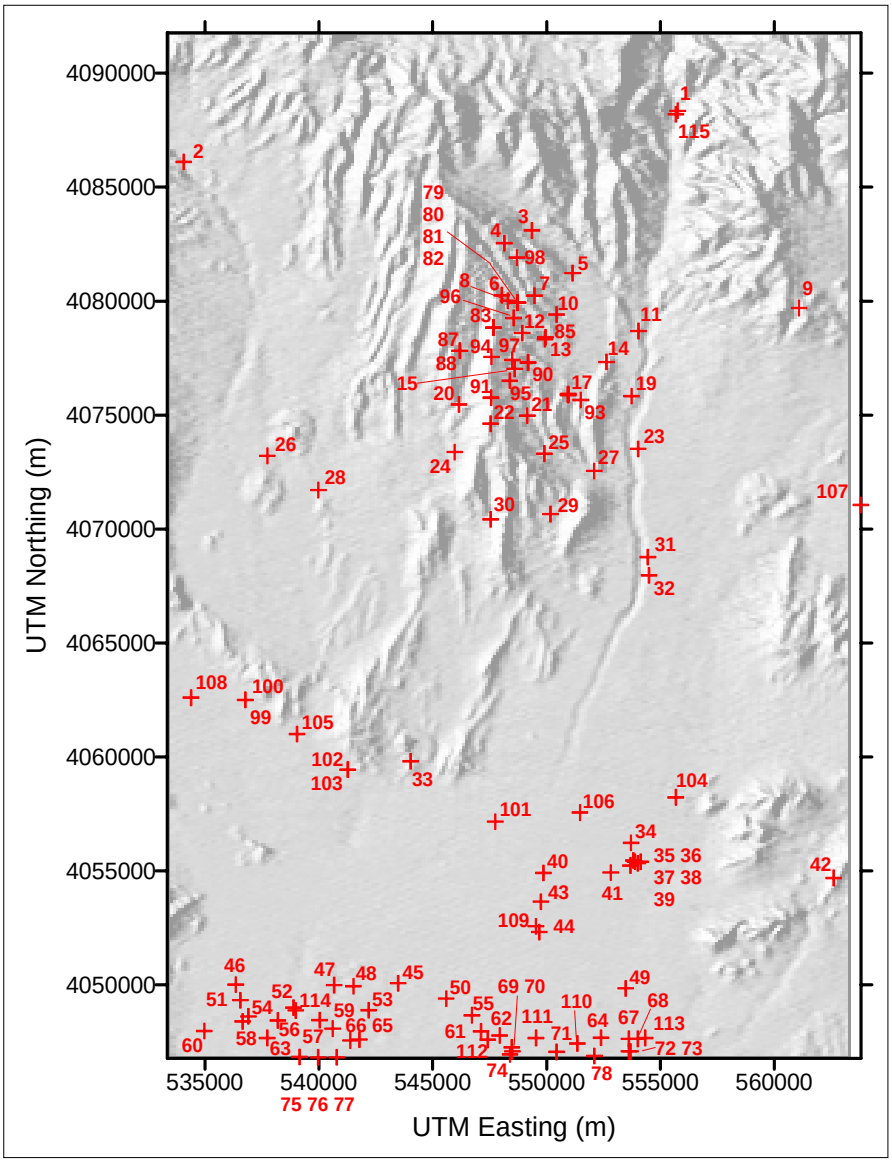

DTN: GS010908312332.002 [163555].

NOTE: Numbers in the figure refer to the label listed in the second column of Table 13.

Figure 22. Location of Observation Wells

For permeability, vertical anisotropy is assigned a value of 10:1 (horizontal to vertical) in the volcanic and valley-fill units in the site-scale SZ flow model. Relatively lower permeability in the vertical direction may occur in stratified media, and the ratio of 10:1 is in the generally

accepted range (CRWMS M&O 1998 [100353], Table 3-2). Furthermore, the relatively high vertical gradient observed in well UE-25p#1 suggests that vertical permeability is lower than horizontal permeability. Well NC-EWDP-2D also exhibited a vertical gradient. The uncertainty associated with the vertical anisotropy is discussed in Section 6.8.3.1.

Specific hydrogeologic features that were thought to potentially impact groundwater flow are also classified as permeability zones. The permeability variable or permeability multiplication factor used for a specific feature is assigned to all of the nodes within that feature. The hydrogeologic features for which special permeability zones were established are primarily faults, fault zones, and areas of chemical alteration (Section 6.5.2). As previously discussed, these features are distinct from the subhorizontal hydrogeologic units identified in the HFM. Each of the identified hydrogeologic features includes multiple geologic formations and represents zones of altered permeability within the individual formations.

Twenty-seven permeability zones were established for model calibration. In addition, permeability multipliers were assigned to four zones that contain geologic features that penetrate a number of hydrogeologic units. The permeability multipliers are used to modify the permeability values assigned to the hydrogeologic units in the area of the geologic features. While the permeability parameter or multiplier values for most zones are optimized during calibration, permeability for the upper carbonate aquifer was assigned a constant value because sensitivity analyses indicate that the model is not sensitive to this parameter value.

The parameters used in the calibration of the SZ flow model are a combination of permeabilities of hydrogeologic units, permeabilities of faults and other features, and permeability multipliers of faults and features. Permeabilities of the 18 hydrogeologic units were chosen as calibration parameters because of both the importance of the parameter in the flow system and the fact that each of the units was identified in the HFM. The parameters that represent these features were added because they were identified as important structural features (e.g., the Solitario Canyon fault), were in the regional-scale model (e.g., the Spotted Range-Mine Mountain zone), or were necessary for some conceptual feature, such as the high head gradient north of Yucca Mountain (east-west barrier). The number of parameters represents a computationally tractable set.

Upper and lower bounds are placed on each permeability variable during parameter optimization. The upper and lower bounds for the permeabilities and permeability multipliers are chosen to reflect maximum and minimum field values (permeability) or a reasonably realistic range of values (permeability multipliers). For example, when the multiplier represents flow in the plane of a fault, the multiplier is allowed to take on values between 1 and 100; when the multiplier represents geochemical alteration, the multiplier is allowed to take values between 0.00001 and 0.50000. The upper bounds for permeability for faults were generally higher than the hydrostratigraphic unit where the fault was situated. The final calibrated values of the parameters are not sensitive to initial parameter values within the range specified, thus giving confidence that the calibration values are unique within the specified bounds of permeability.

A list of permeability zones, including the parameter type assigned to each zone, the upper and low bounds specified for the parameter, and an identification of the parameters optimized during calibration, are provided in Table 14.

Table 14. Calibration Parameters Used in the Saturated-Zone Site-Scale Model

Parameter Name	Geologic Unit or Feature	Calibrated Value	Parameter Type	Minimum Value	Maximum Value
gran	Granites	1.96×10^{-16}	Permeability	1.00×10^{-17}	1.00×10^{-14}
lcla	Lower Clastic Confining Unit	1.00×10^{-16}	Permeability	1.00×10^{-16}	1.00×10^{-14}
lca2	Lower Carbonate Aquifer	5.00×10^{-14}	Permeability	5.00×10^{-14}	1.00×10^{-12}
ucla	Upper Clastic Confining Unit	1.00×10^{-16}	Permeability	1.00×10^{-16}	1.00×10^{-14}
lca1	Lower Carbonate Aquifer Thrust	1.00×10^{-14}	Permeability	1.00×10^{-14}	1.00×10^{-12}
ucar	Upper Carbonate Aquifer	4.08×10^{-14}	Permeability (fixed)	4.08×10^{-14}	4.08×10^{-14}
udif	Undifferentiated Valley Fill	5.00×10^{-15}	Permeability	5.00×10^{-15}	1.00×10^{-12}
ovoc	Older Volcanic Confining Unit	2.00×10^{-16}	Permeability	2.00×10^{-16}	1.00×10^{-11}
ovoa	Older Volcanic Aquifer	5.00×10^{-16}	Permeability	3.00×10^{-16}	1.00×10^{-12}
lvoc	Lower Volcanic Confining Unit	2.00×10^{-15}	Permeability	1.00×10^{-15}	1.00×10^{-11}
tram	Crater Flat-Tram	2.36×10^{-13}	Permeability	1.00×10^{-13}	1.00×10^{-11}
bull	Crater Flat-Bullfrog	1.54×10^{-11}	Permeability	1.00×10^{-13}	8.00×10^{-11}
prow	Crater Flat-Prow Pass	8.00×10^{-12}	Permeability	1.00×10^{-13}	5.00×10^{-11}
uvoc	Upper Volcanic Confining Unit	5.00×10^{-14}	Permeability	4.00×10^{-14}	1.00×10^{-12}
uvoa	Upper Volcanic Aquifer	8.00×10^{-14}	Permeability	8.00×10^{-14}	1.00×10^{-11}
lava	Lava Flow Aquifer	1.00×10^{-12}	Permeability	1.00×10^{-16}	2.00×10^{-12}
lime	Limestone Aquifer	1.00×10^{-12}	Permeability	1.00×10^{-15}	1.00×10^{-11}
vala	Valley Fill Aquifer	5.00×10^{-12}	Permeability	1.00×10^{-13}	8.00×10^{-12}
ewba	East-West Barrier	1.05×10^{-18}	Permeability	1.00×10^{-18}	1.00×10^{-15}
nsba	Solitario Canyon Fault	1.00×10^{-18}	Permeability	1.00×10^{-18}	1.00×10^{-15}
fpb1	Fortymile Wash Fault	10	multiplier	2	100
fpb2	Spotted Range-Mine Mountain Zone	11.7789	Multiplier	1	70
fpb3	Northern Low Perm Zone	7.11×10^{-2}	Multiplier	1.00×10^{-5}	0.5
fpb4	Imbricate Fault Zone	1	Multiplier	1	100
cffz	Crater Flat Fault	5.00×10^{-14}	Permeability	1.00×10^{-15}	5.00×10^{-13}
allu	Alluvial Uncertainty Zone	3.20×10^{-12}	Permeability	1.00×10^{-13}	1.00×10^{-11}
wash	Lower Fortymile Wash Zone	5.00×10^{-12}	Permeability	1.00×10^{-14}	8.00×10^{-12}

Output DTN: LA0304TM831231.002.

6.6.2 Calibration Results

6.6.2.1 Water Levels

The water levels predicted by the calibrated site scale SZ flow model along with the observed water level at each of the calibration target locations is presented in Table 13. The location of each of the target observation wells is shown in Figure 22. The calibration targets (water levels) are from DTN: GS000508312332.001 [149947] and updated in DTN: GS010908312332.002 [163555]. The calibration targets are discussed in Section 6.6.1.3. The distribution of residuals, along with the measured and simulated water-level surfaces, resulting from the calibrated model is provided in Figure 23. It is noted here that the actual water levels (not the interpolated surface) in each well is used for comparison. In the more recent interpretations, such as DTN:

GS010608312332.001 [155307], potentiometric surface map output from USGS (2001 [157611]), the head contours have been smoothed in the area near wells WT-24 and G-2 to reflect perched conditions. The different interpretations of the water-table surface, that is, whether or not wells WT-24 and G-2 are perched, have little impact on the results. This is because those wells were given a low weight (owing to their suspect levels) and do not affect the calibration. Interestingly, the model consistently reports simulated levels in WT-24 and G-2 that are closer to the perched interpretations than the original high water-table values.

A weighting scheme was used in conjunction with the PEST (STN: 10289-5.5-00; Watermark Computing 2002 [161564]) code to focus the calibration in areas where the confidence in the data was high (i.e., the low gradient area) or importance to the TSPA calculations was great (i.e., along the flow path). A low weighting on a target value will cause PEST to essentially ignore the value, and high value will cause PEST to respect the target value at the expense of other observations.

The calibrated SZ flow model has a sum-squared weighted residual of about 27,600, which translates into about a 16-m (weighted) residual for each observation. Without weighting, the sum-squared residual is about 90,000, which corresponds to the approximately 30-m average residual for each observation. It is also worth noting here that compared to the overall head drop in the SZ site-scale model of approximately 500 m, the 30-m average residual amounts to a 6 % error.

As can be seen in Figure 23, the largest head residuals (~80 m) are in the northern part of the model in the high-head gradient area near the East-West barrier. In the figure, a negative residual means that the calibrated value was lower than the target data. These head values are largely the result of the low weighting factor of (0.05) and the uncertainty in these measurements, possibly due to perched conditions. The next highest group of heads borders the East-West barrier and the Solitario Canyon fault. These residuals (~50 m) are most likely the result of 500-m gridblocks not being able to resolve the 780-m to 730-m drop in head in the very short distance just east of the above-mentioned features. There may well be additional complicating factors such as the changing character in the Solitario Canyon fault along its north-south transect. The fault is modeled as a barrier with only one calibration parameter. This may be inadequate to represent the behavior locally of such a long feature. For example well H-5, about 1000 m from the Solitario Canyon fault, has discrepancy between measured and simulated heads of 41 m. The measured head for this well (775 m), located on the east side of the fault, is closer to measured head values on the west side of the fault. Since the majority of wells on the east side are around 735 m, the simulated head for H-5 was close to that value. Luckey et al. (1996 [100465], p. 25) discuss potential causes for the high head measurements at H-5 located just to the east of the Solitario Canyon fault. When comparing the predicted and the observed water-level surfaces, it should be noted that both water-table surfaces are contoured and that the data distribution for both surfaces is not uniform. Evident in the comparison is the low-gradient region in the Fortymile Wash region, the high-gradient region north of Yucca Mountain, and the flow disruption caused by the Solitario Canyon fault. These results indicate that the model adequately represents the current water table in the vicinity of Yucca Mountain.

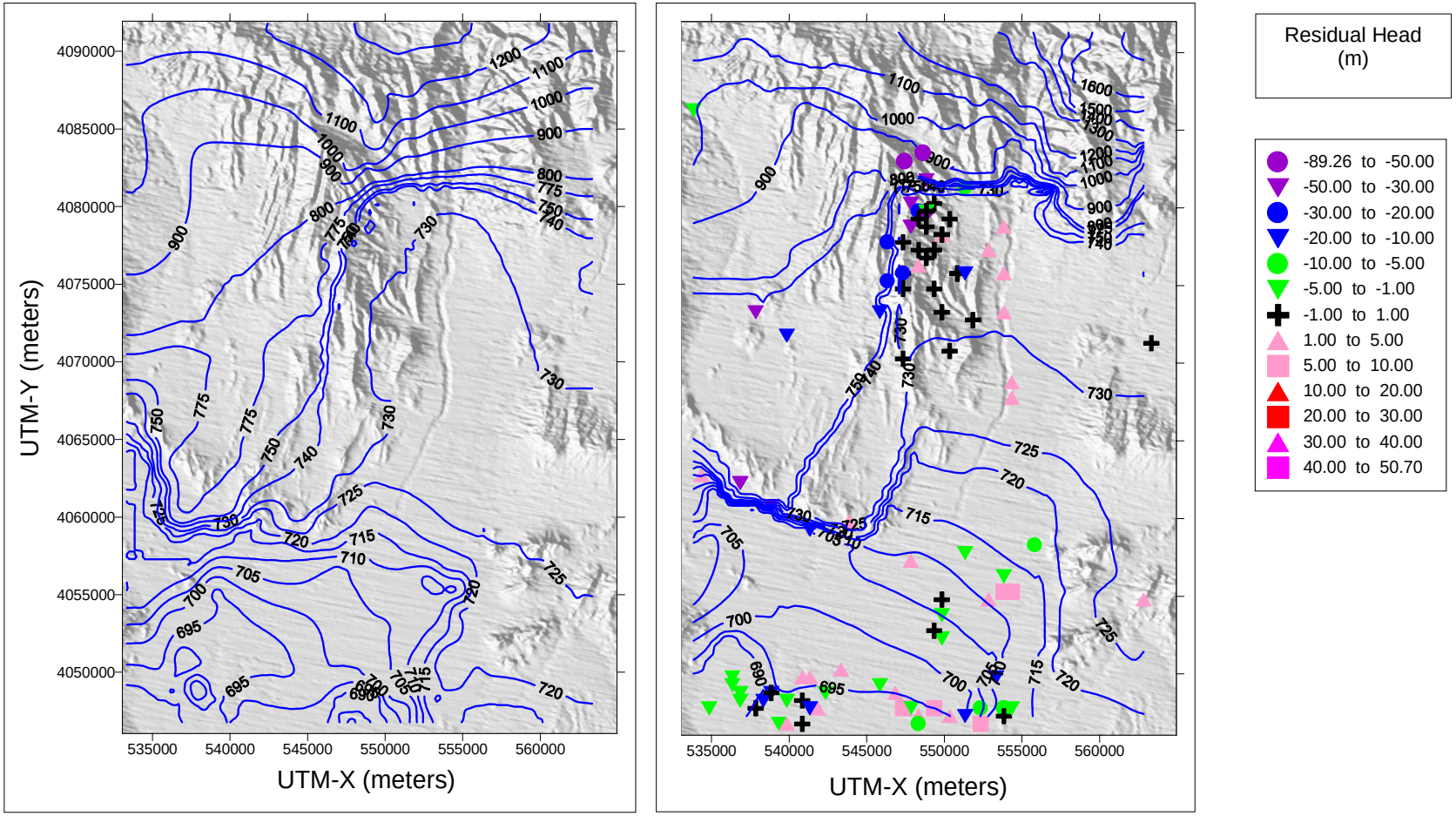

DTN: GS000508312332.001 [149947] (left panel); Output DTN: LA0304TM831231.002 (right panel).

NOTE: Symbols in right panel represent well locations.

Figure 23. Contour Plot of Water-Level Data (left panel) and Simulated Water-Level Data with Residual Heads (right panel)

The recharge map used in the calibration process is described in CRWMS M&O (1999 [130979], Section 4). It is also important to note that during performance-assessment (TSPA-SR) calculations (CRWMS M&O 2000 [139440]), a newer recharge map was used than the one used here. The older map was used for calibration purposes because it was the only map available at the time of calibration. The only differences are in the area of the model associated with the UZ model, and in that area the changes were small. The complete details of the newer recharge map are described in CRWMS M&O (2000 [139440]). The important aspect to be addressed in this report is the effect of the newer recharge map on the calibrated flow model. The differences are given in Table 13 with tenths of a meter difference at most. Thus, it is appropriate for the TSPA to use either recharge map.

6.6.2.2 Comparing Fluxes Derived from the Regional Model with Fluxes Calculated from the Calibrated Model

The SZ flow model describes a small part of the Death Valley regional groundwater flow system. By comparing the SZ flow model with the numerical model of the larger regional system, additional constraints can be applied to the model. The comparison between the two models was also suggested by the Expert Elicitation Panel (CRWMS 1998 [100353]). The numerical model of the regional flow system models a closed system and contains data from spring discharges to help fix the water flux through the system (D'Agnese et al. 1997 [100131]). Thus, it is appropriate to compare the fluxes in the two models. The hydrogeologic framework model is being continuously updated. A fact that diminishes the value of this comparison is the use of different versions of the hydrogeologic framework model in the regional and SZ site scale models. The regional model uses an older hydrogeologic framework model, which is described in D'Agnese et al. (1997) [100131]. The SZ flow model uses a newer hydrogeologic framework model, which is described in USGS 2001 [158608]. In Section 6.6.1.4, the methodology for applying fixed-head boundary conditions on the sides of the SZ flow model was described. With fixed-head boundary conditions, the flux through the boundary is a function of the permeabilities. A comparison of fluxes derived from the regional model and fluxes derived from the calibrated site-scale model are shown in Table 15. In this table, the zones with "N" in the label refer to the northern boundary, those with an "E," the eastern boundary, and so on. The zones are depicted graphically in Figure 24. The comparison is reasonable on the northern and eastern boundaries. The northern boundary, for instance, has a total flux of 189 kg/s across it in the regional model and 169 kg/s across it in the SZ calibrated model. As can be seen in Table 15 and Figure 24, the distribution is different, which is not unexpected because the regional and SZ calibrated models are based on different hydrogeologic models. The match was good on the eastern side of the model with the lower thrust area, E1. The other zones showed small flows in both models. The match between the two models was poor on the western boundary. The southern boundary flux, which is simply a sum of the other boundary fluxes plus the recharge, is also a good match. The difference in southern fluxes (shown as zone S in Table 15) is about 21 percent.

Several factors affect the flux match between the two models: the horizontal and vertical resolution, the hydrologic framework model, and the permeability distribution. The horizontal resolution of the site-scale model is three times finer than the regional model (500-m versus 1500-m gridblock size). The vertical resolution of the site-scale SZ model is an order of magnitude finer than the regional model (39 layers versus 3 layers). The increased resolution of

the site-scale means that fluxes calculated by the site-scale model may depend more strongly on a few units than on the regional-scale model. This fact is important when considering that many of the unit permeabilities in the site-scale SZ model are constrained by field data. The hydrologic framework model used in the regional-scale model is older than that used in the site-scale model (for a complete discussion, see the previous version of this model report, BSC 2001 [155974]). The newer HFM used in the site-scale model differs considerably from the older HFM used in the 1997 regional model, which is why the matching requirements for the fluxes were relaxed for the western boundary and the flux distribution is different on the northern boundary. The last factor affecting the flux distribution in the regional model is the use of permeability classes. In the regional model, permeabilities associated with specific units are not defined (D'Agnese et al. 1997 [100131]). Rather, the permeabilities are grouped into classes, and a class assigned to a particular grid block based on the percentages of the rock types contained in the grid block. Thus, even though the regional-scale model was based on a complex hydrogeologic framework model, the actual model used only four permeability classes. That method of assigning permeabilities made it difficult to reproduce the distribution of fluxes on the side of the site-scale model, if done on a unit-by-unit basis. In turn, this discrepancy makes it difficult to reproduce vertical flow or head gradients if they existed in the regional model because this would require a flux distribution on the lateral boundaries assigned by hydrogeologic unit.

Table 15. Comparison of Regional and Site-Scale Fluxes

Boundary Zone	Regional Flux (kg/s)	Site-Scale Flux (kg/s)	Calibration Target ?
N1	–101.24	–60.0	Yes
N2	–16.48	–33.4	Yes
N3	–53.05282	–30.6	Yes
N4	–18.41	–44.8	Yes
W1	3.45	4.17	No
W2	–71	–0.00719	No
W3	–6.9	–0.0000078	No
W4	2.73	–0.0000223	No
W5	–46.99	–6.85	No
E1	–555.45	–553.9	Yes
E2	–5.46	3.53	Yes
E3	2.65	16.50	Yes
E4	–3.07	16.8	Yes
S	918	724	No

Source: D'Agnese et al. (1997 [100131]); Output DTN: LA0304TM831231.002.

NOTE: A negative value indicates flow into the model.

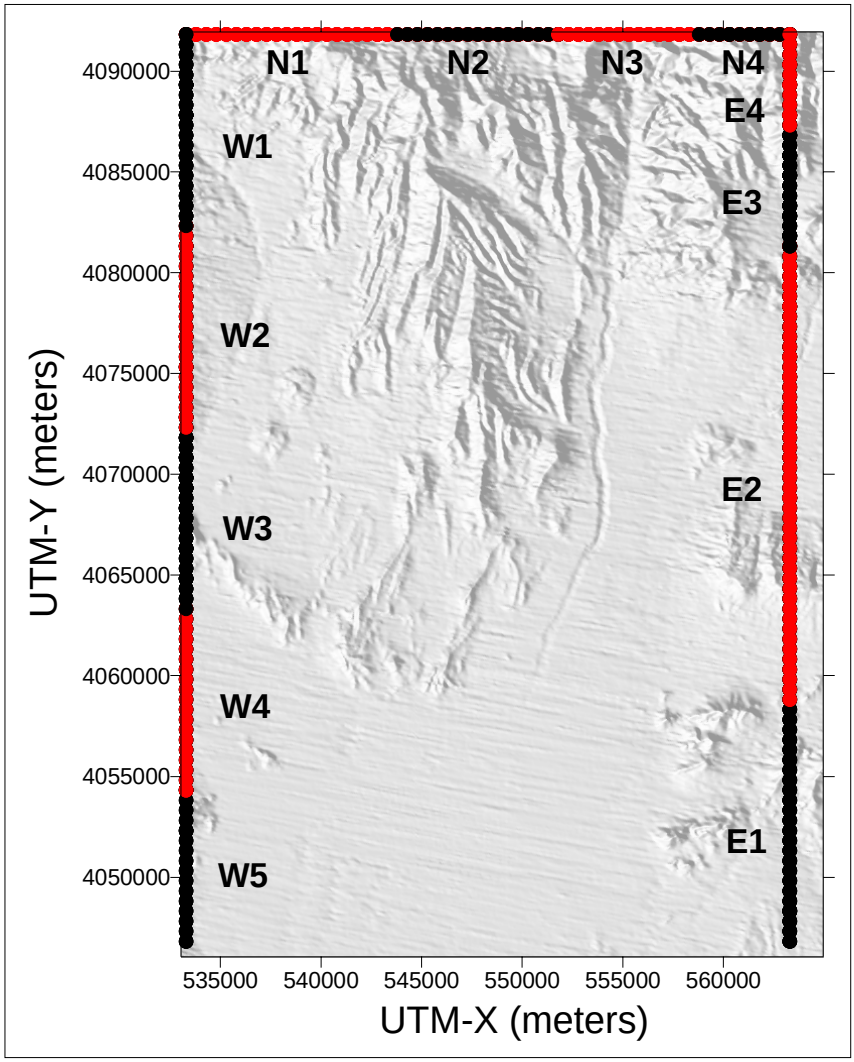

Source: Previous version of this model report (BSC 2001 [155974])

NOTE: Colors are used only to discriminate among flux zones.

Figure 24. Flux Zones Used for Comparing Regional and Site-Scale Fluxes

6.6.2.3 Predicted Flow Paths

The particle-tracking capability of FEHM V 2.20 (STN: 10086-2.20-00; LANL 2003 [161725]) was used to demonstrate flow paths predicted by the calibrated site-scale SZ flow model. One hundred particles were distributed uniformly over the area of the repository and allowed to migrate until they reached the model boundary (Figure 25). The pathways generally leave the repository and travel in a south-southeasterly direction to the 5-km boundary and the 18-km compliance boundary. From the 18-km boundary to the end of the model, the flow paths trend to the south-southwest and generally follow Fortymile Wash. Most of the pathways pass through the designated Imbricate Zone (Zone 91 of Figure 19). Some of the pathways follow fault zones along Fortymile Wash (Zones 57 and 58 of Figure 19). The hydrogeologic units through which the fluid leaving the repository layer passes consist of the Crater Flat group (Bullfrog, Tram, and Prow Pass) with most of the flow in the Bullfrog unit, the Upper Volcanic Aquifer, the Upper Volcanic Confining Unit, the Valley Fill Unit, and the Undifferentiated Valley-Fill Unit. Figure

25 shows a vertical cross section of the path lines. Evident in the figure is the shallow depth of the path lines, which is consistent with data supporting an upward head gradient. In Section 7, the fluid pathways are compared with those inferred by geochemical data.

6.6.2.4 Specific Discharge

Using the calibrated flow model, specific discharge was estimated for a nominal fluid path leaving the repository area and traveling 0 to 5-, 5 to 20-, and 20 to 30-km (0, 3, 12.5, and 18.6 mi). The specific discharge simulated by the flow model for each segment of the flow path from the repository was determined using the median travel time (50th particle) for a group of particles released beneath the repository. By dividing the distance between the boundaries (shown in Figure 25) by the median travel time, values for specific discharge of 0.67 m/yr, 2.3 m/yr, and 2.5 m/yr (2.2, 7.5, and 8.2 ft/yr) were obtained, respectively, for the three segments of the flow path. The expert elicitation panel (CRWMS M&O 1998 [100353], Figure 3-2e) estimated a median specific discharge of 0.71 m/yr (2.3 ft/yr) for the 5-km (3-mi) distance. Thus, good agreement is found between the specific discharge predicted by the calibrated model and that estimated by the expert elicitation panel for this distance. The expert elicitation committee did not consider other travel distances.

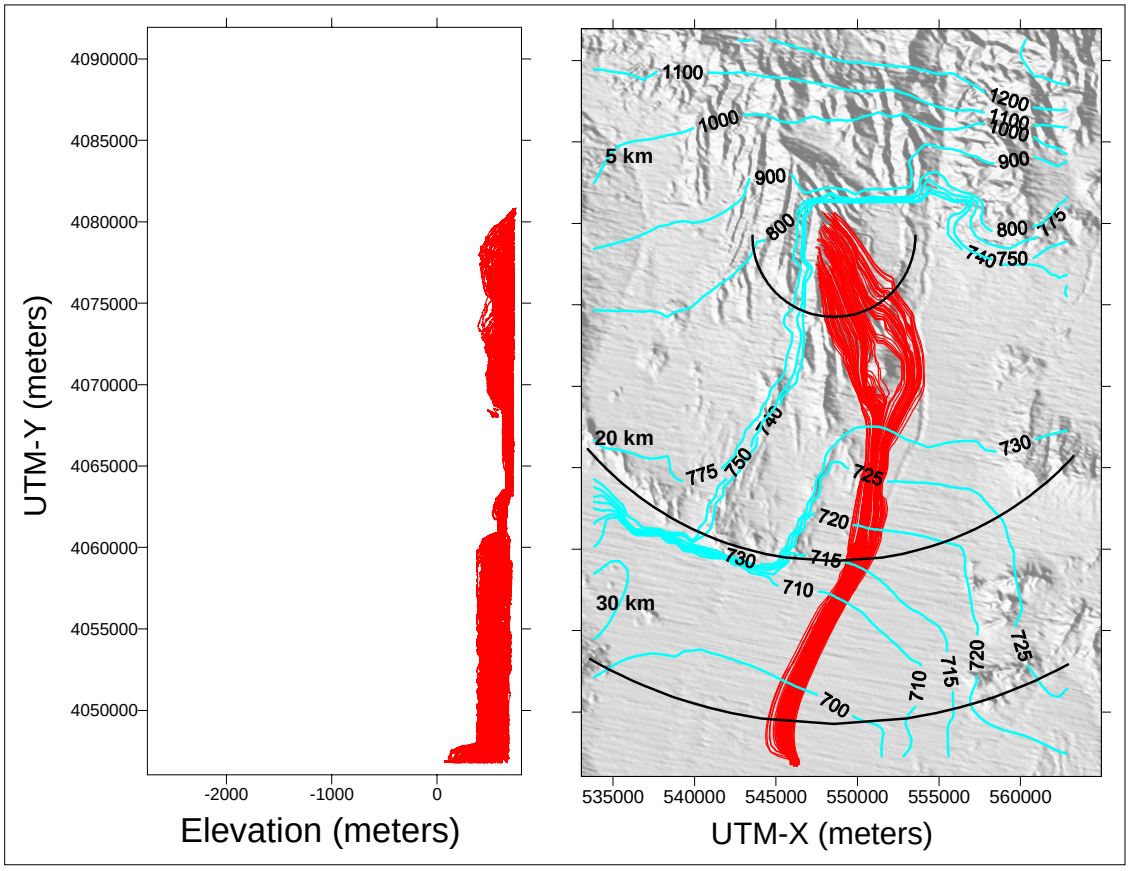

Output DTN: LA0304TM831231.002.

NOTE: Blue lines refer to head contours; red lines refer to particles. Circles correspond to the 5-km boundary and the 18-km and 30-km compliance boundaries. The left panel is the north-south vertical plane; the right panel is the plan view.

Figure 25. Flow Paths from the Repository with Simulated Hydraulic Head Contours

6.7 EVALUATION OF ALTERNATIVE MODELS

6.7.1 Large Hydraulic Gradient ACM

An overview of the Large Hydraulic Gradient ACM is presented below, followed by discussions of the model setup used in evaluating the ACM and of the results of the evaluation. The section concludes with an assessment of the impact of the Solitario Canyon Fault ACM on the site-scale SZ flow model. The evaluation of ACMs associated with the large hydraulic gradient is taken from Zyvoloski et al. (2003) [163341]. The evaluation of the Solitario Canyon Fault ACM is specific to this model report and is not needed for any TSPA or other models.

6.7.1.1 Overview of Large Hydraulic Gradient ACM

The large hydraulic gradient (LHG) north of Yucca Mountain has been a feature of the flow system near Yucca Mountain that has been the subject of interest over the years (see Figure 3). Compared to the very gentle gradient from the repository to points south, the gradient north of the site is much larger. The cause of this gradient is unknown. To simulate the LHG in models, a low-permeability east-west feature has been incorporated into the base-case conceptual model north of Yucca Mountain. Because there is little field evidence for the presence of this feature, alternate conceptualizations are plausible. The Claim Canyon Caldera, north of Yucca Mountain, is an area of extensive hydrothermal alteration that may result in a generalized reduction in permeability in the hydrogeologic units in this area. Permeability changes in similar environments have been studied by economic geologists (Norton and Knapp 1977 [147379]). Alternate conceptualizations have been formulated, which remove the extensive set of features north of Yucca Mountain but divide the model domain along the Claim Canyon Caldera into northern and southern zones, allowing different permeabilities to be assigned in the north versus the south within the same hydrogeologic unit. By creating a distributed region of lower permeability in the northern portion of the model, the LHG can be simulated in the flow domain. Using this basic conceptualization, different models incorporating the northwest-southeast trending fault zone just north of Yucca Mountain, the Ghost Dance Fault, and the Dune Wash Fault have been formulated to evaluate the sensitivity of the base-case model to different conceptualizations of the LHG.

6.7.1.2 Large Hydraulic Gradient ACM Setup

The alternate conceptualizations of the LHG do not make use of the extensive feature set north of Yucca Mountain, and these have been removed from the base-case model grid (Figure 5) thereby simplifying the grid in the alternate conceptualizations considered for the LHG. Instead, the hydrogeologic units have been divided into northern and southern zones at the Claim Canyon Caldera boundary. Differing permeabilities can be assigned in each zone to each hydrologic unit. Two variants of this basic approach are considered: one uses only the alteration zone, whereas the other includes the alteration zone and a zone to represent the northwest-southeast trending fault zone just north of Yucca Mountain (Feature 2 in Figure 5). These models are referred to as the “altered, no fault” (ANF) and “altered, with fault” (AWF) models, respectively. Although there are fewer discrete features in the altered models than in the base-case model, there are actually a greater number of calibration parameters. This increase is a result of breaking the hydrogeologic units into independent northern and southern zones. A third alternate

model, which adds features to the AWF model to account for the Ghost Dance Fault (GDF) and the Dune Wash Fault was also formulated to improve the calibration obtained with the AWF conceptual models. This third alternate conceptual model is referred to as the AWF/GDF model.

The alternative models resulted only in changes to the computation grid that were necessary to implement these alternate formulations of the hydrogeology. The alternative models were calibrated in a manner identical to that previously described for the base-case SZ flow model. Water-level contour maps and particle tracks were generated based on the water levels predicted by the alternative models in a manner similar to that previously described for the base-case SZ flow model.

6.7.1.3 Large Hydraulic Gradient ACM Results

Water levels predicted by the base case and the LHG models at selected observation points are presented in Table 16. The calibrated permeability values, the base-case model, and the LHG model are presented in Table 17. All models did a good job of reproducing the gradient in the flow path downstream of the repository, and each model has similar sum-of-the-squared residuals on an overall basis. However, the simulations of the conceptual models that include the altered zone in the north do a better job of matching water-level observations in the low-gradient region than the simulation with the base-case site-scale model. In addition, all models capture the upward gradient from the Carbonate Aquifer. The close agreement of the calibrated permeabilities of the Bullfrog Tuff from each model also suggests that there are no significant differences in the specific discharge beneath the repository for the various conceptualizations.

The flow paths resulting from the simulations with the various conceptual models are shown in Figures 26 (ANF), 27 (AWF), and 28 (AWF/GDF). Although the flow paths predicted by the ANF and AWF conceptual models are similar to one another, they are noticeably different than the flow paths predicted by the simulations of the base-case model. The base-case model produces flow paths that trend in a southeasterly direction from the repository site (see Figure 24) Further analysis of the flow paths indicates that the fluid particles travel in the same units, predominantly the Bullfrog Tuff and the alluvial units, regardless of the model, and do not reach the Carbonate Aquifer. This is because of the pervasive upward gradient and confining unit that separates the alluvial units and the Carbonate Aquifer. Because the travel times are directly proportional to the permeability values, the travel-time comparison with base-case results can be inferred from the calibrated permeabilities in Table 17. The Bullfrog Tuff has a calibrated value about 30% higher in the AWF/GDF model than in the base-case model. This is within the uncertainty range for specific discharge discussed in Section 6.8.8.

Table 16. Selected Residuals from Models

		Residuals (Model - Measured), m				
Well ID	**Measured Head, masl**	**Base Case Model**	**ANF Model**	**AWF Model**	**AWF/GDF Model**	**Characteristic of Head Measurement**
UE-25 WT #18	730.8	3.83	6.20	1.58	2.75	Low gradient
UE-25 WT #4	730.8	3.63	0.23	0.41	2.65	Low gradient
UE-25 WT #15	729.2	4.65	1.57	1.62	4.15	Low gradient
USW G-4	730.6	4.38	0.65	0.78	3.36	Low gradient
USW SD-6	731.2	3.61	-0.37	-0.28	2.24	Low gradient
USW SD-7	727.6	6.50	3.05	3.16	5.68	Low gradient
USW SD-9	731.1	3.51	-0.29	-0.17	2.41	Low gradient
UE-25 J-11	732.2	-0.63	-0.63	-0.63	-0.57	Low gradient
USW UZ-14	779.0	-44.10	-47.60	-48.20	-45.40	Moderate gradient
USW G-1	754.2	-19.20	-23.00	-23.30	-18.60	Moderate gradient
USW WT-7	775.8	-7.70	-17.50	-17.80	-7.80	Moderate gradient
USW WT-10	776.0	5.50	-3.01	-2.91	-39.80	Moderate gradient
USW H-5 upper	775.5	-40.90	-45.20	-45.30	-42.00	Moderate gradient
USW H-6 lower	775.9	-12.00	-10.20	-10.30	13.50	Moderate gradient
UE-25 WT #6	1034.6	-89.34	-211.76	-289.47	-297.20	Possibly perched
USW G-2	1020.2	-86.41	-209.63	-283.92	-286.40	Possibly perched
UE-25 p #1 (Lwr Intrvl)	752.4	-12.73	-13.90	-14.89	-17.60	Upward gradient

Source: Zyvoloski et. al. (2003 [163341], Table 1). Output DTN: LA0304TM831231.002.

Table 17. Comparison of Selected Parameter Values for Different Conceptual Models

Hydrogeologic Unit or Feature	Permeability (m^2) or Permeability Multiplication Factor(**)			
	Base Case	**ANF***	**AWF***	**AWF/GDF***
Lower Carbonate Aquifer	5.00×10^{-14}	3.29×10^{-14}	3.30×10^{-14}	1.96×10^{-14}
Older Volcanic Confining Unit	2.00×10^{-16}	1.03×10^{-16}	1.00×10^{-16}	5.70×10^{-16}
Older Volcanic Aquifer	5.00×10^{-16}	1.00×10^{-15}	1.00×10^{-15}	1.52×10^{-14}
Lower Volcanic Confining Unit	2.00×10^{-15}	1.28×10^{-16}	1.54×10^{-16}	1.79×10^{-13}
Crater Flat-Tram	2.36×10^{-13}	2.23×10^{-13}	1.73×10^{-13}	3.38×10^{-14}
Crater Flat-Bullfrog	1.54×10^{-11}	2.00×10^{-11}	2.00×10^{-11}	2.02×10^{-11}
Crater Flat-Prow Pass	8.00×10^{-12}	1.01×10^{-13}	1.00×10^{-13}	7.19×10^{-14}
Upper Volcanic Confining Unit	5.00×10^{-14}	1.52×10^{-15}	1.87×10^{-15}	1.55×10^{-14}
Upper Volcanic Aquifer	8.00×10^{-14}	1.00×10^{-14}	1.00×10^{-14}	8.25×10^{-15}
Lava Flow Aquifer	1.00×10^{-12}	4.85×10^{-12}	4.89×10^{-12}	7.81×10^{-12}
Limestone Aquifer	1.00×10^{-12}	1.87×10^{-11}	1.94×10^{-11}	8.26×10^{-11}
Valley Fill Aquifer	5.00×10^{-12}	5.00×10^{-14}	5.01×10^{-14}	4.93×10^{-14}
Lower Carbonate Aquifer (North)	-	3.30×10^{-16}	2.18×10^{-16}	5.00×10^{-16}
Older Volcanic Confining Unit (North)	-	9.59×10^{-16}	1.27×10^{-15}	5.64×10^{-19}
Older Volcanic Aquifer (North)	-	3.28×10^{-16}	3.32×10^{-16}	2.20×10^{-16}
Lower Volcanic Confining Unit (North)	-	1.00×10^{-16}	1.00×10^{-16}	1.08×10^{-15}
Crater Flat-Tram (North)	-	1.00×10^{-16}	1.00×10^{-16}	2.14×10^{-15}
Crater Flat-Bullfrog (North)	-	2.55×10^{-13}	1.00×10^{-13}	1.34×10^{-14}
Crater Flat-Prow Pass (North)	-	6.12×10^{-15}	5.00×10^{-15}	2.83×10^{-14}
Upper Volcanic Confining Unit (North)	-	8.04×10^{-16}	8.00×10^{-16}	9.83×10^{-16}
Upper Volcanic Aquifer (North)	-	3.00×10^{-15}	3.00×10^{-15}	2.52×10^{-14}
Lava Flow Aquifer (North)	-	2.96×10^{-12}	2.99×10^{-12}	1.06×10^{-11}
Limestone Aquifer (North)	-	4.31×10^{-13}	4.42×10^{-13}	5.87×10^{-12}
Fortymile Wash Fault**	10	5.58575	5.61164	-
Spotted Range-Mine Mountain Zone**	11.7789	18.2576	18.2191	-
Imbricate Fault Zone**	1	5	5	-
Crater Flat Fault	5.00×10^{-14}	3.19×10^{-14}	3.47×10^{-14}	4.57×10^{-13}
Crater Flat Fault (North)	-	3.56×10^{-14}	4.52×10^{-14}	1.21×10^{-12}
Highway 95 Fault	-	9.36×10^{-15}	9.60×10^{-15}	1.21×10^{-14}
Alluvial Uncertainty Zone	3.20×10^{-12}	3.00×10^{-12}	3.00×10^{-12}	3.13×10^{-11}
Lower Fortymile Wash Zone	5.00×10^{-12}	5.95×10^{-12}	5.39×10^{-12}	6.81×10^{-12}
Northwest Trending Fault Zone	-	-	3.87×10^{-13}	1.55×10^{-11}

Source: Zyvoloski et. al. (2003 [163341], Table 2). Output DTN: LA0304TM831231.002.

NOTE: * ANF is the acronym for “altered, no fault”
AWF is the acronym for “altered, with fault”
AWF/GDF is the acronym for “altered, with fault/Ghost Dance Fault.”
** Permeability Multiplication Factor

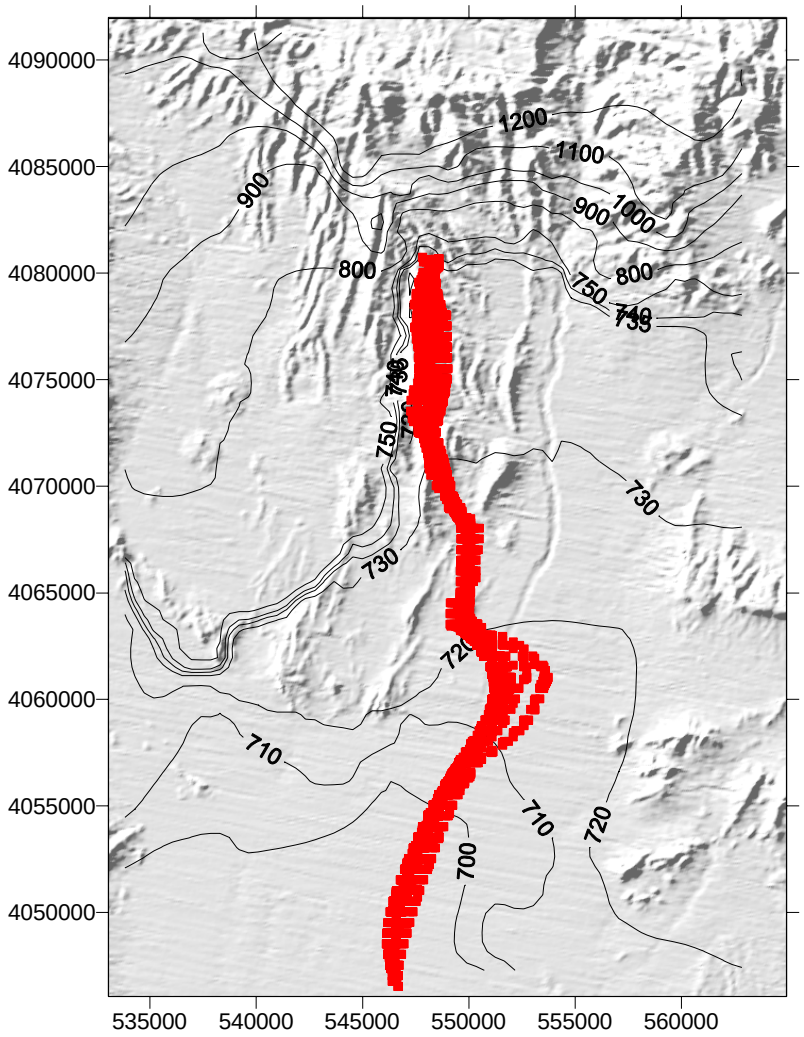

Source: Zyvoloski et. al. (2003 [163341], Figure 6).

NOTE: The red lines indicate flow paths.

Figure 26. Predicted Flow Paths from the Water Table Beneath the Repository for the ANF Model

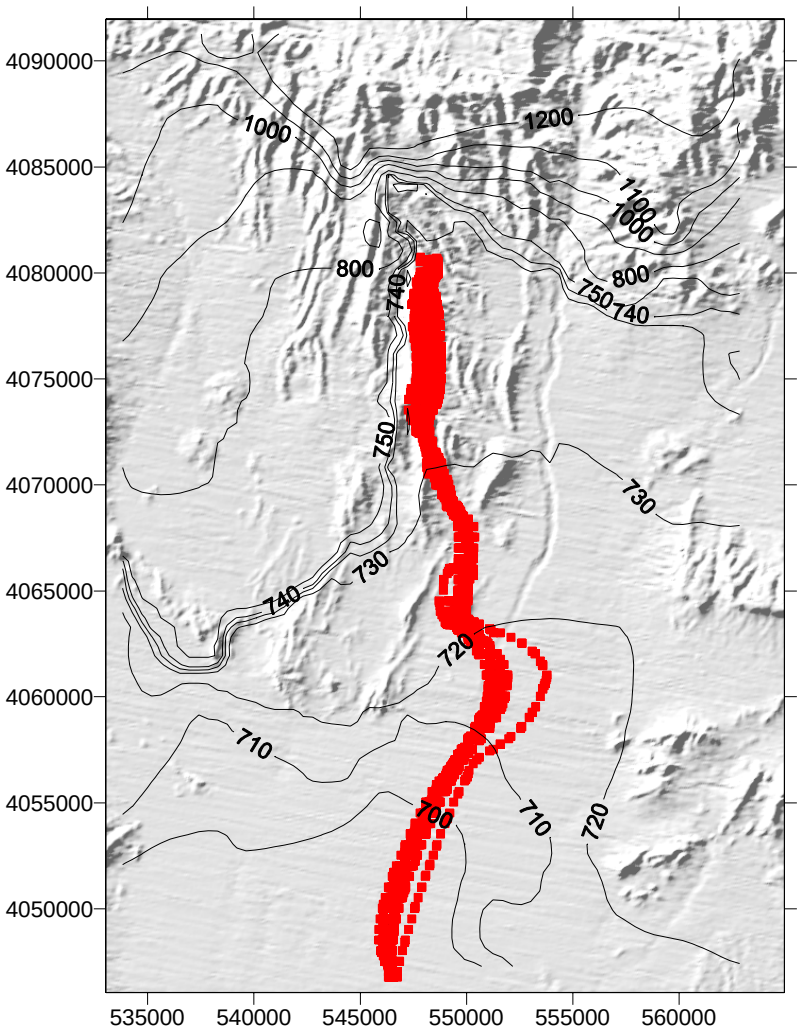

Source: Zyvoloski et. al. (2003 [163341], Figure 7).

NOTE: The red lines indicate flow paths.

Figure 27. Predicted Flow Paths from the Water Table Beneath the Repository for the AWF Model

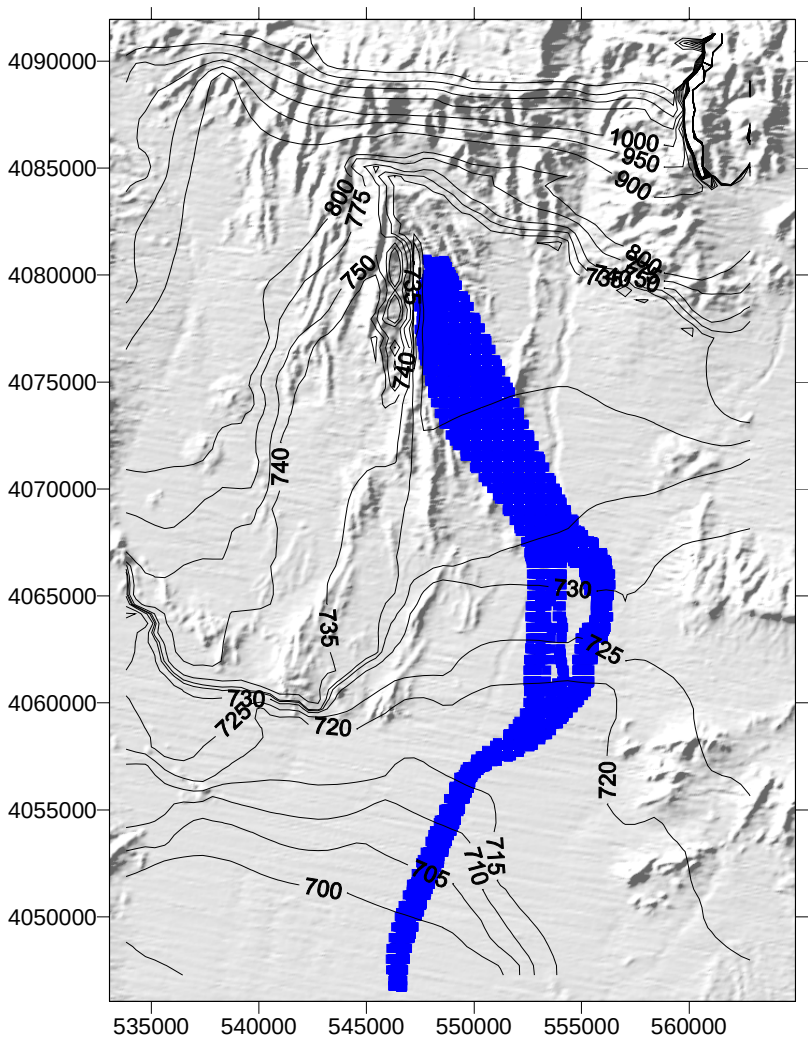

Source: Zyvoloski et. al. (2003 [163341], Figure 8).

NOTE: The blue lines indicate flow paths.

Figure 28. Predicted Flow Paths from the Water Table Beneath the Repository for the AWF/GDF Model

As described in Section 7.3, the flow paths predicted by the base-case model are consistent with the inferred geochemical flow paths shown in Figure 29. The ANF and AWF models produce flow paths of particles leaving the repository that are more southerly in direction than those of the base-case model and, arguably, significantly different than the interpreted flow paths from the geochemistry. The more southeasterly direction predicted by the base-case model is due to the east-west barrier feature that is not present in the ANF and AWF conceptual models. This feature acts as a dam to keep the head elevated in the north, but in the process, also blocks water flow from the north.

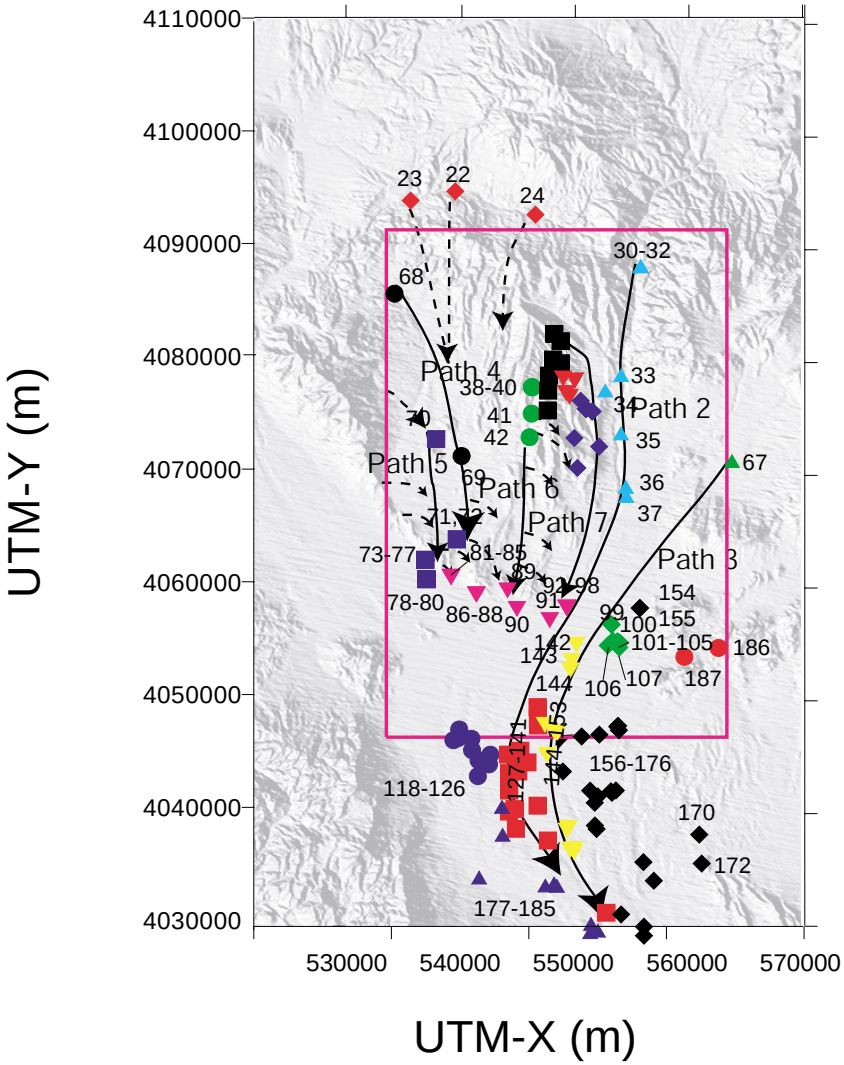

- Timber Mountain (TM)
- Solitario Canyon Wash (SCW)
- Yucca Mountain - Crest (YM-CR)
- Yucca Mountain - Central (YM-C)
- Yucca Mountain - Southeast (YM-SE)
- Jackass Flats
- Crater Flat (CF)
- Crater Flat - Southwest (CF-SW)
- Yucca Mountain - South (YM-S)
- Fortymile Wash North (FMW-N)
- Fortymile Wash - West (FMW-W)
- Fortymile Wash - South (FMW-S)
- Fortymile Wash - East (FMW - E)
- Gravity Fault (GF)
- Amarg. Riv./Fortymile W (AR/FMW)
- Skeleton Hills (SH)
- Funeral Mountains (FMt)
- Lathrop Wells (LW)

Source: BSC (2003 [162657])

Figure 29. Groundwater Flow Paths in SZ Interpreted From Groundwater Chemistry and Isotope Compositions (enlarged from Figure 39a)

Because the ANF and AWF models are forced to honor the available head data, the calibration process adjusts for this blockage by determining permeability distributions that allow water from Crater Flat (west of Yucca Mountain) to enter the repository area. Although the alternate conceptual models produced a level of calibration equal to or better than the original model, this adjustment results in the calibration of these alternate models not achieving as good a match as the base-case model in those few moderate water-level wells (750-780 m) just to the west of Yucca Mountain.

To correct these deficiencies in the ANF and AWF models, the AWF/GDF model was formulated. The AWF/GDF model augments the structures present in the AWF model with two permeability features, the Ghost Dance Fault and the Dune Wash Fault, and an additional four parameters associated with the moderate gradient region. The Ghost Dance Fault runs parallel and to the east of the Solitario Canyon Fault. The Dune Wash Fault is a northwest-southeast trending fault splay of the Ghost Dance Fault. Both features are shown in Figure 5. Calibration with the additional parameters noticeably improves the model in the moderate gradient region, with little deterioration of the overall fit. The more accurate match to the heads in the moderate gradient region results in particle flow paths (Figure 28) that more closely resemble those inferred from geochemistry. Therefore, this model is considered to be a plausible alternative model to the base-case model and an improvement over the other two models that assume only altered rock of lower permeability north of Yucca Mountain. Given the similarities between the predicted flow paths and overall flux through base-case and AWF/GDF models, the conceptual model used to account for the LHG appears to be relatively unimportant to flow leaving the repository area, as long as a good match to the data is achieved. Thus, the base-case model, in its role as a TSPA tool, is completely adequate. The uncertainty associated with the models is discussed in Section 6.8.1.

6.7.1.4 Assessment of the Large Hydraulic Gradient ACM

The base-case model and three conceptual models representing a variety of approaches for interpreting the cause of the LHG north of Yucca Mountain were investigated using a technique of calibration to hard and soft data, followed by a comparison of predicted flow paths from the repository. Although none of the calibrations are unique, several important data sets were matched by all of the conceptual models. The low hydraulic gradient in the area to the south-southeast of Yucca Mountain was modeled accurately in all models, with the alternate conceptual models producing better head matches.

The largest potential differences observed between the base-case and alternate conceptual models are found in the flow paths predicted by the models. The analyses of the base case, ANF, and AWF models show that the flow path could be sensitive to the conceptual model of the LHG. To address the difficulties encountered by the ANF and AWF models in matching heads near the Solitario Canyon Fault, the AWF/GDF model was evaluated. The AWF/GDF model contains additional parameters designed to capture the moderate gradient more accurately. With additional parameterization, this model produces flow paths similar to the base-case model.

The similarity of the base-case and AWF/GDF models suggests that the conceptualization of the LHG has little effect on the site-scale SZ flow model results and that either can be used during performance assessment studies. Apparent differences in flow paths in the ANF and AWF

models are most likely due to not representing accurately the moderate gradient head observations and do not represent important differences in hydrologic conditions for the different conceptual models of the LHG.

6.7.2 Solitario Canyon Fault ACM

An overview of the Solitario Canyon Fault ACM is presented below, followed by discussions of the model setup used in evaluating the ACM and of the results of the evaluation. The section concludes with an assessment of the impact of the Solitario Canyon Fault ACM on the site-scale SZ flow model.

6.7.2.1 Overview of Solitario Canyon Fault ACM

The Solitario Canyon Fault and its east and west branches make up three of the 17 discrete geologic features and regions represented with distinct hydrological properties in the SZ site-scale flow model. The Solitario Canyon Fault separates Crater Flat from Yucca Mountain and is shown in Figure 2. The Solitario Canyon Fault consists of generally north-south trending features just to the west of Yucca Mountain. Both east and west branches consist of generally north-northeast trending linear features, also just to the west of Yucca Mountain. The representation of the Solitario Canyon Fault is an important part of the SZ site-scale flow model because it can potentially control flow from Crater Flat to Fortymile Wash. The impact on the model of these features is to generate a higher head gradient to the west of Yucca Mountain and to impede flow from Crater Flat to Yucca Mountain. This effect on flow is important in determining the amount of alluvial material that groundwater flowing from beneath the repository region passes through en route to the accessible environment.

While the Solitario Canyon Fault has been identified as a major fault in the site-scale model region, conceptual uncertainty remains in the hydrogeologic framework model as to the depth of this fault. This uncertainty translates into uncertainty regarding the likely hydraulic behavior of this feature at depth. The SZ site-scale flow model includes the Solitario Canyon Fault as a discrete feature that extends from the bottom of the model to the top of the water table. The fault is modeled as an anisotropic feature with large permeability along the plane of the fault rather than across it. It is possible that this treatment of the anisotropy is inappropriate where it cuts the Carbonate Aquifer deep in the model domain. To investigate the importance of the Solitario Canyon Fault depth, an alternative conceptualization has been simulated in which the fault extends from the water table only to the top of the Carbonate Aquifer.

6.7.2.2 Solitario Canyon Fault ACM Setup

The SZ site-scale flow model includes the Solitario Canyon Fault as a discrete feature that extends from the bottom of the model to the top of the water table. To investigate the importance of Solitario Canyon Fault depth, an alternative conceptualization was simulated in which the fault extends from the water table only to the top of the Carbonate Aquifer. This alternative was identical to the SZ site-scale flow model in all other respects except for the Solitario Canyon Fault properties. The alternative resulted only in changes to the computation grid that were necessary to implement this alternate formulation of the fault. The alternative model was calibrated in a manner identical to that previously described for the base-case SZ flow model (see Section 6.6). Water-level contour maps and particle tracks were generated based on

the water levels predicted by the alternative model in a manner similar to that previously described for the base-case SZ flow model.

6.7.2.3 Solitario Canyon Fault ACM Results

To investigate the importance of Solitario Canyon Fault depth, an alternative conceptualization was simulated in which the fault extends from the water table only to the top of the Carbonate Aquifer. This alternative is referred to as the Shallow Fault Alternative model. This alternative is identical to the TSPA-SR (CRWMS M&O 2000, Section 2 [153246]) model in all respects except for the Solitario Canyon Fault properties. Table 18 compares the modeled head values from the Shallow Fault Alternative model for the 32 wells in the low-gradient region to the south and east of Yucca Mountain with measured values and values from the base-case model. Locations of the wells in Table 18 are shown in Figure 22. This area was chosen for comparison because of its influence on the specific discharge to the 5-km boundary, which is an important PA measure. To provide a quantitative measure of the calibration of the Shallow Fault Alternative model versus the TSPA-SR model, modeled heads at selected wells and water-level contours over the model domain can be compared. As seen from the comparison of modeled heads in Table 18, this simulation produced essentially the same result as the original TSPA-SR model with the deeper fault zone. For the shallow fault case, however, the calibrated permeability for the fault was approximately 25 percent lower than the permeability for the original deeper fault.

Table 18. Observation Wells with Computed Head Data Compared to Shallow Fault ACM

Site Name	Fig. 22 Label	*x* (UTM) (m)	*y* (UTM) (m)	*z* (elevation) (m)	Head Data (m)	Base-Case Results (m)	Shallow Fault Model Results (m)	Weight
UE-25 WT #18	7	549468	4080238	722.1	730.8	734.67	734.93	20
UE-25 WT #4	10	550439	4079412	709	730.8	734.46	734.70	20
UE-25 WT #15	11	554034	4078694	698.7	729.2	733.87	734.02	20
USW G-4	12	548933	4078602	542.2	730.6	734.5	734.77	20
UE-25 WT #14	14	552630	4077330	703.6	729.7	733.79	733.95	20
USW WT-2	15	548595	4077028	702	730.6	734.18	734.46	20
UE-25 c #1	16	550955	4075933	473.2	730.2	733.92	734.11	20
UE-25 c #3	17	550930	4075902	474.3	730.2	733.92	734.11	20
UE-25 c #2	18	550955	4075871	553.2	730.2	733.9	734.10	20
UE-25 WT #13	19	553730	4075827	703.8	729.1	733.35	733.47	20
USW WT-1	21	549152	4074967	708.4	730.4	733.86	734.05	20

Table 18. Observation Wells with Computed Head Data Compared to Shallow Fault ACM (Continued)

Site Name	Fig. 22 Label	*x* (UTM) (m)	*y* (UTM) (m)	*z* (elevation) (m)	Head Data (m)	Base-Case Results (m)	Shallow Fault Model Results (m)	Weight
USW G-3	22	547543	4074619	318.1	730.5	734.96	738.02	20
UE-25 J-13	23	554017	4073517	354.8	728.4	732.74	732.83	20
UE-25 WT #17	25	549905	4073307	705.4	729.7	733.58	733.70	20
UE-25 WT #3	27	552090	4072550	705.8	729.6	733.08	733.18	20
UE-25 WT #12	29	550168	4070659	702.6	729.5	732.92	732.89	20
USW WT-11	30	547542	4070428	691.9	730.7	733.71	733.43	20
UE-25 J-12	31	554444	4068774	659.6	727.9	731.44	731.48	20
UE-25 JF-3	32	554498	4067974	662.7	727.8	731.15	731.19	20
Cind-R-Lite Well	33	544027	4059809	710.2	729.8	737.49	735.75	20
USW H-1 tube 3	81	548727	4079926	562.5	730.6	734.63	734.89	20
USW H-1 tube 4	82	548727	4079926	680.5	730.8	734.65	734.92	20
UE-25 b #1 lower	85	549949	4078423	–8.8	729.7	735.53	735.84	20
UE-25 b #1 upper	86	549949	4078423	366.2	730.6	734.34	734.58	20
USW H-4 upper	89	549188	4077309	395.5	730.4	734.25	734.51	20
USW H-4 lower	90	549188	4077309	45	730.5	735.1	735.48	20
USW H-3 upper	91	547562	4075759	576.9	731.5	734.48	736.23	20
USW SD-6	94	547578	4077550	725.9	731.2	734.84	735.21	20
USW SD-7	95	548384	4076499	637.7	727.6	734.13	734.43	20
USW SD-9	96	548550	4079256	678.3	731.1	734.64	734.91	20
USW SD-12	97	548492	4077415	696.7	730.0	734.31	734.61	20
UE-25 J-11	107	563799	4071058	687.2	732.2	731.57	731.57	20

Output DTN: LA0304TM831231.002.

NOTE: The extended fault model corresponds to the base-case model.

Groundwater flow paths in the base-case SZ site-scale flow model and in the alternative shallower Solitario Canyon Fault model were evaluated using particle tracking. Particle paths from beneath the repository show similarity between those in the alternative model to those in the base-case model; however, the flow paths in the cross section indicate that the paths crossing the southern branches of the Solitario Canyon Fault do not extend to depths as great as in the base-case flow model (Figures 30, 31, 32, and 33).

6.7.2.4 Assessment of the Solitario Canyon Fault ACM

An analysis of flow paths in the saturated zone beneath Yucca Mountain was completed using an alternative representation of the Solitario Canyon Fault. The results of the analysis were compared to base-case representation of the Solitario Canyon Fault used for SR. The comparison resulted in the following.

- Both alternative conceptualizations of the Solitario Canyon Fault yield the same flow paths from the water table underneath the repository to the accessible environment.

- Particles started to the west of the Solitario Canyon Fault do not extend to depth as great as in the base case (see Figures 31 and 33).

- For the shallow-fault case, the calibrated permeability for the fault was approximately 25 percent lower than for the fault in the base-case model. Thus, travel times for the shallow-fault case will not be shorter than for the base-case model.

- Based on this SZ sub-system analysis, which yielded similar flow path for both conceptualizations of the Solitario Canyon Fault, it is concluded that the alternative representation of the Solitario Canyon Fault will not change the performance documented in the SR documentation.

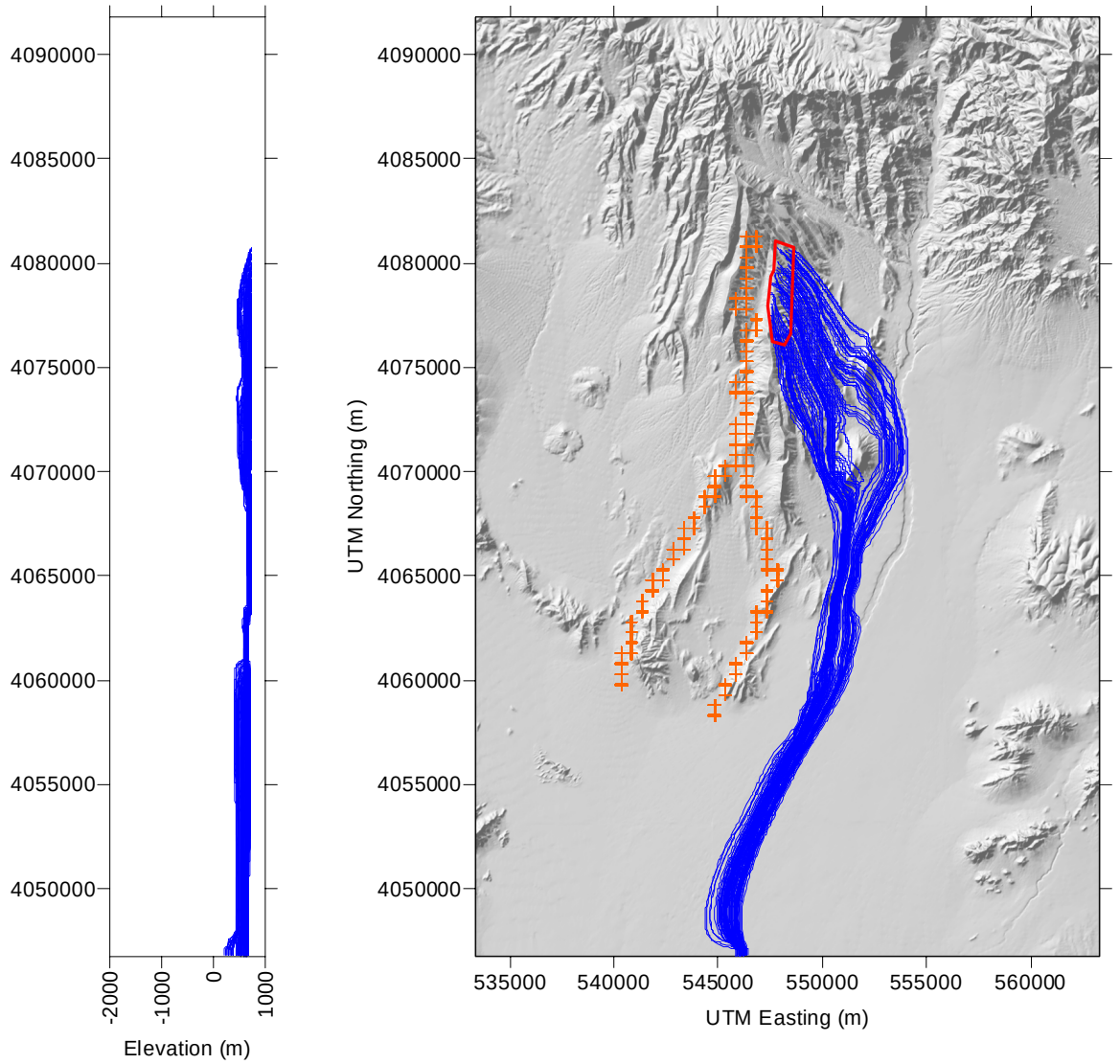

Output DTN: LA0304TM831231.002.

NOTE: Repository outline (shown with the bold red line) and nodes along the Solitario Canyon Fault (shown with orange crosses).

Figure 30. Simulated Groundwater Flow Paths from Beneath the Repository (Blue Lines) for the Base-Case (Deep Solitario Canyon Fault) SZ Site-Scale Flow Model

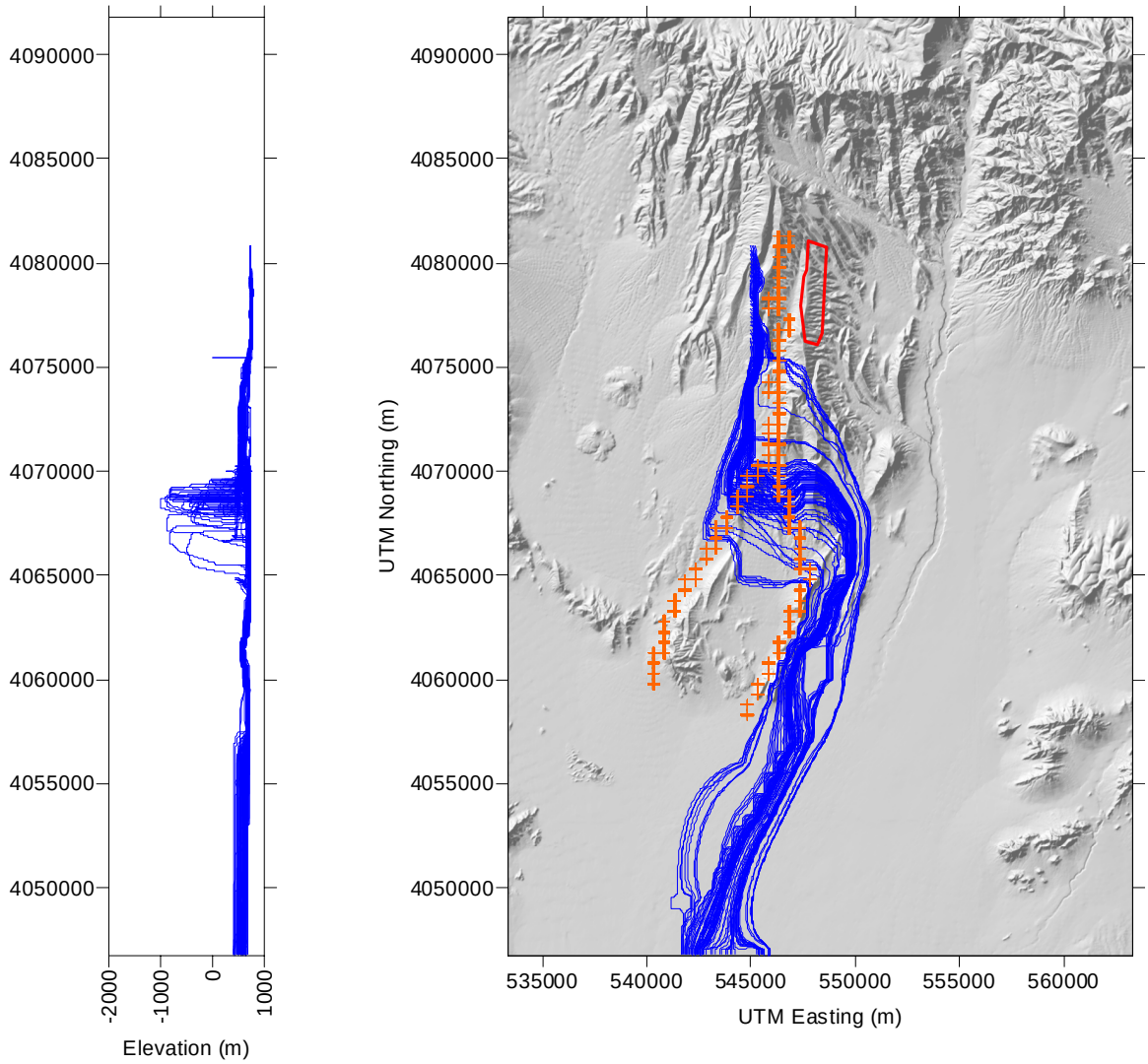

Illustration purposes only.

NOTE: Repository outline (shown with the bold red line) and nodes along the Solitario Canyon Fault (shown with orange crosses).

Figure 31. Simulated Groundwater Flow Paths from the West Side of Solitario Canyon Fault (Blue Lines) for the Base-Case (Deep Solitario Canyon Fault) SZ Site-Scale Flow Model

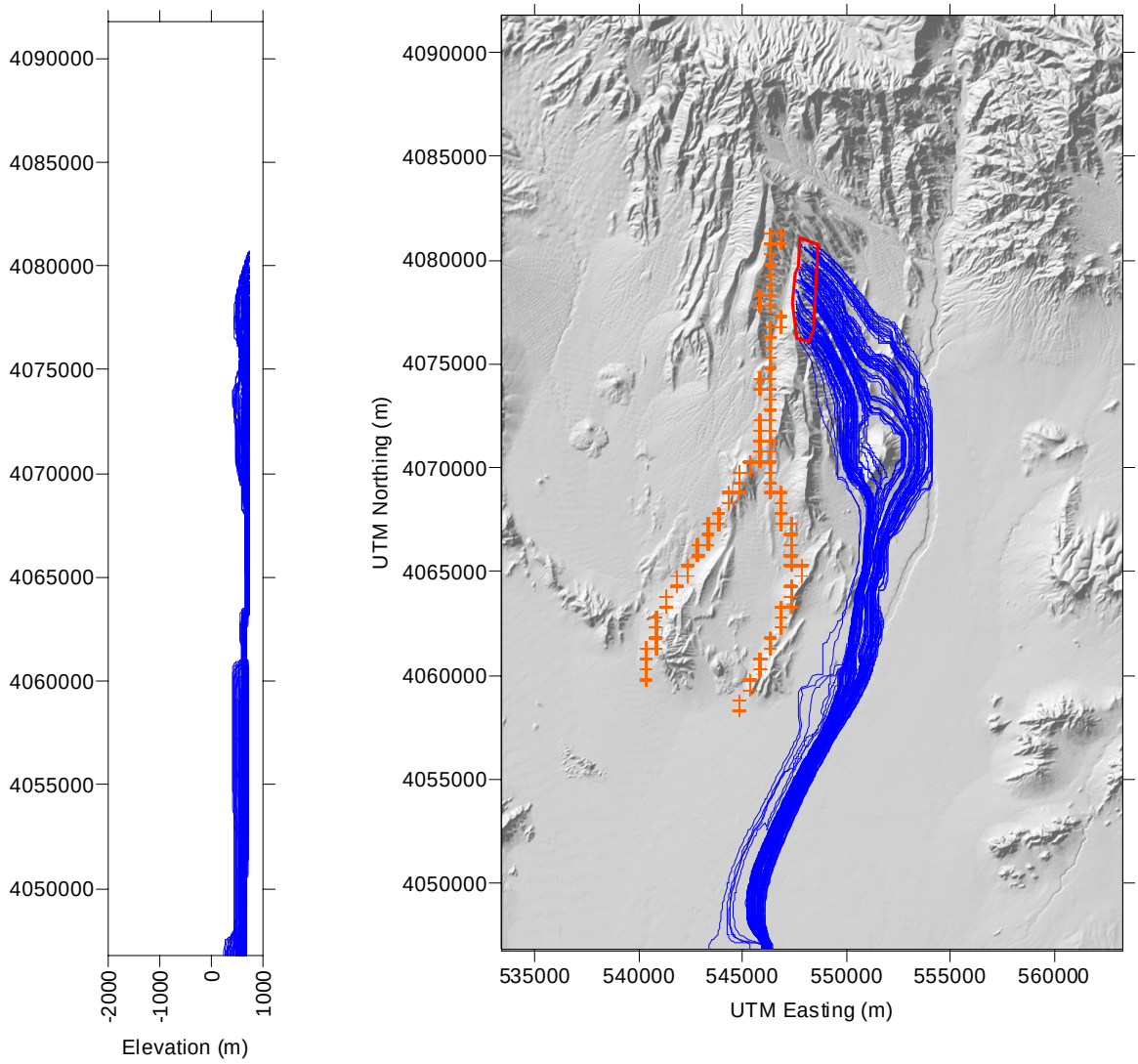

Illustration purposes only.

NOTE: Repository outline (shown with the bold red line) and nodes along the Solitario Canyon Fault (shown with orange crosses).

Figure 32. Simulated Groundwater Flow Paths from Beneath the Repository (Blue Lines) for the Alternative Case (Shallow Solitario Canyon Fault) SZ Site-Scale Flow Model

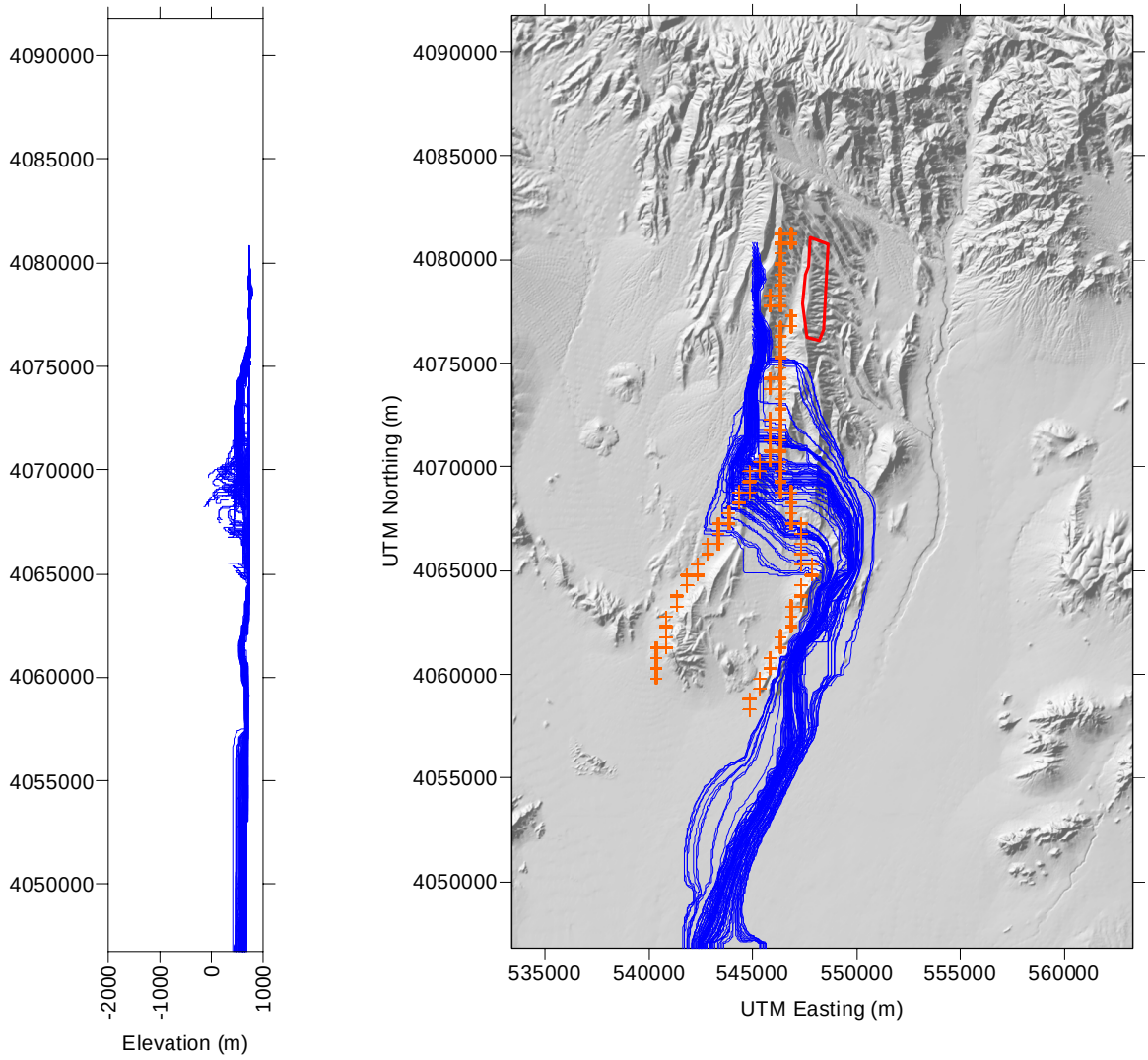

Illustration purposes only.

NOTE: Repository outline (shown with the bold red line) and nodes along the Solitario Canyon Fault (shown with orange crosses).

Figure 33. Simulated Groundwater Flow Paths from the West Side of Solitario Canyon Fault (Blue Lines) for the Alternative Case (Shallow Solitario Canyon Fault) SZ Site-Scale Flow Model

6.8 UNCERTAINTY

Characterizing and understanding the flow through the saturated zone is important for assessing the overall containment strategy for safely storing radioactive materials at the Yucca Mountain repository. Uncertainty in flow modeling arises from a number of sources including, but not limited to, the conceptual model of the processes affecting groundwater flow, water level measurements and simplifications of the model geometry, boundary conditions, hydrogeologic unit extent and depth, and the values of permeability assigned to hydrogeologic units. This section discusses and attempts to quantify uncertainties in the SZ flow model. In addition to the discussion in this section, parameter uncertainty is addressed in the model abstraction document (BSC 2003 [164870]). This document includes additional quantitative analysis on horizontal anisotropy in permeability and groundwater specific discharge.

6.8.1 Model Uncertainty Due to the Large Hydraulic Gradient

An area of a large hydraulic gradient (LHG) north of the high-level radioactive waste repository at Yucca Mountain has been inferred from previous hydraulic head measurements. This area has been a source of controversy and discussion for many years, and its cause is unknown. To simulate this feature in the Yucca Mountain site-scale saturated zone numerical model reported in the previous revision to this model report, a low-permeability east-west feature was incorporated into the model domain north of Yucca Mountain. The presence of this feature has yet to be confirmed by field investigations. More recent data appear to indicate that the gradient in this area may be significantly lower than originally thought, although high gradients still appear to be present in which a low-permeability east-west feature is incorporated into the model domain north of Yucca Mountain.

The sensitivity of the estimated groundwater flow paths and specific discharge to each of the conceptual models of the LHG has been investigated by both recalibrating the numerical model to fit conditions appropriate to each conceptual model and noting the resulting changes in the groundwater flow regime. The site-scale saturated zone flow model uses the uniform permeability of the hydrogeologic units plus permeabilities (or permeability multipliers) associated with features as calibration parameters. As discussed above, the base-case model calibration included low permeability zones and an east-west barrier north of Yucca Mountain to simulate the high gradient area (Figure 5). The new conceptualizations of the LHG do not make use of the extensive feature set north of Yucca Mountain, and these have been removed from the recalibrated model (Figure 6) to simplify it. To incorporate the area of extensive hydrothermal alteration in the Claim Canyon Caldera north of Yucca Mountain, the hydrogeologic units have been divided into distinct northern and southern zones. The two newer models differ from each other only by the inclusion of a zone that represents the northwest-southeast trending fault zone just north of Yucca Mountain (Feature 2 in Figure 6).

Although the number of features used in the newer models is less than in the original SZ site-scale flow model, the number of calibration parameters is more. This increase is a consequence of dividing the hydrogeologic units into northern and southern zones. The list of calibrated versus measured observations for selected observation points (calibration targets) is given in Table 13. In general, the simulations of the newer conceptual models do a better job of matching observations in the low gradient region than the simulation within the original SZ site-scale flow

model. The inclusion of the additional northwest-southeast trending fault zone in the second of the newer conceptual models does not seem to help the calibration.

The flow paths resulting from the simulation of the newer conceptual models and original model are shown in Figures 26, 27, and 28. Although the flow paths predicted by the simulation of the newer conceptual models are similar, they are noticeably different from the flow paths predicted by the simulations of the original base-case conceptual model. The original model produces flow paths that trend in a southeasterly direction from the repository site (Figure 26). This result is consistent with the inferred geochemical path lines shown in Figure 29. The newer models produce path lines of particles leaving the repository that are more southerly in direction than those of the original model (Figures 27 and 28). An in-depth analysis of the path lines indicates that the fluid particles travel in the same units—basically, the Bullfrog Tuff and the alluvial units, regardless of the model, and do not reach the Carbonate Aquifer. The net result of the newer flow paths is a relatively shorter traverse through the alluvial units compared to the paths for the original model. It should be noted that the more southeasterly component of the original model is due to the east-west barrier feature that is not present in the newer models. This feature not only acts as a dam to keep the head elevated in the north but also blocks water from the north, thus, allowing water from Crater Flat to enter the repository area. The newer models lack this feature and allow the water to flow directly south.

6.8.2 Model Uncertainty Due to Perched Water on Flow Paths and Specific Discharge

Perched water was not explicitly modeled in the SZ site-scale flow model, although it is noted here that all three conceptualizations of the LHG produced water levels in wells UE-25 WT#6 and UE-25 G-2 (suspected to be perched) that were much lower than the reported water levels. From Table 17, it can be seen that the original model is about 80 m to 90 m low, indicating a water level of about 930 m in this area to the north of Yucca Mountain; this is consistent with the latest USGS water-level interpretation in that area. The newer models of the LHG yield water levels in the UE-25 WT#6, UE-25 G-2 area that are 130 m lower than the base-case conceptual model, indicating a much more abrupt change in head. This area has the steepest head gradient in the model; thus, it is not surprising that such differences in the models occur. As these head gradients occur over only several elements, addition discretization may be needed to quantify possible effects on flow direction and specific discharge. Fortunately, the LHG is upgradient of the repository and only minimally affect particle flow paths and travel times (see Figure 28).

6.8.3 Model Uncertainty Due to Anisotropy

Both vertical and horizontal anisotropy can affect the flow path, flow direction, and specific discharge.

6.8.3.1 Vertical Anisotropy

The SZ site-scale flow model was calibrated using 115 head measurements from wells within the model domain as described in the previous revision of this model report. Removing background vertical anisotropy from the model had the following effects on computed heads for these wells and lateral boundary fluxes. The difference between heads computed for the target wells with and without background vertical anisotropy was less than the difference between heads

computed using the model and measured heads except for seven of the 115 measurements.

- Well UE-29a 2 HTH is located in the high-gradient region north of Yucca Mountain. Removing background vertical anisotropy resulted in a computed head 23 meters lower than the model.

- Wells USW WT-10 and USW VH-1 are located west of Yucca Mountain. Removing background vertical anisotropy resulted in computed heads 12 meters and 13 meters lower than the model.

- Wells James H. Shaw, Richard Washburn (1), NC-Washburn-1X, and Richard Washburn (3) are located in the Amargosa Desert. Removing background vertical anisotropy resulted in computed heads approximately 1 meter higher than the model.

Differences in fluxes through the boundary flux zones defined in Figure 24 exceeded 30% for only two of the zones, W1 and W4, both of which are located on the western boundary of the site-scale model boundary.

6.8.3.2 Horizontal Anisotropy

Incorporating anisotropy in the area of the north-south trending faults at Yucca Mountain into the calibrated model discussed in the previous revision of this model report resulted in predicted hydraulic heads that were slightly closer to the observed heads than for the model calibration without anisotropy. The differences in predicted heads and their impacts on the specific discharge, the flow path direction, and flow path lengths in volcanic tuffs and alluvium were within the uncertainty ranges used in the TSPA-SR (CRWMS M&O 2000 [153246]). More detailed analyses (including path-line analyses) are being conducted to study the impact of horizontal anisotropy on specific discharge and flow path direction and length. These analyses use the anisotropy distribution specified in Section 6.2.6 of BSC (2003 [162415]).

6.8.4 Uncertainty of Representing Faults with Enhanced Permeability Grid Blocks

Computational limitations (i.e., insufficient memory and/or processor speed) preclude the implementation of a finite-element model of the YMP SZ ($30 \cdot 45$ km^2) that precisely models individual fractures and faults on a one-to-one scale. For example, if the exact location, orientation, and dimensions were known for each fracture/fault in the system, the number of elements (and computation time) required to model the system would increase by several orders of magnitude. Therefore, major faults are conceptualized in the site-scale saturated zone flow model as zones of enhanced permeability that simulate preferential flow in faults with gridblocks that are nominally $500 \cdot 500$ m^2 in the horizontal directions. The situation is somewhat different in the vertical direction. Here, element depth is typically on the order of tens of meters at the fault termination depth (often the top of the regional Carbonate Aquifer). Thus, the depth of a fault zone is as accurate as the available geologic information. Nevertheless, fault properties are necessarily volume-averaged throughout an element. On the one hand, representing faults with $500 \cdot 500$ m^2 elements certainly accounts for the uncertainties in their geographic location. On the other hand, the hydrogeologic properties are “smeared” across a relatively large area, precluding the use of some fault specific site data in the calibration targets. Finally, it should be noted that

Bower et al. (2000 [149161]) studied 10 different grids generated from the same hydrogeologic framework model (similar to that used in the previous revision of this model report) and found that model calibrations were sufficient with $500 \cdot 500\ m^2$ horizontal elements, and that further refinement produced little change in fluxes.

Volume-averaged representations of faults are commonly used in numerical modeling. For example, studies of different conceptual models of the LHG have shown that its (modeled) representation had little impact on resulting flow paths as long as the system potentiometric surface was matched. Furthermore, because element permeability values are calibrated to field observations that are several grid blocks away from faults, it is believed that the large gridblock representation is adequate for the purpose of flow modeling "away" from the fault. A sensitivity study, with the fault represented by smaller grid blocks, could be used to quantify this belief and will be explored in future revisions to this document. While the precise flow regime within the fault may not be representative, overall flow through the system, particularly at the model boundaries, is not significantly affected by the volume-averaged approach. These studies give confidence that the representation of faults is adequate in the SZ site-scale flow model.

6.8.5 Quantification of Groundwater Specific Discharge Uncertainty

The specific discharge down gradient from the repository at Yucca Mountain, along with effective transport porosity, determines the rate at which groundwater and radionuclides move away from Yucca Mountain. The specific discharge, in turn, is a function of both the permeability of the rocks and alluvium and of the hydraulic gradient in this area. The hydraulic gradient, as discussed above, is sufficiently characterized to provide well-constrained input to the transport calculations. The purpose of this section is to discuss the permeability data for the volcanic rocks at Yucca Mountain and elsewhere at the NTS and the application of these data to calculations of specific discharge.

As discussed in Section 6.4, several conceptual models have been evaluated with the common goal of reducing the uncertainty in specific discharge both near the repository and down gradient in the alluvial aquifer. These efforts include:

- Studying different conceptualizations of the Solitario Canyon Fault
- Studying different conceptualizations of the LHG
- Mapping the vertical gradient
- Investigating anisotropy effects
- Investigating repository temperature effects.

Investigating different conceptualizations of the Solitario Canyon Fault is important because this fault regulates flow from Crater Flat (west of the fault) to Fortymile Wash (east of the fault). Conceptualizations include a shallower representation of the fault that terminates at the top of the Carbonate Aquifer (it originally went to the bottom of the SZ site-scale model, well into the Carbonate Aquifer). In the shallow fault model, neither the calibrated permeability of the fault nor the resulting path lines for fluid leaving the repository area change significantly. In both

models, the flow remains primarily in the volcanic units due to an upward gradient in the Carbonate Aquifer. Furthermore, varying the ratio of vertical to horizontal permeabilities also has little effect. The important fault property is the east-west (across the fault) permeability.

Different conceptualizations of the LHG are important because all previous models of the saturated zone near Yucca Mountain required a low permeability feature north of Yucca Mountain to explain the abrupt drop in heads in this area (from 1,200 to 730 m). As discussed in Section 6.4.1, an excellent potentiometric surface calibration was obtained by modeling the large head change with geochemical alteration and ring faulting as a consequence of the formation on the Claim Canyon caldera north of Yucca Mountain. In all models of the LHG, fluid path lines and specific discharge are similar, primarily because this feature is upgradient of any flow that might originate from the repository at Yucca Mountain. The important conclusion to draw is that if the water level calibration is accurate, the conceptualization of the LHG has little effect on specific discharge or flow path.

The mapping of the vertical gradient at the contact between the volcanic and/or alluvial aquifer and the Carbonate Aquifer shows that the vertical gradient is upward along the fluid path lines originating from the repository area. It can be inferred that for all reasonable climate scenarios, the fluid paths will lie in the most permeable volcanic unit (likely the Bullfrog tuff), until they reach (and remain in) the alluvial aquifer. Therefore, it is important to carry forward a conceptualization of the vertical gradient in the site-scale SZ flow model.

The original SZ site-scale model (*Calibration of the Site-Scale Saturated Zone Flow Model*, MDL-NBS-HS-000011 REV 00, CRWMS M&O 2000 [139582]) included a vertical anisotropy ratio of 0.1 in many of the units as described in Section 6.4.3. Included faults were generally modeled as anisotropic features highly conductive along the fault (strike), and vertically of low conductivity in the direction across the fault (Figure 6). Results indicated that the effect of individual fault anisotropy is relatively unimportant. When a fault zone is calibrated to its minimum directional permeability (across the fault), even significant changes in the other directional permeabilities (vertical and strike) contribute little to variation in the model results. For example, the Solitario Canyon Fault zone is calibrated to its across-the-fault permeability. Increasing the vertical permeability by factors of 10 and 1,000 times the across-the-fault value has little effect on model calibrations.

There is an area of special concern in the SZ site-scale flow model with predominately north-south trending faults in the vicinity of Yucca Mountain. This zone, which is described on p. 51 in the previous revision of this model report (*Calibration of the Site-Scale Saturated Zone Flow Model*, MDL-NBS-HS-000011 REV 00 ICN 01, BSC 2001 [155974]), is bounded by a quadrilateral with points (548712,4065570), (554390,4067050), (553647,4080900), (547317,4081090) in UTM coordinates (~88 km^2) and has a north-south to east-west anisotropy ratio in permeability. A detailed analysis of the anisotropy distribution applied to this zone can be found in the scientific analysis report BSC (2003 [162415], Section 6.2.6). In the previous revision of this model report, the effect of horizontal anisotropy in this area was investigated by running the SZ calibrated model with a 5:1 anisotropy ratio. Calibration results were slightly closer to targets with this implementation of anisotropy. Although particle tracking was not performed, it is likely that the fluid path lines leaving the repository will have a more north-south trajectory than the original isotropic model. Particle path-line changes subject to the latest

distribution of horizontal anisotropy in this zone will be studied in more detail in this model report.

Incorporating increases in saturated-zone water temperature changes the specific discharge in a predictable manner. Creating a zone of elevated temperature near the repository simply decreases the travel time (and, thus, the specific discharge) in proportion to the decrease in the fluid viscosity due to temperature change. Increasing the average temperature from 30°C to 80°C along a 5-kilometer path decreases both the viscosity and travel time by a factor of two.

6.8.6 Discussion of the Effect of Hydrogeologic Contact Uncertainty on Specific Discharge

The HFM for the saturated zone site-scale flow model was created by the USGS from a variety of field data and exists in electronic form as Stratamodel surfaces (USGS 2001 [158608], Section 6.1). There is uncertainty in the spatial positions of these surfaces primarily due to lack of data. These surfaces were used to generate the finite-element mesh such that each element is assigned those hydrogeologic properties found at the center of the element. There is interest in how uncertainties in the representation of hydrogeologic-unit horizontal locations affect flux or specific discharge calculations. Due to the coarseness of the finite-element mesh, some horizontal uncertainty in the HFM can be entertained. As long as the horizontal spatial ambiguity in the location of hydrogeologic contacts is less than 250 m (one-half the gridblock dimension), there is essentially no impact on model specific discharge or flux calculations.

Because flow leaving the repository area is confined to a few of the most permeable units, the vertical dimension deserves special consideration. From the SZ flow model, it is known that the fluid leaves the repository area through the Bullfrog Tuff and migrates to alluvial units. The flow paths in areal and vertical views are reproduced in Figure 24. Note that the vertical thickness of the flowing zone varies between 100 and 400 m, and the elevation changes from 300 to 700 m above sea level. From Table 10, the spacing in this part of the finite element mesh varies from 10 to 50 m. Consider, for example, that the uncertainty in the vertical contact location of the Bullfrog Tuff is 50 m in the portion of the model where the flow path is 300 m to 400 m thick. Changing a single element's hydrogeologic designation either to or from Bullfrog Tuff would result in a change to the local specific discharge by no more than a factor of 50/300 (17%). This is well within the overall model tolerances. Unfortunately, the thin flow path between UTM Northing coordinates 4,070,000 and 4,060,000 m can be problematic. Here the fluid flow is vertically constrained to 100 m. If the bottom contact of the Bullfrog Tuff were to change by 50 m, this could result in a change to the specific discharge flux in that area of up to 50%. Fortunately, integrated specific discharge calculations will be affected to a lesser degree. Nevertheless, due to the significant impact of this uncertainty, the uncertainty of the vertical hydrogeologic contact in this area will be examined in future modeling exercises.

The impacts of hydrogeologic contact location uncertainty are summarized below.

- Sensitivity to uncertainty in the hydrogeologic contact surfaces in the horizontal directions is much less than in the vertical direction due to the averaging effect of 500 m grid-block spacing.

- 50-m uncertainty in the vertical hydrogeologic surface can produce up to a 17% change in the local specific discharge near the repository and in the alluvial flow regions.

- 50-m uncertainty in the vertical hydrogeologic surface can produce up to a 50% change in the local specific discharge in the transitional zone, UTM Northing coordinates 4,070,000–4,060,000 m.

Because of the averaging effect across elements in the integrated specific-discharge calculations (0–5 km, 0–20 km), a 50% regional change in a relatively small portion of the 0-km to 20-km compliance boundary affects model results only moderately.

6.8.7 Uncertainty Due to Scaling Issues

Scaling issues are some of the most complex modeling problems to overcome, and it is an active field of contemporary research in geohydrology. Although there are many approaches that address the effects of scaling on model results, none has been widely accepted as the "best" method. Transport models are particularly sensitive to scaling issues both in space and time. For example, distribution coefficients measured on the order of hours to months in the laboratory for a PA model are dubiously applied to transport of contaminants over millennia. Fortunately, flow modeling is much less sensitive to scaling issues in both space and time. First, time scales are relatively unimportant because hydrogeologic properties change little over the course of millennia. While water-level data and infiltration rates may change over such long time periods, any flow model can easily account for these changes given appropriate boundary conditions. Second, while hydrogeologic properties measured through borehole pumping tests may not be appropriate to apply at distances far from the sample site (distance scaling), the SZ flow model described here does not use these measured properties directly. Instead, they are used as calibration targets and to describe parameter estimation limits. Therefore, although it may be inappropriate to assign geologic properties based on distant measurements, the calibration techniques used in this flow model moderate the negative impact of such scaling issues.

6.8.8 Specific Discharge Uncertainty Range

In previous models of the saturated zone, the specific discharge has varied from one-tenth of its nominal value to ten times its nominal value in PA calculations (BSC 2001, Section 6.2.5, [157132]. Based on recent calibration experience and the evaluation of permeability data from Yucca Mountain and other sites presented above, the range may be limited to one-third of its nominal value to three times the nominal value. The nominal value was obtained from the calibration effort described in the previous revision of this model report (BSC 2001 [155974]). Because of the linearity of the numerical model, the calibration of the model can be preserved by scaling the fluxes, recharge, and permeabilities in exactly the same manner. In the discussion below, we focus on the Bullfrog Tuff unit because calibration experience has shown that, for all reasonable scenarios, the fluid particles leaving the repository area travel predominantly in this unit until the transition to the alluvial aquifer.

From the re-evaluation of the permeability data described above and the statistical summary of the permeability data given in Table 19, three important facts emerge. The first is that the upper 95% confidence interval for the mean permeability of the Bullfrog Tuff from the cross-hole tests ($3.4 \cdot 10^{-11}$ m^2) is approximately three times the mean value ($1.4 \cdot 10^{-11}$ m^2). The mean value, in turn, is very close to the nominal calibration value of $1.5 \cdot 10^{-11}$ m^2 obtained for the SZ site-scale model. Second, alternative conceptual models implemented in the numerical model since REV 00 of this model report was written have resulted in a range of estimates for the permeability of the Bullfrog Tuff that vary less than 100% from the nominal permeability value. Third, the permeability data from Yucca Mountain had a practical maximum of $8.0 \cdot 10^{-11}$ m^2 for individual tests in highly fractured intervals in volcanic rock. Although this value exceeds the nominal value by a factor of five, uncertainty in the geometric-mean permeability is a more relevant measure of the uncertainty that should be considered in the numerical model because all units in that model are considered to be homogeneous and should have site-averaged rather than local permeabilities. Large values were measured in cross-hole tests in the C-wells complex near the Midway Valley fault, and, as discussed above, proximity to the fault was probably responsible for these permeability measurements. Based on this evidence, upper limits for permeabilities of the Bullfrog Tuff, and, by inference other units, that are three times the nominal values are realistic and appropriate. By similar reasoning, because the lower 95% confidence interval of the geometric-mean permeability of the Bullfrog Tuff is approximately Σ of the mean value, this ratio is recommended for the lower limit in PA calculations.

In the 18-km compliance region, PA calculations are also strongly influenced by travel of fluid in the alluvial aquifer. Recently, estimates of groundwater specific discharge in the SZ have been obtained from field testing at the Alluvial Testing Complex (ATC) (BSC 2003 [162415], Section 6.5.4.3). The ATC is approximately located at the boundary of the accessible environment, as specified in regulations for the Yucca Mountain Project, 10 CFR 63.302 (10 CFR 63 [156605]). The location of the ATC is approximately 18 km from Yucca Mountain, and testing was performed in the alluvium aquifer. Estimates of groundwater specific discharge at the ATC range from 1.2 m/yr to 9.4 m/yr (DTN: LA0303PR831231.002 [163561]). The simulated average specific discharge in this region of the SZ system, using the SZ transport abstraction model, ranges from 1.9 m/yr to 3.2 m/yr for differing values of horizontal anisotropy in permeability. Correspondingly, the simulated average specific discharge in the volcanic aquifer near Yucca Mountain using the SZ transport abstraction model ranges from 0.31 m/yr to 0.87 m/yr for differing values of horizontal anisotropy in permeability. These results show that the average groundwater specific discharge tends to increase along the flow path from beneath Yucca Mountain to the south. This increase in the specific discharge is due to convergent groundwater flow in this region of the SZ system. These results also indicate that there is general consistency between the simulated specific discharge and the median values of uncertainty ranges estimated for the volcanic aquifer and the alluvial aquifer along the flow path.

Table 19. Statistical Summary of Permeabilities Calculated from Single-Hole and Cross-Hole Tests at Yucca Mountain

Single-Hole Tests

Unit	Topopah Spring Tuff	Calico Hills Formation	Prow Pass Tuff	Bullfrog Tuff	Tram Tuff	Lava Flows	Lithic Ridge Tuff	Pre-Lithic Ridge Tuff (Older tuff)	Middle Volcanic Aquifer	Mixed Tuffs	Carbonate Aquifer
Number of Tests	1	9	14	19	34	0	15	5	10	30	24
Mean	7.84×10^{-13}	9.38×10^{-14}	2.85×10^{-13}	3.07×10^{-14}	1.00×10^{-14}	—	1.09×10^{-14}	4.52×10^{-16}	5.59×10^{-14}	1.34×10^{-15}	7.17×10^{-14}
Lower 95% Confidence Interval for Mean	—	4.45×10^{-14}	8.13×10^{-14}	9.98×10^{-15}	4.03×10^{-15}	—	2.57×10^{-15}	1.87×10^{-18}	6.19×10^{-15}	4.56×10^{-16}	4.69×10^{-14}
Upper 95% Confidence Interval for Mean	—	1.97×10^{-13}	9.95×10^{-13}	9.45×10^{-14}	2.49×10^{-14}	—	4.60×10^{-14}	1.09×10^{-13}	5.05×10^{-13}	3.95×10^{-15}	1.10×10^{-13}
Minimum	—	2.72×10^{-14}	7.77×10^{-15}	2.28×10^{-16}	2.35×10^{-16}	—	8.35×10^{-17}	1.84×10^{-18}	1.85×10^{-16}	1.72×10^{-18}	1.69×10^{-14}
Maximum	—	4.19×10^{-13}	1.40×10^{-11}	1.67×10^{-12}	1.18×10^{-12}	—	1.22×10^{-12}	4.49×10^{-14}	1.40×10^{-12}	3.53×10^{-13}	1.40×10^{-12}

Cross-Hole Tests

	Calico Hills Formation	Prow Pass Tuff	Bullfrog Tuff	Tram Tuff	Middle Volcanic Aquifer
Number of Tests	6	8	13	1	6
Mean	1.68×10^{-13}	2.77×10^{-12}	1.37×10^{-11}	5.39×10^{-11}	1.78×10^{-11}
Lower 95% Confidence Interval for Mean	1.25×10^{-13}	1.78×10^{-12}	5.61×10^{-12}	—	8.33×10^{-12}
Upper 95% Confidence Interval for Mean	2.26×10^{-13}	4.31×10^{-12}	3.36×10^{-11}	—	3.81×10^{-11}
Minimum	1.08×10^{-13}	1.44×10^{-12}	1.08×10^{-12}	—	7.19×10^{-12}
Maximum	2.52×10^{-13}	7.19×10^{-12}	7.55×10^{-11}	—	5.75×10^{-11}

DTN: SNT05082597001.003 [129714] (reference only).

NOTE: Permeability values are given in units of meters-squared (m^2). The Topopah Spring Tuff corresponds to the Upper Volcanic Aquifer (unit 16); the Calico Hills Formation corresponds to the Upper Volcanic Confining Unit (unit 15); and portions of the Lithic Ridge and Pre-Lithic Ridge Tuffs correspond to the Lower Volcanic Confining Unit (unit 11), the Older Volcanic Aquifer (unit 10), and the Older Volcanic Confining Unit (unit 9). The Middle Volcanic Aquifer includes the Prow Pass, Bullfrog, and Tram Tuffs and associated bedded units (Luckey et al. 1996 [100465], Figure 7). Other units correspond to hydrogeologic units of the same name.

The additional data from the ATC both constitute new information on the specific discharge in the SZ and significantly reduce uncertainty in the specific discharge relative to the assessment by the expert elicitation panel. The range of estimated specific discharge at the ATC spans about a factor of 7.8 (i.e., 1.2 m/yr to 9.4 m/yr). This indicates a range of uncertainty in specific discharge that is somewhat less than one order of magnitude, which is considerably less than the degree of uncertainty from the SZ Expert Elicitation Project (CRWMS M&O 1998 [100353], p. 3-43). Consequently, the uncertainty distribution for the groundwater specific discharge is reevaluated to reflect the reduced uncertainty. From this information, an uncertainty distribution in specific discharge is constructed, in which 80% of the probability is between one-third and three times the best estimate of specific discharge. Note that the details, including figures, of the specific discharge distribution and associated sampling techniques are contained in BSC (2003 [164870], Section 6).

6.8.9 Remaining Uncertainties in Specific Discharge Estimates

The analyses and corresponding assignment of an uncertainty range for the groundwater specific discharge assumes that the porous continuum approach is appropriate for the fractured volcanic tuffs. A remaining uncertainty is whether or not the continuum approach can be employed at the scale of the model. An alternate conceptual model not yet explicitly examined is one in which most of the flow from Yucca Mountain moves through faults rather than through the unfaulted rock. To test this alternate model, the known faults need to be included explicitly in the numerical grid of the site-scale flow and transport model. Although the grid-generation and flow-calculation capabilities exist to do this, the need to calibrate the model efficiently and perform particle-tracking transport simulations has taken priority and led to the adoption of structured grids that make explicit inclusion of faults difficult. Important faults are included in the model to capture their impact on flow. Furthermore, the adoption of a range that includes larger specific discharge values and smaller effective porosities introduces realizations that replicate the behavior of a fault-dominated flow and transport system. Therefore, the suite of performance assessment transport simulations currently used likely encompasses the range of behavior that will be obtained with a fault-based flow and transport model.

6.9 DESCRIPTION OF BARRIER CAPABILITY

This model report is a compilation of information and processes affecting flow in the saturated zone around Yucca Mountain. As such it provides a description of the saturated zone barrier flow component. The two main features of the barrier described here are: (1) the specific discharge, which affects the travel time of the radionuclides that may be released at the water table beneath the repository horizon and travel to the accessible environment; and (2) the flow paths that will affect the travel length and, therefore, travel times.

The base-case result for specific discharge ranges from 0.5 to 3 m/yr, depending on the part of the flow path. The average particle flow path itself is likely to travel southeast as it leaves the repository area and follow Fortymile Wash, where it encounters large amounts of alluvial material. Travel times are expected in the thousands of years (BSC 2003 [164870], Sections 6.6 and 6.7).

Uncertainty affects the permeability range and the flow paths. These parameters, with the head gradient, comprise the components of the specific discharge calculations. The largest uncertainty range for permeability was that of the Bullfrog Tuff in which the mean value, $1.4 \cdot 10^{-11}$ m^2, varied by a factor of 3. The flow paths proved to be relatively independent of the ACM provided the moderate and low gradient observations were adequately represented in the calibrated numerical model.

Outputs from this model report will be used in the site-scale SZ transport model report (BSC 2003 [162419]) to generate both concentrations-versus-time and concentrations-versus-distance curves that are needed to demonstrate the capabilities of the saturated zone barrier and the transport barrier.

7. VALIDATION

Model validation is the process of testing the appropriateness of the conceptual, mathematical, and numeric representation of the system being modeled. The SZ site-scale flow model is designed to provide an analysis tool that facilitates understanding of flow in the aquifer beneath and down gradient from the repository. The flow model is also a computational tool to provide the flow fields for performing radionuclide migration predictions in the saturated zone. For these predictions to be credible, it must be demonstrated that the SZ flow model has been validated for its intended use. This statement means that there is established "confidence that a mathematical model and its underlying conceptual model adequately represents with sufficient accuracy the phenomenon, process, or system in question" (AP-SIII.10Q, *Models*, Section 3.14).

The validation activities for the SZ flow model are carried out according to the *Technical Work Plan for: Saturated Zone Flow and Transport Modeling and Testing* (BSC 2003 [163965]), Section 2.2), which requires Level-II model validation of the SZ flow model based on its relative importance to the performance of the repository system. The TWP states that the validation activities "will include those listed as items a) through f) in Appendix B of the *Scientific Processes Guidelines Manual* (SPGM), MIS-WIS-MD-000001" (BSC 2002 [160313]). In addition, the TWP states that post-model development validation will consist of a comparison of simulated flow paths with those derived from hydrochemistry and isotope analyses together with one of the following comparisons between:

- Predicted and observed hydraulic heads not used during model development and calibration, including recently available potentiometric data.

- Calibrated hydraulic parameters and those derived from hydraulic testing at locations where the hydraulic data and resulting parameter values were not used during model development and calibration. At locations where sufficient new data are available, the validation has been extended to a comparison of the specific discharge calculated using predicted and observed values of both hydraulic gradient and permeability.

- Comparison of predicted and observed temperatures in SZ wells. A thermal model based on the site-scale SZ flow model is used to predict temperatures in the SZ wells.

All these options have been chosen for the validation of the SZ flow model. The comparison of predicted and observed hydraulic heads is presented in Section 7.1. This comparison focuses on the new water level data recently obtained as part of the Nye County Early Warning Drilling Program (NC-EWDP) (DTN: MO9909NYEEWDP0.000 [119613], Phase I - Fiscal Year 1999 Nye County Early Warning Drilling Program Data Package). A comparison of predicted and observed water levels for all the new water level data is presented; but for purposes of post-model development validation, the comparison focuses on new water level data obtained in the anticipated flow path from the repository. A comparison of predicted and observed gradients along the flow path from the repository is also presented to evaluate the impact of difference between observed and predicted water levels on the computation of specific discharge. Specific discharge is directly proportional to the hydraulic gradient. As previously established in the SZ TWP (BSC 2003 [163965], Section 2.2), validation is considered acceptable if the differences between simulated and observed hydraulic gradients are not greater than 50% of the observed

hydraulic gradient along the flow path from the water table directly beneath the repository to the compliance boundary at the accessible environment (differences may be greater than 50% away from this flow path). The 50% criterion used here is within the range (a factor of 3 smaller or larger) used for representing uncertainty in the specific discharge for calculations used directly by TSPA.

The comparison of specific discharges based on calibrated hydraulic parameters (permeability values) and those derived from hydraulic testing is presented in Section 7.2. This section begins by providing a summary discussion of the data from Yucca Mountain and nearby areas available for determining the permeability of the hydrogeologic units represented in the base-case flow model. These data are compared to the permeability values established during the calibration of the base-case flow model. However, since these permeability data were used to constrain permeability parameters during model calibration, these comparisons are not suitable for formal post-model development validation. Rather, these comparisons are provided in support of model validation as a confidence-building activity.

New permeability measurements are available from the Alluvial Testing Complex (ATC) (BSC [162415], Section 6. These permeability measurements were not previously used during model development and calibration and, as such, are suitable for post model development validation. These measurements have been taken along the flow path from the repository. A comparison of these measurements with calibrated permeabilities is also presented in Section 7.2. In addition, since both new water-level data and permeability measurements are available at the ATC, predicted and observed values of both hydraulic gradient and permeability at this location are used to calculate specific discharge. These calculated specific discharge values are compared to the model-simulated specific discharge for the test location for purposes of post-model development validation. Furthermore, the ATC tracer test also independently provides estimates of specific discharge from groundwater flow velocity for a range of flowing porosity (DTN: LA0303PR831231.002 [163561]; BSC 2003 [162415], Section 6.5.4.3); a comparison was also made between the calibrated and the test-derived specific discharge values at the ATC. As previously established in the SZ TWP (BSC 2003 [163965], Section 2.2), validation is considered acceptable if the difference between specific discharge values are within the factor of 3 used in TSPA simulations.

The comparison of the predicted flow pathways and those derived from the hydrochemistry and isotope analysis is presented in Section 7.3. The hydrochemistry and isotope analysis was not used during model development and calibration and, consequently, is suitable for post-model development validation. As previously established in the SZ TWP (BSC 2003 [163965], Section 2.2), the flow-path comparison is considered acceptable if the flow paths predicted by the model are enveloped by those flow paths inferred from hydrochemical and isotope analyses.

The comparison of predicted and observed temperatures in SZ wells is presented in Section 7.4. A thermal model based on the site-scale SZ flow model is used to predict temperatures in the SZ wells. This validation method involves the evaluation of the model's ability to simulate the magnitudes and spatial distribution of temperature differences observed in wells in the SZ. This activity constitutes post-model development validation of the site-scale SZ flow model because the temperature data represent an independent data set that was not used in construction or calibration of the model. As previously established in the SZ TWP (BSC 2003 [163965],

Section 2.2), the validation criteria consist of a quantitative comparison between the measured and simulated temperatures in wells and qualitative comparison of spatial patterns for observed wells. The calibration target of ±10°C was selected because of the wide range of temperatures and existence of hydrothermal upwelling observed in the saturated zone near Yucca Mountain.

7.1 COMPARISON OF OBSERVED AND PREDICTED NYE COUNTY WATER LEVELS

Since the calibration of the base-case model, a number of additional wells have been installed as part of the Nye County EWDP. These additions include both wells installed at new locations and wells completed at depths different from those previously available at existing locations. Comparison of the water levels observed in the new Nye County EWDP wells with water levels predicted by the base-case model at these new locations and depths offers an opportunity to validate the base-case model. In addition, water-level measurements from the new Nye County EWDP wells provide additional data for use in comparing the measured and predicted hydraulic gradients along the flow path from the repository. This comparison can be used to validate the base-case model quantitatively.

The base-case model was calibrated using 115 water-level and head measurements from wells within the model domain as described in Section 6.6.1.3. Eight of these measurements were from wells drilled and completed as part of the Nye County EWDP. Measured and predicted heads for these wells, along with their coordinates, are shown in Table 20. The locations of these wells are shown in Figure 34.

Table 20. Nye County EWDP Wells Used as Calibration Targets in the Base-Case Model Calibration with Observed and Predicted Water Levels

Well ID	*x* (UTM) (m)	*y* (UTM) (m)	*z* (elevation) (m)	Observed Head (m)	Modeled Head (m)	Residual Error (m)
NC-EWDP-1DX shallow	536768	4062502	413.5	786.8	763.9	-22.9
NC-EWDP-1S probe 1	536771	4062498	747.8	787.1	773.3	-13.8
NC-EWDP-2D	547744	4057164	507.2	706.1	709.3	-3.2
NC-EWDP-3D	541273	4059444	376.7	718.3	703.9	-14.4
NC-EWDP-3S probe 2	541269	4059445	719.1	719.8	702.5	-17.3
NC-EWDP-5SB	555676	4058229	603.9	723.6	718.0	-5.6
NC-EWDP-9SX probe 2	539039	4061004	721.2	767.3	732.5	-34.8
NC-Washburn-1X	551465	4057563	668.8	714.6	714.6	0.0

DTN: GS010908312332.002

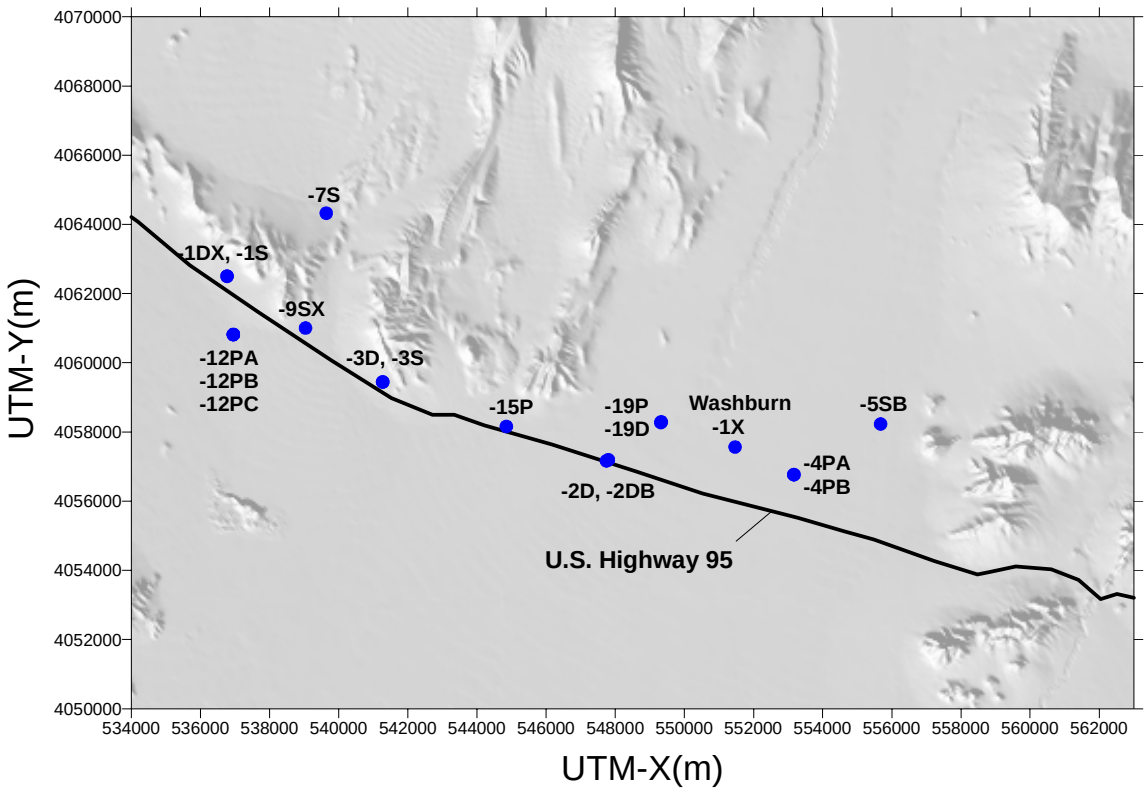

DTN: GS010908312332.002[163555] (coordinates for well locations).

NOTE: The coordinates for well locations can be found in Table 21.

Figure 34. Locations of Nye County EWDP Wells

With the addition of the new EWDP wells, the number of water-level observations available in the Nye County area has increased to 26. These wells are identified in Table 21, and the location of these wells are shown in Figure 34. As indicated in Table 21, water-level data from new completion intervals at previously existing well locations are now available and, for the purpose of this comparison, are replacing water levels previously available at this location. It should also be noted that although NC-EWDP-2D, NC-EWDP-3D, and NC-Washburn-1X were previously used as calibration targets for the base-case model, water levels from these wells are included in Table 21.

Examination of the residuals reported in Table 21 indicates that the errors in predicted water levels are highly dependent on their location within the site-scale model domain. Well clusters NC- EWDP-1, -9, and -12 are all located in the western portion of the Nye County study area, along Highway 95 and south of Crater Flat. The residuals observed in this cluster range from +13.9 m to -35.6 m. As can be seen from comparing Figures 3 and 34, these wells are located in an area of rapid water-level changes, along the Highway 95 fault, and the model is not able to replicate fully the steep head gradients observed in this area. However, similar residual errors were observed using the water-level data available during model calibration, indicating that the calibrated model is able to predict the new water levels now available in this area in a manner similar to the calibration targets originally available in this area. The new data do indicate significant vertical gradients at the NC-EWDP-1 well cluster, which the calibrated model is not

able to reproduce. NC-EWDP-7S is located north of these wells. The residual observed here was -60.5 m, but this well is located on a paleospring deposit at the southern end of Crater Flat. All of these wells are located in the southern portion of the Crater Flat flow system. Consequently, the errors observed in this area of the model domain are not likely to influence significantly the flow system from the repository. A residual of -19.9 m was also observed for well NC-EWDP-1P, which is located northeast of well NC-EWDP-7S in the lower Solitario Fault area. This area is also one of significant water-level change.

Table 21. Comparison of Water Levels Observed and Predicted at Nye County EWDP Wells

Site Name	*x* (UTM) (m)	*y* (UTM) (m)	*z* (elevation) (m)	Observed Head (m)	Modeled Head (m)	Residual Error (m)
NC-EWDP-1DX, shallow	536768	4062502	585.7	786.8	756.7	-30.1
NC-EWDP-1DX, deep	536768	4062502	133.1	748.8	762.7	13.9
NC-EWDP-1S, P1	536771	4062498	751.8	787.1	767.3	-19.8
NC-EWDP-1S, P2	536771	4062498	730.8	786.8	767.3	-19.5
NC-EWDP-2DB	547800	4057195	-77.0	713.3	717.0	3.7
NC-EWDP-2D	547744	4057164	507.1	706.1	709.2	3.1
NC-EWDP-3D	541273	4059444	377.9	718.3	703.7	-14.6
NC-EWDP-3S, P2	541269	4059445	682.8	719.8	702.5	-17.3
NC-EWDP-3S, P3	541269	4059445	642.3	719.4	702.6	-16.8
NC-EWDP-5SB	555676	4058229	707.8	723.6	718.0	-5.6
NC-EWDP-9SX, P1	539039	4061004	765.3	766.7	731.7	-35.0
NC-EWDP-9SX, P2	539039	4061004	751.3	767.3	731.7	-35.6
NC-EWDP-9SX, P4	539039	4061004	694.8	766.8	731.7	-35.1
NC-Washburn-1X	551465	4057563	687.0	714.6	714.5	-0.1
NC-EWDP-4PA	553167	4056766	687.0	717.9	715.5	-2.4
NC-EWDP-4PB	553167	4056766	582.5	723.6	715.5	-8.1
NC-EWDP-7S	539638	4064323	826.6	830.1	769.6	-60.5
NC-EWDP-12PA	536951	4060814	666.7	722.9	705.3	-17.6
NC-EWDP-12PB	536951	4060814	666.7	723.0	705.3	-17.7
NC-EWDP-12PC	536951	4060814	713.7	720.7	704.3	-16.4
NC-EWDP-15P	544848	4058158	716.9	722.5	711.0	-11.5
NC-EWDP-19P	549329	4058292	694.7	707.5	713.2	5.7
NC-EWDP-19D	549317	4058270	549.7	712.8	713.2	0.4

DTN: GS010908312332.002 [163555] (first five columns); Output DTN: LA0304TM831231.002.

NOTE: *z*-elevation refers to the mid point of the monitored open interval of an uncased well.

The observed residuals tend to improve as the wells are located further to the east. The residual errors at the NC-EWDP-3 well cluster range from -14.6 m to -17.3 m. With an observed residual of -11.5 m at NC-EWDP-15P, the residuals decrease in well locations further east. At the NC-EWDP-19 cluster location (the ATC), the residuals improve further, with observed values of only +0.4 and +5.7 m. The residuals in this general area at NC-Washburn-1X, NE-EWDP-4, and NC-EWPD-5 are similarly low. These wells are in the predicted flow path from the repository. Thus, these additional water-level data confirm the base-case model's capability to predict water levels accurately in this portion of the flow path from the repository.

To further validate the base-case model, a comparison of the hydraulic gradients along the flow path from the repository observed through field data and predicted by the base-case model has been performed. These gradients have a direct impact on the prediction of specific discharge along the flow path from the repository and can be used to determine if the model meets the validation criterion of not having an effect on the specific discharge greater than 50%.

The water-level data from a series of six wells extending from the immediate area of the repository to the new Nye County EWDP well 19P is presented in Figure 35. The predicted and observed hydraulic gradient observed between the identified wells is presented in Table 22. The location of these wells is shown in Figures 22 and 34. It should be noted that only the hydraulic gradient calculated for the last segment actually involves new water level data not previously used during the base-case flow model development and calibration. Consequently, only a comparison of predicted and observed hydraulic gradients from this segment meets the requirement of post model development validation. The comparison of predicted and observed hydraulic gradients along the remainder of the flow path from the repository is presented as a confidence building activity.

As Figure 35 and Table 22 indicate, the observed and predicted gradients along the flow path are in good agreement, except in the very northernmost part of the flow path. The wells were selected because they were on or close to the predicted flow path and included wells that were on the east and west of the Solitario Canyon fault. Another candidate well not selected, H-5, is discussed in Section 6.6.2.1. The discrepancies in water levels observed and predicted between wells H-6 and WT-2 are the result of the manner in which the model accounts for the effect of the splay of the Solitario Canyon fault, which lies in the general area of these wells. However, it should be noted that while the model does not accurately predict the precise location for the drop in head across the fault, largely because of the 500-m gridblocks, the overall hydraulic gradient predicted between H-6 and WT-2 agrees reasonably well with the value (34%). Regarding the segment between WT-2 and WT-1, for which simulated hydraulic gradient differs from the observed by 60%, in absolute terms the difference between both the observed and simulated hydraulic gradients is very close to zero (note that the water table is very flat in that area and the accuracy of land surface altitude is 0.1 m {USGS 2001 [157611]}). Overall, therefore, the comparisons between simulated and observed hydraulic gradients along the flow path are deemed acceptable and in compliance with the 50% validation criterion of BSC (2003 [163965], Section 2.2).

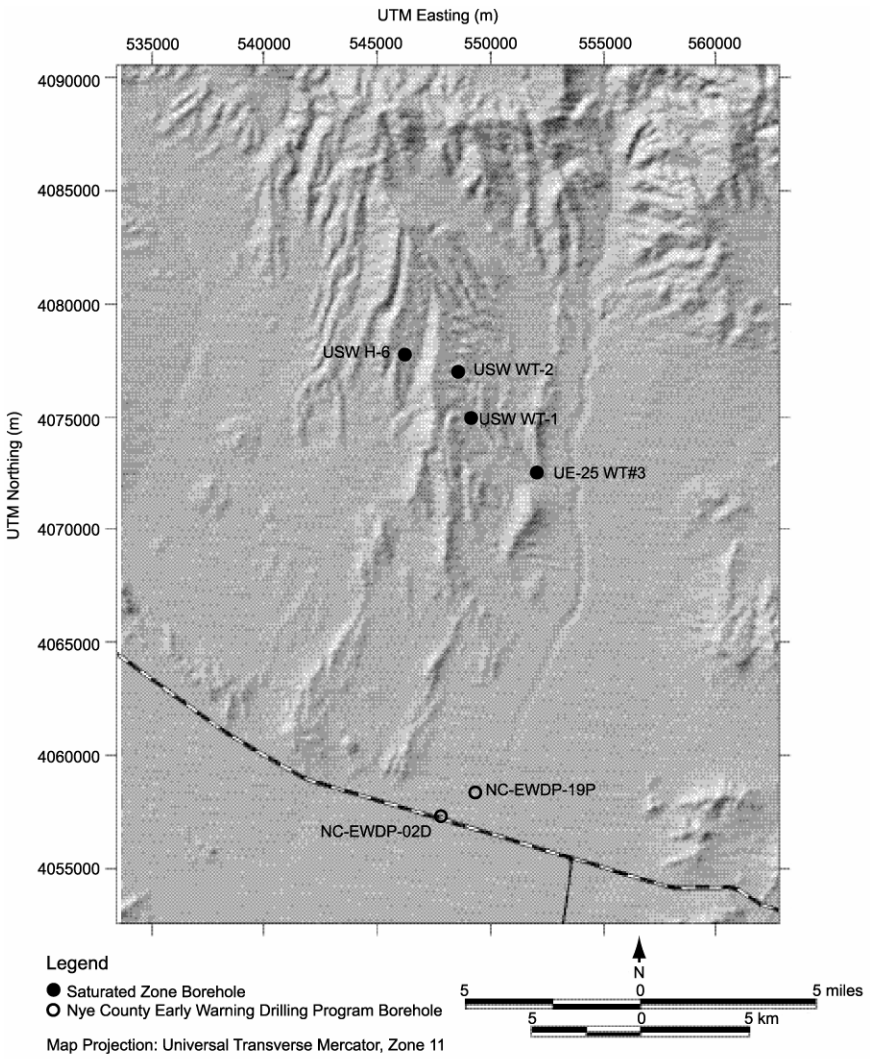

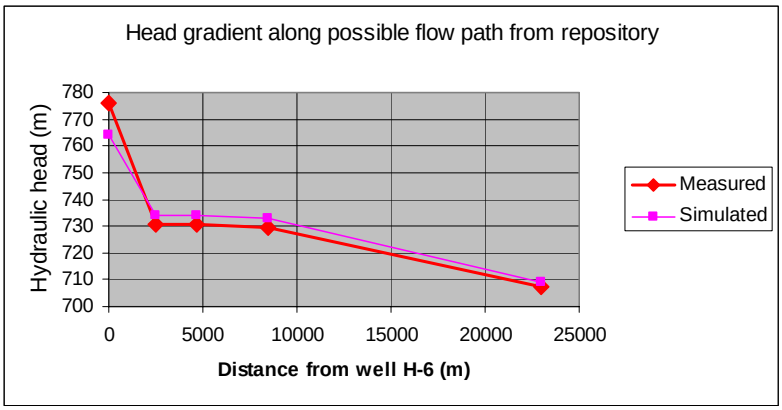

DTN: GS000508312332.001 [149947]. Output DTN: LA0304TM831231.002.

NOTE: Data results computed from Table 13.

Figure 35. Measured and Simulated Head Along Flow Path

Table 22. Predicted and Observed Hydraulic Gradient for Identified Wells

Flow Segment	ΔH/ΔL (Measured)	ΔH/ΔL (Simulated)
H-6 to WT-2	0.0118	0.0078
WT-2 to WT-1	0.000094	0.00015
WT-1 to WT-3	0.00021	0.00021
WT-3 to 19P/2D	0.0015	0.0016

DTN: GS000508312332.001 [149947]. Output DTN: LA0304TM831231.002.

NOTE: Data results computed from Table 13.

7.2 COMPARISON OF SPECIFIC DISCHARGE BASED ON PERMEABILITY DATA AND ATC TRACER TEST RESULTS

The numerical model was calibrated by adjusting permeability values for individual hydrogeologic units in the model until the sum of the weighted-residuals squared (the objective function) was minimized. The residuals include the differences between the measured and simulated hydraulic heads and the differences between the groundwater fluxes simulated with the regional- and the site-scale models. Permeabilities estimated from hydraulic tests were neither formally included in the calibration as prior information nor were considered in the calculation of the objective function. The field-derived permeabilities were instead used to guide the selection of bounds on the permissible range of permeabilities to be considered during the calibration and to check on the reasonableness of the final permeability estimates produced by the calibration. However, since these permeability data were used to constrain permeability parameters during model calibration, these measurements are not suitable for formal post-model-development validation. Rather, they are presented and discussed below in support of model validation as a confidence-building activity. New permeability measurements are available from the ATC. These permeability measurements were not previously used during model development and calibration and, as such, are suitable for post-model-development validation. A comparison of calibrated permeability values with those newly obtained values from the ATC is presented below. The impact of the differences between these values on the determination of specific discharge is also evaluated. In addition, an analysis of the combined impact of differences between predicted and observed hydraulic gradients and permeabilities at the ATC on specific discharge is presented below.

Discussions of the permeability data from the Yucca Mountain Area and nearby Nevada Test Site (NTS) as well as the Apache Leap site in Arizona are presented in the following subsections. A discussion of the general inferences about permeability that can be drawn from regional observations is also presented. Following these discussions, a comparison of calibrated with measured permeability values is presented, including the analysis of the potential impact of calibrated permeability values on groundwater specific discharge.

7.2.1 Newer Permeability Data

Note that information contained in Section 7.2.1 was acquired or reviewed since the previous revision of this report (BSC 2001 [155974]).

Many factors can be expected to affect the permeability of the volcanic rocks at Yucca Mountain, including: (1) the tendency of the rock either to fracture or to deform plastically in response to stress; (2) the ability of the rock to maintain open fractures, which is a function of the strength of the rock and overburden stress; (3) proximity to major zones of deformation, such as fault zones; and, (4) the degree of mineralization or alteration that would tend to seal fractures and faults. Other factors being equal, rocks that tend to fracture are at shallow depth, have high compressive strength, are located in a fault zone, or are unmineralized and would be expected to have high permeabilities compared to rocks that do not possess these attributes. In addition to actual variations in permeability, the scale of measurement may also influence the permeability value determined by a test. This effect is most often observed when results of permeability tests conducted on cores that do not incorporate fractures are compared to the results of tests conducted in boreholes that contain fractured intervals. At Yucca Mountain, the relatively high permeabilities estimated from cross-hole tests compared to single-hole tests in the same rock unit have also been attributed to the effects of scale (Geldon et al. 1998 [129721]). In this case, the cause of the permeability increase in the cross-hole tests is attributed to the greater likelihood of including relatively rare but highly transmissive and continuous features in the larger rock volume sampled by the cross-hole tests. This assumption is re-evaluated below on the basis of recent analyses of air-injection tests conducted at the Apache Leap test site near Globe, Arizona. Permeability data from single- and multiple-borehole hydraulic tests at Yucca Mountain and single-borehole tests elsewhere at the Nevada Test Site (NTS) have been compiled and compared to permeabilities estimated during calibration of the SZ site-scale flow model. Several aspects of the data merit further discussion.

7.2.1.1 Calico Hills

First, the mean permeability estimated for the Calico Hills Formation from single-hole tests ($k = 7.8 \cdot 10^{-14}$ m^2) is of the same order as that estimated from cross-hole tests ($k = 1.7 \cdot 10^{-13}$ m^2). This observation indicates that factors other than the test method and the scale of the test are influencing results. One such factor may be proximity to faults. Several of the single-hole tests conducted in the Calico Hills Formation were performed in the highly faulted area near borehole UE-25 b#1, whereas faults were present only at deeper stratigraphic horizons at the C-wells where the cross-hole tests were done (Geldon et al. 1998 [129721], Figure 3). Nonetheless, geologic contacts with open partings may also have enhanced permeability in the Calico Hills Formation at the C-wells (Geldon et al. 1998 [129721], Figure 5). Second, both estimates of the mean Calico Hills Formation permeability are either larger than the mean permeability estimated for the Carbonate Aquifer from Yucca Mountain data ($k = 0.072 \cdot 10^{-12}$ m^2) or comparable to mean permeabilities estimated for the Carbonate Aquifer from data elsewhere at the NTS ($k = 0.6 \cdot 10^{-12}$ m^2). Although the permeability of the Calico Hills Formation may be locally higher than the mean permeability of the Carbonate Aquifer, it is unlikely that this relation between the two formation permeabilities can exist in general. The Carbonate Aquifer, along with the alluvial aquifers, is widely viewed as a major water-supply source in southern Nevada (Dettinger 1989 [154690]). In contrast, the Calico Hills Formation has properties similar to

those of rocks deemed suitable for nuclear weapons tests below the water table at Pahute Mesa. The rocks at Pahute Mesa had properties (low intrinsic permeability due to zeolitization and sparse, poorly connected fractures) that were predicted, and later observed, to result in only small amounts of seepage into open test chambers during their construction (Blankennagel and Weir 1973 [101233], pp. B30–B31). Similar rocks in the unsaturated zone at Rainier Mesa produced perched water from isolated fault zones during construction of tunnels into the mesa; however, because the fault zones drained quickly and fault zones intersected later during tunneling also initially produced water, the fault zones were inferred to be relatively isolated both horizontally and vertically (Thordarson 1965 [106585], pp. 42–43). At Yucca Mountain, the apparently widespread presence of perched water on top of the zeolitic Calico Hills Formation in northern Yucca Mountain (Patterson 1999 [158824]) indicates that the formation generally has low permeability compared to the rate of water percolation through the unsaturated zone, which has been estimated to average 1 to 10 mm/yr in the vicinity of the repository under the present climate (Flint et al. 1998 [100033]). Water flowing under a unit gradient at a rate of 10 mm/yr ($3.17 \cdot 10^{-10}$ m/s) would pass through a rock having a permeability of $3.23 \cdot 10^{-17}$ m^2 (assuming a viscosity of 0.001 N-s/m^2 and a water density of 1000 kg/m^3); so the field-scale vertical permeability of the Calico Hills Formation, which includes the effects of fracturing, presumably has permeabilities less than this value. The geometric-mean hydraulic conductivity for the zeolitic Calico Hills Formation, based on core measurements, is $4.5 \cdot 10^{-11}$ m/s (Flint 1998 [100033], Table 7), comparable to the low hydraulic conductivity value ($3.23 \cdot 10^{-17}$ m^2) previously thought as necessary for perched water.

7.2.1.2 Alluvial Testing Complex (ATC)

From July through November 2000, pumping tests were conducted in hole NC-EWDP-19D1. The first test involved production from the entire saturated thickness of 136 m (446 ft). The results indicated a transmissivity of about 21 m^2/day (223 ft^2/day) and an average hydraulic conductivity of 0.5 ft/day, approximately equivalent to a permeability of $0.2 \cdot 10^{-12}$ m^2. Subsequently, four screened intervals having a combined thickness of 84 m (276 ft) were tested individually. The combined transmissivities of these intervals totaled about 145 m^2/day (1,600 ft^2/day), far exceeding the transmissivity determined for the initial open-hole test. There are at least two likely causes for the discrepancy. First, pumping apparently resulted in further well development, as fine materials were drawn into the well and discharged with the water. Second, the screened intervals are probably interconnected hydraulically, consistent with the complexity of fluvial-alluvial depositional environments, so that actual thicknesses of the producing zones were significantly greater than the screened intervals. The average permeability of the section is probably greater than the initial permeability determined from the open-hole test ($0.2 \cdot 10^{-12}$ m^2) but less than those calculated for the two deeper screened intervals, $1.5 \cdot 10^{-12}$ m^2 and $3.3 \cdot 10^{-12}$ m^2. Although thin, discontinuous zones may locally have higher permeabilities, these results indicate that significantly thick (>10 m) and areally extensive zones at NC-EWDP-19D1 probably have average permeabilities between $0.1–1 \cdot 10^{-12}$ m^2.

7.2.1.3 Apache Leap

Fractured welded tuffs and relatively unfractured nonwelded tuffs occur both above and below the water table. Permeabilities measured in the unsaturated zone at Yucca Mountain using air may, therefore, have some relevance to the permeability values of similar rocks located below

the water table. In the unsaturated zone, air-injection tests have been conducted from surface-based boreholes in both welded and nonwelded tuffs (LeCain 1997 [100153]) and from test alcoves in and adjacent to the Ghost Dance Fault zone in the densely welded Topopah Spring Tuff (LeCain et al. 2000 [144612]). At Yucca Mountain, no water-injection tests were done in these same intervals to directly compare to the results of the air-injection tests. However, some understanding of the probable relation between permeabilities estimated from air- and water-injection tests at Yucca Mountain can be made on the basis of tests in non- to partially welded tuff at the Apache Leap experimental site in Arizona, where borehole air- and water-injection tests were made at ambient moisture conditions in the same depth intervals (Rasmussen et al. 1993 [154688]). The Apache Leap data (Rasmussen et al. 1993, Figure 5b [154688]) showed a somewhat complex relation between permeabilities calculated from the two types of tests. Air-injection tests resulted in lower permeabilities than water-injection tests in borehole intervals for which permeabilities calculated using both fluids indicated that fractures were sparse or absent. In these intervals, matrix pore water probably obstructed air movement. However, in test intervals for which air and water permeabilities were both relatively high, the air-injection tests resulted in permeabilities comparable to or higher than permeabilities from the water-injection tests. In these intervals, both fluids probably moved into drained fractures. Additionally, because gravitational influences on air are not as pronounced as for water in the unsaturated zone, air had more possible pathways for movement than water, so air permeabilities were often higher than water permeabilities. Overall, the correlation between air and water permeabilities from the borehole injection tests at Apache Leap was $r = 0.876$ (Rasmussen et al. 1993, Figure 5b [154688]).

The test data from Apache Leap indicate that permeabilities calculated from air-injection test data in the unsaturated zone at Yucca Mountain probably provide good approximations to the water permeabilities, particularly in the densely welded intervals where drained fractures dominate the overall air permeability. The surface-based tests in four boreholes at Yucca Mountain showed that the highest air permeabilities (up to $54.0 \cdot 10^{-12}$ m^2) were present at depths less than 50 m in the Tiva Canyon Tuff, presumably because low lithostatic stresses at these depths allowed fractures to open (LeCain 1997 [100153], Figures 7 to 10). However, permeabilities in the Tiva Canyon Tuff typically decreased rapidly with depth, so that the permeabilities at depths greater than 50 m were less than 10^{-11} m^2. The geometric-mean permeabilities of the Tiva Canyon Tuff in the four boreholes varied between $3.4 \cdot 10^{-12}$ and $8.4 \cdot 10^{-12}$ m^2 (LeCain 1997 [100153], Table 1), with an overall geometric-mean permeability of $4.7 \cdot 10^{-12}$ m^2 based on a total of 23 tests. Geometric-mean permeabilities of the Topopah Spring Tuff at the four boreholes varied between $0.3 \cdot 10^{-12}$ and $1.7 \cdot 10^{-12}$ m^2 (LeCain 1997 [100153], Table 5) with an overall geometric-mean permeability of $0.75 \cdot 10^{-12}$ m^2 based on the results of 153 tests.

Recent work by Vesselinov et al. (2001 [154706]) at the Apache Leap site has demonstrated that permeabilities determined from multiple single-well air-injection tests and simultaneous numerical inversion of multiple cross-hole air-injection tests provided comparable estimates of the mean permeability of the test volume. However, when the cross-hole tests were analyzed individually with an approach equivalent to type-curve analyses, which requires the assumption of a uniform permeability field and a particular flow geometry (spherical), the resulting mean permeability estimated for the test volume was several orders of magnitude higher than the

mean permeability estimated from the single-hole analyses or the more detailed simultaneous numerical inversion of the cross-hole tests. The simultaneous numerical inversion of the cross-hole tests did result in larger calculated variance in permeabilities than was estimated from the multiple single-hole tests, a result that may have been caused by round-off error associated with the numerical inversion. The conclusions of this work relevant to the present analysis are that the mean permeabilities would not be a function of test methodology (single-hole or cross-hole analyses) except for the inability of standard cross-hole type-curve methods to account for heterogeneity and departures of the actual flow field from the assumed flow geometry.

7.2.1.4 Ghost Dance Fault

Cross-hole air-injection tests conducted in and adjacent to the Ghost Dance fault resulted in geometric-mean permeability values of $4.1 \cdot 10^{-12}$ m^2 for the hanging wall of the fault, $14.6 \cdot 10^{-12}$ m^2 for the main fault zone (defined by a zone of significantly higher fracture density), and $7.8 \cdot 10^{-12}$ m^2 for the footwall (LeCain et al. 2000 [144612], Table 13). These permeabilities were higher than the permeabilities measured in the same units elsewhere from the surface-based boreholes and 2 to 10 times higher than the permeabilities estimated for the Ghost Dance fault and adjacent rock from single-hole tests conducted from an exploratory borehole drilled before alcove excavation (LeCain et al. 2000 [144612], p. 26).

Air permeabilities have also been estimated at Yucca Mountain from measured subsurface pneumatic pressure changes that occur in response to barometric changes at land surface (Kwicklis 1999 [157414]; Ahlers et al. 1999 [109715]). Because subsurface pneumatic pressure changes are described by a diffusivity equation (Weeks 1978 [108841]), assumptions need to be made about the effective air-filled porosity to estimate permeability to air. Ahlers et al. (1999 [109715]) calculated only air diffusivity. Assuming the entire drained porosity of the matrix to be the effective air-filled porosity for air flow, Kwicklis (1999 [157414]) estimated permeabilities for the Tiva Canyon Tuff to be between $0.2 \cdot 10^{-12}$ and $10.0 \cdot 10^{-12}$ m^2 and for the Topopah Spring Tuff to be between $1.0 \cdot 10^{-12}$ and $50.0 \cdot 10^{-12}$ m^2 (Kwicklis 1999, Tables 9–12 [157414]). The value of $50.0 \cdot 10^{-12}$ m^2 was estimated for a thin (22 m) interval at borehole NRG-6 that fracture logs indicated were highly fractured. Generally, however, permeabilities of about $10.0 \cdot 10^{-12}$ m^2 were adequate to match the subsurface pneumatic pressure response in the Topopah Spring Tuff. The differences between the permeabilities obtained for the Tiva Canyon Tuff and the Topopah Spring Tuff by LeCain (1997 [100153]) and by Kwicklis (1999 [157414]) may be due to anisotropy, scale effects, or to assumptions made by Kwicklis (1999 [157414]) about air-filled porosity.

7.2.1.5 Tuffaceous Formations

The Prow Pass Tuff, Bullfrog Tuff, and Tram Tuff of the Crater Flat Group contain both non- to partially-welded margins and partially- to densely-welded interiors (Bish and Chipera 1989 [101195]; Loeven 1993 [101258]). The initially vitric non- to partially welded margins of these units have been largely altered to zeolites during hydrothermal events as a result of their thermodynamically unstable glass composition and their initially high permeabilities (Broxton et al. 1987 [102004]). The partially to densely welded parts of these units have devitrified to mostly quartz and feldspar and have higher matrix permeabilities than the non- to partially welded zeolitized margins (Loeven 1993 [101258]; Flint 1998 [100033]). Additionally, because

the welded parts of the tuffs have a greater tendency to fracture, the densely welded parts of these units generally have higher secondary permeability. Thus, unless faults are locally present, the densely welded parts of the Prow Pass Tuff, Bullfrog Tuff, and Tram Tuff are expected to have substantially higher permeability than the nonwelded margins.

The densely welded parts of the Prow Pass Tuff, Bullfrog Tuff, and Tram Tuff are likely to have mean permeabilities that are less than the mean air permeabilities of the Tiva Canyon ($k = 4.7 \cdot 10^{-12}$ m^2) or Topopah Spring ($k = 0.75 \cdot 10^{-12}$ m^2) Tuffs estimated from air-permeability tests. This likelihood is because greater lithostatic stresses at depth tend to close fractures and successive hydrothermal events have caused increasing degrees of alteration with depth (Broxton et al. 1987 [102004]). Figure 36 shows the geometric-mean permeabilities from the single-hole air-permeability tests for the Tiva Canyon and Topopah Spring Tuffs and the geometric-mean single-hole water permeabilities calculated for the Calico Hills Formation and the Prow Pass, Bullfrog, Tram, and Lithic Ridge Tuffs as a function of relative stratigraphic position. The single-hole permeabilities show the expected trends with depth. Conversely, the trends in the cross-hole permeability data from the C-wells (see Figure 37 in Section 7.2.6) are exactly opposite the trends one would expect to see based on geologic reasoning; these trends do, however, reflect the proximity of each hydrogeologic unit to the Midway Valley Fault, which intersects the C-wells in the upper part of the Tram Tuff (Geldon et al. 1998, Figure 3 [129721]). Thus, it appears that permeability trends with depth at the C-wells are controlled by local conditions and do not reflect general trends in permeability established by the single-hole tests and expected from geologic reasoning.

Overall, an upper limit of $60 \cdot 10^{-12}$ m^2 in the most critical alluvial formations is expected, and this value is used in the PEST V 5.5, (STN: 10289-5.5-00; Watermark Computing 2002 [161564]) model calibrations.

7.2.2 Implications of Permeability Data on Specific Discharge Estimates

The depth-dependent trends in mean hydrogeologic-unit permeabilities indicated by the combined air-permeability data from the unsaturated zone and the water-permeability data from the saturated zone (Figure 36) are consistent with the trends expected as higher lithostatic stresses and more intense hydrothermal alterations close fractures at increasing depths. Conversely, permeabilities measured from cross-hole tests at the C-wells (Figure 36) indicate trends that reflect proximity to the Midway Valley fault. Recent studies at the Apache Leap site in Arizona have indicated that single-hole and cross-hole tests should yield the same mean permeabilities once heterogeneity and departures from idealized flow geometries are properly taken into account. Therefore, except for the Calico Hills Formation, the single-hole permeabilities reflect the true permeabilities of the hydrogeologic units in unfaulted areas and can be used to represent the hydrogeologic-unit permeabilities in specific-discharge calculations or in numerical models, provided the effects of faults are also accounted for in some manner. The geometric-mean permeability estimated for the Calico Hills Formation was probably unduly biased toward that of faulted locations by data from boreholes UE-25 b#1 and UE-25 J-13. In unfaulted areas, the Calico Hills Formation permeability is probably several orders of magnitude

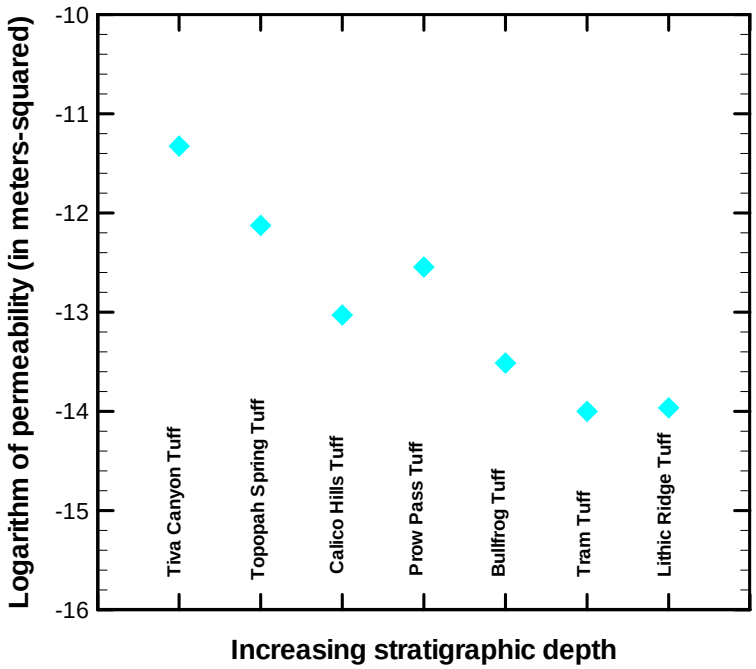

DTN: GS960908312232.012 [114124] (Tiva and Topopah units); SNT05082597001.003 [129714] (all other units). Used for corroboration only.

Figure 36. Comparison of Unsaturated-Zone and Saturated-Zone Permeabilities

less than the geometric-mean permeability calculated from the single-hole tests. The similarity of geometric-mean permeability values from cross-hole air-permeability testing in the Ghost Dance fault ($k = 14.6 \cdot 10^{-12}$ m^2) and the maximum permeabilities from cross-hole testing at the C-wells ($54.0 \cdot 10^{-12}$ m^2) indicate that values of $10.0 \cdot 10^{-12}$ to $50.0 \cdot 10^{-12}$ m^2 may be appropriate as fault zone properties in numerical models so long as the modeled width reflects the true width of the fault; otherwise, the permeabilities in the model should be adjusted to preserve the overall transmissivity of the faults. The maximum permeability values that have been calculated for faulted locations at the C-wells and alcoves in the Ghost Dance fault provide upper bounds on the permeability values that would be representative of the tuffs at unfaulted locations ($k = 50.0 \cdot 10^{-12}$ m^2). The expected values of the tuffs are provided by the geometric means calculated from the single-hole tests and are one to several orders of magnitude less than this likely upper bound.

7.2.3 Permeability Data from the Yucca Mountain Area

Permeability data from single-hole and cross-hole tests were collected in the Yucca Mountain area from the early 1980s to the present day Nye County wells. The test results published up to 1997 were compiled in DTN: SNT05082597001.003 [129714] (for reference only). A statistical analysis of this data set is presented in this section. In addition to permeability data previously

available during the development of the base-case model, additional permeability measurements are now available from the ATC. These data are reported below as well.

7.2.3.1 Single-Hole Tests

The statistical analysis that follows required that the test results be grouped. This grouping was done by first compiling the permeability estimates for individual hydrogeologic units, where possible, and by considering progressively more general groupings for those cases in which the test interval spanned several hydrogeologic units. For instance, in cases in which the test interval was in the Prow Pass Tuff, with or without some portion of the adjacent bedded tuffs, the test results were grouped with other permeability estimates for the Prow Pass Tuff. If other units within the Middle Volcanic Aquifer (MVA), as defined by Luckey et al. (1996 [100465], Figure 7), were also present in the test interval along with the Prow Pass Tuff, the test results were considered to represent the MVA. If hydrogeologic units other than those in the MVA were present in the test interval along with the Prow Pass Tuff, the permeability estimate for the test was grouped with the most general category, which is the mixed tuffs. The mixed-tuff category includes data for all tests that would not fit into a more restrictive category. All tuffs older than the Lithic Ridge Tuff are listed as Pre-Lithic Ridge Tuffs ("Older Tuffs"). The other categories were named for the hydrogeologic unit to which they pertain and are believed to be self-explanatory.

There were several instances in which several kinds of hydraulic tests (injection, drawdown, or recovery) were conducted in the same depth interval in the same borehole. The results of these tests could have been treated in several different ways. For example, (1) the data for a particular depth interval could have been averaged and only the single average value considered in the statistical summary, in which case the statistical uncertainty could be interpreted as reflecting only the effects of spatial variability, or (2) all of the permeabilities that resulted from testing of the interval could have been used to calculate the summary statistics, which was done in this report. By considering multiple measurements from the same test interval, this statistical analysis attempts to reflect the effects of measurement uncertainty as well as the effects of spatial variability.

The base-10 logarithms of the permeabilities were calculated in the original revision of this report (*Calibration of the Site-Scale Saturated Zone Flow Model*, MDL-NBS-HS-000011 REV 00, CRWMS M&O 2000 [139582]), and a statistical analysis was performed on the log-transformed values for each category (CRWMS M&O [139582]). The antilogarithms of the statistical parameters for each category were calculated and are listed in Table 19. The analysis indicates that the deepest tuffs, which are the Pre-Lithic Ridge Tuffs (Pre-Tlr), and the mixed tuff group have the lowest permeabilities, and the Topopah Spring Tuff and Prow Pass Tuff have the largest permeabilities. Where they could be calculated, the 95-percent confidence limits indicate that the mean permeability values are constrained within relatively narrow limits, except for the Pre-Lithic Ridge Tuffs.

The results also indicate that the Calico Hills Formation (Tac), which is a zeolitized tuff that functions as the Upper Volcanic Confining Unit (Luckey et al. 1996 [100465], Figure 7), has a higher permeability than the Bullfrog Tuff (Tcb) and the Carbonate Aquifer. This paradoxical result may reflect the fact that, because it is unsaturated in the western half of Yucca Mountain,

the Calico Hills Formation could be hydraulically tested only in the highly faulted eastern half of Yucca Mountain, whereas the other units were also tested in less intensely faulted areas to the west.

Single-well hydraulic testing of the saturated alluvium in well NC-EWDP-19D1 of the ATC was conducted between July 2000 and November 2000. During this testing, a single-well test of the alluvium aquifer to a depth of 812 feet (ft) (247.5 m) below land surface was initiated to determine the transmissivity and hydraulic conductivity of the entire alluvium system at the NC-EWDP-19D1 location. In addition, each of the four intervals in the alluvium in NC-EWDP-19D1 were isolated and hydraulically tested to obtain transmissivity and associated hydraulic conductivity. This interval testing program was initiated in an effort to evaluate heterogeneity in hydraulic properties over the thickness of the alluvium at the NC-EWDP-19D1 location to help determine the conceptual model of flow in the saturated alluvium south of Yucca Mountain. The results of this testing are presented in Table 23.

Table 23. Transmissivities, Hydraulic Conductivities, and Permeabilities Determined in the Single-Well Hydraulic Tests Conducted in the Alluvium in NC-EWDP-19D1 between July and November 2000

Test Interval (ft below land surface)[a]	***Apparent* Transmissivity of Interval [b] (ft^2/day)**	***Apparent* Transmissivity of Total Saturated Alluvium [c] (ft^2/day)**	**Hydraulic Conductivity Based on Sand Pack Thickness[d] (ft/day)**	**Hydraulic Conductivity Based on Distance from Water Table[e] (ft/day)**	**Permeability (m^2)**
		Combined-Interval Test			
Four combined intervals	223	223	0.5	0.5	2.7×10^{-13}
		Isolated-Interval Tests			
#1: 412–437	66	335	2.0	0.75	2.71×10^{-13}
#2: 490–519	7.5	N/A	0.23	0.04	1.44×10^{-14}
#3: 568–691	223	291	1.74	0.65	2.35×10^{-13}
#4. 717–795	300	300	3.57	0.67	2.42×10^{-13}

Source: BSC 2003, Section 6.4.1 [162415]).

NOTE:
(a) Depths correspond to upper and lower extent of sand packs
(b) Transmissivity, as obtained directly from applying the Neuman (1975 [150321]) solution to the drawdown in the interval tested, of the saturated alluvium from the water table to the bottom of the screen being tested. Ignoring screen #2, which is affected by a local clay layer, these transmissivities increase monotonically as the depth of the screen being tested increases.
(c) Transmissivity calculated from the screens #1, #3, and #4 interval tests for the entire saturated alluvium thickness tested by multiplying the transmissivity value in the second column, which is for the interval from the water table to the bottom of the screen being tested, by the ratio of 446 ft (the total saturated alluvium thickness tested) over the depth from the water table to the bottom of the screen being tested. Thus, for screen #1, 66 x (446/88) = 334.5 ≈ 335 ft^2/day. For screen #3, 223 x (446/342) = 290.8 ≈ 291 ft^2/day. No corrections are needed for the combined-interval test nor for the screen #4 test.
(d) Assumes that interval thickness is the thickness of the interval sand pack.
(e) Assumes that interval thickness is the distance from the water table to the bottom of the screened interval being pumped.

7.2.3.2 Cross-Hole Tests

Permeability data from cross-hole tests were compiled, grouped, and analyzed in a manner similar to the permeability data for the single-hole tests (see Table 19). The cross-hole data originate from tests conducted at the C-wells complex. Whereas the permeabilities of the Calico Hills formation are similar for both the single- and cross-hole tests, the permeabilities of the Prow Pass Tuff (Tcp), Bullfrog Tuff, Tram Tuff of the Crater Flat Group (Tct), and the MVA calculated from the cross-hole tests are one to several orders of magnitude greater than the mean permeabilities calculated from the single-hole tests. The differences in the mean permeability values between the single- and cross-hole tests generally have been attributed to the larger volume of rock affected by the cross-hole tests (Geldon et al. 1997 [100397]), which allows a larger number of possible flow paths, including relatively rare, high-transmissivity flow paths, to be sampled during the test. However, some of the increase in permeability attributed to the effects of scale may also be due to the presence of a breccia zone associated with the Midway Valley fault in the Bullfrog Tuff and Tram Tuff at boreholes UE-25 c#2 and UE-25 c#3 (Geldon et al. 1997 [100397], Figure 3). Thus, some of the difference in the mean permeabilities calculated for the single-hole and cross-hole tests may be due both to local conditions in the vicinity of the C-wells and to scale.

A cross-hole hydraulic test was also conducted at the ATC in January 2002. During this test, borehole NC-EWDP-19D1 was pumped in the open-alluvium section, while IM1 and IM2 were used as monitoring wells. IM1 was packed off, isolating each of four intervals in the alluvium section, while IM2 had only one packer inflated, isolating the alluvium section from the intervals below it. The analyses of the drawdown data from IM2 resulted in an estimated transmissivity value of 3,300 ft^2/day (0.00355 m^2/s). The transmissivity estimate is approximately an order-of-magnitude higher than the 300 ft^2/day (0.000322 m^2/s) value obtained from single-hole testing in 19D1. The differences between cross-hole and single-well tests are likely the result of large head losses in the single-hole testing due to the well efficiency of 19D1. The tested interval in IM2, from the water table to the bottom of screen #4, is 438 ft (133.5 m). Therefore, the intrinsic permeability measured in this test is 2.7×10^{-12} m^2.

7.2.4 Permeability Data from the Nevada Test Site

Data from reports pertaining to the NTS were examined to help constrain permeability estimates for hydrogeologic units that were either not tested or that underwent minimal testing at Yucca Mountain. These permeability data, as well as more qualitative observations concerning the permeability of some of the hydrogeologic units in the site-model area, are summarized in the following sections. Additionally, these reports, including Blankennagel and Weir (1973 [101233]), Winograd and Thordarson (1975 [101167]), and Laczniak et al. (1996 [103012]), describe the hydrogeologic controls on groundwater movement at the NTS, thereby providing a regional perspective for groundwater flow at Yucca Mountain. Assessments of permeability data from the NTS for the Lower Carbonate Aquifer, the Valley-Fill Aquifer, the Welded-Tuff Aquifer, and the Lava-Flow Aquifer are presented below.

7.2.4.1 Lower Carbonate Aquifer (unit 4)

The results of hydraulic tests in the Lower Carbonate Aquifer were reported for eight boreholes by Winograd and Thordarson (1975 [101167], Table 3). For two of the boreholes, only transmissivity estimates based on specific capacity were made. At boreholes for which permeability estimates based on drawdown curves were also available, the estimates based on specific capacity were much lower than the estimates based on the drawdown curves. At five boreholes where both drawdown and recovery tests were conducted, the permeabilities estimated from recovery tests were several times higher than those estimated from drawdown tests. Both the drawdown and recovery data exhibited complex responses to pumping that were attributed to test conditions as well as to aquifer properties. These responses were manifested on log-linear plots of time versus drawdown as straight-line segments with distinct breaks in slope. Because they were unable to explain the differences in the results from the drawdown and recovery tests, Winograd and Thordarson (1975 [101167], p. C25) advised against the use of the transmissivities estimated from the recovery tests. The transmissivities estimated from drawdown tests in the Lower Carbonate Aquifer are listed for six boreholes in Table 24 along with thicknesses of the test intervals and the calculated permeabilities. The permeabilities in m^2 were calculated from the hydraulic conductivity values using a viscosity of 0.001 Pascal seconds, a density of 1000 kg/m^3, and a gravitation acceleration of 9.81 m/s^2. These viscosity and density values are appropriate for test temperatures of about 25°C. The actual test temperatures were not reported by Winograd and Thordarson (1975 [101167]) but may have been substantially higher (greater than 50°C) than the temperatures assumed in this calculation, in which case the calculated permeabilities may overestimate the true permeabilities measured by the tests by a factor of 2 to 3. A statistical analysis of the base-10 logarithms of the permeabilities listed in Table 23 resulted in an estimated mean permeability for the Carbonate Aquifer of 6.0×10^{-13} m^2. The 95% lower and upper confidence limits for the mean permeability were 1.39×10^{-13} and 2.58×10^{-12} m^2, respectively.

Table 24. Permeabilities Calculated for the Lower Carbonate Aquifer

Well	Thickness (ft)	Transmissivity[a] (gpd/ft)[b]	Hydraulic Conductivity (gpd/ft^2)	Permeability (m^2)
67-73	281	20,000	71.2	3.44×10^{-12}
67-68	996	39,000	39.2	1.89×10^{-12}
66-75	753	11,000	14.6	7.05×10^{-13}
88-66	872	1,300	1.49	7.19×10^{-14}
75-73	750	3,800	5.07	2.45×10^{-13}
84-68	205	2,400	11.7	5.65×10^{-13}

Source: Winograd and Thordarson (1975 [101167], Table 3).

NOTE: [a] These transmissivities were estimated by Winograd and Thordarson (1975 [101167], Table 3) from drawdown curves.

[b] gpd is gallons per day.

Statistics for the logarithm of permeability (log *k*) are

Mean = –12.224
Standard deviation = 0.605
Median = –12.999
Lower 95% confidence level for mean = –12.858
Upper 95% confidence level for mean = –11.5887.

In addition to providing quantitative estimates of the permeability, Winograd and Thordarson (1975 [101167]) made several qualitative observations regarding the distribution of permeability within the Carbonate Aquifers.

- The permeability data for the Carbonate Aquifer showed no systematic decrease either with depth beneath the top of the aquifer or beneath the land surface (p. C20). The inference that groundwater may circulate freely within the entire thickness of the Lower Carbonate Aquifer is not negated by chemical data, which indicate no significant increase in the dissolved-solids content to depths of several thousand feet (p. C103).

- No major caverns were detected during drilling in the Lower Carbonate Aquifer, despite the fact that approximately 16,000 feet (4877 m) of the Lower Carbonate Aquifer was penetrated in 26 holes drilled in 10 widely separated areas, including over 5,000 feet (1524 m) at 13 holes beneath the Tertiary/pre-Tertiary unconformity, where caverns might be expected to exist (p. C19). Drill-stem tests in three holes in the Rock Valley and Yucca Flat indicated negligible to moderate permeability immediately below the unconformity (p. C20).

- Outcrop evidence indicates that klippen, which are the upper plates of low-angle thrust faults and gravity slump faults, have a higher intensity of fracturing and brecciation than rock below the fault planes and may have above-average porosity and permeability (pp. C19 to C20). Specific capacity data for five wells penetrating the upper plates of low-angle faults in southern Yucca Flat and the northwestern Amargosa Desert indicated relatively high transmissibilities for these plates (p. C28).

- The presence of hydraulic barriers within the Lower Carbonate Aquifer is indicated in the hydraulic response in two-thirds of the wells pumped, indicating that zones of above-average transmissibility may often not be connected to each other (p. C116). However, this observation needs to be reconciled with hydraulic and chemical evidence supporting the existence of a “mega channel” extending over 40 miles (64 km) between southern Frenchman Flat and the discharge area at Ash Meadows (Winograd and Pearson 1976 [108882]).

7.2.4.2 Valley-Fill Aquifer (unit 20)

The Valley Fill Aquifer, as defined by Winograd and Thordarson (1975 [101167], Table 1, p. C37) is composed of alluvial fan, fluvial, fanglomerate, lake-bed, and mudflow deposits in depressions created by post-Pliocene block faulting. Thus defined, the Valley Fill Aquifer of Winograd and Thordarson (1975 [101167]) probably includes the Valley Fill Aquifer (unit 20), the Valley-Fill Confining Unit (unit 19), and the Undifferentiated Valley Fill (unit 8) defined for the present study.

Transmissivity estimates for the Valley-Fill Aquifer were made at six boreholes in Emigrant Valley, Yucca Flat, and Frenchmen Flat (Winograd and Thordarson 1975 [101167], Table 3). For two of the boreholes, only transmissivity estimates based on specific capacity data were available. However, these estimates are considered unreliable because of the lack of agreement with transmissivity estimates based on drawdown or recovery curves at boreholes in which both

types of estimates were made. The transmissivity estimates made from drawdown and recovery curves were consistent with each other at wells where both types of tests were conducted, in which case the transmissivity values from the drawdown and recovery curves were averaged to produce the transmissivity estimates listed in Table 25. Values used for the viscosity, density, and gravity terms in the expression for permeability are the same as those used for the Lower Carbonate Aquifer. Based on a statistical analysis of the logarithm of the permeabilities listed in Table 24, the mean permeability of the valley fill is 1.57×10^{-12} m^2, and the 95 percent lower and upper confidence limits for the mean permeability are 1.61×10^{-13} and 1.54×10^{-11} m^2, respectively. The relatively high mean permeability calculated for the valley fill is probably more reflective of the permeability of the Valley-Fill Aquifer (unit 20) and, possibly, the Undifferentiated Valley Fill (unit 8) of this study than of the Valley-Fill Confining Unit (unit 19).

Table 25. Permeability Estimates for the Valley-Fill Aquifer

Well	Thickness (ft)	Transmissivity (gpd/ft)	Hydraulic Conductivity (gpd/ft^2)	Permeability (m^2)
74-70 [b]	511	2,200 [a]	4.31	2.08×10^{-13}
74-70 [a]	217	9,350 [b]	43.1	2.08×10^{-12}
83-68	264	12,700 [b]	48.1	2.32×10^{-12}
91-74	264	33,500 [c]	126.9	6.12×10^{-12}

Source: Winograd and Thordarson (1975 [101167], Table 3).

NOTE: Permeability estimates based on transmissivity data from Winograd and Thordarson (1975 [101167], Table 3). gpd is gallons per day.

[a] Average is the arithmetic sum of the results of one drawdown and two recovery tests.

[b] Average is the arithmetic sum of the results of one drawdown and one recovery test.

[c] Representative Value is the result of one recovery test.

Statistics for the logarithm of permeability (log *k*) are

Mean = –11.803
Standard deviation = 0.623
Median = –11.658
Lower 95% confidence level for mean = –12.794
Upper 95% confidence level for mean = –10.812.

In addition to providing the quantitative estimates of the permeability of the valley fill summarized in this section, Winograd and Thordarson (1975 [101167]) also made numerous observations regarding the permeability of the valley fill at particular locations in the area of the NTS. Of special interest to this report are those observations made for the valley fill in the Amargosa Desert. Winograd and Thordarson (1975 [101167], pp. C84 to C85) noted that hydraulic head contours south of Lathrop Wells (now Amargosa Valley) probably reflect the effects of upward leakage from the Lower Carbonate Aquifer into poorly permeable valley fill along the Gravity fault and associated faults and of the drainage of this water to more permeable sediments farther west. Immediately west of the Gravity fault, gravity data indicate that downward displacement of the pre-Tertiary rocks west of the fault is 500 to 1,500 ft (152.4 to 457.2 m) at a location one mile east of Lathrop Wells and 1,200 to 2,200 ft (365.8 to 670.6m) at a point one mile southeast of the inferred intersection of the Specter Range Thrust fault and the Gravity fault. The low permeability of the valley fill immediately west of the Gravity fault was

indicated by drillers' logs, which showed that the valley fill in this area was mainly clay, and also by analogy with the lakebed sediments southwest of the spring line at Ash Meadows, where groundwater discharging from the Lower Carbonate Aquifer into the sediments across the Gravity fault is forced to the land surface by the low permeability of the sediments. Winograd and Thordarson (1975 [101167], p. C85) argued that the discharge across the Gravity fault near Lathrop Wells was probably small because only the lower-most part of the Lower Carbonate Aquifer is present in the area and the Lower Clastic Aquitard, which underlies the Carbonate Aquifer at shallow depths, would probably not transmit much water.

7.2.4.3 Welded-Tuff Aquifer (unit 16)

The Welded Tuff Aquifer corresponds to the Upper Volcanic Aquifer (unit 16) of Table 11. Results of hydraulic tests conducted in the Welded Tuff Aquifer were reported by Winograd and Thordarson (1975 [101167], Table 3) for four wells, but only two wells, both in Jackass Flats, had transmissivity estimates based on drawdown curves. Well 74-57 tested the Topopah Spring Tuff and well 74-61 tested both the Topopah Spring Tuff and the Basalt of Kiwi Mesa. Permeabilities calculated from the drawdown curves at these wells are listed in Table 26. The geometric mean permeability based on the estimated permeabilities in Table 26 is 5.3×10^{-12} m^2.

Table 26. Permeability Estimates for the Welded-Tuff Aquifer

Well	Thickness (ft)	Transmissivity (gpd/ft)	Hydraulic Conductivity (gpd/ft^2)	Permeability (m^2)
74-61	290	28,000	96.6	4.7×10^{-12}
74-57	547	68,000	124.3	6.0×10^{-12}

Source: Winograd and Thordarson (1975 [101167], Table 3)

NOTE: Permeability estimates based on transmissivities determined from drawdown curves (Winograd and Thordarson 1975 [101167], Table 3).

gpd is gallons per day.

Statistics: The geometric mean permeability is 5.3×10^{-12} m^2.

7.2.4.4 Lava-Flow Aquifer (unit 17)

Rhyolitic lavas and welded and nonwelded tuffs fill the Silent Canyon caldera complex, which now lies buried beneath Pahute Mesa by younger tuffs, erupted from the Timber Mountain caldera complex to the south (Blankennagel and Weir 1973 [101233], p. 6; Laczniak et al. 1996 [103012], p. 36). The permeabilities of the lava flows beneath Pahute Mesa are assumed to be an appropriate analog for the Lava Flows (unit 17) near Yucca Mountain.

A qualitative comparison of the water-producing attributes of the lavas and tuffs based on the concept of specific capacity (in gal/min/ft of drawdown) indicated that despite considerable overlap in their water-yield potential, the lavas generally were the most transmissive rocks tested, followed by the welded tuffs and, finally, the zeolitized nonwelded tuffs (Blankennagel

and Weir 1973 [101233], Figure 4). Pumping tests were conducted in 16 boreholes at Pahute Mesa, including 14 in which the major water production came from the rhyolitic lava flows (Blankennagel and Weir 1973 [101233], Table 3). The borehole names, uncased saturated thickness, measured transmissivities, and calculated hydraulic conductivities and permeabilities associated with these 14 tests are given in Table 27. The mean permeability of the rhyolitic lava is estimated to be 2.67 x 10^{-13} m^2, with 95 percent lower and upper confidence limits of 9.18 x 10^{-14} and 7.76 x 10^{-13} m^2, respectively. However, these estimates should be viewed as approximate lower bounds because other, less permeable rocks (welded and nonwelded tuffs) are present in the test interval, and these less permeable rocks would cause the transmissivity to be lower than the transmissivity that would be expected if only lava had been present. Resistivity logs indicated that nonwelded tuffs could constitute as much as 73 percent of the upper 2000 ft of saturated rock at the boreholes listed in (Blankennagel and Weir 1973 [101233], Table 2). Because most of the water pumped from the lava enters the wells from zones that constitute only 3 to 10 percent of the total saturated thickness (Blankennagel and Weir 1973 [101233], p. 11), permeabilities in the lava may be locally much higher than the calculated mean value.

Table 27. Permeabilities of the Lava-Flow Aquifer

Well	Uncased, Saturated Thickness (ft)[a]	Transmissivity (gpd/ft)[b]	Hydraulic Conductivity (gpd/ft^2)	Permeability (m^2)
UE-18r	3,375	23,000	6.82	3.28 x 10^{-13}
TW-8	4,422	185,000	41.8	2.01 x 10^{-12}
UE19b-1	2,310	56,000	24.2	1.17 x 10^{-12}
UE19c	2,099	12,000	5.72	2.75 x 10^{-13}
UE-19d	5,129	20,000	3.90	1.88 x 10^{-13}
UE-19fs	2,214	11,000	4.97	2.39 x 10^{-13}
UE-19gs	1,858	30,000	16.1	7.77 x 10^{-13}
UE-19h	1,383	140,000	101.0	4.87 x 10^{-12}
UE-19I	5,104	1,400	0.274	1.32 x 10^{-14}
U-20a-2	2,434	18,000	7.40	3.56 x 10^{-13}
UE-20d	2,047	44,000	21.5	1.03 x 10^{-12}
UE-20e-1	4,573	8,300	1.82	8.73 x 10^{-14}
UE-20f	9,230	1,000	0.108	5.21 x 10^{-15}
UE-20h	4,701	11,000	2.34	1.13 x 10^{-13}

Source: Blankennagel and Weir (1973 [101233], Table 3).

NOTE: [a] Uncased, saturated thickness was calculated as the depth to water or depth of casing, whichever was greater, minus the depth of the well. The depth to water was used for TW-8, where the casing was perforated.

[b] gpd is gallons per day

Statistics for the logarithm of permeability (log *k*) are:

Mean = –12.574
Standard deviation = 0.803
Median = –12.521
Lower 95% confidence level for mean = –13.037
Upper 95% confidence level for mean = –12.110

7.2.5 Inferences about Permeability from Regional Observations

In addition to the permeability values from the NTS summarized in the previous section, Winograd and Thordarson (1975 [101167]) made numerous qualitative evaluations of the relative magnitude of permeability for different hydrogeologic units. These evaluations were based on examination of core for fractures and mineral infilling, the geologic setting and the magnitude of discharge of springs in the region, and the correspondence between changes in hydraulic gradients and the underlying hydrogeologic unit. Sections 7.2.3.1 through 7.2.3.3 focus on qualitative assessments of hydrogeologic units that have little actual test data and for which the qualitative evaluations, thus, assume relatively more importance.

7.2.5.1 Lower Clastic Aquitard (unit 3)

The Lower Clastic Aquitard of Winograd and Thordarson (1975 [101167], Table 1) corresponds to the Lower Clastic Confining Unit (unit 3) of Table 11. According to Winograd and Thordarson (1975 [101167], p. C43), the large-scale transmissivity of the Lower Clastic Aquitard is probably controlled by its interstitial permeability, which, based on the hydraulic conductivity of 18 cores (Winograd and Thordarson 1975 [101167], Table 4), ranges from 3.4 x 10^{-20} to 4.8 x 10^{-18} m^2 and has a median value of 9.7 x 10^{-20} m^2. Although the Lower Clastic Aquitard is highly fractured, Winograd and Thordarson (1975 [101167], p. C43) argued that fractures probably do not augment the interstitial permeability of the unit on a regional scale to the same degree as in the Lower Carbonate Aquifer for the following reasons:

- The argillaceous formations within the unit have a tendency to deform plastically, that is, by folding, rather than by fracturing. Thus, fracture continuity across the Lower Clastic Aquitard is disrupted by the argillaceous layers.

- Micaceous partings and argillaceous laminae tend to seal the fractures in the brittle quartzite parts of the unit, reducing or eliminating the ability of the fractures to transmit water.

- The clastic rocks that constitute the unit have a low solubility; therefore, solution channels, which can further enhance permeability along fractures in carbonate rocks, are not likely to be present in this unit.

The low permeability of the Lower Clastic Aquitard compared to the carbonate rocks also was indicated by the observation that, in the Spring Mountains, the total discharge issuing from the Lower Clastic Aquitard is only a small fraction of the total discharge of the springs in the Lower Carbonate Aquifer (Winograd and Thordarson 1975 [101167], pp. C42 to C43, C53). The comparatively low permeability of the Clastic Aquitard also is indicated by a head drop across the Lower Clastic Aquitard of 2000 ft (609.6 m) over a distance of less than eight miles (12.8 km) (an apparent hydraulic gradient of 250 ft/mile (47.6 m/km)) in the hills northeast of Yucca Flat (Winograd and Thordarson 1975 [101167], Plate 1). In contrast, the hydraulic gradient in the Carbonate Aquifer ranges from 5.9 ft/mile (1.12 m/km) or less along the axis of the potentiometric trough in Yucca Flat to 20 ft/mile (3.8 m/km) along the flanks of the trough (Winograd and Thordarson 1975 [101167], p. C71).

7.2.5.2 Upper Clastic Aquitard (unit 5)

The Upper Clastic Aquitard is equivalent to the Upper Clastic Confining Unit (unit 5) of Table 11. The Upper Clastic Aquitard corresponds to the Eleana Formation, which consists of argillite, quartzite, conglomerate, and limestone (Winograd and Thordarson 1975 [101167], Table 1). The upper two-thirds of the unit consists mainly of argillite, whereas the lower one-third of the unit is principally quartzite (Winograd and Thordarson 1975 [101167], p. C118). Winograd and Thordarson (1975 [101167], p. C43) argued that fractures were unlikely to remain open in the rock at depth because of the plastic deformation behavior of the rock, which is evidenced by tight folds, and the fact that the formation serves as a glide plane for several thrust faults at the NTS. No core-scale permeability measurements exist, but based on analogy with the Lower Clastic Aquitard, its interstitial permeability probably is less than 1×10^{-4} gpd/ft^2 (4.8×10^{-18} m^2) (Winograd and Thordarson 1975 [101167], p. C43). In the hills northwest of Yucca Flat, an approximately 2,000-ft (607.6 m) drop in hydraulic head in the pre-Tertiary rocks over a distance of less than 10 miles (an apparent hydraulic gradient of 200 ft/mile (38m/km)) suggests a comparatively low regional permeability for the Upper Clastic Aquitard. However, because land-surface elevation changes abruptly over this same distance and because water-table elevations often mimic ground-surface elevations, it is not possible to isolate the effects of permeability from the effects of topography on the head gradient in this area.

7.2.5.3 Faults

A summary of the possible effects of faults on groundwater movement in the Death Valley region was recently presented by Faunt (1997 [100146]). The transmissivity of faults was described by Faunt (1997 [100146], p. 30) to be a function of many factors:

- The orientation of the fault relative to the minimum horizontal stress in the region.
- The amount and type of fill material in the fault.
- The relative transmissivities of hydrogeologic units juxtaposed by offset across the fault.
- The solubility and deformation behavior of the rock adjacent to the fault.
- Recent seismic history.

7.2.5.3.1 Orientation of Faults Relative to the Minimum Horizontal Stress in the Region

In the vicinity of Yucca Mountain, the mean orientation of the minimum horizontal stress is 306 ± 11 degrees (Faunt 1997 [100146], Table 4-4), so that faults with traces oriented north-northeast are expected to be more open and permeable than faults with traces oriented in directions that place them in either a shear or a compressive state. Faults oriented northwest, or perpendicular to the maximum horizontal stress direction, would be expected to be least transmissive, all other factors being equal. One example cited by Faunt (1997 [100146], pp. 34–35) to illustrate that northeast-southwest trending structures that may have relatively high transmissivity is the "megachannel" formed in the Spotted Range-Mine Mountain shear zone between Frenchman Flat and Ash Meadows. The presence of a highly transmissive zone in the Carbonate Aquifer was indicated by a potentiometric trough in this area and relatively young carbon-14 ages of groundwater discharging from springs at the distal end of the trough (Winograd and Pearson 1976 [108882]).

7.2.5.3.2 Amount and Type of Infilling Material in the Fault

Fine-grained gouge or clayey infilling material can cause faults to become poorly transmissive, even if their orientation relative to the stress field indicates they have the potential to be highly transmissive. The effects of deformation behavior, solubility, and infilling material in the Clastic Aquitards and Carbonate Aquifer were discussed in the sections "Lower Clastic Aquitard" (Section 7.2.5.1) and "Upper Clastic Aquitard" (Section 7.2.5.2). Solution channels along faults in the carbonate rock have the potential to further enhance the transmissivity of faults in this unit.

7.2.5.3.3 Relative Transmissivities of Hydrogeologic Units Juxtaposed by Offset Across the Fault

Where faults juxtapose hydrogeologic units with contrasting permeabilities, the hydrologic effects caused by juxtaposition may be difficult to isolate from the effects of the fault properties themselves. As indicated in Faunt (1997 [100146], Figure 16), an increase in the local head gradient compared to the regional gradient can occur across a fault if:

- The fault is closed, thereby blocking flow.
- The fault is open, thereby redirecting flow.
- The permeability of the material downgradient of the fault is low compared to the upgradient material so that flow across the fault is blocked.
- The permeability of the material downgradient of the fault is high compared to the upgradient material so that flow can drain away from the fault faster than it can be delivered by the upgradient material.

Evidence that springs in Ash Meadows are caused by the juxtaposition of poorly permeable sediments and rocks downgradient of the Carbonate Aquifer across the Gravity fault was presented in Winograd and Thordarson (1975 [101167], p. C82). Hydraulic data in southern Indian Springs Valley were interpreted by Winograd and Thordarson (1975 [101167], p. C67 to C68) to indicate the presence of two hydraulic barriers related to the Las Vegas shear zone: (1) a northern barrier caused by the juxtaposition of the Lower Clastic Aquitard and Lower Carbonate Aquifer; and (2) a southern barrier, which was attributed to the presence of gouge along a major fault zone.

7.2.5.3.4 Recent Seismic History

The seismic history of the faults may indicate which faults have undergone recent movement. Recent movement on a fault may serve to break calcite or silica cement or other material that may have closed the fault. A map showing which faults or fault segments near Yucca Mountain have undergone recent movement was developed by Simonds et al. (1995 [101929]). Of the faults that have been mapped near the repository area, only the Solitario Canyon fault and short segments of the Bow Ridge fault near Exile Hill show evidence of late Quaternary (or more recent) movement.

7.2.6 Comparing Permeability Data to Calibrated Permeability Values

To check if the permeabilities estimated by PEST V 2.0 (STN: 10302-2.0-00; Watermark Computing 2002 [161564]) during the calibration of the base-case model are reasonable, the logarithms of permeabilities estimated during calibration of the model are compared to the mean logarithms of permeability estimated from pump-test data from Yucca Mountain in Figure 37 and to data from elsewhere at the NTS in Figure 38. Where they could be estimated, the 95-percent confidence limits for the mean logarithm of the permeability data also are shown in Figures 37 and 38. For the Calico Hills Formation, the Prow Pass Tuff, the Bullfrog Tuff, the Tram Tuff, and the MVA, permeabilities are shown for both the single-hole and for the cross-hole tests at the C-wells complex.

The calibrated permeabilities for the Calico Hills Formation, the Pre-Lithic Ridge Tuffs, and the Carbonate Aquifer are within the 95 percent confidence limits of the mean permeabilities estimated from single-hole pump test analyses at Yucca Mountain (Figure 37). The calibrated permeability for the Bullfrog Tuff is within the 95 percent confidence limits of the mean-measured permeability determined from the cross-hole tests. The calibrated permeability of the Prow Pass Tuff is slightly higher than the mean permeability estimated from the cross-hole tests, whereas the calibrated permeability of the Tram Tuff is between the mean permeabilities estimated for the unit from the single-hole and cross-hole tests (Figure 37).

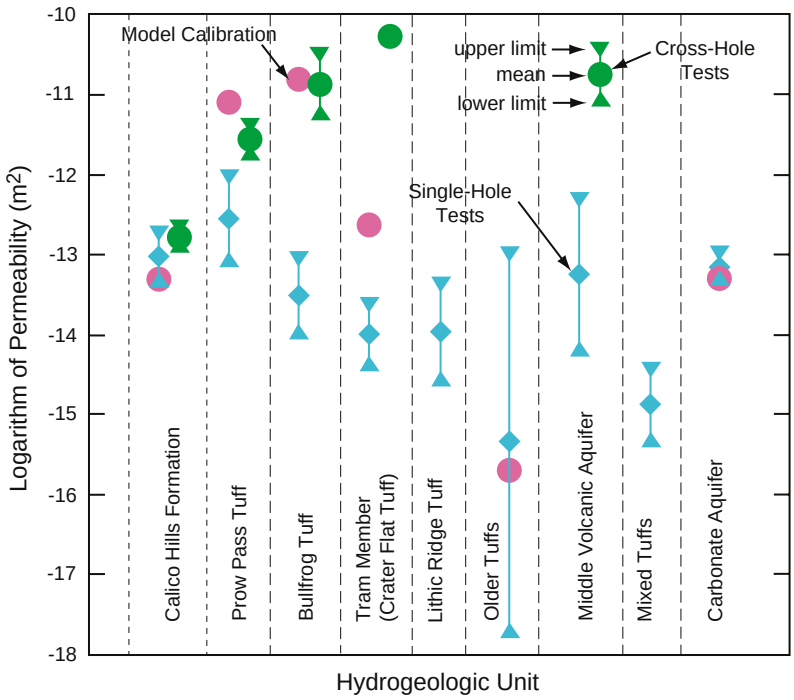

DTN: SNT05082597001.003 [129714] (reference only).

Figure 37. Logarithms of Permeabilities Estimated during Model Calibration Compared to Mean Logarithms of Permeability Determined from Pump-Test Data from Yucca Mountain

The mean measured permeability of the Carbonate Aquifer is higher elsewhere at the NTS than either the mean-measured permeability at Yucca Mountain or the calibrated permeability for the Carbonate Aquifer (Figures 37 and 38). The calibrated permeabilities for the Alluvial Aquifer and the Lava-Flow Aquifer are within or very close to the 95 percent confidence limits for the mean permeabilities of these units. The calibrated permeability for the Upper Volcanic Aquifer is about two orders of magnitude less than the mean-measured permeability of this unit.

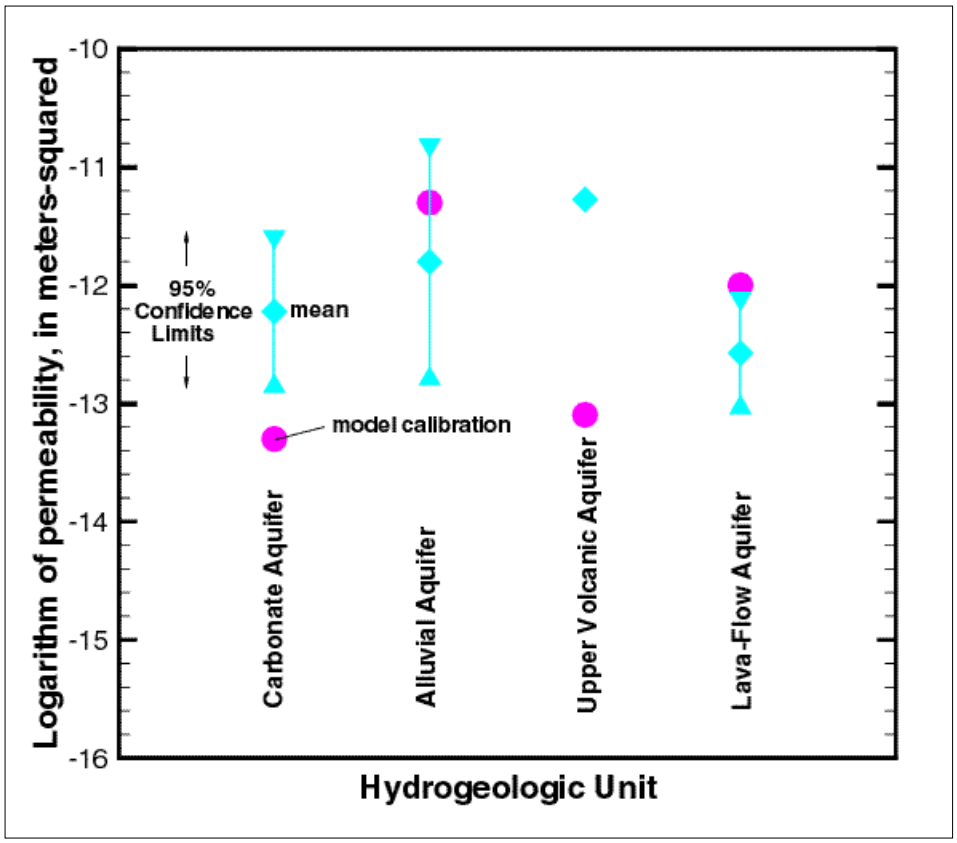

DTN: SNT05082597001.003 [129714] (for reference only).

Figure 38. Logarithms of Permeabilities Estimated during Model Calibration Compared to Mean Logarithms of Permeability Determined from Pump-Test Data from the Nevada Test Site

Overall, the calibrated permeabilities are consistent with most of the permeability data from Yucca Mountain and elsewhere at the NTS, except for the Upper Volcanic Aquifer. The calibrated permeability of the Tram Tuff is lower than the mean permeability derived from the cross-hole tests but higher than the permeability estimated from the single-hole tests. The relatively high permeability estimated for the Tram Tuff from the cross-hole tests may be at least partially attributable to local conditions at the site of these tests. A breccia zone is present in the Tram Tuff at boreholes UE-25 c#2 and UE-25 c#3 (Geldon et al. 1997 [100397], Figure 3), which is a factor that may have caused a local enhancement in the permeability of the Tram Tuff.

The permeability data recently obtained from single-hole and cross-hole testing in the alluvial testing complex have not been included in Figure 38. As indicated in Section 7.2.1, while the permeabilities reported from the single-hole tests for the alluvial materials are about an order of magnitude less than the calibrated value, the cross-hole tests yield a permeability measurement similar to the calibrated permeability values for the alluvial aquifer.

While the calibrated permeability of the many geologic units and features represented in the site-scale flow model may indirectly influence to a limited extent the specific discharge predicted by the base-case model, the calibrated permeabilities of those geologic units along the flow path from the repository to the compliance boundary most directly determine the specific discharge predicted by the base-case model. Particle tracking using the base-case model (see Section 7.3.1) has indicated that fluid particles migrating from the repository generally travel downward until they reach the Crater Flat Bullfrog unit. Because of the high permeability of the Bullfrog unit, the particles remain in that unit until it ends. At this point, fluid particles generally enter the alluvial portion of the flow system after briefly transitioning the Upper Volcanic Confining Unit. The flow path through the alluvial deposits is represented in the base-case model by the Alluvial Uncertainty Zone and the Lower Fortymile Wash Zone. Thus, those calibrated permeabilities that most directly control the prediction of specific discharge by the base-case model are those for the Bullfrog Unit and the Alluvial Uncertainty and Lower Fortymile Wash zones.

The calibrated value for the Bullfrog unit was 1.54×10^{-11} m^2 (see Table 14). As shown in Table 19, the mean permeability for the cross-hole measurements of the Bullfrog unit at Yucca Mountain was 1.37×10^{-11} m^2. Thus, the calibrated permeability for the Bullfrog unit was only 12 % greater than the mean of the measured value.

As indicated in Section 7.2.3.2, cross-hole tests have been performed in the alluvial material at the ATC in borehole NC-EWDP-19D. Borehole NC-EWDP-19D is located in the southern portion of the Alluvial Uncertainty Zone established in the base-case model. The calibrated permeability for the Alluvial Uncertainty Zone was 3.20×10^{-12} m^2. The permeability measured during the cross-hole tests at NC-EWDP-19D was 2.7×10^{-12} m^2. Thus, the calibrated permeability for the Alluvial Uncertainty Zone was only 19% greater than the measured value.

Since both new water-level data and permeability measurements are available at the ATC, predicted and observed values of both hydraulic gradient and permeability at this location can be used to calculate specific discharge. These calculated specific discharge values can then be compared to evaluate their combined impact on specific discharge for purposes of post-model development validation. As previously discussed in Section 7.1, the predicted hydraulic gradient between WT-3 and 19P/2D is only 7 percent greater that the observed gradient between these two locations (see Table 22). As indicated above, the calibrated permeability for the Alluvial Uncertainty Zone was 19% greater than the measured value at the ATC. Since the combined effect of the differences between predicted and observed values of these parameters on specific discharge is the product of their individual impacts, the calculated specific discharge based on the predicted value of hydraulic gradient and the calibrated value of permeability is only 27 percent greater than the value calculated using the respective observed values of these parameters. This result meets the validation criteria of being within a factor of 3 (BSC 2003 [163965], Section 2.2) used in the SZ transport abstraction model.

The 18-km compliance region described in Section 6.8.8 and the SZ transport abstraction model (BSC (2003 [164870]) are strongly influenced by groundwater flow in alluvium. Estimates of groundwater specific discharge in the SZ were recently obtained from field testing at the Alluvial Testing Complex (ATC) (BSC 2003 [162415], Section 6.5.4.3). The ATC is located approximately 18 km from Yucca Mountain at the boundary of the accessible environment as specified in 10 CFR 63.302 (10 CFR 63 [156605]). The ATC testing was performed in the alluvium aquifer. Estimates of groundwater specific discharge at the ATC range from 1.2 m/yr to 9.4 m/yr. For the details of flow porosity in alluvium, see DTN: LA0303PR831231.002 [163561] (BSC 2003 [162415], Section 6.5.4.3). For the expected flow porosity in the alluvium of 0.18, the test-derived specific discharge ranges from 2.4 to 7.3 m/yr. The simulated average specific discharge in this region of the SZ system, using the SZ transport abstraction model, ranges from 1.9 m/yr to 3.2 m/yr for differing values of horizontal anisotropy in permeability ranging from 0.05 to 20 (BSC 2003 [162415], Section 6.5.4.3). For the mean horizontal anisotropy, the simulated average specific discharge is approximately 2.8 m/yr for the ATC test location (BSC 2003 [164870], Section 6.5.1.2). This specific discharge is within a factor of 1.2 of the lower end of test-derived value (2.4 m/yr) and a factor 2.6 of the upper end value (7.3 m/yr), which meets the validation criterion of being within a factor of 3 (BSC 2003 [163965], Section 2.2). Therefore, the data from the ATC field testing both constitute new specific discharge in the SZ information and significantly reduce uncertainty in the specific discharge relative for use in SZ transport abstraction model. The remaining uncertainty is propagated accordingly into the SZ transport abstraction model (BSC (2003 [164870]), Section 6). Specifically, an uncertainty distribution in specific discharge is constructed, in which 80% of the probability is between one-third and three times the best estimate of specific discharge, with an additional 10% assigned to the lower tail of 1/30 of the expected value and 10% to the upper tail of 10 times the expected value of specific discharge. Additionally, the uncertainty in effective porosity is captured through the use of a truncated normal distribution as used in the SZ transport abstraction model (BSC 2003 [163870]). The details of the uncertainty distributions of specific discharge and effective porosity in the alluvium and their associated sampling techniques are contained in BSC 2003 [164870]), Sections 6.5.2.1 and 6.5.2.3, respectively.

7.3 COMPARISON OF HYDROCHEMICAL DATA TRENDS WITH CALCULATED PARTICLE PATHWAYS

The base-case flow and transport model was used to simulate the movement of a conservative tracer from various segments along the boundaries in the model. The location of these boundary segments and their numerical designations in the model are shown in Figure 24. The goal of these simulations was to provide an understanding of where groundwater at any location in the flow system may have originated and to what extent groundwaters originating from various locations may mix. These simulation results are then qualitatively evaluated in the context of the understanding gained from the analysis of the hydrochemical and isotopic data discussed in the previous sections and summarized here in the next section.

7.3.1 Hydrochemical Data Flow Path Summary

Groundwater flow paths and mixing zones were identified in the analyses of the areal distributions of measured and calculated geochemical and isotopic parameters, scatterplots, and inverse mixing and reaction models with PHREEQC (Parkhurst and Appelo 1999 [159511]). This summary describes the basis for the flow paths drawn in Figure 39.

Flow paths of tracer particles were calculated for the base-case flow and transport model. The particles were started in the vicinity of the repository footprint and allowed to transport downstream to the compliance boundary. The results are shown in Figure 39b. Also shown in Figure 39 (a and b) are flow paths deduced from the hydrochemistry data (BSC 2003 [162657] Section 6.7.11). Chemical and isotopic compositions were measured for groundwater samples taken from a number of wells in the area of the SZ site-scale flow model. As explained in detail in BSC (2003 [162657] Section 6.7.11), graphical analysis was done of the variations in the concentrations of the chloride (Cl^-), sulphate (SO_4^{2-}), HCO_c^-, and SiO_2 ions and in the oxygen isotopic ratio (δ^{18}O) and the hydrogen isotopic ratio (δD) to estimate plausible flow lines. Of particular interest are the flow paths labeled # 2 and #7 from this analysis (Figure 39a). Flow Path #7, which is derived from hydrochemistry data, originates in the vicinity of the repository footprint and generally overlaps the model-calculated flow paths as seen in Figure 39b. Flow Path #2 is also of interest here, although it originates northeast of the repository, because it closely bounds Flow Path #7 to the east.

Flow Path #1 traces the movement of groundwater southeastward from Oasis Valley through the Amargosa Desert along the axis of the Amargosa River to its confluence with Fortymile Wash. This flow path is identified from both areal plots of Cl and scatterplots of SO_4 versus Cl that support this flowpath and mixing zone. The same data indicate that groundwater flow southward from the CF-SW wells toward the AR and FMW-W wells is improbable. Groundwater along this flowpath becomes more dilute in the AR/FMW wells as it becomes increasingly mixed with groundwater near Fortymile Wash. Upstream of this mixing zone, high groundwater ^{14}C activities and variable δD and $\delta^{18}O$ compositions at the AR wells indicate the presence of relatively young recharge in the groundwater due to ephemeral runoff in the Amargosa River channel or to irrigation in the area.

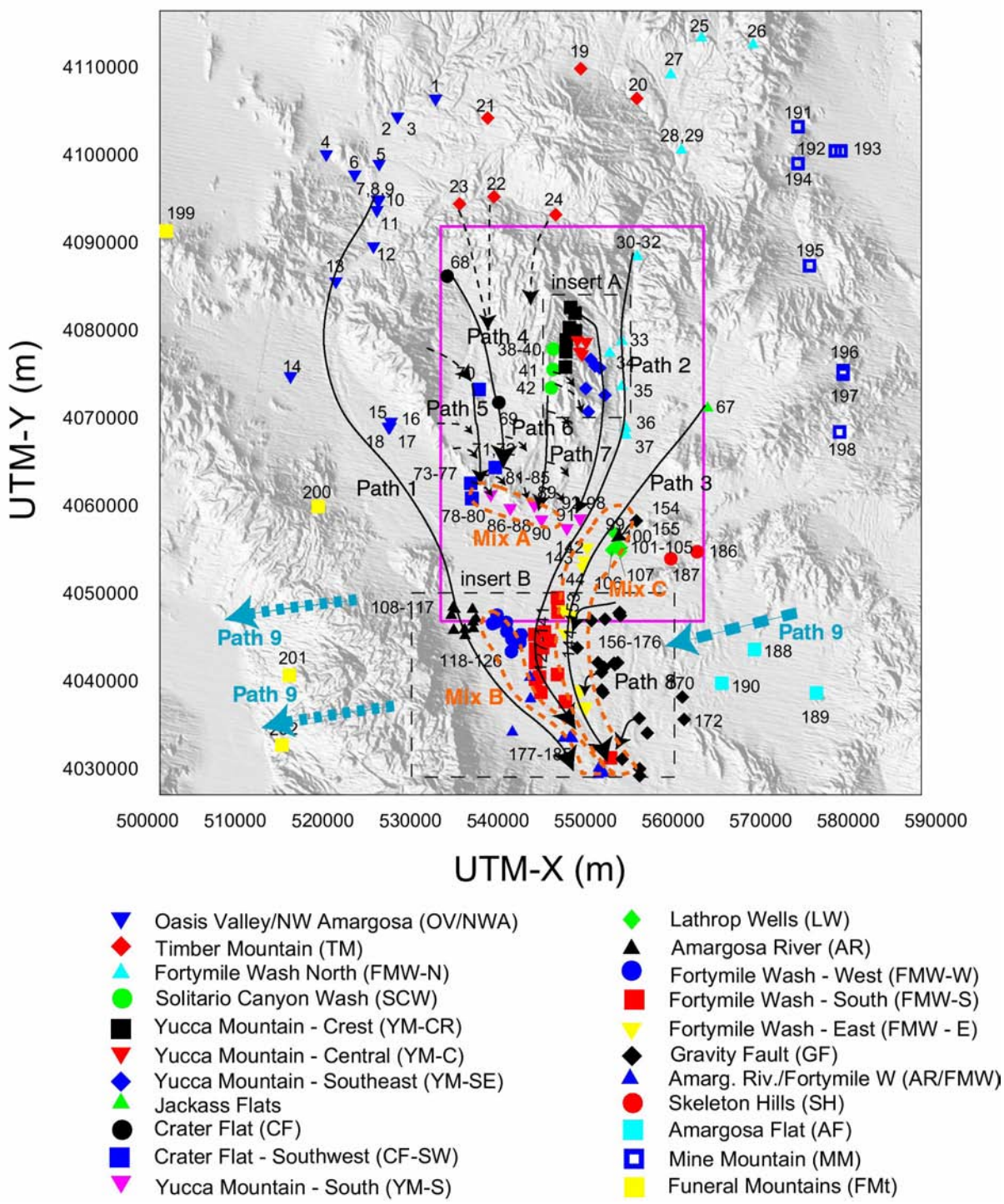

Source: BSC (2003 [162657]).

Figure 39a. Groundwater Flow Paths and Mixing Zones Interpreted From Groundwater Chemistry and Isotope Compositions

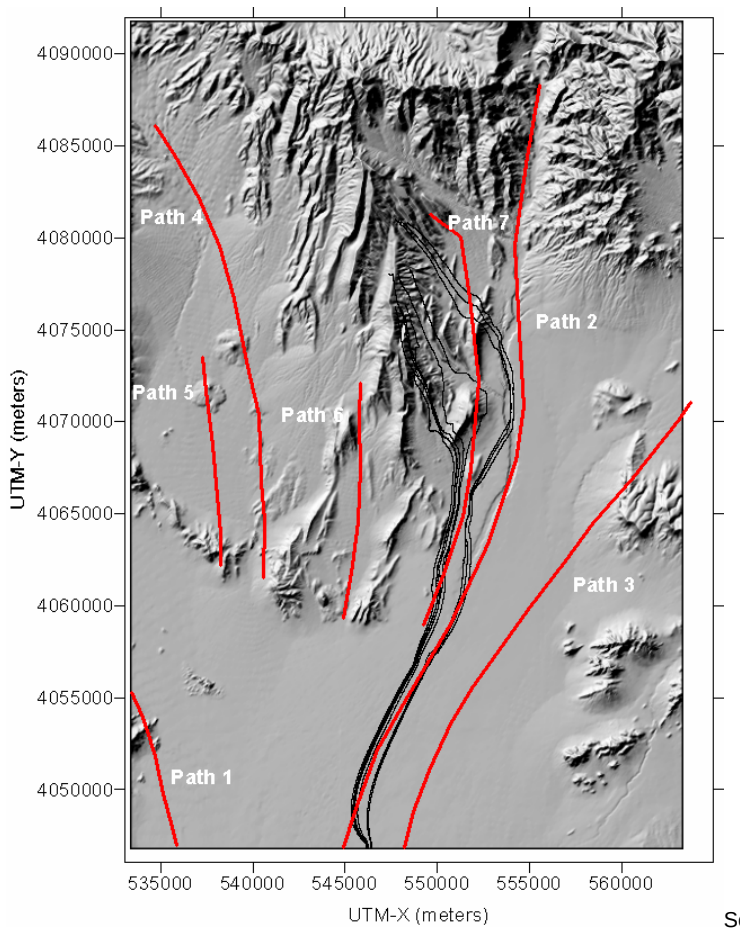

Source: BSC (2003 [162657]).

Figure 39b. Transport Pathways Deduced from Hydrochemistry Data (in red, enlarged from Figure 39a) Overlaying Flow Paths Calculated from the SZ Transport Model (in black) for Tracer Particles Starting at the Repository Footprint

Flow Path #2 traces the movement groundwater from the Fortymile Canyon area southward along the axis of Fortymile Wash into the Amargosa Desert. Groundwater along the northern part of this flow path is distinguished from groundwater at Yucca Mountain by δD and $\delta^{18}O$ compositions that are heavier and/or more offset from the Yucca Mountain meteoric water line than the groundwater found under Yucca Mountain. It is inferred that the groundwater found along the FMW-S wells in the Amargosa Desert is derived, in part, from groundwater flow from the FMW-N wells, based on the similarly dilute SO_4 and Cl compositions of these groundwaters. Differences in the δD compositions of the FMW-N and FMW-S groundwaters are attributed to the effects of changing climatic conditions on the δD composition of recharge, as indicated by the relationship between δD values and ^{14}C activities for these groundwaters. Groundwater flow from the FMW-N area wells southward into the Amargosa Desert along the axis of the wash is also compatible with expected and observed chemical evolution trends between the two areas, such as down-gradient increases in pH, calcite saturation indices, and HCO_3 and SiO_2 concentrations. Some part of the groundwater along Fortymile Wash may also be derived by

recharge from overland flow, based on the observation that ^{14}C activities do not decrease systematically southward in either the northern or southern segments of the wash. Groundwater from the eastern and western parts of the Amargosa Desert is a relatively minor component of FMW-S area groundwater, based on the much higher solute contents and distinct isotopic compositions of groundwaters adjacent to the FMW-S area wells.

Flow Path #3 traces the movement of groundwater from Jackass Flats in the vicinity of well J-11 (Site 67) as it moves along the western edge of the Lathrop Wells area wells and arcs southward through the FMW-E area wells. The identification of groundwater from Jackass Flat in this mixture of groundwaters is possible because the high SO_4/low $\delta^{34}S$ characteristics of groundwater from well J-11 distinguish it from the high SO_4 /high $\delta^{34}S$ groundwater characteristic of the Gravity fault and the low SO_4 /low $\delta^{34}S$ groundwater of the Fortymile Wash area on scatterplots of $\delta^{34}S$ versus 1/ SO_4 concentration. A source for this high SO_4 groundwater from Jackass Flats rather than from the Gravity fault area is also indicated by the light $\delta^{13}C$ of groundwater along this flow path.

Flow Path #4 traces the movement of groundwater from the lower Beatty Wash area into northwestern Crater Flat. This groundwater flows predominantly southward in Crater Flat through Site 69 (borehole VH-1) and Site 86 (NC-EWDP-3D). The chemistry and isotopic composition of this groundwater appears to be a mixture of subequal amounts of groundwater from Sites 22 and 23 in lower Beatty Wash, with much smaller amounts of recharge from local runoff in Crater Flat or groundwater flow from Site 24. Groundwater from Site 68 (Gexa Well 4), which may be groundwater from Site 23 modified by recharge from surface runoff, also contributes groundwater to this flow path. Scatterplots of δD versus Cl and PHREEQC (Parkhurst and Appelo 1999 [159511]) inverse models show that a mixture of groundwater from Sites 22 and 23 is required to account for both the relatively low Cl concentrations and the light δD and $\delta^{18}O$ values that are characteristic of this flow path; small amounts of recharge from local runoff or flow from Site 24 are also needed in this mixture to decrease the $\delta^{13}C$ of the lower Beatty Wash groundwater toward the lighter $\delta^{13}C$ values found at borehole VH-1.

Most groundwater at Timber Mountain north of Yucca Mountain is characterized by $\delta^{13}C$, which is too heavy (-6 to 0) and too low in ^{14}C to be a major source of groundwater at Yucca Mountain. The absence of significant amounts of Timber Mountain groundwater beneath Yucca Mountain is also indicated by the extremely low $\delta^{87}Sr$ and high Sr of the Timber Mountain groundwater compared to Yucca Mountain. The extremely light $\delta^{13}C$ and high $\delta^{87}Sr$ of groundwater in northern Yucca Mountain compared to Timber Mountain groundwater indicates that groundwater from the Timber Mountain/Beatty Wash area does not flow directly south through northern Yucca Mountain. Groundwater in well ER-EC-07 (Site 24) in upper Beatty Wash has a high ^{14}C activity and $\delta^{13}C$ and $\delta^{87}Sr$ values similar to those of groundwater in the Solitario Canyon Wash area and areas south of Drill Hole Wash at Yucca Mountain. Some groundwater from the area of ER-EC-07 in upper Beatty Wash could be present in Yucca Mountain groundwater south of Drill Hole Wash and along Solitario Canyon Wash if Sr sorption on the rock removed most of the Sr from the Beatty Wash area along its flow path.

Flow Path #5 traces the movement of groundwater between the SW Crater Flat group wells. Groundwaters in this well grouping have relatively uniform and distinctive chemical and isotopic

compositions compared to groundwaters in adjacent areas. In particular, groundwaters in the CF-SW group have higher concentrations of most major ions (but lower concentrations of F and SiO_2), and relatively heavy $\delta^{18}O$ and δD compared to groundwaters that characterize Flow Path #4. The $\delta^{18}O$ and δD values of groundwaters in the CF-SW group are similar to those of groundwater from Species Spring (Rose et al. 1997 [144725]), which is a perched spring at Bare Mountain, suggesting that the CF-SW group groundwaters are derived principally from local recharge and runoff from Bare Mountain. Dashed west- and southwest-oriented lines schematically illustrate this flow. Groundwater in the Oasis Valley is among the lightest groundwater in the Yucca Mountain area, eliminating flow from Oasis Valley under Bare Mountain as a possible source of groundwater in southwest Crater Flat. The similar chemical and isotopic characteristics of groundwater at the up-gradient well in the CF-SW group (Site 70 – borehole VH-2) and down-gradient wells in this group indicate predominantly north-south flow in southwest Crater Flat. PHREECQ (Parkhurst and Appelo 1999 [159511]) models of groundwater evolution between Sites 70 and 73 confirm this flow path. Importantly, the chemically distinct groundwater along this flow pathway is not observed in boreholes to the south in the Amargosa Desert (AR and FMW-S groups).

Flow Path #6 traces the movement of groundwater from Site 42 (well WT-10) southward toward Sites 89 (Cind-R-Lite well) and 90 (well NC-EWDP-15P). This flow path is identified from PHREEQC (Parkhurst and Appelo 1999 [159511]) models that indicate that groundwater from the Cind-R-Lite well is formed from subequal amounts of groundwater from well WT-10 and local Yucca Mountain recharge (represented by perched water from borehole SD-7) and a small percentage (10 to 15 percent) of groundwater from the Carbonate Aquifer. A small amount (5 percent) of groundwater from the vicinity of Site 69 (borehole VH-1) may also be present in this mixture. Although the dominant flow direction from well WT-10 may be southward along the Solitario Canyon fault, some flow toward the southeast may be possible, based on an analysis of the chemistry at well NC-EWDP-19D (see below). Hence, a small amount of leakage southeast is indicated on this flow path.

Flow Path #7 traces the movement of groundwater from northern Yucca Mountain southeastward toward YM-SE wells in the Dune Wash area and then southwestward along the western edge of Fortymile Wash. The upper segment of this flow path is motivated by the high groundwater $^{234}U/^{238}U$ activity ratios found in the northern Yucca Mountain and Dune Wash areas. High $^{234}U/^{238}U$ activity ratios (> 7) typify both perched water and groundwater along and north of Drill Hole Wash but not groundwater along Yucca Crest at borehole SD-6 or perched water at borehole SD-7. Based on the conceptual model for the evolution of $^{234}U/^{238}U$ activity ratios, dissolution of thick vitric tuffs that underlie the Topopah Spring welded tuff along Yucca Crest south of Drill Hole Wash would be expected to decrease the $^{234}U/^{238}U$ activity ratios of deep unsaturated-zone percolation south of the Wash. High $^{234}U/^{238}U$ activity ratios are expected only where these vitric tuffs are absent, as in northern Yucca Mountain. Results of a PHREEQC (Parkhurst and Appelo 1999 [159511]) model of the evolution of groundwater between Site 44 (well WT-24) in northern Yucca Mountain and Site 65 (well WT-3) in the Dune Wash area are consistent with this segment of Flow Path #7. The southern segment of Flow Path #7 is based on PHREEQC models of groundwater evolution between well WT-3 and various depth intervals of well NC-EWDP-19D (Sites 92-98). Groundwater at well NC-EWDP-19D has low Cl and SO_4 concentrations that are characteristic of groundwater at well WT-3. The light $\delta^{18}O$ and δD values eliminate Fortymile Wash as a possible source of the dilute groundwater at well NC-

EWDP-19D. An alternative set of PHREEQC models was developed that interprets the groundwater at NC-EWDP-19D to result from the mixing of groundwater from well WT-10 and local southern Yucca Mountain recharge, as represented by perched water from borehole SD-7. Both sets of models explain the major ion chemistry and $\delta^{13}C$ values of groundwater at NC-EWDP-19D. The arrows leading from Flow Path #6 toward NC-EWDP-19D reflect this alternative groundwater path. It should also be noted that the $\delta^{18}O$ and δD values of groundwater at well NC-EWDP-19D are substantially lighter than groundwater at either wells WT-3 or WT-10, requiring that climate change be invoked as a possible explanation for their differences.

Although the predominant direction of flow from the Solitario Canyon area is southward along the Solitario Canyon fault, evidence for the leakage of small amounts of groundwater eastward across the fault is provided by similarities of ion concentrations and isotopic values among the Solitario Canyon Wash (SCW) and Yucca Mountain Crest area (YM-CR) wells. The chemical and isotopic resemblance indicates that groundwater as far east as borehole H-4 may have some component of groundwater from the Solitario Canyon Wash area. The short southeast-oriented dashed lines from Solitario Canyon Group wells schematically illustrate this leakage.

Flow Path #8 schematically demonstrates leakage of groundwater from the Carbonate Aquifer (Gravity Fault and Amargosa Flat Groups) across the Gravity fault. Hydrogeologists and geochemists have recognized this leakage across the fault for many years (Winograd and Thordarson 1975 [101167]; Claassen 1985 [101125]). The Carbonate Aquifer component in this groundwater is recognized by the many of the same chemical and isotopic characteristics that typify groundwater discharging from the Carbonate Aquifer at Ash Meadows. These characteristics include high concentrations of Cl, SO_4, Ca and Mg, low SiO_2 concentrations, heavy $\delta^{13}C$ values, low ^{14}C activities, and comparable $\delta^{18}O$ and δD values as the Ash Meadows groundwater. Westward seepage of this groundwater mixes with the southward flow of groundwater along flow path #3 to produce groundwater with compositions intermediate between the two. Evidence for these flow paths is best defined in groundwater composition of some of the more westerly samples of the Gravity Fault Group, such as found at Sites 160, 161, 175, and 175. These flow pathways are also compatible with the hydraulic gradient and the present understanding of the regional groundwater flow patterns (e.g., Lacziak et al. 1996 [103012]). These mixing relations are discussed below in the context of Mixing Zone C in this section.

Flow Path #9 is drawn to illustrate schematically deep underflow of groundwater from the Carbonate Aquifer east of and including the Gravity Fault and Amargosa Flat Groups, beneath the Amargosa Desert and the Funeral Mountains, to the discharge points in Death Valley. The similarity in the chemical and isotopic characteristics of groundwater found in the Gravity fault area and groundwater that discharges from springs at Sites 201 (Nevares Spring) and 202 (Travertine Spring) support this interpretation. The dissimilarity in Cl, Mg, and SiO_2 concentrations in these springs compared to the groundwater from the alluvial aquifer along the Amargosa River (AR grouping) suggests that this alluvial groundwater is not the predominant source of the spring discharge in Death Valley.

7.3.2 Mixing Zones

Figure 39a highlights three zones within which there is good evidence for mixing as demonstrated by linear relationships between various solutes and isotopes on cross-correlation plots.

Mixing Zone A is identified from groundwaters in the YM-S and CF-SW group wells along Interstate 95. The mixing zone is demonstrated by groundwater compositions of samples 81 to 85, 89, and 90 that are intermediate between the compositionally distinct groundwater of the Carbonate Aquifer and the dilute groundwater of the volcanic aquifer that is interpreted to have originated in the Yucca Mountain area (see Flow Path #6 discussion). The source of the carbonate groundwater in samples 89 and 90 is unclear, but evidence favors a carbonate source similar to that of the SW Crater Flat group.

Mixing Zone B consists of samples from the FMW-W, AR/FMW, and a few samples from the FMW-S groups. The zone is identified by groundwaters with compositions that are intermediate between the relatively high salinity groundwater compositions of the Amargosa River Group and the dilute groundwater of the FMW-S group. Flow Path #1 is drawn to avoid Mixing Zone B and to indicate the flow of groundwater from the Amargosa River group toward Site 181, which has a similar groundwater composition and is interpreted to represent undiluted groundwater from the Amargosa River group.

Mixing Zone C consists of all samples from the Lathrop Wells and FMW-E groups, a few of the more westerly samples from the Gravity Fault Group, and at least one sample (Site 141) from the FMW-S group. The mixing zone is characterized by small percentages of the distinctively high SO_4 groundwater from Site 67 (borehole J-11). This distinct hydrochemical signature persists in variable percentages as far south as Site 150. Groundwaters with this distinctive signature are mixed to variable degrees with dilute water from the FMW-S group to the west or groundwater from the Carbonate Aquifer (Gravity Fault Group) to the east.

An important conclusion derived from the identification of these mixing zones is that they document and illustrate qualitatively the extent of transverse dispersivity along certain flow pathways. The mixing zones also illustrate that although some flow pathways may remain intact for great distances (e.g., Flow Paths #1 and #2), even these most persistent flow paths eventually lose their distinct character largely through mixing. This is best illustrated in the southern Amargosa Desert where Flow Paths #1, #2, and #3 (with contributions from Flow Path #8) converge and mix. The distinct end-member groundwaters of the AR and FMW-S groups, representing Flow Paths #1 and #2, appear to be absent at the southern boundary of the study area. It is possible that these end-member groundwaters have not yet been sampled. However, the proximity of mixed groundwater samples in the southern part of the study area (samples 141, 174, 175, 183, 184, and 185) leaves little room for unmixed (end member) groundwater to move through the area. The hydrochemical data are interpreted to indicate that groundwaters from distinct sources that merge in the Amargosa Desert eventually loose their hydrochemically distinct character and flow southward as partially mixed samples.

Flow paths from the repository predicted by the base-case model and shown in Figure 39b can be compared to those identified using geochemical analysis and shown in Figure 39a. A comparison of these flow paths indicates that the flow paths from the repository predicted by the base-case model generally correspond well with those identified through geochemical analysis and are enveloped by possible flow paths deduced from the geochemical analysis. The generally good agreement between the two sets of flow paths qualitatively supports the validation of the base-case model, particularly in demonstrating the capability of the base-case model to simulate flow paths accurately from the repository to the compliance boundaries.

7.4 THERMAL MODELING

Measurements of temperature in the SZ constitute an independent data set that was not used in the calibration of the SZ site-scale flow model and may be used to support the validation of the flow model. The transport of heat in the geosphere occurs generally upward toward the Earth's surface, leading to higher temperatures with depth. However, heat is also redistributed by groundwater flow, and temperature can potentially serve as a tracer for the movement of groundwater in the SZ. To evaluate heat transport in the SZ, modeling of heat transport through conduction only and through conduction with convective transport was undertaken. The validation of the base-case model using simulations of heat transport and measured values of temperature in the SZ is documented in the following section. Modeling of heat transport through conduction only is presented first, followed by a presentation of modeling of heat transport through both conduction and convection. The direct comparison of temperature with groundwater movement is complicated by spatial uncertainty in thermal properties, overburden thickness, and heat flux. Despite these inherent limitations, an acceptable comparison between observed and simulated temperatures was achieved. The work presented in this section is taken from the paper Arnold et al. (2003 [164473]) and is not used for any other purpose than to provide additional support in the validation of the SZ flow model.

7.4.1 Conduction-Only Modeling

Heat transport in the geosphere is a function of thermal conduction and advective movement with groundwater flow. Simulation of coupled groundwater flow and heat transport in the SZ is a more complete description of natural geothermal processes in the SZ system. Simulations of heat conduction alone are used to assess the relative importance of conduction with regard to the observed temperatures in the system. In addition, the conduction-only model of the SZ is calibrated with respect to observed temperatures and provides a starting point for coupled thermal simulations that have been optimized with regard to thermal conduction.

The base-case flow model is used as the basis for the modeling of heat conduction. The model domain and definitions of the hydrogeologic units are retained from the base-case model. Values of thermal conductivity are designated on a unit-by-unit basis. The thermal boundary conditions on the bottom and top boundaries of the base-case model are defined and adjusted in the thermal calibration process.

7.4.1.1 Temperature and Thermal Properties Data

Data on temperatures in the SZ are taken from temperature profiles measured in wells within the SZ site-scale model area. These data are from Yucca Mountain Project wells and from the newer Nye County Early Warning Drilling Program wells and are compiled in Table 28. The temperature data in Table 28 were extracted at 200-m intervals from these temperature logs, starting at the water table. A total of 94 observed temperatures in 35 wells were obtained.

Table 28. Temperature Data from Boreholes

Well ID	UTM Easting (m)	UTM Northing (m)	Elevation (m)	Temperature (^oC)	Data Tracking Number *
USWG-1	548306	4080016	754	29.6	GS950408318523.001
USWG-1	548306	4080016	554	35.8	GS950408318523.001
USWG-1	548306	4080016	354	39.2	GS950408318523.001
USWG-1	548306	4080016	154	44.9	GS950408318523.001
USWG-1	548306	4080016	-46	50.4	GS950408318523.001
USWG-1	548306	4080016	-246	55.7	GS950408318523.001
USWG-1	548306	4080016	-446	62.1	GS950408318523.001
USWG-2	548143	4082542	1028	29.6	GS950408318523.001
USWG-2	548143	4082542	828	32.3	GS950408318523.001
USWG-2	548143	4082542	628	38.4	GS950408318523.001
USWG-2	548143	4082542	428	46.6	GS950408318523.001
USWG-2	548143	4082542	228	55.1	GS950408318523.001
USWG-3	547543	4074619	729	33	GS950408318523.001
USWG-3	547543	4074619	529	35.3	GS950408318523.001
USWG-3	547543	4074619	329	39.7	GS950408318523.001
USWG-3	547543	4074619	129	43	GS950408318523.001
USWG-4	548933	4078602	729	30	GS950408318523.001
USWG-4	548933	4078602	529	34.5	GS950408318523.001
USWH-1	548727	4079926	730	32.8	GS950408318523.001
USWH-1	548727	4079926	530	35.4	GS950408318523.001
USWH-1	548727	4079926	330	39.3	GS950408318523.001
USWH-1	548727	4079926	130	44.2	GS950408318523.001
USWH-1	548727	4079926	-70	50.1	GS950408318523.001
USWH-1	548727	4079926	-270	56.2	GS950408318523.001
USWH-1	548727	4079926	-470	61.6	GS950408318523.001

Table 28 (Continued). Temperature Data from Boreholes

Well ID	UTM Easting (m)	UTM Northing (m)	Elevation (m)	Temperature (^oC)	Data Tracking Number
USWH-3	547562	4075759	732	33.3	GS950408318523.001
USWH-3	547562	4075759	532	37.2	GS950408318523.001
USWH-3	547562	4075759	332	41.1	GS950408318523.001
USWH-4	549188	4077309	730	30.7	GS950408318523.001
USWH-4	549188	4077309	530	32.8	GS950408318523.001
USWH-4	549188	4077309	330	33.7	GS950408318523.001
USWH-4	549188	4077309	130	38.3	GS950408318523.001
USWH-4	549188	4077309	30	40.2	GS950408318523.001
USWH-5	547668	4078841	774	35.1	GS950408318523.001
USWH-5	547668	4078841	574	37.1	GS950408318523.001
USWH-5	547668	4078841	374	40.3	GS950408318523.001
USWH-6	546188	4077816	776	34	GS950408318523.001
USWH-6	546188	4077816	576	36.1	GS950408318523.001
USWH-6	546188	4077816	376	44	GS950408318523.001
USWH-6	546188	4077816	176	51.2	GS950408318523.001
UE-25b1H	549949	4078423	731	31.8	GS950408318523.001
UE-25b1H	549949	4078423	531	34.6	GS950408318523.001
UE-25b1H	549949	4078423	331	35.4	GS950408318523.001
UE-25b1H	549949	4078423	131	39.2	GS950408318523.001
UE-25p1	551501	4075659	730	33.6	GS950408318523.001
UE-25p1	551501	4075659	530	38.2	GS950408318523.001
UE-25p1	551501	4075659	330	41.9	GS950408318523.001
UE-25p1	551501	4075659	130	48.1	GS950408318523.001
UE-25p1	551501	4075659	-70	55.6	GS950408318523.001
UE-25p1	551501	4075659	-270	57.5	GS950408318523.001
UE-25p1	551501	4075659	-470	55.4	GS950408318523.001
USWVH-1	539976	4071714	898	27	GS930208318523.001
USWVH-1	539976	4071714	698	32	GS930208318523.001
USWVH-1	539976	4071714	498	35	GS930208318523.001
USWVH-1	539976	4071714	298	36	GS930208318523.001
USWVH-2	537738	4073214	811	27	GS930208318523.001
USWVH-2	537738	4073214	611	30	GS930208318523.001
USWVH-2	537738	4073214	411	35	GS930208318523.001
USWVH-2	537738	4073214	211	36	GS930208318523.001
USWVH-2	537738	4073214	11	38	GS930208318523.001
USWVH-2	537738	4073214	-189	52	GS930208318523.001
J-13WW	554017	4073517	729	30.2	GS950408318523.001

Table 28 (Continued). Temperature Data from Boreholes

Well ID	UTM Easting (m)	UTM Northing (m)	Elevation (m)	Temperature (^{o}C)	Data Tracking Number
J-13WW	554017	4073517	529	30.7	GS950408318523.001
J-13WW	554017	4073517	329	33.1	GS950408318523.001
J-13WW	554017	4073517	129	35.8	GS950408318523.001
USWWT-1	549152	4074967	731	30.1	GS950408318523.001
USWWT-2	548595	4077028	730	31.5	GS950408318523.001
UE-25WT3	552090	4072550	730	33.1	GS950408318523.001
UE-25WT4	550439	4079412	728	31.4	GS950408318523.001
UE-25WT6	549352	4083103	1029	28.4	GS950408318523.001
USWWT-7	546151	4075474	776	33.8	GS950408318523.001
USWWT-10	545964	4073378	775	38.8	GS950408318523.001
USWWT-11	547542	4070428	730	35.2	GS950408318523.001
UE-25WT12	550168	4070659	730	32.9	GS950408318523.001
UE-25WT13	553730	4075827	729	28.5	GS950408318523.001
UE-25WT14	552630	4077330	730	29.9	GS950408318523.001
UE-25WT15	554034	4078694	729	27.5	GS950408318523.001
UE-25WT16	551146	4081234	737	32.3	GS950408318523.001
UE-25WT17	549905	4073307	729	31.1	GS950408318523.001
UE-25WT18	549468	4080238	731	31.2	GS950408318523.001
NC-EWDP-1S	536771	4062498	787	21.7	MO0008NYE02997.033
NC-EWDP-2DP	547744	4057164	706	24.1	Nye Co. web site
NC-EWDP-3D	541273	4059444	717	26.6	MO0008NYE02997.033
NC-EWDP-3D	541273	4059444	517	26.3	MO0008NYE02997.033
NC-EWDP-3D	541273	4059444	317	28.4	MO0008NYE02997.033
NC-EWDP-3D	541273	4059444	117	42.3	MO0008NYE02997.033
NC-EWDP-5SB	555676	4058229	724	29.2	Nye Co. web site
NC-EWDP-7S	539558	4064317	830	24.5	Nye Co. web site
NC-EWDP-7S	539558	4064317	630	31.7	Nye Co. web site
NC-EWDP-12PA	536905	4060766	723	32.7	Nye Co. web site
NC-EWDP-12PC	536871	4060808	721	29.5	Nye Co. web site
NC-EWDP-19P	549237	4058265	713	26.2	Nye Co. web site
UE-25a#1	549925	4078330	731	31.5	GS950408318523.001
UE-25a#1	549925	4078330	531	34.1	GS950408318523.001

NOTE: The DTNs listed in the table {GS950408318523.001 [107244], MO0008NYE02997.033 [155290], GS930208318523.001 [145763], and the Nye Co. web site (Nye County Nuclear Waste Repository Project Office 2000 [149364])} are the sources of information for each entry. This table is used as reference only.

Values of thermal conductivity for the hydrogeologic units in the conduction-only model are taken from a variety of sources and are listed in Table 29. For hydrogeologic units that are generally stratified and for which multiple thermal conductivity measurements are available, vertical and horizontal thermal conductivity are estimated separately. Harmonic averaging is appropriate for effective conductivity in the vertical direction in which stratified variations in conductivity occur in series. Arithmetic averaging is appropriate for effective conductivity in the horizontal direction in which variations in conductivity generally occur in parallel.

Table 29. Thermal Conductivity of SZ Hydrogeologic Units

Model Zone Number	Hydrogeologic Unit	Horizontal Thermal Conductivity (W/m K)	Vertical Thermal Conductivity (W/m K)	Source
2	Granite	2.40	2.40	Sass et al. (1984 [153174])
3	Lower Clastic Confining Unit	2.49	2.49	Sekiguchi (1984 [163363])
4	Lower Carbonate Aquifer	4.95	4.55	Sass et al. (1988 [100644])
5	Upper Clastic Confining Unit	2.49	2.49	Sekiguchi (1984 [163363])
6	Lower Carbonate Aquifer (Thrust)	4.95	4.55	Sass et al. (1988 [100644])
7	Upper Carbonate Aquifer	3.61	3.03	Ryder (1997 [163364])
8	Undifferentiated Valley Fill (North)	1.60	1.60	*
9	Older Volcanic Confining Unit	1.87	1.86	Sass et al. (1988 [100644])
10	Older Volcanic Aquifer	2.00	2.00	Sass et al. (1988 [100644])
11	Lower Volcanic Confining Unit	1.87	1.86	Sass et al. (1988 [100644])
12	Tram Tuff	1.75	1.72	Sass et al. (1988 [100644])
13	Bullfrog Tuff	1.63	1.60	Sass et al. (1988 [100644])
14	Prow Pass Tuff	1.45	1.43	Sass et al. (1988 [100644])
15	Upper Volcanic Confining Unit	1.21	1.20	Sass et al. (1988 [100644])
16	Upper Volcanic Aquifer	1.67	1.56	Brodsky et al. (1997 [100653])
17	Lava-Flow Aquifer	2.09	2.09	Lagedrost and Capps (1983 [163366])
18	Limestone Aquifer	3.61	3.03	Ryder (1997 [163364]])
20	Valley-Fill Aquifer	1.00	1.00	Wollenberg et al. (1983 [163359])
23	Undifferentiated Valley Fill (South)	1.00	1.00	Wollenberg et al. (1983 [163359])

NOTE: * Estimate based on unit consisting predominantly of volcanic material.
This table is for reference only.
The thermal conductivity values in Sass et al. (1988 [100644]) are found in Section 2-17.

Sass et al. (1984 [153174]) investigated thermal conductivity measurements on several rock types, including granite, using the steady-state divided bar, line source, and half-space probe techniques. Two thermal conductivities are given for granite, at 23°C (Sass et al. (1984 [153174]), p. 17), one derived using the divided bar technique, 2.40 W $m^{-1}K^{-1}$, and the other, 2.27 W $m^{-1}K^{-1}$, using the half-space probe technique. The authors suggest thermal conductivity values using the divided bar technique be used for materials that are easily machineable, anisotropic, and nonfriable materials. Granite falls within this category. For this reason, the YMP regional heat flow model uses 2.40 W $m^{-1}K^{-1}$ as the thermal conductivity of granite.

Sekiguchi (1984 [163363]) presents thermal conductivities for several rock types, including silty-sandstone, based on three empirical equations, all a function of porosity, fluid type, and mineralogy. He determined a thermal conductivity range for "silty-sandstone" of which a value listed as the primary thermal conductivity for silty-sandstone is bounded (Sekiguchi 1984 [163363], Table 1). Consequently, it is believed that 2.49 W/m K, which is the primary thermal conductivity for silty-sandstone given in Sekiguchi (1984 [163363]), is appropriate for the regional scale geothermal simulations.

Site-specific thermal conductivity data are reported for dolomite by Sass et al. (1988 [100644]). Thirteen Lone Mountain dolomite core samples were taken from borehole UE-25 p#1 at depths 1310.4 to 1801.6 m. Sass et al. (1988 [100644] Appendix 3, p. 118, Table 3-5) derived thermal conductivity measurements at ambient room temperatures of about 25°C. From these values, an harmonic-averaged and an arithmetic effective thermal conductivity are developed. The harmonic-averaged thermal conductivity, 4.55 W/m K, is to be used for heat flow in the vertical direction; the arithmetic-averaged value, 4.95 W/m K, is to be used for heat flow in the horizontal direction.

There are no site-specific thermal conductivity measurements for limestone. Consequently, limestone thermal conductivity derived from similar rock types is used. Limestone has been considered as one of the material components to be included in a backfill mixture for Yucca Mountain and has been discussed in Ryder (1997 [163364], Section 3.2, p. 10). The range listed in Ryder's 1997 report is based on the author's literature search. Values appropriate for temperatures below 50°C for limestone thermal conductivity (3.03–3.61 W/m K) are used in the site-scale heat flow model for the vertical and horizontal thermal conductivities.

There are numerous site-specific thermal conductivity measurements for the various tuff units incorporated in the analysis. These values are reported by Sass et al. (1988 [100644]) and Brodsky (1997 [100653]). Two effective thermal conductivities are derived, one in the vertical direction, the other in the horizontal direction, from cores lithologies representative of each hydrogeologic unit. Thermal conductivity in the vertical direction is derived by first harmonically averaging thermal conductivities for each individual borehole. Then the harmonic averages from individual boreholes are arithmetically averaged. Thermal conductivity in the horizontal direction is derived by simply arithmetically averaging data from the same hydrogeologic units. The number of samples used in the analysis ranged from 7 for the Prow Pass Tuff to 58 for the Upper Volcanic Aquifer.

Thermal conductivity measurements for 11 core samples from three boreholes drilled through the Pomona Member Basalt, located in Washington State, are used to derive an effective basalt thermal conductivity. Thermal conductivity measurements were taken at temperatures ranging between 21°C to 506°C. To derive a thermal conductivity for 30°C, a simple linear interpolation for thermal conductivity values measured at ~22°C to 50°C is used. The 11 interpolated values are arithmetically averaged resulting in a thermal conductivity of 2.09 W/m K.

There are no site-specific data on the thermal conductivity of saturated alluvium. Smyth et al. (1979 [163360]) report values of thermal conductivity ranging from 0.5 to 1.2 W/m K for soils, indurated, and unconsolidated alluvium at varying degrees of saturation. Wollenberg et al. (1983 [163359], p. 97) give an estimated value of 1.0 W/m K for the thermal conductivity of typical alluvium under saturated or near-saturated conditions. For the units that are predominantly alluvium, 1.0 W/m K is taken as a representative estimate of the thermal conductivity. Because considerable uncertainty exists in the thermal conductivity of alluvium in the SZ site-scale model domain, sensitivity analyses were conducted to evaluate the impact of this parameter on the calibration of the conduction-only model, as described later.

7.4.1.2 Thermal Conduction Model Setup

The FEHM input files for the base-case model are used as the starting point for the SZ site-scale thermal conduction model. Input macros related to fluid flow are removed from the input file, a heat-conduction-only solution is indicated, and thermal boundary conditions are added. The lateral boundaries of the SZ site-scale thermal conduction model are set as no thermal flow. This is appropriate, given the primarily vertical nature of geothermal heat transport and the relatively thin dimension of the model in the vertical direction (2.75 km thick x 30 km x 45 km). The bottom boundary is specified heat flux to reflect upward heat transport from the deeper crust. The upper boundary condition is temperature-dependent heat flux, in which the heat flux to the land surface is calculated as a function of the simulated temperature at the water table and the specified temperature at the land surface.

7.4.1.2.1 Thermal Boundary Conditions on the Upper Boundary

The thermal boundary condition at the upper boundary of the SZ site-scale thermal conduction model requires that the temperature at the land surface and the effective conductance from the water table to the land surface be specified. The temperature at the land surface is specified based on an estimate of the average annual surface temperature. The effective thermal conductance of the UZ is a function of several factors, including thickness of the UZ, rock type, and downward percolation of groundwater through the UZ; however, only thickness of the UZ is included here. The spatially varying effective thermal conductance of the UZ is estimated in the calibration process, as explained later.

The average annual surface temperature for the SZ site-scale thermal model domain is estimated using a relationship relating temperature to elevation (Section 6.5.3.7). This simple linear relationship for average surface temperature is:

$$T_s = T_{ref} - \lambda(Z_s - Z_{ref}) \qquad \text{(Eq. 12)}$$

where

T_s is the average surface temperature

T_{ref} is the average temperature at a reference location

λ is the rate of change in temperature with elevation

Z_s is the surface elevation

Z_{ref} is the surface elevation at the reference location.

Using values of mean surface temperature and elevations from the locations of boreholes NRG-6 and NRG-7 (DTN: GS950208312232.003 [105572]), the value of λ is 0.009^{o}C/m (Section 6.5). The reference average surface temperature and reference elevation at the location of borehole NRG-6 are 18.23^o C and 1231 m, respectively.

This relationship is applied to the SZ site-scale thermal model domain to estimate the average annual surface temperature, as shown in Figure 40. Estimated average surface temperature varies as a function of elevation from about 10° C in northern parts of the area to greater than 22°C at the lower elevations in the southern part of the domain. The spatially varying values of estimated average surface temperature shown in Figure 40 are used as the upper boundary condition of the SZ site-scale thermal model.

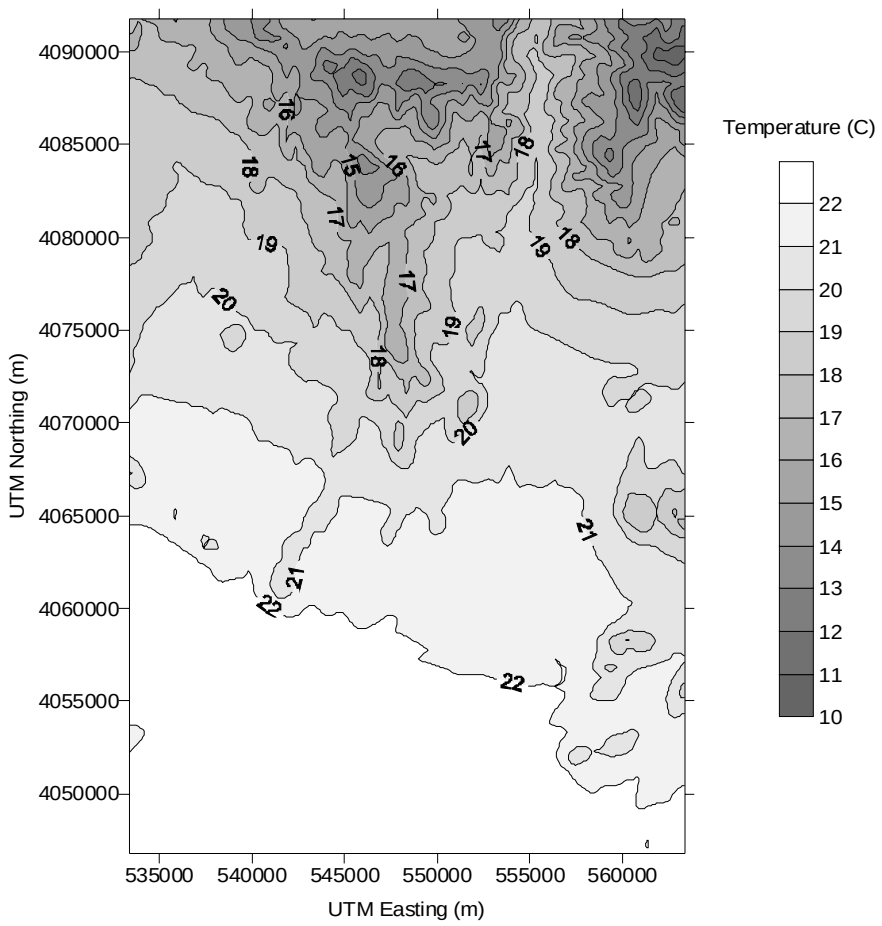

Source: Arnold et al. (2003 [164473]).

Figure 40. Computed Average Annual Surface Temperature for the SZ Site-Scale Thermal Model Area

The thermal conductance of the UZ at the upper boundary of the SZ site-scale thermal conduction model is inversely proportional to the thickness of the UZ, which varies considerably across the area of the model. The UZ acts as a thermal "blanket" to geothermal heat flow from the SZ, so the higher conductance occurs where the UZ is thin and lower conductance occurs where the UZ is relatively thick. Figure 41 shows a plot of the thickness of the UZ, which varies from less than 50 m in the south and in Fortymile Canyon to greater than 1000 m in the north. The values of UZ thickness shown in Figure 41 are used to calculate spatially varying values of thermal conductance for the upper boundary condition in the SZ site-scale thermal conduction model.

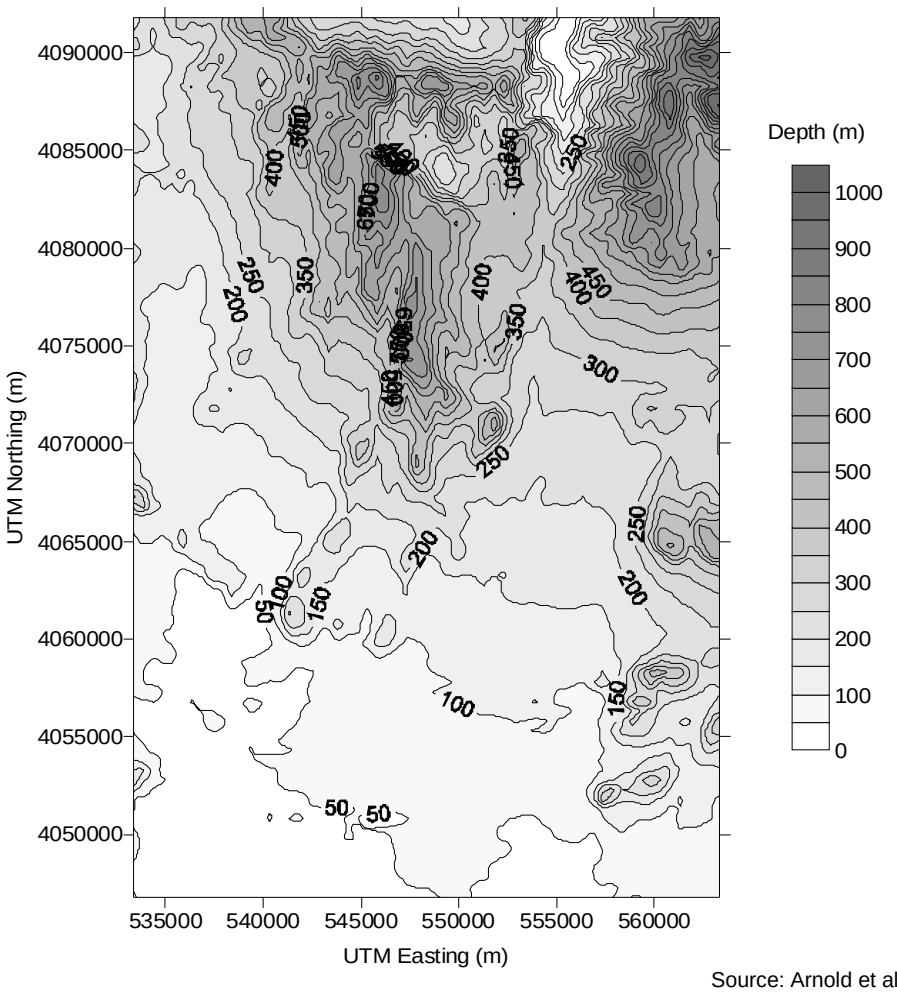

Source: Arnold et al. (2003 [164473]).

Figure 41. Depth to the Water Table in the SZ Site-Scale Model Area

Considerable uncertainty exists in the effective thermal conductivity of the UZ. In addition, thermal conductivity of the UZ varies as a function of rock type and heat flow may be influenced by downward percolation of groundwater in the UZ, as noted above. Because of these uncertainties, the effective thermal conductance at the upper boundary is treated as a calibration parameter in the heat conduction-only modeling for the SZ. The inverse proportionality to UZ thickness is preserved in the calibration process, but the overall effective thermal conductance is adjusted proportionally during thermal calibration.

7.4.1.2.2 Thermal Boundary Conditions on the Lower Boundary

The lower thermal boundary condition of the SZ site-scale thermal conduction model is assigned a uniform value of specified heat flux. Variations in the geothermal heat flux may occur at the scale of the SZ site-scale model domain; however, there is not sufficient information on variations in deep heat flow to justify assigning spatial variations in heat flux at the bottom boundary of the model. The lower boundary of the SZ site-scale thermal conduction model is relatively deep at 2750 m below the water table, so variations in heat flux due to topographic effects and groundwater flow are significantly less than at shallower depths.

The estimated geothermal heat flux from measurements of temperature profiles in wells at Yucca Mountain is about 40 mW/m^2 (Sass et al. 1988, p. 2 [100644]). This value of heat flux is considerably lower than the regional average of about 85 mW/m^2. Because there is considerable uncertainty in the appropriate value of heat flux at the lower boundary of the SZ site-scale thermal conduction model, this parameter is varied in the thermal calibration process to match the observed temperatures.

7.4.1.3 Thermal Model Calibration

The SZ site-scale thermal conduction model was calibrated by adjusting the upper and lower thermal boundary conditions in a trial-and-error method. (The simulated temperatures at the water table in the calibrated conduction-only model are shown in Figure 42.) The model was run to steady-state thermal conditions and the simulated temperatures were compared to the observed temperatures in a cross plot, such as shown in Figure 43. The calibration process sought to minimize the coefficient of determination (R^2) for this cross plot. The calibration also attempted to place the least-squares line fit to the cross plot along a 45° line, as shown by the dashed red line in Figure 43. Precise optimization of the conduction-only model was not required for the purposes of this analysis because the ultimate goal was to examine coupled groundwater flow and heat transport.

The best calibration of the SZ site-scale thermal conduction model is obtained with a uniform heat flux of 35 mW/m^2 at the lower boundary and an equivalent thermal conductivity of 0.3 W/m K for the UZ at the upper boundary. The calibrated value of the heat flux at the lower boundary of 35 mW/m^2 is somewhat lower than the estimate from Sass et al. (1988 [100644], Section 2-17), but is within the estimated range of error (40 ± 9 mW/m^2) from that study. The calibrated value of the equivalent thermal conductivity for the UZ is quite low relative to the units in the SZ. However, this equivalent value may also account for the effects of unsaturated conditions, variations in rock type, and percolation of groundwater.

As mentioned above, the simulated temperatures at the water table in the calibrated conduction-only model are shown in Figure 42. The values of simulated temperature are projected onto the water-table surface, and the topographic surface is shown in this figure. There is considerable variation in the simulated temperature at the water table, primarily as a function of the UZ.

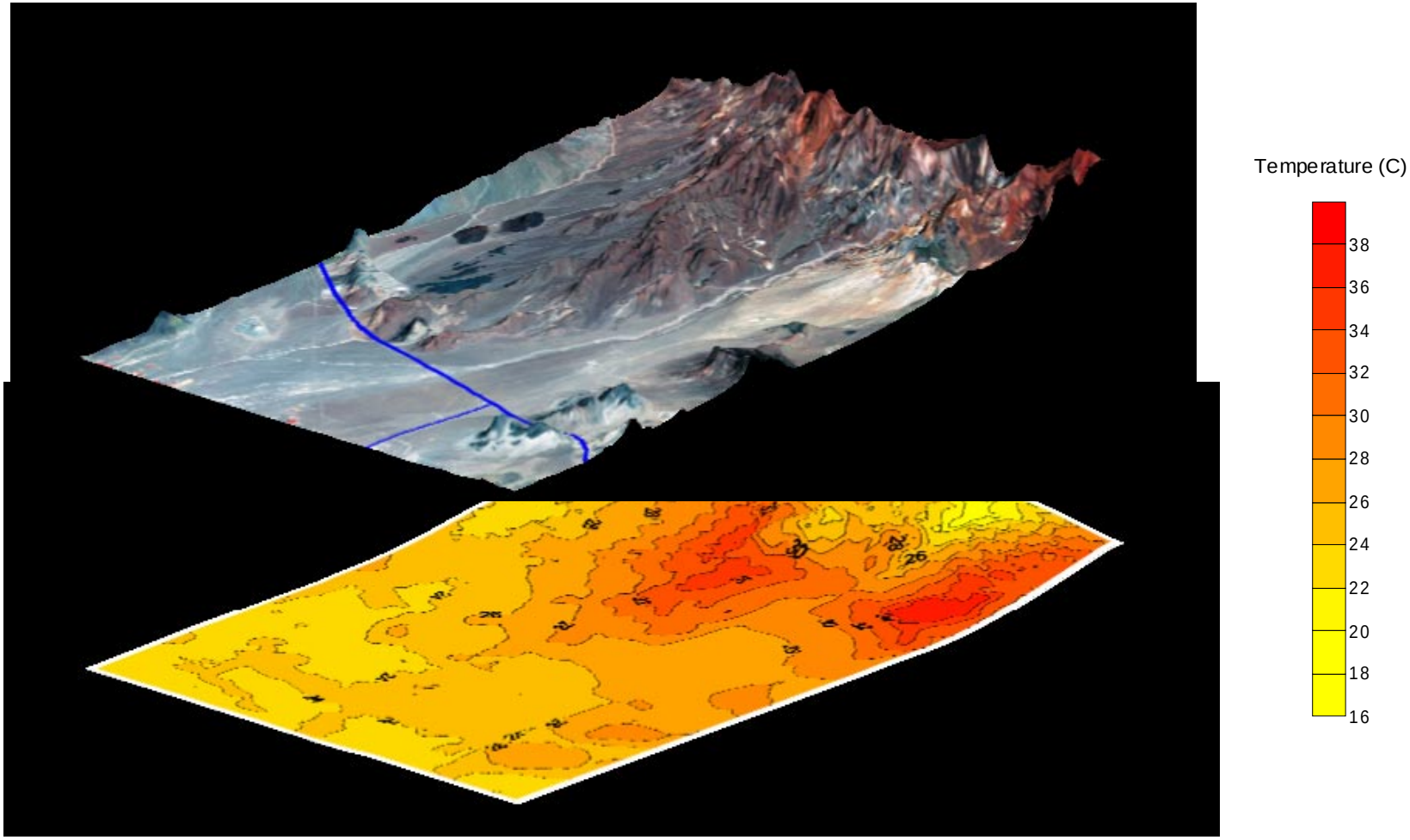

Source: Arnold et al. (2003 [164473]).

Figure 42. Simulated Temperatures at the Water Table for the Thermal Conduction Model

The higher simulated temperatures correspond to the relatively thick UZ under Yucca Mountain in the north-central portion of the area and under the Calico Hills in the northeastern part of the model. The lower simulated temperatures occur in areas where the water table is closer to the land surface, in the southern part of the model, and under Fortymile Canyon in the north. The pattern of simulated temperatures at the water table is influenced to a lesser extent by refraction of heat flow in the Lower Carbonate Aquifer with its higher thermal conductivity.

A plot of the 94 observations of temperatures in wells versus simulated temperatures for the calibrated thermal conduction model is shown in Figure 43. This cross plot indicates that there is generally good agreement between observed and simulated temperatures in the model. The R^2 value for these results is 0.80. There is an apparent tendency for the calibrated model to underestimate temperatures between 20°C and 35°C, to overestimate temperatures between 35°C and 50°C, and to underestimate temperatures over 50°C.

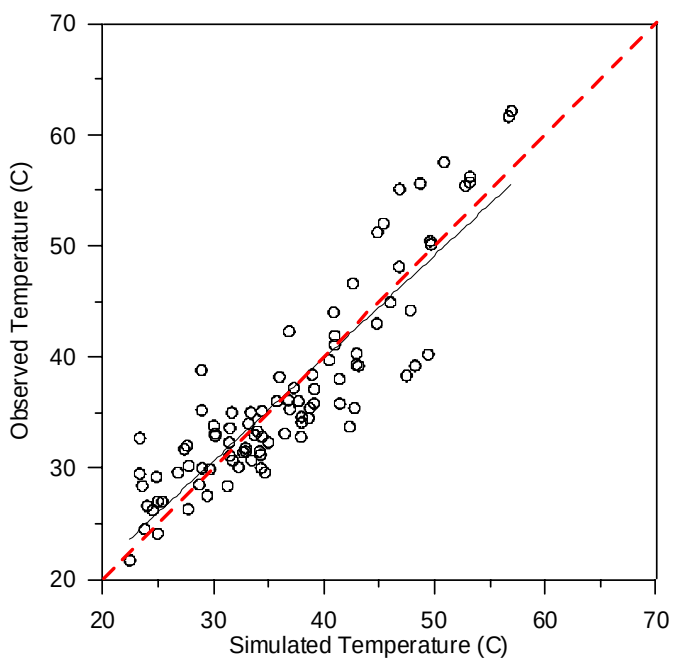

Source: Arnold et al. (2003 [164473]).

Figure 43. Simulated Temperatures Versus Observed Temperatures for the Thermal Conduction Model

The residuals in simulated temperature are defined as the simulated temperature minus the observed temperature at a given location. A histogram of the residuals in simulated temperature in the calibrated SZ site-scale conduction-only model is shown in Figure 44. These residuals are approximately normally distributed, with maximum errors in simulated temperature of less than 10°C. The average residual is –0.3°C. A majority of the simulated temperatures are within 3°C of the observed temperature at that location. These characteristics of the residuals indicate that

the calibrated heat conduction-only model is fairly accurate and unbiased with regard to errors in simulated temperature.

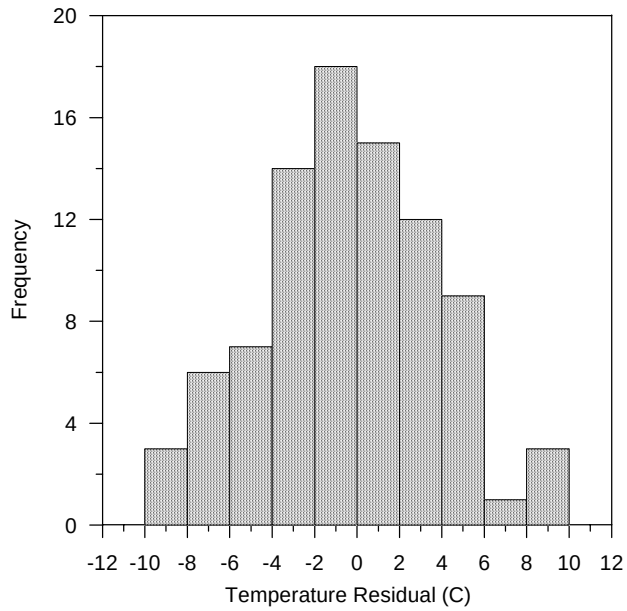

Source: Arnold et al. (2003 [164473]).

Figure 44. Histogram of Residuals in Simulated Temperature for the Thermal Conduction Model

The spatial distribution of residuals in simulated temperature at the water table is examined in the map shown in Figure 45. This figure indicates that there is some systematic pattern to the spatial distribution of residuals in simulated temperature. The positive residuals tend to cluster near and to the east of Yucca Mountain; whereas, the residuals farther to the south and immediately to the north of Yucca Mountain tend to be negative. The positive residuals indicate that the simulated temperature at the water table is too high.

One explanation for the clustering of positive residuals near the crest of Yucca Mountain is that these are locations of significant downward percolation of groundwater through the UZ. Downward percolating groundwater tends to suppress the geothermal gradient and would cause lower temperatures at the water table. Because the heat conduction-only model does not account for this process at the upper boundary, it tends to overestimate the temperature at these locations, leading to the positive residuals. The negative residuals may correspond to locations at which groundwater flow in the SZ is upward. This process is also not accounted for in the heat conduction-only model. Consequently, the simulated temperatures would be too low at these locations.

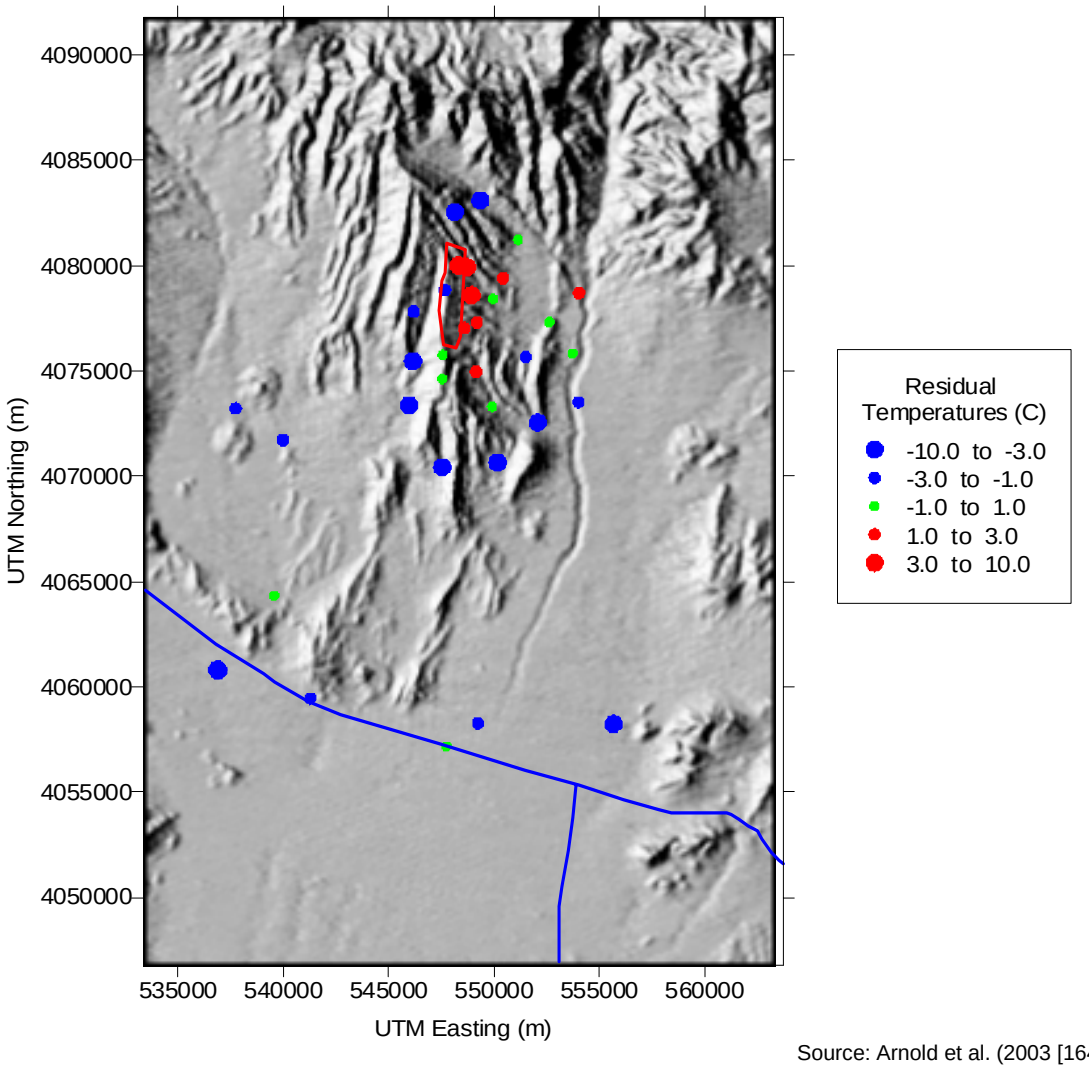

Source: Arnold et al. (2003 [164473]).

Figure 45. Residuals in Simulated Temperature at the Water Table for the Thermal Conduction Model

7.4.1.4 Sensitivity to Thermal Conductivity in the Alluvium

Sensitivity of the SZ site-scale heat conduction-only model to the thermal conductivity of the alluvium was evaluated using a higher value (1.6 W/m K) and a lower value (0.5 W/m K) for this parameter. The results indicate relatively little sensitivity of the model calibration to this parameter, with the R^2 varying from 0.777 to 0.783 over this range of parameter values. Simulated temperatures near the water table are not very sensitive to the thermal conductivity of the alluvium below them, but simulated temperatures deeper in the valley-fill regions of the model are significantly higher for the lower value of thermal conductivity of the alluvium (and *vice versa* for the higher value). This low sensitivity to the thermal conductivity in the alluvium

is primarily due to the general lack of deep temperature observations in wells in the alluvium that would constrain temperatures.

7.4.1.5 Results and Discussion of Conduction-Only Thermal Modeling

Steady-state heat conduction in the SZ site-scale model domain is simulated to assess heat transport by conduction only. The resulting calibrated SZ site-scale thermal conduction model provides a relatively accurate, unbiased match to the observed temperatures in wells in the Yucca Mountain area. Comparison of observed temperatures to simulated temperatures results in a value of 0.80 for the R^2. The approximately normal statistical distribution of residuals in simulated temperature indicates that errors in the model are essentially random and not reflective of any systematic misrepresentation of the thermal transport processes in the SZ. There are some systematic spatial variations in the residuals in simulated temperatures, but these are generally understandable in terms of the coupled groundwater flow and heat transport processes that are not included in the conduction-only model.

Thermal transport in the SZ is dominated by conductive geothermal heat flow at the scale of the SZ site-scale model domain. The results of the calibration of the conduction-only model indicate that at least 80% of the variability in the observed temperatures can be explained by thermal conduction, based on the coefficient of determination from observed versus simulated temperatures. The redistribution of heat by groundwater flow in the UZ and SZ, particularly by vertical groundwater flow, may account for a significant portion of the remaining variability in observed temperatures.

The spatial distribution of observations of temperature may limit the interpretation and modeling of heat transport in the SZ site-scale model area. Most of the temperature logs from wells are concentrated near Yucca Mountain, and almost all the measurements at depths of greater than a few hundred meters below the water table are in this area. Conclusions regarding the heat flux at the bottom boundary of the SZ site-scale model are most accurate for the area near Yucca Mountain but may be much less applicable elsewhere in the model domain.

7.4.2 Coupled Thermal Modeling

Coupled thermal modeling of groundwater flow and heat transport provides a more complete representation of thermal transport processes in the SZ than the conduction-only modeling. Groundwater flow redistributes heat in both the lateral and vertical directions. In addition, variations in the density and viscosity of groundwater as a function of temperature influence the groundwater flow field. These coupled processes result in a more challenging numerical modeling task for the coupled thermal model, relative to the conduction-only model.

7.4.2.1 SZ Site-Scale Coupled Thermal Model Setup

The base-case flow model and the SZ site-scale thermal conduction model are used as the basis for the modeling of coupled thermal transport. The calibrated upper and lower thermal boundary conditions from the conduction-only model are used in the coupled thermal model. The lateral groundwater flow boundary conditions of the base-case flow model are adjusted for use in the coupled thermal model. The specified head boundary conditions at the lateral boundaries of the base-case flow model are converted to values of specified pressure for the coupled thermal model. The temperature of groundwater flowing into the coupled thermal model at the lateral boundaries is specified to be equal to the simulated temperatures at those nodes in the SZ site-scale thermal conduction model. Similarly, the specified groundwater flux from recharge on the upper boundary of the coupled thermal model is specified to be at the simulated temperatures from the conduction-only model.

The SZ site-scale coupled thermal model is run to steady-state thermal and flow conditions for comparison to the observed temperatures in wells. Joint calibration of the coupled thermal model to water-level and temperature measurements was not possible given the long computer run-times necessary to achieve a steady-state solution. Ideally, joint calibration of the SZ site-scale model would provide explicit constraints on the groundwater flow field. Nonetheless, the uncalibrated coupled heat and groundwater flow model can provide independent validation of the flow model and subjective indications to improve the flow model.

The resulting steady-state, simulated temperatures at the water table for coupled groundwater flow and thermal transport are shown in Figure 46. Simulated temperatures at the water table for the coupled model differ significantly from the conduction-only model in the area directly to the east of Yucca Mountain and in a small area in Crater Flat. The simulated temperatures are generally higher in the area between Yucca Mountain and Fortymile Wash in the coupled model, indicating significant upward vertical advective heat transfer in this area of the model. The smaller area of higher simulated temperatures in Crater Flat indicates another area of simulated upward groundwater flow.

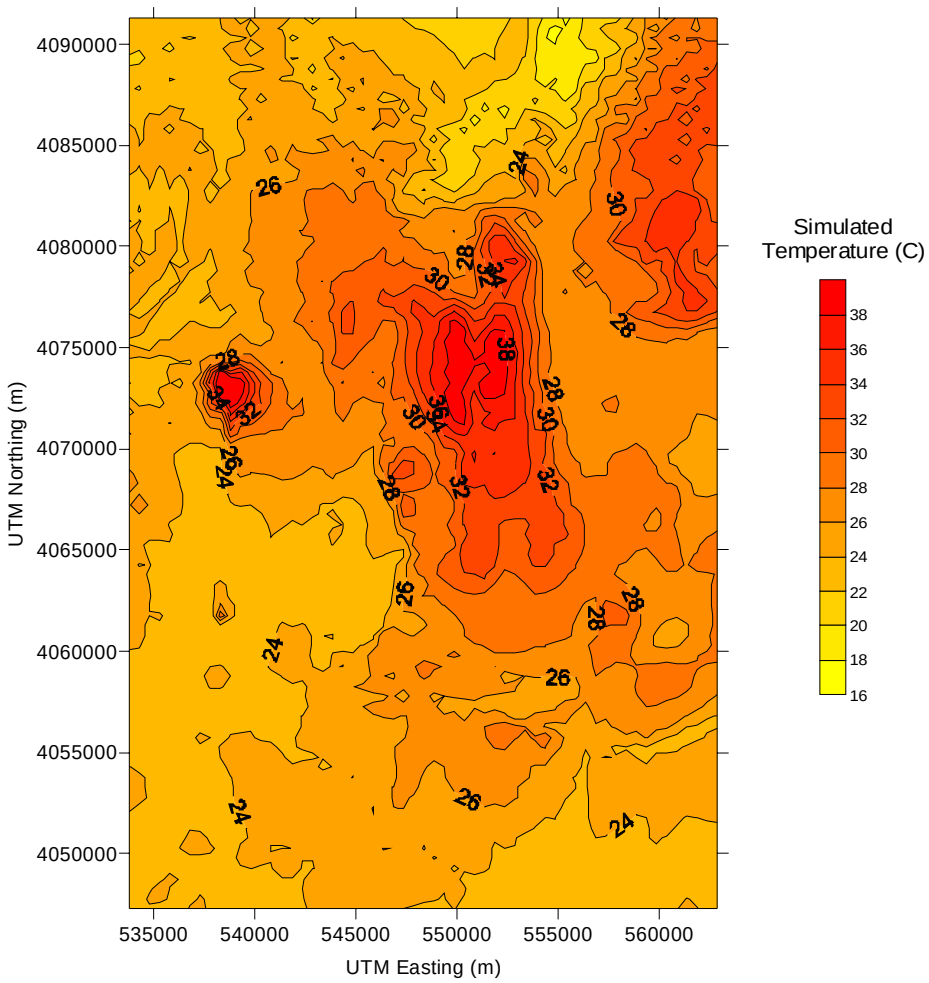

Source: Arnold et al. (2003 [164473]).

Figure 46. Simulated Temperatures at the Water Table for the Coupled Thermal Model

Results of combining the calibrated base-case flow model and the calibrated thermal conduction model indicate a significant reduction in the R^2 of observed and simulated temperatures from the conduction-only model (0.62 versus 0.80). A plot of simulated temperatures versus observed temperatures for the coupled heat and groundwater flow model is shown in Figure 47. The statistical distribution of residuals in simulated temperature for the coupled model has a broader range than for the conduction-only model with an average of –0.13°C. Note in Figure 47 that the simulated temperatures for the deeper, higher-temperature measurement locations have both positive and negative residuals from the coupled model, whereas, the conduction-only model consistently underestimated the temperatures at these locations (Figure 43).

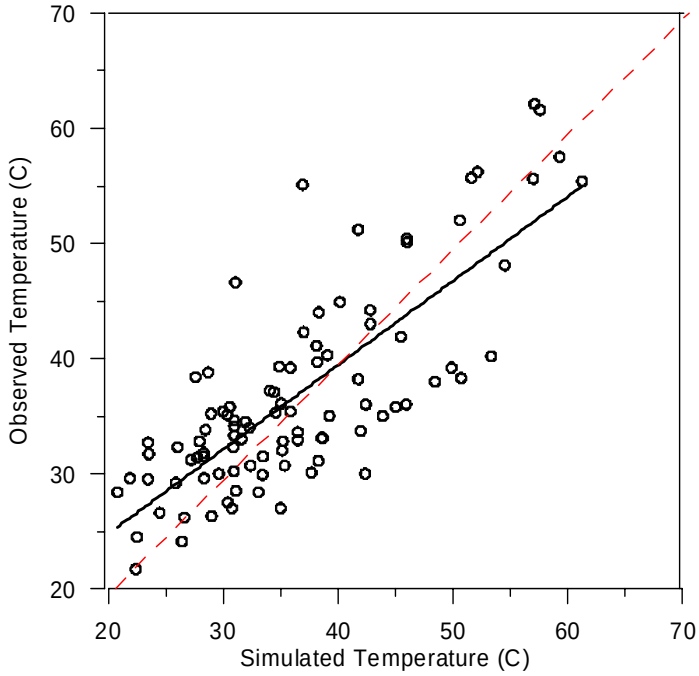

Source: Arnold et al. (2003 [164473]).

Figure 47. Simulated Temperatures Versus Observed Temperatures for the Coupled Thermal Model

The spatial distribution of residuals in simulated temperature at the water table for the SZ coupled thermal model is examined in the map shown in Figure 48. The largest positive residuals generally occur in the area to the east and southeast of Yucca Mountain and in a relatively small area in Crater Flat. The largest negative residuals occur to the north of Yucca Mountain.

7.4.2.2 Results and Discussion of Coupled Thermal Modeling

The calibrated SZ site-scale thermal conduction model provides a relatively accurate, unbiased match to the observed temperatures in wells in the Yucca Mountain area. The approximately normal statistical distribution of residuals in simulated temperature indicates that errors in the model are essentially random and not reflective of any systematic misrepresentation of the thermal transport processes in the SZ.

Thermal transport in the SZ is dominated by conductive, predominantly vertical, geothermal heat flow at the scale of the SZ site-scale model domain. The results of the calibration of the conduction-only model indicates that at least 80% of the variability in the observed temperatures can be explained by thermal conduction, based on the coefficient of determination from observed versus simulated temperatures.

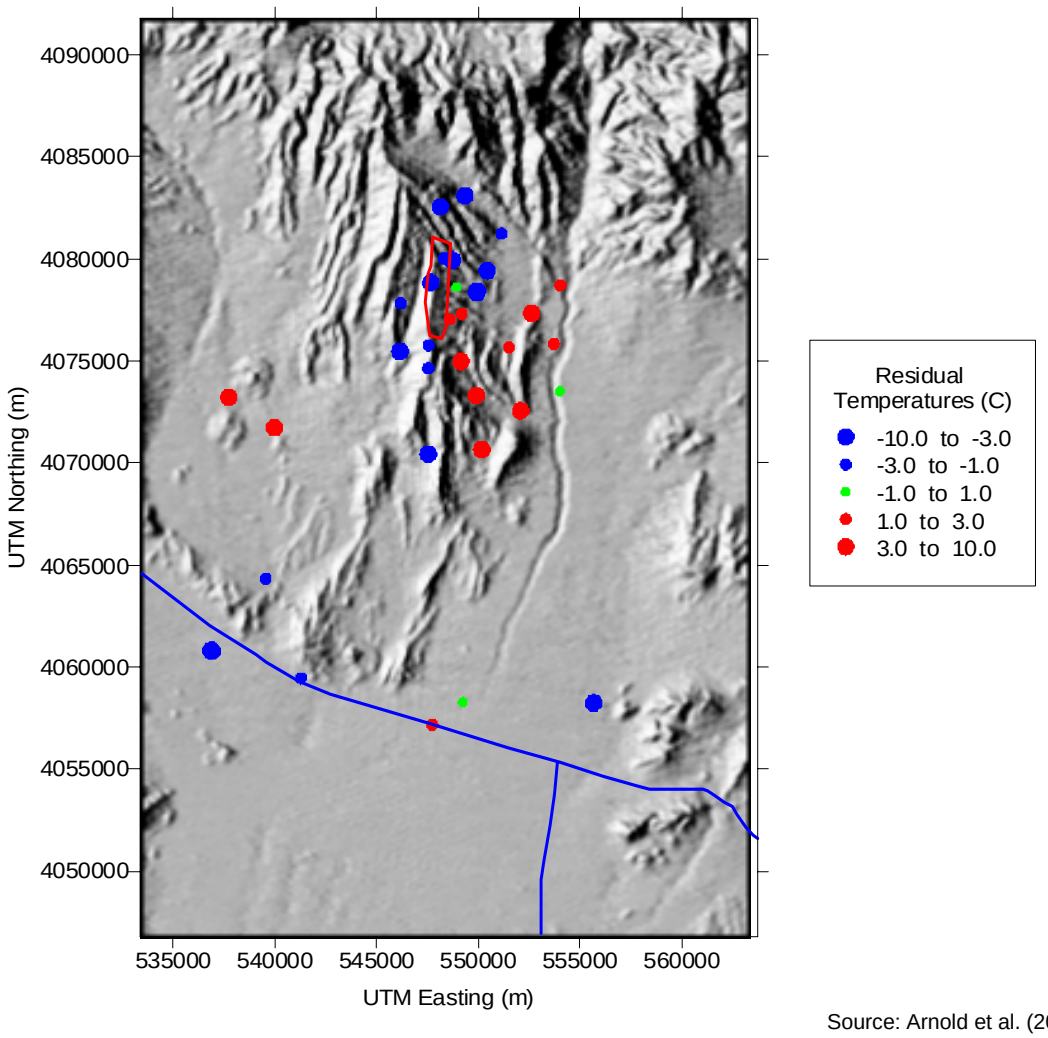

Source: Arnold et al. (2003 [164473]).

Figure 48. Residuals in Simulated Temperature at the Water Table for the Coupled Thermal Model

The results of the coupled thermal transport model show that this jointly uncalibrated model is unbiased, but less accurate than the heat conduction-only model. The pattern of residuals in simulated temperatures suggests that the groundwater flow model overestimates upward groundwater flow in the region to the east and southeast of Yucca Mountain and in one area of Crater Flat, leading to larger positive residuals. The groundwater flow model also apparently overestimates downward groundwater flow to the north of Yucca Mountain and the large hydraulic gradient, resulting in larger negative residuals in this area. The results of the coupled thermal modeling provide addidtional confidence in the SZ site-scale flow model in a general sense, but also indicate some specific areas in the model where the simulation of vertical groundwater flow could be improved.

In the technical work plan governing this modeling task, a criterion was established for the independent validation of the base-case flow model with the ambient temperature data (BSC 2003 [163965]). This criterion stated that the coupled model would constitute an independent

validation of the flow model if the simulated temperatures were within 10°C of the measured temperatures. The uncalibrated coupled thermal transport model of the SZ does meet this criterion (85 of the 94 simulated temperatures are within 10°C of the measured temperatures). Thus, the validation criteria are generally met. However, the spatial pattern of residuals in temperature indicates that the accuracy of the base-case flow model could be improved in several areas. The SZ site-scale flow model overestimates the upward vertical flow of groundwater in the area to the east and southeast of Yucca Mountain, and this flow could be controlled by reducing the vertical permeability in this area. The anomalously high, simulated temperatures in a small area of Crater Flat in the coupled model are apparently the result of an unrealistic discontinuity in the HFM that strongly focuses groundwater flow upward in this region.

7.5 VALIDATION SUMMARY

The base-case flow model has met the validation criteria established for the validation activities completed to date. A comparison of the predicted and recently obtained water levels from the newly installed Nye County EWDP wells demonstrates that the base-case flow model can reliably predict the water levels and gradients along the flow path from the repository. An analysis of the impact of the differences between observed and predicted hydraulic gradients on the specific discharge along the flow path from the repository has identified only a minimal impact on the specific discharge, which easily meets the validation criteria previously established for this comparison. A comparison of the permeability measurements from the ATC with the calibrated permeability value for the alluvium has similarly indicated close agreement between calibrated and measured values. An analysis of the impact of differences between calibrated and measured permeability on the specific discharge along the flow path from the repository has also demonstrated only a minimal impact on the specific discharge, which easily meets the validation criteria previously established for this comparison. An analysis of the combined impact on the specific discharge of the difference between observed and predicted hydraulic gradients and permeability values in the area of the ATC has similarly indicated minimal impact that easily meets the validation criteria previously established for this comparison. The comparison between the flow paths predicted by the base-case model and those indicated by hydrochemical analysis has demonstrated close agreement between these flow paths, with the flow paths derived from hydrochemical analysis generally enveloping those predicted by the base-case model. Thermal modeling has indicated that the thermal model developed from the base-case model is capable of modeling thermal transport in the SZ reasonably well, and comparisons of the predicted with the observed temperatures generally meet the validation criteria previously established for the thermal modeling. The successful meeting of the validation criteria required for a Level II model validation provides the appropriate level of confidence required for the use of the base-case flow model in the overall total system performance assessment of the repository system.

8. CONCLUSIONS

The SZ site-scale flow model is the culmination of enormous efforts incorporating volumes of geologic, hydrologic-testing, and geochemistry data into a coherent representation of flow through the saturated zone near Yucca Mountain. This model is based upon a 3-D finite element mesh with 500×500 m^2 horizontal elements, which grid convergence studies have shown to represent the hydrogeologic framework adequately without introducing significant numerical error. Additionally, the model's vertical resolution varies from 10 m to 500 m; the higher resolution is near the water table in the area under Yucca Mountain. This model is calibrated to and faithfully reproduces two important data sets: the observed potentiometric surface (water level data) and boundary fluxes obtained from the SZ regional-scale flow model. In addition, the SZ site-scale flow model matches other data both quantitatively and qualitatively. These data include permeability values derived from single-well and multiple-well tests, hydrochemical data, temperature data, and specific-discharge values estimated by the expert elicitation panel (CRWMS M&O 1998, Section 3.2 [100353]).

The SZ site-scale flow model matches much of the existing SZ-related data, particularly with respect to the inferred fluid pathways below the repository area. Although the model is meant to represent the SZ accurately, when parameter uncertainty could be resolved no further, parameter values were selected to err on the side of conservatism. The hydrochemical data were used as a quality check for path-line direction. The SZ model produced path lines from the repository area that agree with those inferred from geochemical information. However, there was a bias in the calibration, notably in the low-gradient area where the calibrated heads were consistently 3-4 m higher than the observations. This bias should be investigated in the future.

When using the SZ site-scale flow model for TSPA calculations, there are three limitations that must be noted with regard to the following:

- Changes to calibration parameter values. Some calibration parameters can be varied over a moderate range, and the overall calibration is not adversely affected. For example, calibration was performed assuming isotropic horizontal permeabilities, while PA model runs incorporate a range of anisotropic permeabilities. If using anisotropic permeabilities resulted in poor model calibration, further model development would be required to avoid this. Fortunately, in preliminary PA modeling, the calibration was not impacted (it even improved slightly for some choices of the anisotropy ratio).

- Useable path-line distances. The continuum approach used for the SZ site-scale flow model requires large gridblocks that effectively average fracture and rock matrix properties. To produce meaningful results, the flow path should be long compared to the gridblock size. Because the gridblock size is 500 m, a minimum distance of 2 kilometers is recommended for path lines used in PA calculations.

- Overall model recharge fluxes. Because the SZ site-scale flow model is linear, recharge fluxes may be changed to reflect uncertainty in specific discharge, so long as the boundary fluxes and permeabilities are changed proportionally.

8.1 SUMMARY OF MODELING ACTIVITIES

The SZ site-scale flow model was developed in several stages. First, the hydrogeology of a region around Yucca Mountain was numerically characterized with the Death Valley Regional Flow System model (SZ regional-scale model). Second, a detailed conceptual model of flow processes was developed for a smaller region (i.e., the site-scale) appropriate for TSPA-LA calculations. Third, a numerical model of groundwater flow was developed and calibrated (i.e., the SZ site-scale flow model). Fourth, a series of validation activities were completed to provide confidence in the SZ site-scale flow model and its output. Finally, results of this model were provided and the associated uncertainties were discussed (required before the start of TSPA-LA calculations).

8.1.1 Saturated-Zone Flow Characterization

Much information is available about the regional-scale hydrogeology at Yucca Mountain, both from site characterization activities as well as from numerous additional hydrogeologic studies that have been conducted at the NTS. Specifically, sufficient information is available to describe the stratigraphy, structure, and hydraulic properties of component media, recharge and discharge regions, and groundwater flow paths.

The climate in the Yucca Mountain area is arid, and the water table varies from hundreds of meters below ground surface in the northern part of the model to tens of meters below ground surface in the southern part of the model. Natural recharge to the SZ is from precipitation percolating through the unsaturated zone. Recharge occurs primarily in mountainous areas where there is more snow and rainfall (i.e., both Yucca Mountain including regions of higher elevation to the north and northeast, and the Spring Mountains 50 km (31 mi) southeast of Yucca Mountain). Estimates of recharge rates at the regional scale are based on empirical relationships, and the SZ regional-scale model ensures equal SZ recharge and discharge. Flow paths in the SZ are well characterized at the regional scale because numerous water-level measurements are available.

The fluxes from the SZ regional-scale flow model were used as targets because this model represents a comprehensive water balance of the Death Valley hydrologic system with fluxes constrained by data from spring flows and infiltration rates. Boundary fluxes can help link the SZ site-scale flow model to other global-water-balance data, if necessary. The SZ site-scale flow model reasonably matched the flux data from the SZ regional-scale flow model (up to 21% error on the southern boundary).

In the area near Yucca Mountain, water-level measurements, hydraulic testing in wells, and geochemical analyses provide additional information about groundwater flow in the SZ. Water-level measurements indicate considerable differences in the magnitude of the hydraulic gradient between areas to the north (large hydraulic gradient), west (moderate hydraulic gradient), and southeast (low hydraulic gradient) of Yucca Mountain. The hydraulic gradient drives flow from the repository to the south and southeast. A vertical, upward hydraulic gradient from the underlying carbonate aquifer and the deeper volcanic units is also observed immediately downgradient of Yucca Mountain. Data on groundwater chemistry indicate significant spatial

variability in geochemical and isotopic composition that results from differences in flow paths, recharge locations, and groundwater age.

Due to the long period of time over which the performance of the Yucca Mountain repository must be evaluated, the possible impacts of a future wetter climate must be considered. The general locations of areas of recharge and discharge depend primarily on the topography of the land surface. Modeling studies suggest that increased recharge would result in a higher water table and steeper hydraulic gradients. Field mapping of the occurrence of zeolites and paleospring deposits has confirmed that a higher water table existed during past wetter climates and supports numerical simulations of the possible impacts of climate change. Consequently, wetter climates in the future are expected to result in faster groundwater flow rates along present-day flow paths. The impacts of increased water table are discussed in the SZ site-scale transport model report (BSC 2003, Section 6.4 [162419]).

As groundwater in the Death Valley system moves from recharge to discharge areas, flow rates and paths depend largely on the hydraulic properties of the media along the flow paths. Geologic studies have identified the important rock types and their spatial distribution. The rock types that play the largest role in regional hydrogeology are Paleozoic carbonates, Quaternary-Tertiary volcanic rocks, and Quaternary-Tertiary sediments and volcanic tuffs that fill structural depressions (referred to as valley-fill material in portions of this report). Relatively shallow flow occurs in the volcanic rocks and valley fill (primarily alluvium), and deeper flow occurs in the regionally extensive carbonate aquifer. Along the inferred shallow flow path, groundwater flow paths originate in volcanic rocks near the repository site and continue into younger valley-fill deposits at greater distances.

The permeability of the volcanic rocks in the vicinity of Yucca Mountain is increased by the presence of fractures. An extensive suite of field observations, interpretations of borehole logs, boreholes hydrologic tests, lab-scale tests, and field tracer tests (C-wells complex) confirm that fractures enhance groundwater flow in the volcanic rocks. However, flow in the alluvium occurs through the primary porosity of these sediments.

8.1.2 Conceptual Model of Site-Scale Flow

The SZ site-scale conceptual model is a synthesis of what is known about flow processes at the scale required for TSPA-LA calculations. This knowledge builds upon, and is consistent with, information that has accumulated at the regional scale, but it is more detailed because a higher density of data is available at the site-scale.

Information from geologic maps and cross sections, borehole data, fault-trace maps, and geophysical data were used to construct a 3-D interpretation (HFM) of the hydrostratigraphy and geologic structure of the SZ site-scale flow model. Rock stratigraphies within the framework model are grouped into 18 hydrogeologic units that are classified as having either relatively large permeability (aquifers) or relatively small permeability (confining units). The framework model specifies the position and geometry of these hydrogeologic units. In addition, the framework model identifies major faults that affect groundwater flow.

The source of most of the groundwater flow in the SZ site-scale flow model is lateral flow through the western, northern, and eastern boundaries. A small portion (approximately 5 percent) of the total flux through the SZ site-scale flow model is from precipitation and surface runoff infiltrating along Fortymile Wash. Outflow from the site-scale region is chiefly through the southern boundary. A small amount of water is removed by pumping wells located in the Amargosa Valley near the southern boundary of the model domain. As groundwater moves away from the repository, it first flows through a series of welded and nonwelded volcanic tuffs. These flow paths pass into alluvium.

8.1.3 Mathematical Model and Numerical Approach

The mathematical basis (and associated numerical approaches) of the site-scale SZ flow model is designed to assist in quantifying the uncertainty in the permeability of rocks in the geologic framework model and to represent accurately all included flow process. An automated parameter estimation approach is used to obtain the distribution of rock permeabilities yielding hydraulic heads that best matched measured values, as well as lateral-flow rates across model boundaries that are compatible with results from the SZ regional-scale flow model.

Calculations of groundwater flow (specific-discharge field) are made under steady-state assumptions. The approach of not explicitly representing fractures in the volcanic rocks is reasonable at the scale required for the TSPA-LA (tens of kilometers) but is not accurate at length scales shorter than the dimensions of model grid blocks (<500 m).

8.1.4 Model Validation and Confidence Building

Confidence in the results of the mathematical model was built by comparing: 1) calculated to observed hydraulic heads; 2) predicted to measured permeabilities; 3) lateral flow rates to those calculated by the SZ regional-scale flow model; and 4) predicted and measured groundwater temperatures. In addition, it was confirmed that the flow paths leaving the region of the repository are consistent with those inferred both from gradients of measured head and from independent water-chemistry data. The alternate model will be presented in a revision to this document and will be used to provide more confidence by comparing it to the SZ base-case model.

8.2 OUTPUTS

The technical output from this model comprises the SZ site-scale flow model and associated input and output files (base-case flow files). Output from the SZ site-scale flow model consists of the flow fields for the site-scale area that will be integrated into the SZ site-scale transport model and used to generate radionuclide breakthrough curves. Specifically, the output from the SZ site-scale flow model contains the specific discharge and the flow paths from the water table beneath the repository horizon to the accessible environment.

The computer files associated with the SZ site-scale flow model are contained in *SZ Flow and Transport Model, Hydrogeologic Surface Files* (DTN: LA0304TM831231.001) and *SZ Site-Scale Flow Model, FEHM Files for Base Case* (DTN: LA0304TM831231.002).

8.3 OUTPUT UNCERTAINTY

This section describes remaining uncertainties with the two technical outputs of this model report: specific discharge and flow paths. The section also recommends how the uncertainty associated with the outputs should be considered.

8.3.1 Specific Discharge Uncertainty Range

In previous SZ site-scale flow models for PA calculations, the specific discharge was varied from one-tenth of its nominal value to 10 times its nominal value. Since the uncertainty in permeability directly translates into the uncertainty in specific discharge, assuming a constant head gradient, experience gained in investigating permeability values during calibration is applicable to specific discharge. Based on recent calibration experience and the evaluation of permeability data from Yucca Mountain and other sites, this range may be reduced to one-third of its nominal value to three times the nominal value. The nominal value was obtained from the calibration effort described in this model report. Because the model is linear, calibration is preserved by scaling the fluxes, recharge, and permeabilities proportionally. It should also be noted that this scaling does not cause any permeabilities to exceed the limits imposed in the calibration process for any hydrogeologic unit along the flow path. In the discussion below, the focus is on the Bullfrog Tuff unit because calibration experience has shown that, for all reasonable scenarios, the fluid particles leaving the repository area travel primarily through this unit before entering the alluvial aquifer.

From the re-evaluation of the permeability data described above and the statistical summary of the permeability data given in Table 19, three important facts emerge. First, the upper 95% confidence interval for the mean permeability of the Bullfrog Tuff from the cross-hole tests (3.4×10^{-11} m^2) is approximately three times the mean value (1.1×10^{-11} m^2). The mean value, in turn, is very close to the nominal calibration value of 1.5×10^{-11} m^2 obtained for the SZ site-scale flow model. Second, alternative conceptual models implemented in the numerical model since the previous version of this report (BSC 2001 [155974]) was written have resulted in a range of estimates for the permeability of the Bullfrog Tuff that vary by less than 100% of the nominal permeability value. Third, the permeability data from Yucca Mountain had a practical maximum of 7.6×10^{-11} m^2 from individual tests (see Table 19) in highly fractured intervals in volcanic rock. Although this value exceeds the nominal value by a factor of five, uncertainty in the geometric-mean permeability is a more relevant measure of the uncertainty. Additionally, the intrinsic model formulation requires homogeneity within an element (volume-averaged permeability). Recall that large permeability measurements from the C-wells complex were probably due to their proximity to the Midway Valley fault. Overall, these arguments support the range of permeabilities being within three times the nominal value. Similarly, because the lower 95% confidence interval of the geometric-mean permeability of the Bullfrog Tuff is approximately one-third of the mean value, this ratio is recommended for the lower limit in PA calculations. It should be noted that low permeabilities do not negatively impact modeled performance at this location. When the SZ site-scale model was run with permeabilities of three times and one-third of the nominal value, overall model calibration remained within acceptable tolerances.

In the 18-km compliance region, performance assessment calculations are strongly influenced by travel of fluid particles in the alluvial aquifer. Recent aquifer tests in well NC-EWDP-19D Table 23) and permeability data for the NTS suggest that the variability of the alluvial aquifer permeability is less than that of the volcanic rocks. In particular, three of the four tests produced permeability values that were within a factor of 2 of the mean value. Thus, the permeability ratio ranges derived from the Bullfrog Tuff analysis described above should be sufficient to bound the uncertainty in the alluvial aquifer permeability for the 18-km compliance calculations.

8.3.2 Flow Paths Uncertainty

The flow paths from the water table beneath the repository to the accessible environment directly affect breakthrough curves and associated radionuclide travel times. Because the flow paths are both close to the water table and transition from the volcanic tuffs to the alluvium, flow-path uncertainty directly affects the length of flow in the volcanic tuffs and in the alluvium. Uncertainty in flow paths is affected by anisotropy in hydraulic properties of the volcanic tuffs. Large-scale anisotropy and heterogeneity were implemented in the SZ site-scale flow model through direct incorporation of known hydraulic features, faults, and fractures. Small-scale anisotropy was derived from analysis of hydraulic testing at the C-wells (*Saturated Zone In-Situ Testing*, BSC 2003 [162415], Section 6.2.6). This scientific analysis report also recommends an uncertainty range in anisotropy that should be used in the SZ site-scale flow model to account for uncertainty in the flow paths. For isotropic permeability, flow-path length is approximately 24.5 km. For anisotropy ratios of 20 and 0.05, flow path lengths are 22 and 27 km, respectively. This is an acceptable range of variability in model results.

9. INPUTS AND REFERENCES

9.1 DOCUMENTS CITED

The following is a list of the references cited in this document. Column 1 represents the unique six-digit numerical identifier (the Document Input Reference System [DIRS] number), which is placed in the text following the reference callout (e.g., BSC 2002 [158966]). The purpose of these numbers is to assist the reader in locating a specific reference in the DIRS database. Within the reference list, multiple sources by the same author and date (e.g., BSC 2002) are sorted alphabetically by title.

109715 Ahlers, C.F.; Finsterle, S.; and Bodvarsson, G.S. 1999. "Characterization and Prediction of Subsurface Pneumatic Response at Yucca Mountain, Nevada." *Journal of Contaminant Hydrology, 38*, (1-3), 47-68. New York, New York: Elsevier. TIC: 244160.

164473 Arnold, B.W.; Zyvoloski, G.A.; Economy, K.; and Wallace, M. "Thermal Transport in the Saturated Zone Site-Scale Model at Yucca Mountain." *Proceedings of the 10th International High-Level Radioactive Waste Management Conference (IHLRWM), March 30-April 2, 2003, Las Vegas, Nevada.* La Grange Park, Illinois: American Nuclear Society. TIC: 254559.

101195 Bish, D.L. and Chipera, S.J. 1989. *Revised Mineralogic Summary of Yucca Mountain, Nevada*. LA-11497-MS. Los Alamos, New Mexico: Los Alamos National Laboratory. ACC: NNA.19891019.0029.

101233 Blankennagel, R.K. and Weir, J.E., Jr. 1973. *Geohydrology of the Eastern Part of Pahute Mesa, Nevada Test Site, Nye County, Nevada*. Professional Paper 712-B. Washington, D.C.: U.S. Geological Survey. TIC: 219642.

149161 Bower, K.M.; Gable, C.W.; and Zyvoloski, G.A. 2000. *Effect of Grid Resolution on Control Volume Finite Element Groundwater Modeling of Realistic Geology*. LA-UR-001870. [Los Alamos, New Mexico: Los Alamos National Laboratory]. TIC: 248256.

100653 Brodsky, N.S.; Riggins, M.; Connolly, J.; and Ricci, P. 1997. *Thermal Expansion, Thermal Conductivity, and Heat Capacity Measurements for Boreholes UE25 NRG-4, UE25 NRG-5, USW NRG-6, and USW NRG-7/7A.* SAND95-1955. Albuquerque, New Mexico: Sandia National Laboratories. ACC: MOL.19980311.0316.

102004 Broxton, D.E.; Bish, D.L.; and Warren, R.G. 1987. "Distribution and Chemistry of Diagenetic Minerals at Yucca Mountain, Nye County, Nevada." *Clays and Clay Minerals, 35*, (2), 89-110. Long Island City, New York: Pergamon Press. TIC: 203900.

155974 BSC (Bechtel SAIC Company) 2001. *Calibration of the Site-Scale Saturated Zone Flow Model*. MDL-NBS-HS-000011 REV 00 ICN 01. Las Vegas, Nevada: Bechtel SAIC Company. ACC: MOL.20010713.0049.

159356 BSC (Bechtel SAIC Company) 2001. *Development of Numerical Grids for UZ Flow and Transport Modeling*. ANL-NBS-HS-000015 REV 00 ICN 01. Las Vegas, Nevada: Bechtel SAIC Company. ACC: MOL.20020211.0002.

154657 BSC (Bechtel SAIC Company) 2001. *FY01 Supplemental Science and Performance Analyses, Volume 1: Scientific Bases and Analyses.* TDR-MGR-MD-000007 REV 00. Las Vegas, Nevada: Bechtel SAIC Company. ACC: MOL.20010712.0062.

158606 BSC (Bechtel SAIC Company) 2001. *Geochemical and Isotopic Constraints on Groundwater Flow Directions, Mixing, and Recharge at Yucca Mountain, Nevada. ANL-NBS-HS-000021 REV 00 ICN 2*. Las Vegas, Nevada: Bechtel SAIC Company. ACC: MOL.20020128.0434.

157132 BSC (Bechtel SAIC Company) 2001. *Input and Results of the Base Case Saturated Zone Flow and Transport Model for TSPA.* ANL-NBS-HS-000030 REV 00 ICN 01. Las Vegas, Nevada: Bechtel SAIC Company. ACC: MOL.20011112.0068.

156965 BSC (Bechtel SAIC Company) 2001. *Probability Distribution for Flowing Interval Spacing*. ANL-NBS-MD-000003 REV 00 ICN 02. Las Vegas, Nevada: Bechtel SAIC Company. ACC: MOL.20010625.0304.

160313 BSC (Bechtel SAIC Company) 2002. *Scientific Processes Guidelines Manual*. MIS-WIS-MD-000001 REV 01. Las Vegas, Nevada: Bechtel SAIC Company. ACC: MOL.20020923.0176.

158966 BSC (Bechtel SAIC Company) 2002. *The Enhanced Plan for Features, Events, and Processes (FEPs) at Yucca Mountain.* TDR-WIS-PA-000005 REV 00. Las Vegas, Nevada: Bechtel SAIC Company. ACC: MOL.20020417.0385.

160109 BSC (Bechtel SAIC Company) 2003. *Development of Numerical Grids for UZ Flow and Transport Modeling.* ANL-NBS-HS-000015 REV 01. Las Vegas, Nevada: Bechtel SAIC Company. ACC: DOC.20030404.0005.

162657 BSC (Bechtel SAIC Company) 2003. *Geochemical and Isotopic Constraints on Groundwater Flow Directions and Magnitudes, Mixing, and Recharge at Yucca Mountain*. ANL-NBS-HS-000021 REV 01A. Las Vegas, Nevada: Bechtel SAIC Company. ACC: MOL.20030604.0164.

162289 BSC (Bechtel SAIC Company) 2003. *Repository Design, Repository/PA IED Subsurface Facilities*. 800-IED-EBS0-00401-000-00C. Las Vegas, Nevada: Bechtel SAIC Company. ACC: ENG.20030303.0002.

162415 BSC (Bechtel SAIC Company) 2003. *Saturated Zone In-Situ Testing*. ANL-NBS-HS-000039 REV 00A. Las Vegas, Nevada: Bechtel SAIC Company. ACC: MOL.20030602.0291.

162419 BSC (Bechtel SAIC Company) 2003. *Site-Scale Saturated Zone Transport*. MDL-NBS-HS-000010 REV 01A. Las Vegas, Nevada: Bechtel SAIC Company. ACC: MOL.20030626.0180.

164870 BSC (Bechtel SAIC Company) 2003. *SZ Flow and Transport Model Abstraction.* MDL-NBS-HS-000021 REV 00. Las Vegas, Nevada: Bechtel SAIC Company. ACC: DOC.20030818.0007.

163128 BSC (Bechtel SAIC Company) 2003. *Features, Events, and Processes in SZ Flow and Transport.* ANL-NBS-MD-000002 REV 02A. Las Vegas, Nevada: Bechtel SAIC Company. ACC: MOL.20030823.0129.

163965 BSC (Bechtel SAIC Company) 2003. *Technical Work Plan for: Saturated Zone Flow and Transport Modeling and Testing*. TWP-NBS-MD-000002 REV 01. Las Vegas, Nevada: Bechtel SAIC Company. ACC: DOC.20030618.0021.

161770 Canori, G.F. and Leitner, M.M. 2003. *Project Requirements Document*. TER-MGR-MD-000001 REV 01. Las Vegas, Nevada: Bechtel SAIC Company. ACC: DOC.20030404.0003.

101125 Claassen, H.C. 1985. *Sources and Mechanisms of Recharge for Ground Water in the West-Central Amargosa Desert, Nevada—A Geochemical Interpretation*. U.S. Geological Survey Professional Paper 712-F. Washington, [D.C.]: United States Government Printing Office. TIC: 204574.

100126 CRWMS M&O 1998. "Geology." *Book 1 - Section 3 of Yucca Mountain Site Description*. B00000000-01717-5700-00019 REV 00. Las Vegas, Nevada: CRWMS M&O. ACC: MOL.19980729.0049.

100353 CRWMS M&O 1998. *Saturated Zone Flow and Transport Expert Elicitation Project*. Deliverable SL5X4AM3. Las Vegas, Nevada: CRWMS M&O. ACC: MOL.19980825.0008.

130979 CRWMS M&O 1999. *Recharge and Lateral Groundwater Flow Boundary Conditions for the Saturated Zone Site-Scale Flow and Transport Model*. ANL-NBS-MD-000010 REV 00. Las Vegas, Nevada: CRWMS M&O. ACC: MOL.19991118.0188.

139582 CRWMS M&O 2000. *Calibration of the Site-Scale Saturated Zone Flow Model*. MDL-NBS-HS-000011 REV 00. Las Vegas, Nevada: CRWMS M&O. ACC: MOL.20000825.0122.

139440 CRWMS M&O 2000. *Input and Results of the Base Case Saturated Zone Flow and Transport Model for TSPA.* ANL-NBS-HS-000030 REV 00. Las Vegas, Nevada: CRWMS M&O. ACC: MOL.20000526.0330.

153246 CRWMS M&O 2000. *Total System Performance Assessment for the Site Recommendation*. TDR-WIS-PA-000001 REV 00 ICN 01. Las Vegas, Nevada: CRWMS M&O. ACC: MOL.20001220.0045

143665 CRWMS M&O 2000. *Total System Performance Assessment for the Site Recommendation.* TDR-WIS-PA-000001 REV 00. Las Vegas, Nevada: CRWMS M&O. ACC: MOL.20001005.0282

101043 Czarnecki, J.B. 1984. *Simulated Effects of Increased Recharge on the Ground-Water Flow System of Yucca Mountain and Vicinity, Nevada-California*. Water-Resources Investigations Report 84-4344. Denver, Colorado: U.S. Geological Survey. ACC: HQS.19880517.1750.

100377 Czarnecki, J.B.; Faunt, C.C.; Gable, C.W.; and Zyvoloski, G.A. 1997. *Hydrogeology and Preliminary Calibration of a Preliminary Three-Dimensional Finite-Element Ground-Water Flow Model of the Site Saturated Zone, Yucca Mountain, Nevada*. Administrative Report. Denver, Colorado: U.S. Geological Survey. ACC: MOL.19980204.0519.

100131 D'Agnese, F.A.; Faunt, C.C.; Turner, A.K.; and Hill, M.C. 1997. *Hydrogeologic Evaluation and Numerical Simulation of the Death Valley Regional Ground-Water Flow System, Nevada and California*. Water-Resources Investigations Report 96-4300. Denver, Colorado: U.S. Geological Survey. ACC: MOL.19980306.0253.

120425 D'Agnese, F.A.; O'Brien, G.M.; Faunt, C.C.; and San Juan, C.A. 1999. *Simulated Effects of Climate Change on the Death Valley Regional Ground-Water Flow System, Nevada and California*. Water-Resources Investigations Report 98-4041. Denver, Colorado: U.S. Geological Survey. TIC: 243555.

100027 Day, W.C.; Dickerson, R.P.; Potter, C.J.; Sweetkind, D.S.; San Juan, C.A.; Drake, R.M., II; and Fridrich, C.J. 1998. *Bedrock Geologic Map of the Yucca Mountain Area, Nye County, Nevada*. Geologic Investigations Series I-2627. Denver, Colorado: U.S. Geological Survey. ACC: MOL.19981014.0301.

154690 Dettinger, M.D. 1989. *Distribution of Carbonate-Rock Aquifers in Southern Nevada and the Potential for Their Development, Summary of Findings, 1985-88*. Summary Report No. 1. Carson City, Nevada: State of Nevada. ACC: NNA.19940412.0056.

103415 Dudley, W.W., Jr. and Larson, J.D. 1976. *Effect of Irrigation Pumping on Desert Pupfish Habitats in Ash Meadows, Nye County, Nevada*. Professional Paper 927. Washington, D.C.: U.S. Geological Survey. ACC: MOL.20010724.0312.

100633 Ervin, E.M.; Luckey, R.R.; and Burkhardt, D.J. 1994. *Revised Potentiometric-Surface Map, Yucca Mountain and Vicinity, Nevada*. Water-Resources Investigations Report 93-4000. Denver, Colorado: U.S. Geological Survey. ACC: NNA.19930212.0018.

100146 Faunt, C.C. 1997. *Effect of Faulting on Ground-Water Movement in the Death Valley Region, Nevada and California*. Water-Resources Investigations Report 95-4132. Denver, Colorado: U.S. Geological Survey. ACC: MOL.19980429.0119.

100033 Flint, L.E. 1998. *Characterization of Hydrogeologic Units Using Matrix Properties, Yucca Mountain, Nevada*. Water-Resources Investigations Report 97-4243. Denver, Colorado: U.S. Geological Survey. ACC: MOL.19980429.0512.

144110 Forsyth, P.A. 1989. "A Control Volume Finite Element Method for Local Mesh Refinement." *[Proceedings, Tenth] SPE Symposium on Reservoir Simulation, Houston, Texas, February 6-8, 1989*. SPE 18415. Pages 85-96. Richardson, Texas: Society of Petroleum Engineers. TIC: 247068.

154365 Freeze, G.A.; Brodsky, N.S.; and Swift, P.N. 2001. *The Development of Information Catalogued in REV00 of the YMP FEP Database*. TDR-WIS-MD-000003 REV 00 ICN 01. Las Vegas, Nevada: Bechtel SAIC Company. ACC: MOL.20010301.0237.

101173 Freeze, R.A. and Cherry, J.A. 1979. *Groundwate*r. Englewood Cliffs, New Jersey: Prentice-Hall. TIC: 217571.

129721 Geldon, A.L.; Umari, A.M.A.; Earle, J.D.; Fahy, M.F.; Gemmell, J.M.; and Darnell, J. 1998. *Analysis of a Multiple-Well Interference Test in Miocene Tuffaceous Rocks at the C-Hole Complex, May-June 1995, Yucca Mountain, Nye County, Nevada*. Water-Resources Investigations Report 97-4166. Denver, Colorado: U.S. Geological Survey. TIC: 236724.

100397 Geldon, A.L.; Umari, A.M.A.; Fahy, M.F.; Earle, J.D.; Gemmell, J.M.; and Darnell, J. 1997. *Results of Hydraulic and Conservative Tracer Tests in Miocene Tuffaceous Rocks at the C-Hole Complex, 1995 to 1997, Yucca Mountain, Nye County, Nevada*. Milestone SP23PM3. [Las Vegas, Nevada]: U.S. Geological Survey. ACC: MOL.19980122.0412.

103010 Kilroy, K.C. 1991. *Ground-Water Conditions in Amargosa Desert, Nevada-California, 1952-87*. Water-Resources Investigations Report 89-4101. Carson City, Nevada: U.S. Geological Survey. TIC: 209975.

100909 Kotra, J.P.; Lee, M.P.; Eisenberg, N.A.; and DeWispelare, A.R. 1996. *Branch Technical Position on the Use of Expert Elicitation in the High-Level Radioactive Waste Program.* NUREG-1563. Washington, D.C.: U.S. Nuclear Regulatory Commission. TIC: 226832.

157414 Kwicklis, E.M. 1999. "Determination of Pneumatic Diffusivity." *Hydrogeology of the Unsaturated Zone, North Ramp Area of the Exploratory Studies Facility, Yucca Mountain, Nevada.* Rousseau, J.P.; Kwicklis, E.M.; and Gillies, D.C., eds. Water-Resources Investigations Report 98-4050. Denver, Colorado: U.S. Geological Survey. ACC: MOL.19990419.0335.

103011 La Camera, R.J. and Locke, G.L. 1997. *Selected Ground-Water Data for Yucca Mountain Region, Southern Nevada and Eastern California, Through December 1996*. Open-File Report 97-821. Carson City, Nevada: U.S. Geological Survey. ACC: MOL.20010724.0311.

103012 Laczniak, R.J.; Cole, J.C.; Sawyer, D.A.; and Trudeau, D.A. 1996. *Summary of Hydrogeologic Controls on Ground-Water Flow at the Nevada Test Site, Nye County, Nevada*. Water-Resources Investigations 96-4109. Carson City, Nevada: U.S. Geological Survey. TIC: 226157.

163366 Lagedrost, J.F. and Capps, W. 1983. *Thermal Property and Density Measurements of Samples Taken from Drilling Cores from Potential Geologic Media*. BMI/ONWI-522. Columbus, Ohio: Battelle Memorial Institute, Office of Nuclear Waste Isolation. ACC: MOL.20030609.0316.

100153 LeCain, G.D. 1997. *Air-Injection Testing in Vertical Boreholes in Welded and Nonwelded Tuff, Yucca Mountain, Nevada*. Water-Resources Investigations Report 96-4262. Denver, Colorado: U.S. Geological Survey. ACC: MOL.19980310.0148.

144612 LeCain, G.D.; Anna, L.O.; and Fahy, M.F. 2000. *Results from Geothermal Logging, Air and Core-Water Chemistry Sampling, Air-Injection Testing, and Tracer Testing in the Northern Ghost Dance Fault, Yucca Mountain, Nevada, November 1996 to August 1998*. Water-Resources Investigations Report 99-4210. Denver, Colorado: U.S. Geological Survey. TIC: 247708.

101258 Loeven, C. 1993. *A Summary and Discussion of Hydrologic Data from the Calico Hills Nonwelded Hydrogeologic Unit at Yucca Mountain, Nevada*. LA-12376-MS. Los Alamos, New Mexico: Los Alamos National Laboratory. ACC: NNA.19921116.0001.

100465 Luckey, R.R.; Tucci, P.; Faunt, C.C.; Ervin, E.M.; Steinkampf, W.C.; D'Agnese, F.A.; and Patterson, G.L. 1996. *Status of Understanding of the Saturated-Zone Ground-Water Flow System at Yucca Mountain, Nevada, as of 1995*. Water-Resources Investigations Report 96-4077. Denver, Colorado: U.S. Geological Survey. ACC: MOL.19970513.0209.

150321 Neuman, S.P. 1975. "Analysis of Pumping Test Data from Anisotropic Unconfined Aquifers Considering Delayed Gravity Response." *Water Resources Research, 11*, (2), 329-342. Washington, D.C.: American Geophysical Union. TIC: 222414.

147379 Norton, D. and Knapp, R.B. 1977. "Transport Phenomena in Hydrothermal Systems: The Nature of Porosity." *American Journal of Science, 277*, 913-936. New Haven, Connecticut: Yale University, Kline Geology Laboratory. TIC: 247599.

163274 NRC (U.S. Nuclear Regulatory Commission) 2003. *Yucca Mountain Review Plan, Final Report*. NUREG-1804, Rev. 2. Washington, D.C.: U.S. Nuclear Regulatory Commission, Office of Nuclear Material Safety and Safeguards. TIC: 254568.

107770 NRC (U.S. Nuclear Regulatory Commission) 1998. "Proposed Rule: 10 CFR Part 63---'Disposal of High-Level Radioactive Wastes in a Proposed Geologic Repository at Yucca Mountain, Nevada'." SECY-98-225. [Washington, D.C.: U.S. Nuclear Regulatory Commission]. Accessed October 30, 1999. TIC: 240520. http://www.nrc.gov/NRC/COMMISSION/SECYS/1998-225scy.html

149364 Nye County Nuclear Waste Repository Project Office. 2000. "Early Warning Drilling Program." Pahrump, Nevada: Nye County. Accessed April 24, 2000. TIC: 247627. http://www.nyecounty.com/ewdpmain.htm.

149438 Oatfield, W.J. and Czarnecki, J.B. 1989. *Hydrogeologic Inferences from Drillers Logs and from Gravity and Resistivity Surveys in the Amargosa Desert, Southern Nevada*. Open-File Report 89-234. Denver, Colorado: U.S. Geological Survey. TIC: 200468.

159511 Parkhurst, D.L. and Appelo, C.A.J. 1999. *User's Guide to PHREEQC (Version 2)—A Computer Program for Speciation, Batch-Reaction, One-Dimensional Transport, and Inverse Geochemical Calculations*. Water-Resources Investigations Report 99-4259. Denver, Colorado: U.S. Geological Survey. TIC: 253046.

158824 Patterson, G.L. 1999. "Occurrences of Perched Water in the Vicinity of the Exploratory Studies Facility North Ramp." *Hydrogeology of the Unsaturated Zone, North Ramp Area of the Exploratory Studies Facility, Yucca Mountain, Nevada*. Rousseau, J.P.; Kwicklis, E.M.; and Gillies, D.C., eds. Water-Resources Investigations Report 98-4050. Denver, Colorado: U.S. Geological Survey. ACC: MOL.19990419.0335.

101466 Pollock, D.W. 1988. "Semianalytical Computation of Path Lines for Finite-Difference Models." *Ground Water, 26*, (6), 743-750. Worthington, Ohio: National Water Well Association. TIC: 226464.

159398 Potter, C.J.; Dickerson, R.P.; Sweetkind, D.S.; Drake, R.M., II.; San Juan, C.A.; Taylor, E.M.; Fridrich, C.J.; and Day, W.C. 2001. *Geologic Map of the Yucca Mountain Region, Nye County, Nevada*. Administrative Report. Denver, Colorado: U.S. Geological Survey. ACC: MOL.20020416.0184.

103316 Press, W.H.; Teukolsky, S.A.; Vetterling, W.T.; and Flannery, B.P. 1992. *Numerical Recipes in Fortran 77, The Art of Scientific Computing. Volume 1 of Fortran Numerical Recipes*. 2nd Edition. Cambridge, United Kingdom: Cambridge University Press. TIC: 243606.

154688 Rasmussen, T.C.; Evans, D.D.; Sheets, P.J.; and Blanford, J.H. 1993. "Permeability of Apache Leap Tuff: Borehole and Core Measurements Using Water and Air." *Water Resources Research, 29*, (7), 1997-2006. [Washington, D.C.]: American Geophysical Union. TIC: 245278.

144725 Rose, T.P.; Kenneally, J.M.; Smith, D.K.; Davisson, M.L.; Hudson, G.B.; and Rego, J.H. 1997. *Chemical and Isotopic Data for Groundwater in Southern Nevada*.

UCRL-ID-128000. Livermore, California: Lawrence Livermore National Laboratory. TIC: 243649.

163364 Ryder, E.E. [1996]. *Backfill Generic Concept 1: Effective Thermal Conductivity*. Preliminary Information. Albuquerque, New Mexico: Sandia National Laboratories. ACC: MOL.19971117.0330.

153174 Sass, J.H.; Kennelly, J.P., Jr.; Smith, E.P.; and Wendt, W.E. 1984. *Laboratory Line-Source Methods for the Measurement of Thermal Conductivity of Rocks Near Room Temperature*. Open-File Report 84-91. Menlo Park, California: U.S. Geological Survey. ACC: NNA.19920814.0125.

100644 Sass, J.H.; Lachenbruch, A.H.; Dudley, W.W., Jr.; Priest, S.S.; and Munroe, R.J. 1988. *Temperature, Thermal Conductivity, and Heat Flow Near Yucca Mountain, Nevada: Some Tectonic and Hydrologic Implications*. Open-File Report 87-649. [Denver, Colorado]: U.S. Geological Survey. TIC: 203195.

100075 Sawyer, D.A.; Fleck, R.J.; Lanphere, M.A.; Warren, R.G.; Broxton, D.E.; and Hudson, M.R. 1994. "Episodic Caldera Volcanism in the Miocene Southwestern Nevada Volcanic Field: Revised Stratigraphic Framework, 40Ar/39Ar Geochronology, and Implications for Magmatism and Extension." *Geological Society of America Bulletin, 106*, (10), 1304-1318. Boulder, Colorado: Geological Society of America. TIC: 222523.

163363 Sekiguchi, K. 1984. "A Method for Determining Terrestrial Heat Flow in Oil Basinal Areas." *Tectonophysics, 103*, 67-69, Table 1, p. 73. Amsterdam, The Netherlands: New York, New York: Elsevier. TIC: 254626

101929 Simonds, F.W.; Whitney, J.W.; Fox, K.F.; Ramelli, A.R.; Yount, J.C.; Carr, M.D.; Menges, C.M.; Dickerson, R.P.; and Scott, R.B. 1995. *Map Showing Fault Activity in the Yucca Mountain Area, Nye County, Nevada*. Miscellaneous Investigations Series Map I-2520. Denver, Colorado: U.S. Geological Survey. TIC: 232483.

163360 Smyth, J.R.; Crowe, B.M.; Halleck, P.M.; and Reed, A.W. 1979. *A Preliminary Evaluation of the Radioactive Waste Isolation Potential of the Alluvium-Filled Valleys of the Great Basin*. LA-7962-MS. Los Alamos, New Mexico: Los Alamos Scientific Laboratory. TIC: 202303.

145287 Streeter, V.L. and Wylie, E.B. 1979. *Fluid Mechanics*. 7th Edition. New York, New York: McGraw-Hill. TIC: 4819.

106585 Thordarson, W. 1965. *Perched Ground Water in Zeolitized-Bedded Tuff, Rainier Mesa and Vicinity, Nevada Test Site, Nevada*. TEI-862. Washington, D.C.: U.S. Geological Survey. ACC: NN1.19881021.0066.

101490 Tompson, A.F.B. and Gelhar, L.W. 1990. "Numerical Simulation of Solute Transport in Three-Dimensional, Randomly Heterogeneous Porous Media." *Water*

Resources Research, 26, (10), 2541-2562. Washington, D.C.: American Geophysical Union. TIC: 224902.

101060 Tucci, P. and Burkhardt, D.J. 1995. *Potentiometric-Surface Map, 1993, Yucca Mountain and Vicinity, Nevada*. Water-Resources Investigations Report 95-4149. Denver, Colorado: U.S. Geological Survey. ACC: MOL.19960924.0517.

158608 USGS (U.S. Geological Survey) 2001. *Hydrogeologic Framework Model for the Saturated-Zone Site-Scale Flow and Transport Model*. ANL-NBS-HS-000033 REV 00 ICN 02. Denver, Colorado: U.S. Geological Survey. ACC: MOL.20011112.0070.

154625 USGS (U.S. Geological Survey) 2001. *Water-Level Data Analysis for the Saturated Zone Site-Scale Flow and Transport Model*. ANL-NBS-HS-000034 REV 00 ICN 01. Denver, Colorado: U.S. Geological Survey. ACC: MOL.20010405.0211.

157611 USGS (U.S. Geological Survey) 2001. *Water-Level Data Analysis for the Saturated Zone Site-Scale Flow and Transport Model*. ANL-NBS-HS-000034 REV 01. Denver, Colorado: U.S. Geological Survey. ACC: MOL.20020209.0058.

143606 Verma, S. and Aziz, K. 1997. "A Control Volume Scheme for Flexible Grids in Reservoir Simulation." *Proceedings, SPE Reservoir Simulation Symposium, 8-11, June 1997, Dallas, Texas*. SPE 37999, 215-227. Richardson, Texas: Society of Petroleum Engineers. TIC: 247097.

154706 Vesselinov, V.V.; Illman, W.A.; Hyun, Y.; Neuman, S.P.; Di Federico, V.; and Tartakovsky, D.M. 2001. "Observation and Analysis of a Pronounced Permeability and Porosity Scale-Effect in Unsaturated Fractured Tuff." *Fractured Rock 2001, An International Conference Addressing Groundwater Flow, Solute Transport, Multiphase Flow, and Remediation in Fractured Rock, March 26-28, 2001, Toronto, Ontario, Canada*. Kueper, B.H.; Novakowski, K.S.; and Reynolds, D.A., eds. Smithville, Ontario, Canada: Smithville Phase IV. TIC: 249909.

101062 Waddell, R.K. 1982. *Two-Dimensional, Steady-State Model of Ground-Water Flow, Nevada Test Site and Vicinity, Nevada-California*. Water-Resources Investigations Report 82-4085. Denver, Colorado: U.S. Geological Survey. ACC: NNA.19870518.0055.

103022 Walker, G.E. and Eakin, T.E. 1963. *Geology and Ground Water of Amargosa Desert, Nevada-California*. Ground-Water Resources – Reconnaissance Series Report 14. Carson City, Nevada: State of Nevada, Department of Conservation and Natural Resources. TIC: 208665.

108841 Weeks, E.P. 1978. *Field Determination of Vertical Permeability to Air in the Unsaturated Zone*. Geological Survey Professional Paper 1051. Washington, D.C.: U.S. Government Printing Office. TIC: 218986.

130510 Wen, X-H. and Gomez-Hernandez, J.J. 1996. "The Constant Displacement Scheme for Tracking Particles in Heterogeneous Aquifers." *Ground Water, 34*, (1), 135-142. Worthington, Ohio: Water Well Journal Publishing. TIC: 246656.

108882 Winograd, I.J. and Pearson, F.J., Jr. 1976. "Major Carbon 14 Anomaly in a Regional Carbonate Aquifer: Possible Evidence for Megascale Channeling, South Central Great Basin." *Water Resources Research, 12*, (6), 1125-1143. Washington, D.C.: American Geophysical Union. TIC: 217731.

101167 Winograd, I.J. and Thordarson, W. 1975. *Hydrogeologic and Hydrochemical Framework, South-Central Great Basin, Nevada-California, with Special Reference to the Nevada Test Site*. Geological Survey Professional Paper 712-C. Washington, [D.C.]: United States Government Printing Office. ACC: NNA.19870406.0201.

129796 Winterle, J.R. and La Femina, P.C. 1999. *Review and Analysis of Hydraulic and Tracer Testing at the C-Holes Complex Near Yucca Mountain, Nevada*. San Antonio, Texas: Center for Nuclear Waste Regulatory Analyses. TIC: 246623.

163359 Wollenberg, H.A.; Wang, J.S.Y.; and Korbin, G. 1983. *An Appraisal of Nuclear Waste Isolation in the Vadose Zone in Arid and Semiarid Regions (with Emphasis on the Nevada Test Site).* LBL-15010. Berkeley, California: University of California, Lawrence Berkeley Laboratory. TIC: 211058.

101171 Zyvoloski, G. 1983. "Finite Element Methods for Geothermal Reservoir Simulation." *International Journal for Numerical and Analytical Methods in Geomechanics, 7*, (1), 75-86. New York, New York: John Wiley & Sons. TIC: 224068.

163341 Zyvoloski, G.; Kwicklis, E.; Eddebbarh, A.A.; Arnold, B.; Faunt, C.; and Robinson, B.A. 2003. "The Site-Scale Saturated Zone Flow Model for Yucca Mountain: Calibration of Different Conceptual Models and their Impact on Flow Paths." *Journal of Contaminant Hydrology*, 62-63, 731-750. [New York, New York]: Elsevier. TIC: 254340.

100615 Zyvoloski, G.A.; Robinson, B.A.; Dash, Z.V.; and Trease, L.L. 1997. *User's Manual for the FEHM Application–A Finite-Element Heat- and Mass-Transfer Code*. LA-13306-M. Los Alamos, New Mexico: Los Alamos National Laboratory. TIC: 235999.

9.2 CODES, STANDARDS, REGULATIONS, AND PROCEDURES

156605 10 CFR 63. Energy: Disposal of High-Level Radioactive Wastes in a Geologic Repository at Yucca Mountain, Nevada. Readily available.

164786 AP-2.22Q, Rev. 1, ICN 0. Classification Analyses and Maintenance of the Q-List. Washington, D.C.: U.S. Department of Energy, Office of Civilian Radioactive Waste Management. ACC: DOC.20030807.0002.

165023 AP-SI.1Q, Rev. 5, ICN 2. Software Management. Washington, D.C.: U.S. Department of Energy, Office of Civilian Radioactive Waste Management. ACC: DOC.20030902.0003.

165553 AP-SIII.10Q, Rev. 2, ICN 0. Models. Washington, D.C.: U.S. Department of Energy, Office of Civilian Radioactive Waste Management. ACC: DOC.20030929.0003.

9.3 SOFTWARE

153238 Landmark Graphics. 1998. *Software Code: STRATAMODEL*. V4.1.1. SGI System, PC. 10121-4.1.1-00.

150459 LANL (Los Alamos National Laboratory) 2000. *Software Routine: READPATHS_3.0*. V1.0. MDL-NBS-HS-000011. (Routine not used outside of this report)

149148 LANL (Los Alamos National Laboratory) 2001. *Software Code: LaGriT*. V1.0. 10212-1.0-00.

149910 LANL (Los Alamos National Laboratory) 2001. *Software Code: NETPATH*. V2.13. Platform: PC, OS: WINDOWS NT, DOS Emulation. 10303-2.13-00.

161725 LANL (Los Alamos National Laboratory) 2003. *Software Code: FEHM*. V2.20. SUN, PC. 10086-2.20-00.

LANL 2003. *Software Routine: prepare_features_for_surfer*. V 1.0. (Routine not used outside of this report).

163069 LANL 2003. *Software Code: STRAT2AVS*. V 1.0. SGI with Irix64 operating system. 11028-1.0-00.

LANL 2003. Software routine: write_temps. V 1.0. (Routine not used outside of this report).

163835 Sandia National Laboratories (SNL) 2002. *Software Code: WTCONVYD*. V 1.00. SUN,Solaris 8; PC, Windows 98. 10815-1.0-00.

163072 SNL 2002. *Software Code: Ext_Rech*. V 1.0. Sun UltraSPARC - SunOS 5.7. 109058-1.0-00.

163070 SNL 2002. *Software Code: Extract*. V 1.0. Sun UltraSPARC - SunOS 5.7. 10955-1.0-00.

163071 SNL 2002. *Software Code: Extract*. V 1.1. Sun UltraSPARC - SunOS 5.7. 10955-1.1-00.

163073 SNL 2002. *Software Code: Mult_Rech*. V 1.0. Sun UltraSPARC - SunOS 5.7. 10959-1.0-00.

163344 SNL 2003. *Software Code: SZ_Convolute.* V2.2. PC, Windows 2000. 10207-2.2-00. (Used as reference only)

163074 SNL 2002. *Software Code: Xread_Distr_Rech*. V 1.0. Sun UltraSPARC - SunOS 5.7. 10960-1.0-00.

163075 SNL 2002. *Software Code: Xread_Distr_Rech_-UZ*. V 1.0. Sun UltraSPARC - SunOS 5.7. 10961-1.0-00.

163076 SNL 2002. *Software Code: Xread_Reaches*. V 1.0. Sun UltraSPARC - SunOS 5.7. 10962-1.0-00.

163077 SNL 2002. *Software Code: Xwrite_Flow_New*. V 1.0-125. Sun UltraSPARC - SunOS 5.7. 10963-1.0-125-00.

163078 SNL 2002. *Software Code: Zones*. V 1.0. Sun UltraSPARC - SunOS 5.7. 10957-1.0-00.

161564 Watermark Computing 2002. *Software Code: PEST*. V5.5. SUN, PC, Linux. 10289-5.5-00.

9.4 SOURCE DATA, LISTED BY DATA TRACKING NUMBER

149947 GS000508312332.001. Water-Level Data Analysis for the Saturated Zone Site-Scale Flow and Transport Model. Submittal date: 06/01/2000.

155307 GS010608312332.001. Potentiometric-Surface Map, Assuming Perched Conditions North of Yucca Mountain, in the Saturated Site-Scale Model. Submittal date: 06/19/2001. (Used as reference only).

163555 GS010908312332.002. Borehole Data from Water-Level Data Analysis for the Saturated Zone Site-Scale Flow and Transport Model. Submittal date: 10/02/2001. (Used as reference only)

162874 GS010908314221.001. Geologic Map of the Yucca Mountain Region, Nye County, Nevada. Submittal date: 01/23/2002

163087 GS030208312332.001. HFM Final Output - Hydrogeologic Framework Model for the Saturated-Zone Site-Scale Flow and Transport Model. Submittal date: 02/10/2003.

145763 GS930208318523.001. Temperature and Thermal Conductivity in Wells Near Yucca Mountain. Submittal date: 02/16/1993. (Used as reference only).

107244 GS950408318523.001. Temperature, Thermal Conductivity, and Heat Flow Near Yucca Mountain, Nevada. Submittal date: 04/21/1995. (Used as reference only)

105572 GS950208312232.003. Data, Including Water Potential, Pressure and Temperature, Collected from Boreholes USW NRG-6 and USW NRG-7A from Instrumentation through March 31, 1995. Submittal date: 02/13/1995. (Used as reference only.)

105121 GS960808312144.003. Hydrogeologic Evaluation and Numerical Simulation of the Death Valley Regional Ground-Water Flow System, Nevada and California, Using Geoscientific Information Systems. Submittal date: 08/29/1996. (Used as reference only)

114124 GS960908312232.012. Comparison of Air-Injection Permeability Values to Laboratory Permeability Values. Submittal date: 09/26/1996. (Used as reference only).

163561 LA0303PR831231.002. Estimation of Groundwater Drift Velocity from Tracer Responses in Single-Well Tracer Tests at Alluvium Testing Complex. Submittal date: 03/18/2003. (Used as reference only).

154733 MO0102DQRBTEMP.001. Temperature Data Collected from Boreholes Near Yucca Mountain in Early 1980's. Submittal date: 02/21/2001.

155290 MO0008NYE02997.033. EWDP Phase 1 Water and Elevation Data from Westbay Instrumented Wells, 05/06/99 - 10/18/99. Submittal date: 08/10/2000. (Used as reference only.)

119613 MO9909NYEEWDP0.000. Phase I-Fiscal Year 1999 Nye County Early Warning Drilling Program Data Package. Submittal date: 09/16/1999. (Used as reference only)

132867 SN9908T0581999.001. Recharge and Lateral Groundwater Flow Boundary Conditions for the Saturated Zone (SZ) Site-Scale Flow and Transport Model. Submittal date: 08/19/1999.

129714 SNT05082597001.003. TSPA-VA (Total System Performance Assessment-Viability Assessment) Saturated Zone (SZ) Base Case Modeling Analysis Results. Submittal date: 02/03/1998. (Used as reference only).

9.5 OUTPUT DATA, LISTED BY DATA TRACKING NUMBER

LA0304TM831231.002. SZ Site-Scale Flow Model, FEHM Files for Base Case. Submittal date: 04/14/2003.

LA0304TM831231.001 SZ Flow and Transport Model, Hydrogeologic Surface Files Submittal date: 04/7/2003.

Attachment I: Dune Wash and Ghost Dance Fault Traces

Fault Definition							Input Data *Dune Wash*		
							Fault #1		**Faul**
Charac. Name	**Fault #**	**X-Values (m)**	**Y-Values (m)**	**Slope**	**y-intercept**	**Equation of Line Per Fault**	**X (m)**	**Y (m)**	**X (m)**
Dune Wash	1	5.490930E+05	4.076094E+06	-2.0222	5.1865E+06	y = -2.02x + 5.187E+06	5.50E+05	4074260.2	5.49E+05
		5.514580E+05	4.071312E+06				5.50E+05	4074159.1	5.49E+05
	2	5.490926E+05	4.076095E+06	-7.2716	8.0689E+06	y = -7.272x + 8.069E+06	5.50E+05	4074058	5.49E+05
		5.489543E+05	4.077101E+06				5.50E+05	4073956.9	5.49E+05
Ghost Dance	1	5.479613E+05	4.074277E+06	5.6048	1.0031E+06	y = 5.605x + 1.003E+06	5.50E+05	4073855.8	5.49E+05
		5.481646E+05	4.075416E+06				5.50E+05	4073754.6	5.49E+05
	2	5.480965E+05	4.072914E+06	-12.4134	1.0877E+07	y = -12.413x + 1.088E+07	5.50E+05	4073653.5	5.49E+05
		5.481473E+05	4.072283E+06				5.50E+05	4073552.4	5.49E+05
	3	5.479624E+05	4.074277E+06	-10.2601	9.6964E+06	y = -10.260x + 9.696E+06	5.50E+05	4073451.3	5.49E+05
		5.480958E+05	4.072908E+06				5.50E+05	4073350.2	5.49E+05
	4	5.481645E+05	4.075416E+06	5.5758	1.0190E+06	y = 5.576x + 1.019E+06	5.51E+05	4073249.1	5.49E+05
		5.482137E+05	4.075690E+06				5.51E+05	4073148	5.49E+05
	5	5.487323E+05	4.078346E+06	-18.5553	1.4260E+07	y = -18.555x + 1.426E+07	5.51E+05	4073046.9	5.49E+05
		5.487398E+05	4.078208E+06				5.51E+05	4072945.8	5.49E+05
	6	5.488261E+05	4.079209E+06	0.5747	3.7638E+06	y = 0.575x + 3.764E+06	5.51E+05	4072844.7	5.49E+05
		5.473227E+05	4.078345E+06				5.51E+05	4072743.6	5.49E+05
	7	5.487393E+05	4.078208E+06	14.0504	-3.6318E+06	y = 14.050x - 3.632E+06	5.51E+05	4072642.5	5.49E+05
		5.486228E+05	4.076572E+06				5.51E+05	4072541.3	5.49E+05
	8	5.486228E+05	4.076571E+06	2.1527	2.8956E+06	y = 2.153x + 2.896E+06	5.51E+05	4072440.2	5.49E+05
		5.482131E+05	4.075689E+06				5.51E+05	4072339.1	5.49E+05

All Grey areas represent info that was inputed by recorder for use in computation of output data

lt #2	*Ghost Dance* Fault #1		Fault #2		Fault #3		Fault #4		Fault #5		Fault #6	
Y (m)	X (m)	Y (m)	X (m)	Y (m)	X (m)	Y (m)	X (m)	Y (m)	X (m)	Y (m)	X (m)	Y (m)
4076695.6	5.48E+05	4074325.8	5.48E+05	4072907.8	5.48E+05	4074271.1	5.48E+05	4075446.5	5.49E+05	4078334.1	5.47E+05	4078349.2
4076673.8	5.48E+05	4074353.8	5.48E+05	4072883	5.48E+05	4074209.5	5.48E+05	4075457.7	5.49E+05	4078329.5	5.47E+05	4078377.9
4076652	5.48E+05	4074381.9	5.48E+05	4072858.1	5.48E+05	4074148	5.48E+05	4075468.8	5.49E+05	4078324.8	5.47E+05	4078406.7
4076630.2	5.48E+05	4074409.9	5.48E+05	4072833.3	5.48E+05	4074086.4	5.48E+05	4075480	5.49E+05	4078320.2	5.47E+05	4078435.4
4076608.4	5.48E+05	4074437.9	5.48E+05	4072808.5	5.48E+05	4074024.9	5.48E+05	4075491.1	5.49E+05	4078315.6	5.48E+05	4078464.1
4076586.6	5.48E+05	4074465.9	5.48E+05	4072783.7	5.48E+05	4073963.3	5.48E+05	4075502.3	5.49E+05	4078310.9	5.48E+05	4078492.9
4076564.7	5.48E+05	4074494	5.48E+05	4072758.8	5.48E+05	4073901.7	5.48E+05	4075513.4	5.49E+05	4078306.3	5.48E+05	4078521.6
4076542.9	5.48E+05	4074522	5.48E+05	4072734	5.48E+05	4073840.2	5.48E+05	4075524.6	5.49E+05	4078301.6	5.48E+05	4078550.3
4076521.1	5.48E+05	4074550	5.48E+05	4072709.2	5.48E+05	4073778.6	5.48E+05	4075535.7	5.49E+05	4078297	5.48E+05	4078579.1
4076499.3	5.48E+05	4074578	5.48E+05	4072684.4	5.48E+05	4073717.1	5.48E+05	4075546.9	5.49E+05	4078292.4	5.48E+05	4078607.8
4076477.5	5.48E+05	4074606	5.48E+05	4072659.5	5.48E+05	4073655.5	5.48E+05	4075558	5.49E+05	4078287.7	5.48E+05	4078636.5
4076455.7	5.48E+05	4074634.1	5.48E+05	4072634.7	5.48E+05	4073593.9	5.48E+05	4075569.2	5.49E+05	4078283.1	5.48E+05	4078665.3
4076433.9	5.48E+05	4074662.1	5.48E+05	4072609.9	5.48E+05	4073532.4	5.48E+05	4075580.3	5.49E+05	4078278.4	5.48E+05	4078694
4076412	5.48E+05	4074690.1	5.48E+05	4072585	5.48E+05	4073470.8	5.48E+05	4075591.5	5.49E+05	4078273.8	5.48E+05	4078722.7
4076390.2	5.48E+05	4074718.1	5.48E+05	4072560.2	5.48E+05	4073409.3	5.48E+05	4075602.6	5.49E+05	4078269.2	5.48E+05	4078751.5
4076368.4	5.48E+05	4074746.2	5.48E+05	4072535.4	5.48E+05	4073347.7	5.48E+05	4075613.8	5.49E+05	4078264.5	5.48E+05	4078780.2
4076346.6	5.48E+05	4074774.2	5.48E+05	4072510.6	5.48E+05	4073286.1	5.48E+05	4075624.9	5.49E+05	4078259.9	5.48E+05	4078808.9
4076324.8	5.48E+05	4074802.2	5.48E+05	4072485.7	5.48E+05	4073224.6	5.48E+05	4075636.1	5.49E+05	4078255.2	5.48E+05	4078837.7
4076303	5.48E+05	4074830.2	5.48E+05	4072460.9	5.48E+05	4073163	5.48E+05	4075647.2	5.49E+05	4078250.6	5.48E+05	4078866.4
4076281.2	5.48E+05	4074858.3	5.48E+05	4072436.1	5.48E+05	4073101.5	5.48E+05	4075658.4	5.49E+05	4078246	5.48E+05	4078895.1

Fault #7		Fault #8	
X (m)	Y (m)	X (m)	Y (m)
5.49E+05	4076644.5	5.48E+05	4075876.6
5.49E+05	4076714.7	5.48E+05	4075898.1
5.49E+05	4076785	5.48E+05	4075919.6
5.49E+05	4076855.2	5.48E+05	4075941.2
5.49E+05	4076925.5	5.48E+05	4075962.7
5.49E+05	4076995.7	5.48E+05	4075984.2
5.49E+05	4077066	5.48E+05	4076005.8
5.49E+05	4077136.2	5.48E+05	4076027.3
5.49E+05	4077206.5	5.48E+05	4076048.8
5.49E+05	4077276.7	5.48E+05	4076070.3
5.49E+05	4077347	5.48E+05	4076091.9
5.49E+05	4077417.2	5.48E+05	4076113.4
5.49E+05	4077487.5	5.48E+05	4076134.9
5.49E+05	4077557.7	5.48E+05	4076156.4
5.49E+05	4077628	5.48E+05	4076178
5.49E+05	4077698.3	5.48E+05	4076199.5
5.49E+05	4077768.5	5.48E+05	4076221
5.49E+05	4077838.8	5.48E+05	4076242.6
5.49E+05	4077909	5.48E+05	4076264.1
5.49E+05	4077979.3	5.48E+05	4076285.6

Dune Wash and Ghost Dance Fault Traces

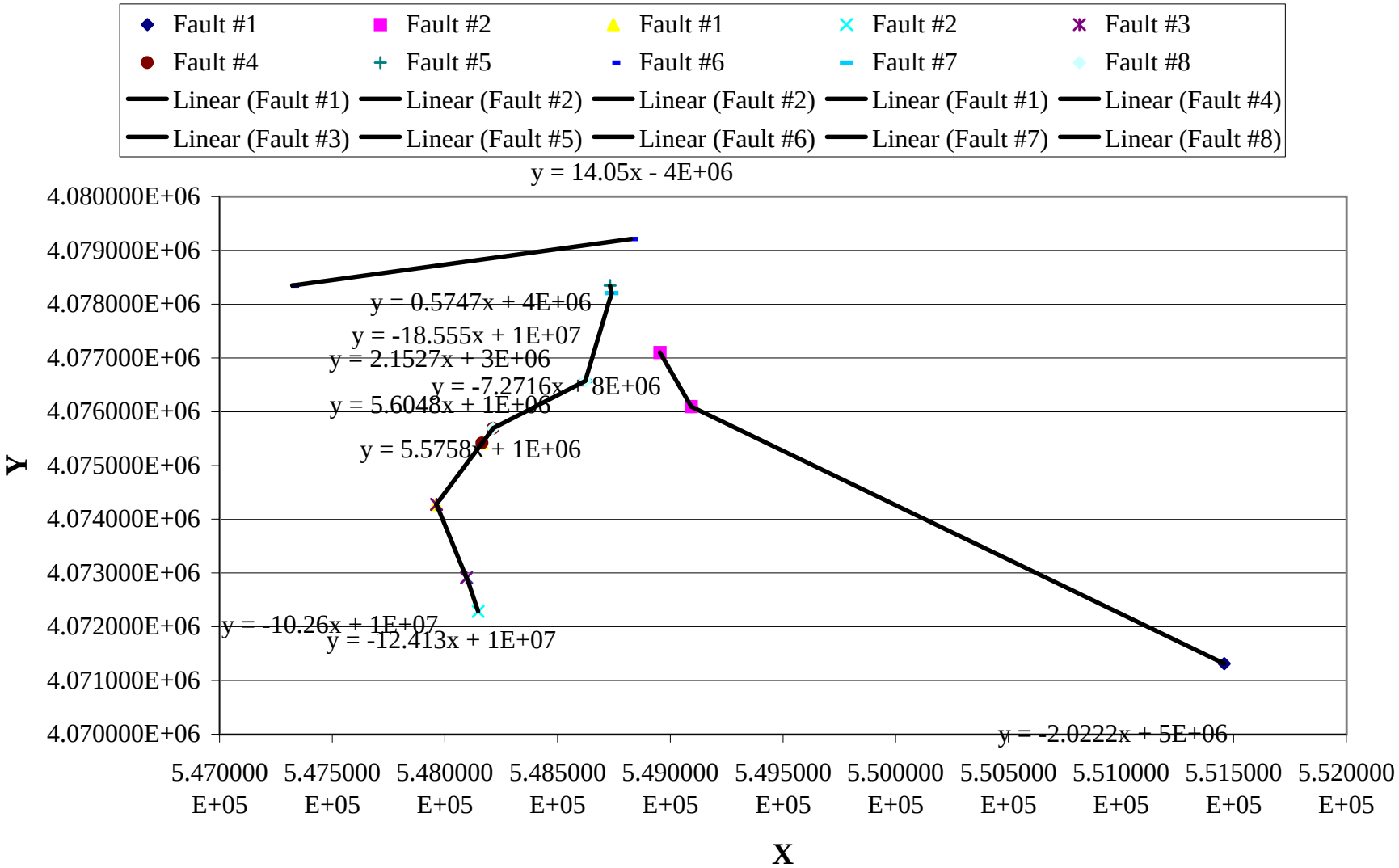

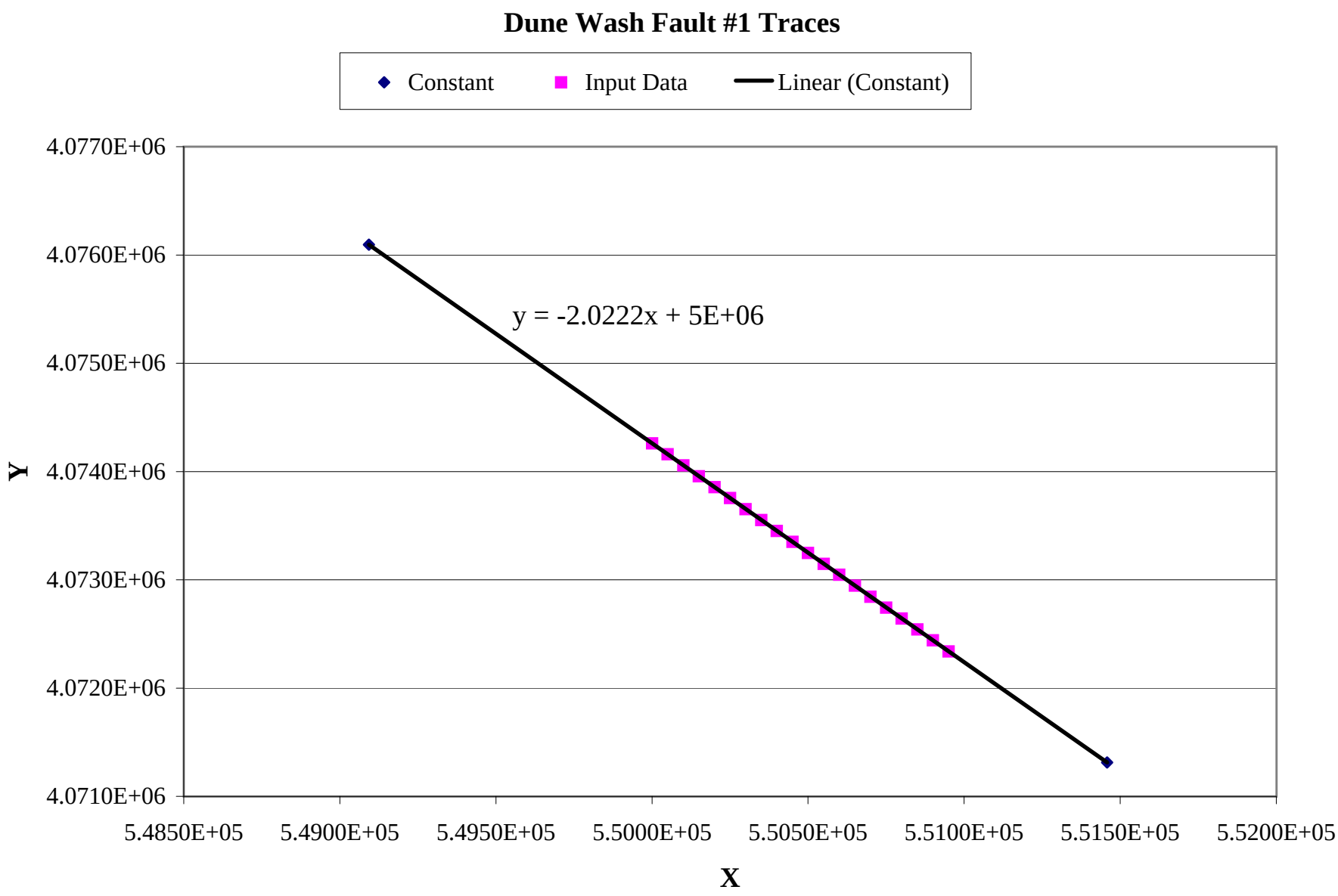
Dune Wash Fault #1 Traces
Constant
Input Data
Linear (Constant)
y = -2.0222x + 5E+06
4.0770E+06
4.0760E+06
4.0750E+06
4.0740E+06
4.0730E+06
4.0720E+06
4.0710E+06
Y
5.4850E+05
5.4900E+05
5.4950E+05
5.5000E+05
5.5050E+05
5.5100E+05
5.5150E+05
5.5200E+05
X

Dune Wash Fault #2 Traces
Constant
Input Data
Linear (Constant)
y = -7.2716x + 8E+06
4.0772E+06
4.0770E+06
4.0768E+06
4.0766E+06
4.0764E+06
4.0762E+06
4.0760E+06
Y
5.4894E+05
5.4896E+05
5.4898E+05
5.4900E+05
5.4902E+05
5.4904E+05
5.4906E+05
5.4908E+05
5.4910E+05
X

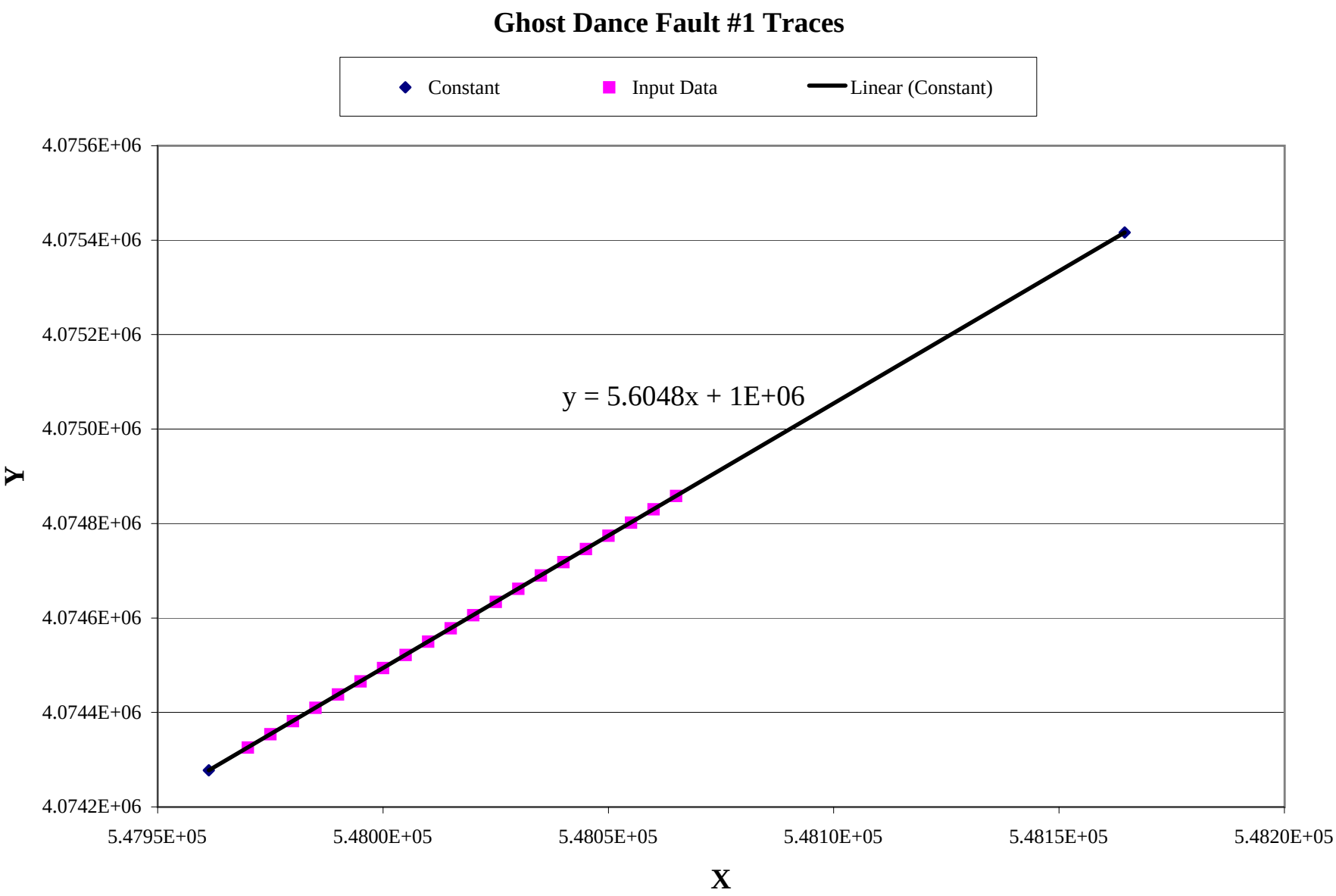
Ghost Dance Fault #1 Traces
Constant
Input Data
Linear (Constant)
y = 5.6048x + 1E+06
4.0756E+06
4.0754E+06
4.0752E+06
4.0750E+06
4.0748E+06
4.0746E+06
4.0744E+06
4.0742E+06
Y
5.4795E+05
5.4800E+05
5.4805E+05
5.4810E+05
5.4815E+05
5.4820E+05
X

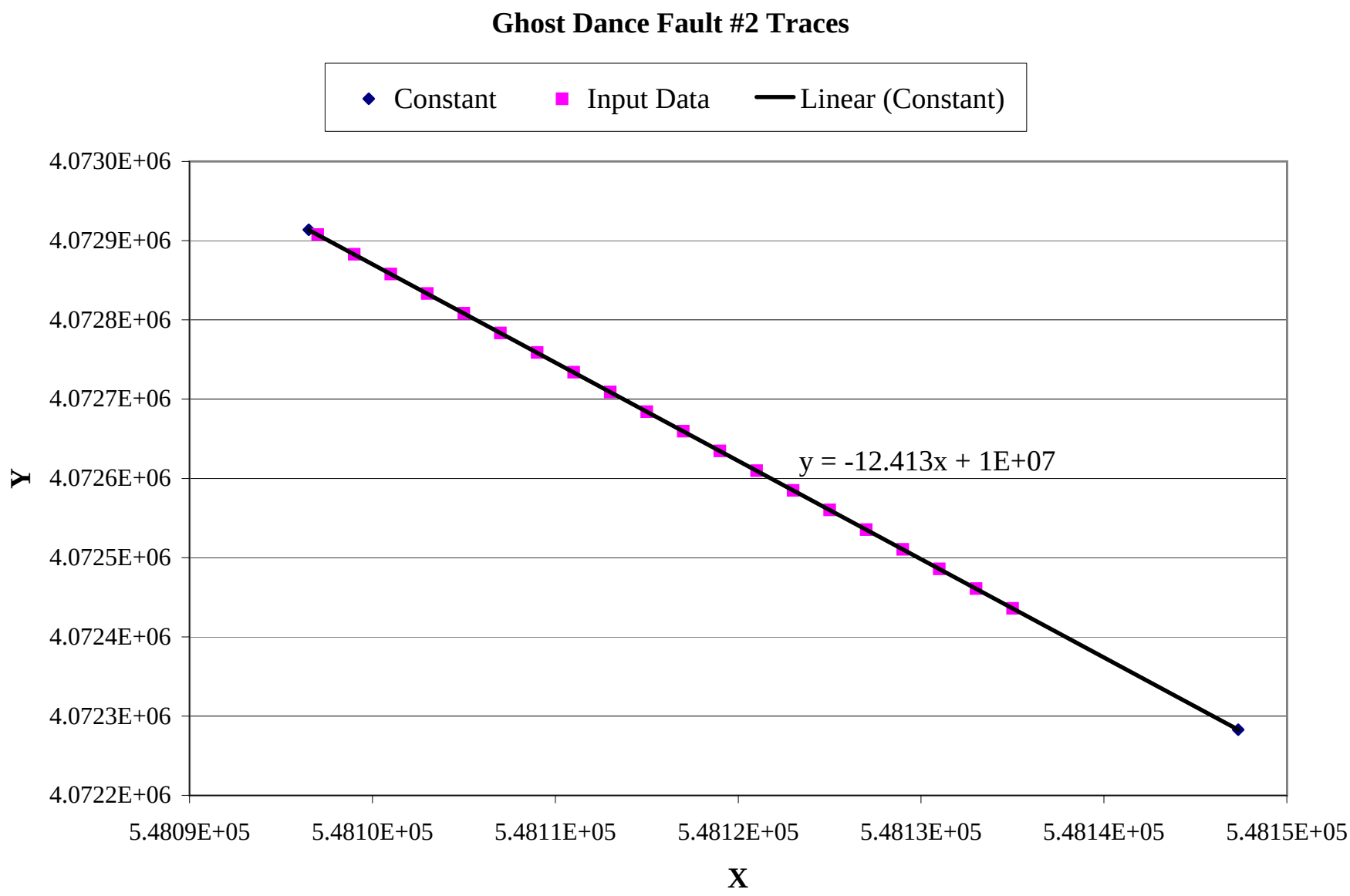
Ghost Dance Fault #2 Traces
Constant
Input Data
Linear (Constant)
y = -12.413x + 1E+07
4.0730E+06
4.0729E+06
4.0728E+06
4.0727E+06
4.0726E+06
4.0725E+06
4.0724E+06
4.0723E+06
4.0722E+06
Y
5.4809E+05
5.4810E+05
5.4811E+05
5.4812E+05
5.4813E+05
5.4814E+05
5.4815E+05
X

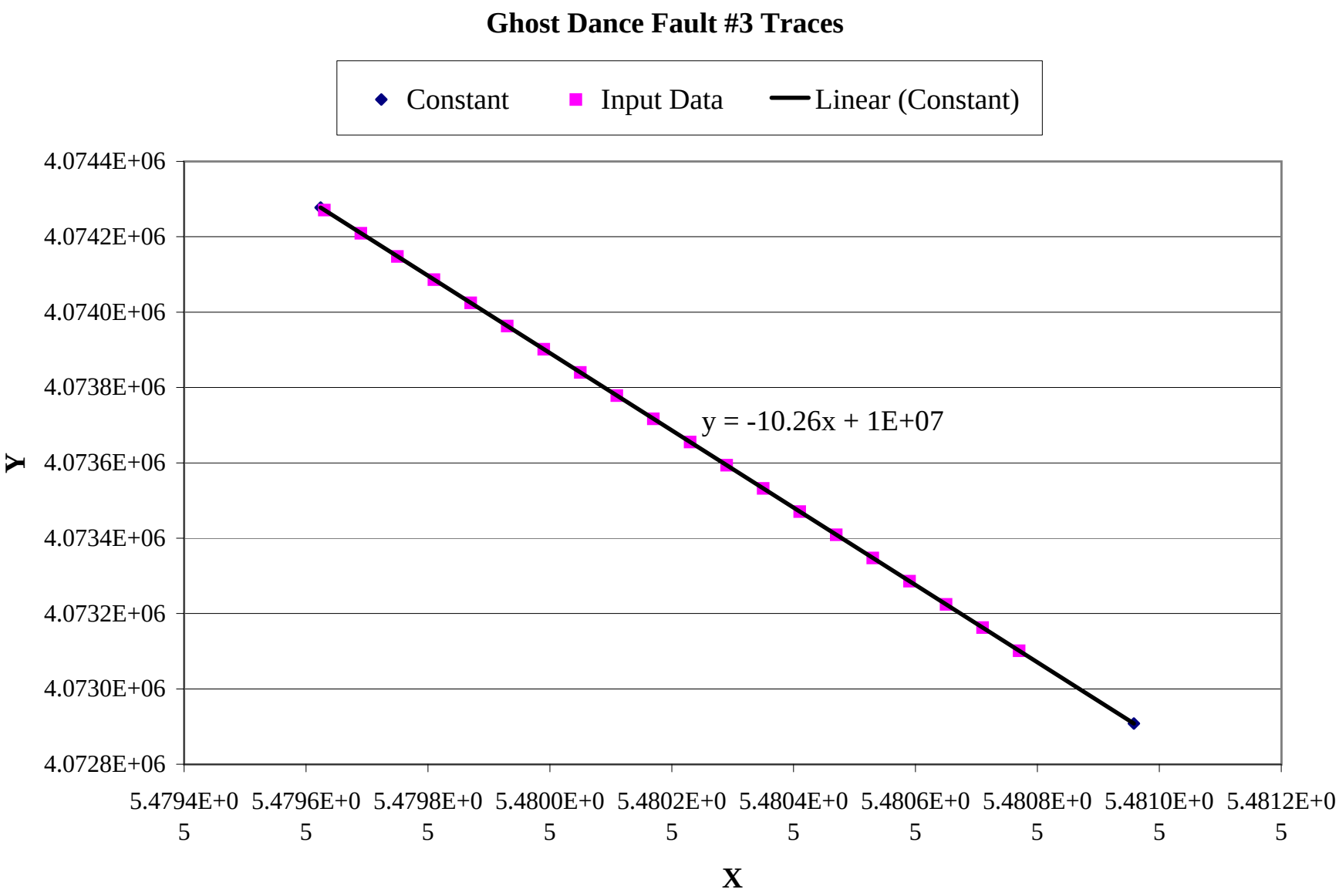
Ghost Dance Fault #3 Traces
Constant
Input Data
Linear (Constant)
y = -10.26x + 1E+07
4.0744E+06
4.0742E+06
4.0740E+06
4.0738E+06
4.0736E+06
4.0734E+06
4.0732E+06
4.0730E+06
4.0728E+06
Y
5.4794E+05
5.4796E+05
5.4798E+05
5.4800E+05
5.4802E+05
5.4804E+05
5.4806E+05
5.4808E+05
5.4810E+05
5.4812E+05
X

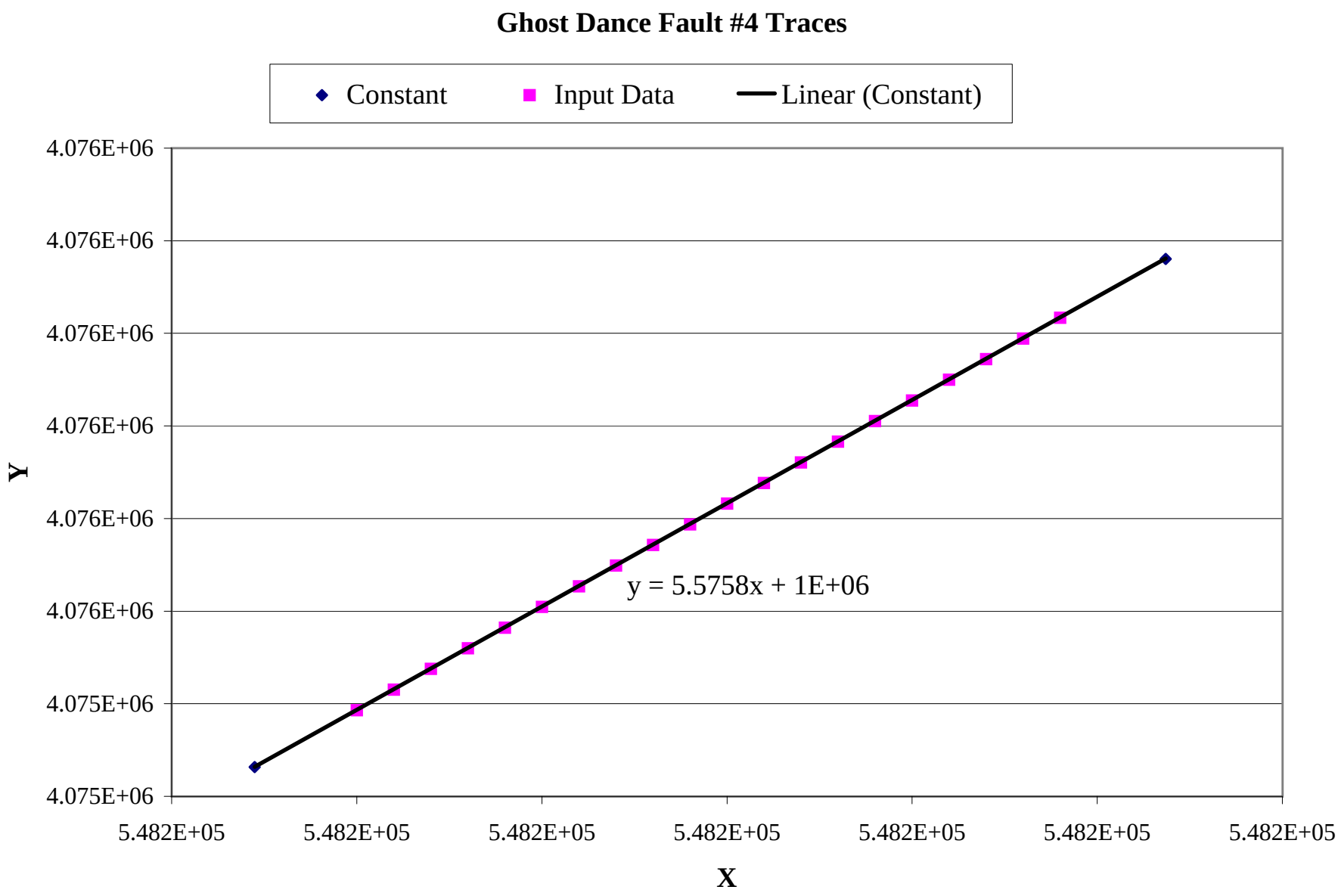
Ghost Dance Fault #4 Traces
Constant
Input Data
Linear (Constant)
4.076E+06
4.076E+06
4.076E+06
4.076E+06
4.076E+06
4.076E+06
4.075E+06
4.075E+06
Y
y = 5.5758x + 1E+06
5.482E+05
5.482E+05
5.482E+05
5.482E+05
5.482E+05
5.482E+05
5.482E+05
X

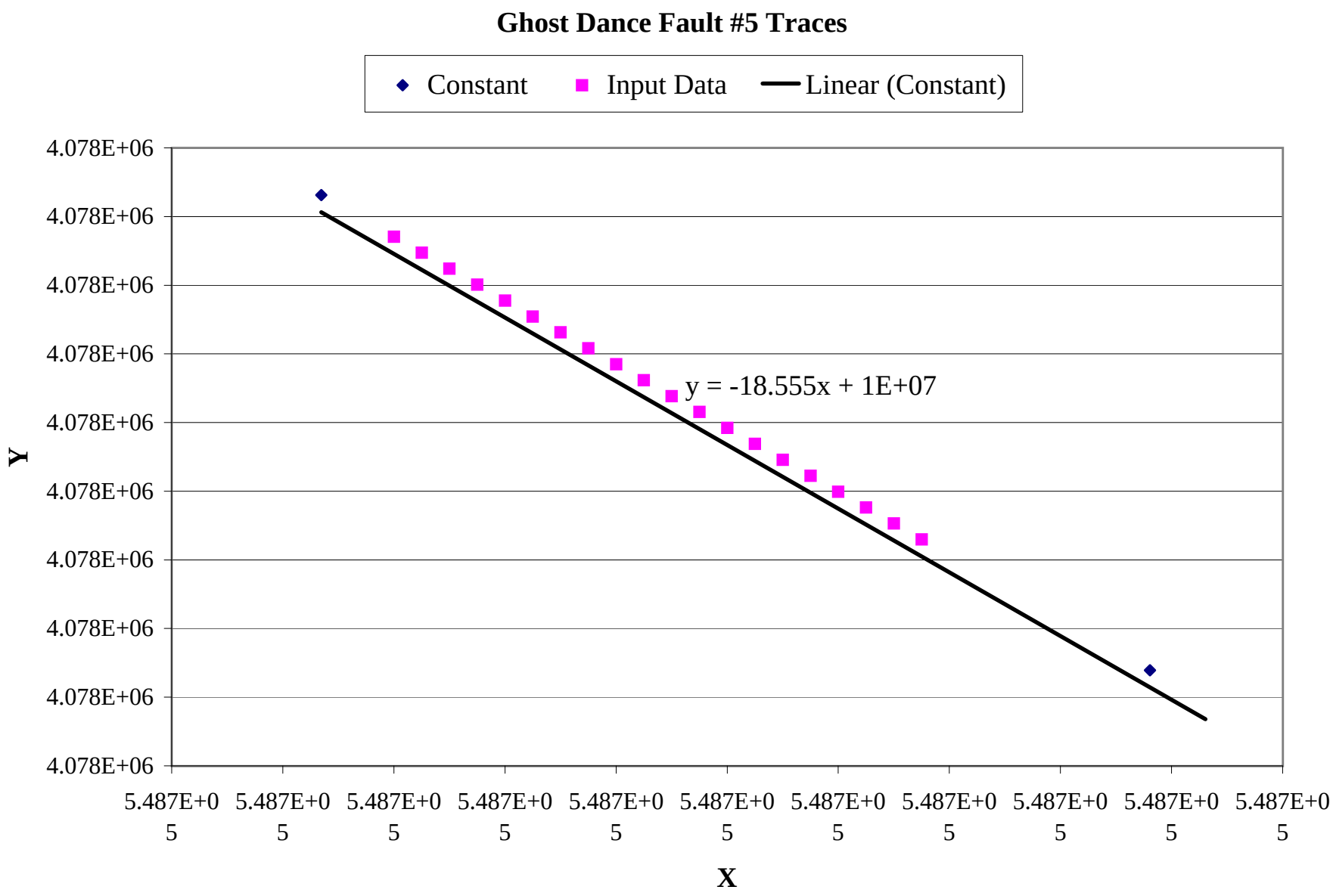
Ghost Dance Fault #5 Traces
Constant
Input Data
Linear (Constant)
y = -18.555x + 1E+07
4.078E+06
4.078E+06
4.078E+06
4.078E+06
4.078E+06
4.078E+06
4.078E+06
4.078E+06
4.078E+06
4.078E+06
Y
5.487E+05
5.487E+05
5.487E+05
5.487E+05
5.487E+05
5.487E+05
5.487E+05
5.487E+05
5.487E+05
5.487E+05
5.487E+05
X

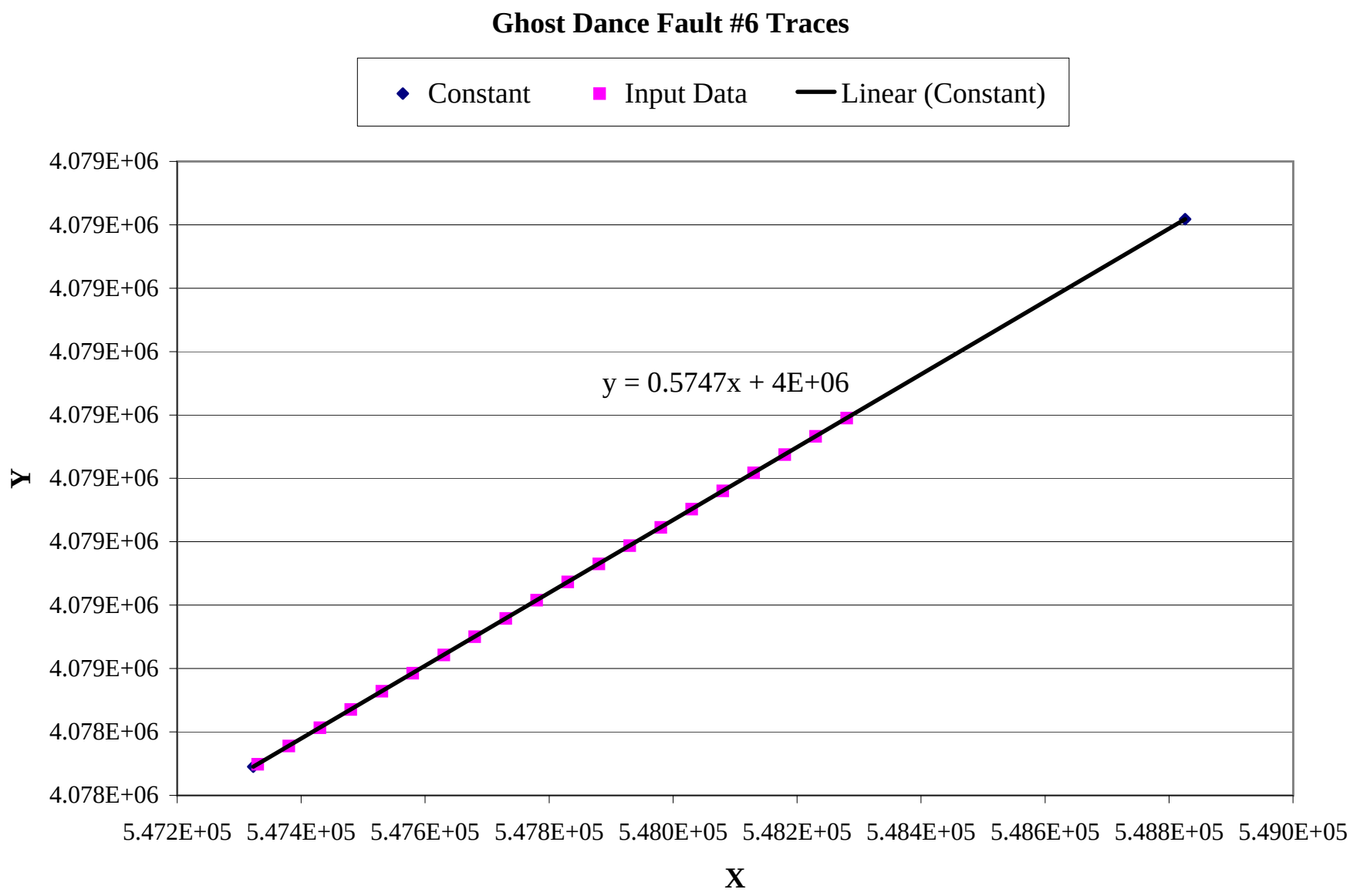
Ghost Dance Fault #6 Traces
Constant
Input Data
Linear (Constant)
y = 0.5747x + 4E+06
4.079E+06
4.079E+06
4.079E+06
4.079E+06
4.079E+06
4.079E+06
4.079E+06
4.079E+06
4.079E+06
4.078E+06
4.078E+06
Y
5.472E+05
5.474E+05
5.476E+05
5.478E+05
5.480E+05
5.482E+05
5.484E+05
5.486E+05
5.488E+05
5.490E+05
X

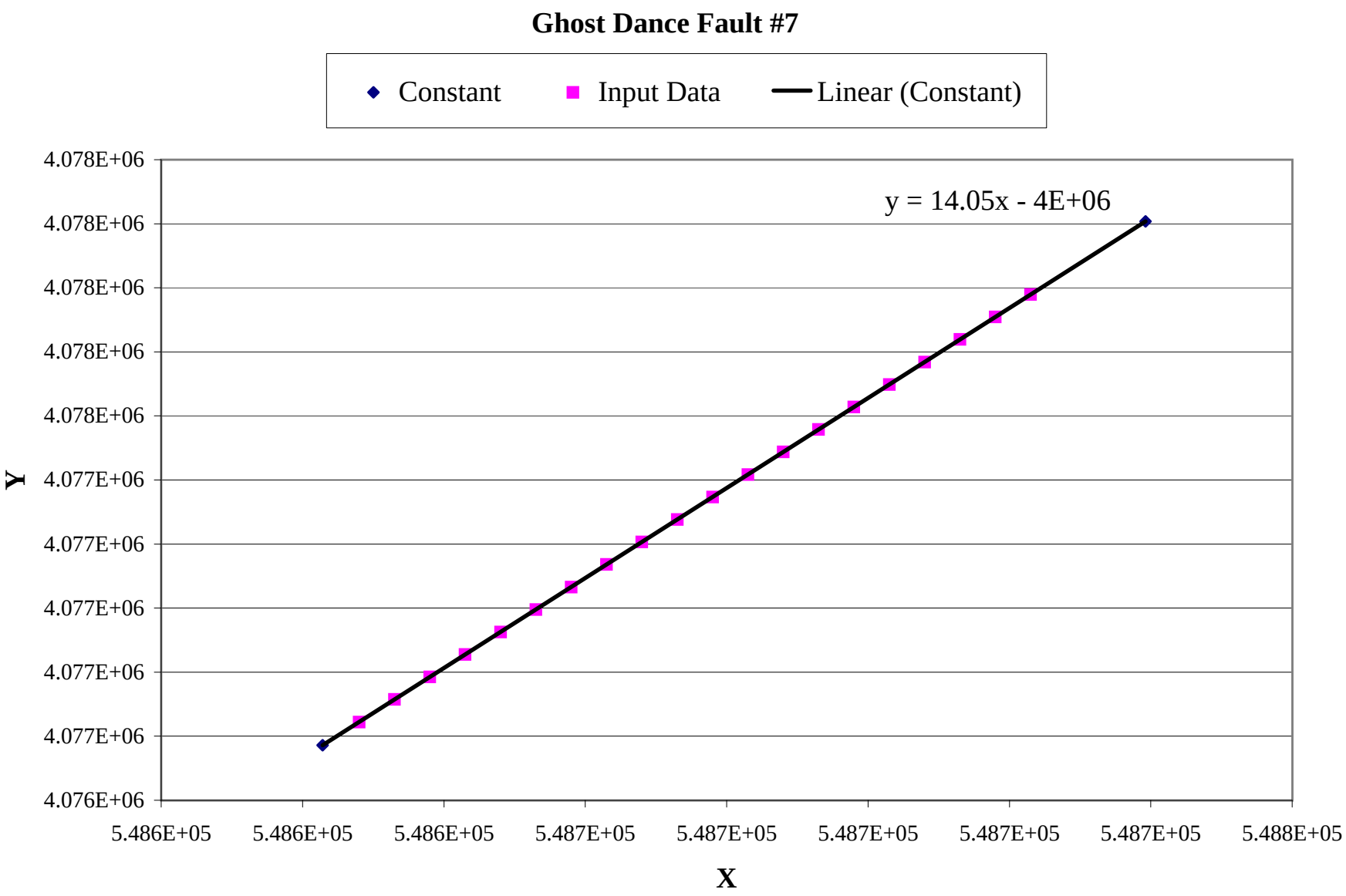
Ghost Dance Fault #7
Constant
Input Data
Linear (Constant)
y = 14.05x - 4E+06
4.078E+06
4.078E+06
4.078E+06
4.078E+06
4.078E+06
4.077E+06
4.077E+06
4.077E+06
4.077E+06
4.077E+06
4.076E+06
Y
5.486E+05
5.486E+05
5.486E+05
5.487E+05
5.487E+05
5.487E+05
5.487E+05
5.487E+05
5.488E+05
X

Ghost Dance Fault #8 Traces
Constant
Input Data
Linear (Constant)
y = 2.1527x + 3E+06
4.077E+06
4.077E+06
4.077E+06
4.076E+06
4.076E+06
4.076E+06
4.076E+06
4.076E+06
4.076E+06
4.076E+06
4.076E+06
4.076E+06
Y
5.482E+05
5.482E+05
5.483E+05
5.483E+05
5.484E+05
5.484E+05
5.485E+05
5.485E+05
5.486E+05
5.486E+05
5.487E+05
X